Elucidating the role of the adhesion and degranulation promoting adaptor protein (ADAP) in innate immune cells during *Listeria monocytogenes* infection in mice

Dissertation

zur Erlangung des akademischen Grades

doctor rerum naturalium (Dr. rer. nat.)

genehmigt durch die Fakultät für Naturwissenschaften der
Otto-von-Guericke-Universität Magdeburg

von M. Sc. Martha Agnes Luise Böning

geb. am 08.12.1989 in Templin

Gutachter: Prof. Dr. Dunja Bruder
              Prof. Dr. Sven Hammerschmidt

eingereicht am: 28.06.2021

verteidigt am: 12.10.2021

Supervisors:

Prof. Dr. Dunja Bruder
Prof. Dr. Burkhart Schraven

Preamble

Results of the present work were published in:

Böning, M. A. L.; Trittel, S.; Riese, P.; van Ham, M.; Heyner, M.; Voss, M.; Parzmair, G. P.; Klawonn, F.; Jeron, A.; Guzman, C. A.; Lothar, J.; Schraven, B.; Reinhold, A. and Bruder, D. ADAP promotes degranulation and migration of NK cells primed during *in vivo Listeria monocytogenes* infection in mice. *Front. Immunol.*, **2020**, *10*, 3144. https://doi.org/10.3389/fimmu.2019.03144.

Text sections and graphs from the above mentioned publication were used in sections 4.1.1, 4.1.2, 4.1.3 and 5.

Results of the present work were submitted for publication in *Frontiers in Immunology* (status: 25.06.2021):

Böning, M. A. L.; Parzmair, G. P.; Jeron, A., Düsedau, H. P.; Kershaw, O.; Xu, B.; Relja, B.; Schlüter, D.; Dunay, I. R.; Reinhold, A.; Schraven, B. and Bruder, D. Enhanced susceptibility of ADAP-deficient mice to *Listeria monocytogenes* infection is associated with altered phagocyte phenotype and function. Manuscript submitted.

Text sections and graphs from the above mentioned submitted manuscript were used in sections 4.2.1, 4.2.2, 4.2.3, 4.2.4 and 5.

Vorwort

Teilergebnisse der vorliegenden Arbeit wurden veröffentlicht in:

Böning, M. A. L.; Trittel, S.; Riese, P.; van Ham, M.; Heyner, M.; Voss, M.; Parzmair, G. P.; Klawonn, F.; Jeron, A.; Guzman, C. A.; Lothar, J.; Schraven, B.; Reinhold, A. and Bruder, D. ADAP promotes degranulation and migration of NK cells primed during *in vivo Listeria monocytogenes* infection in mice. *Front. Immunol.*, **2020**, *10*, 3144. https://doi.org/10.3389/fimmu.2019.03144.

Textabschnitte sowie Grafiken der oben genannten Publikation wurden in den Abschnitten 4.1.1, 4.1.2, 4.1.3 sowie 5 verwendet.

Teilergebnisse der vorliegenden Arbeit wurden zur Veröffentlichung eingereicht in *Frontiers in Immunology* (Stand: 25.06.2021):

Böning, M. A. L.; Parzmair, G. P.; Jeron, A., Düsedau, H. P.; Kershaw, O.; Xu, B.; Relja, B.; Schlüter, D.; Dunay, I. R.; Reinhold, A.; Schraven, B. and Bruder, D. Enhanced susceptibility of ADAP-deficient mice to *Listeria monocytogenes* infection is associated with altered phagocyte phenotype and function. Manuskript eingereicht.

Textabschnitte sowie Grafiken des oben genannten eingereichten Manuskripts wurden in den Abschnitten 4.2.1, 4.2.2, 4.2.3, 4.2.4 sowie 5 verwendet.

Contents

List of publications

Böning, M. A. L.; Trittel, S.; Riese, P.; van Ham, M.; Heyner, M.; Voss, M.; Parzmair, G. P.; Klawonn, F.; Jeron, A.; Guzman, C. A.; Lothar, J.; Schraven, B.; Reinhold, A. and Bruder, D. ADAP promotes degranulation and migration of NK cells primed during *in vivo Listeria monocytogenes* infection in mice. *Front. Immunol.*, **2020**, *10*, 3144. https://doi.org/10.3389/fimmu.2019.03144.
Impact Factor (2020): 5.085

Others

Schmidt, I. H. E.; Gildhorn, C.; **Böning M. A. L.**; Kulow, V. A.; Steinmetz, I. and Bast, A. *Burkholderia Pseudomallei* modulates host iron homeostasis to facilitate iron availability and intracellular survival. *PLoS Negl Trop Dis.* **2018**, 12;*12* (1). https://doi.org/10.1371/journal.pntd.0006096.
Impact Factor (2018): 4.487

Conference contributions

Martha AL Böning, Andreas Jeron, Gerald P Parzmair, Burkhart Schraven & Dunja Bruder. *Role of the Adhesion and degranulation-promoting adaptor protein (ADAP) in natural killer cells during bacterial infection* (**Poster presentation**). International Graduate School for Infection Research, Summer School on Infection Research. **2018**. Wernigerode. Germany.

Martha AL Böning, Andreas Jeron, Gerald P Parzmair, Annegret Reinhold, Burkhart Schraven & Dunja Bruder. *Role of ADAP in NK cell-activation and in the initiation of innate immunity to bacterial infections* (**Oral Presentation**). Natural Killer Cell Symposium. **2018**. Hamburg, Germany.

Martha AL Böning, Martin Voss, Andreas Jeron, Gerald P Parzmair, Maxi Scheiter, Lothar Jänsch, Burkhart Schraven, Annegret Reinhold & Dunja Bruder. *The adhesion and degranulation-promoting adaptor protein (ADAP) is involved in effector cytokine release, degranulation and migration of NK cells primed during in vivo Listeria monocytogenes infection in mice* (**Oral Presentation**). 23. Symposium der FG Infektionsimmunologie "Infektion und Immunabwehr". **2019**. Burg Rothenfels, Germany.

Martha AL Böning, Gerald P Parzmair, Andreas Jeron, Peggy Riese, Stephanie Trittel, Maxi Scheiter, Martin Voss, Lothar Jänsch, Carlos A Guzman, Burkhart Schraven, Annegret Reinhold & Dunja Bruder. *Cytokine release, degranulation and migratory capacity of NK cells depends on ADAP during Listeria monocytogenes infection of mice* (**Oral Presentation and Poster presentation**). II Joint Conference of the German Society for Immunology and the Italian Society for Immunology, Clinical Immunology and Allergology (SIICA), Satellite NK cell Symposium. **2019**. München, Germany.

Martha AL Böning, Gerald P Parzmair, Andreas Jeron, Henning P Düsedau, Xu Baolin, Olivia Kershaw, Borna Relja, Ildiko Rita Dunay, Dirk Schlüter, Annegret Reinhold, Burkhart Schraven & Dunja Bruder. *Enhanced susceptibility of ADAP-deficient mice to Listeria monocytogenes infection is associated with altered neutrophil phenotype and function* (**ePoster talk**). Novel Concepts in Innate Immunity. **2021**. The conference took place digitally.

Abstract

The adhesion and degranulation-promoting adaptor protein (ADAP) serves as a multifunctional scaffold and is involved in the formation of immune signaling complexes. To date only limited and moreover conflicting data exist regarding the role of ADAP in innate immune cells and its contribution in antibacterial immunity during *in vivo* infection remains largely elusive.

The first part of this thesis extends existing knowledge on the role of ADAP in NK cells to *in vivo* infection with the intracellular pathogen *Listeria monocytogenes* (*Lm*). *Ex vivo* analysis of infection-primed NK cells revealed impaired cytotoxic capacity in NK cells lacking ADAP (ADAPko), indicated by reduced CD107a surface expression and inefficient perforin production. However, ADAP-deficiency had no global effect on NK cell morphology or intracellular distribution of CD107a-containing vesicles. Proteomic definition of ADAPko and wild type NK cells did not uncover obvious differences in protein composition during the steady state and similar early response patterns were induced in NK cells upon infection independent of genotype. In line with protein network analyses that suggested an altered migration phenotype in naïve ADAPko NK cells, *in vitro* migration assays uncovered significantly reduced migration of both naïve as well as infection-primed ADAPko NK cells compared to wild type NK cells. In conclusion, during systemic *Lm* infection in mice ADAP is essential for efficient cytotoxic capacity and migration of NK cells.

The second part of the thesis builds on previous, so far unpublished data from our group showing that ADAPko mice are highly susceptible to infection with *Lm*. Enhanced immunopathology in infected tissues and an overall increased morbidity and mortality was associated with an excessive infiltration of neutrophils and inflammatory monocytes. Despite high phagocyte numbers in spleen and liver, ADAPko mice only inefficiently controlled pathogen growth hinting at a functional impairment of infection-primed phagocytes. Indeed, flow cytometric analysis of hallmark pro-inflammatory mediators and whole genome transcriptional profiling of neutrophils and inflammatory monocytes uncovered broad molecular alterations in the inflammatory program following their activation in the ADAP-deficient host. Strikingly, *ex vivo* phagocytosis assay revealed impaired phagocytic capacity of neutrophils derived from *Lm*-infected ADAPko mice. Together these data suggest that an alternative priming of phagocytes in ADAP-deficient mice during *Lm* infection induces marked alterations in the inflammatory profile of phagocytes that contributes to enhanced immunopathology while at the same time limits their capacity to eliminate the pathogen and to prevent the fatal outcome of the infection.

Zusammenfassung

Das Adapterprotein ADAP (*adhesion and degranulation-promoting adapter protein*) ist als multifunktionales Protein an der Bildung von Immunsignalkomplexen beteiligt. Bis heute existieren nur begrenzte und darüber hinaus widersprüchliche Daten bezüglich der Rolle von ADAP in Zellen des angeborenen Immunsystems und dessen Beitrag zur antibakteriellen Immunität während einer *in vivo* Infektion bleibt weitgehend unklar.

Der erste Teil dieser Dissertation erweitert das vorhandene Wissen bezüglich der Rolle von ADAP in NK-Zellen durch Nutzung eines *in vivo* Infektionsmodells mit dem intrazellulären Pathogen *Listeria monocytogenes* (*Lm*). *Ex vivo* Analysen von ADAP-defizienten (ADAPko) NK-Zellen, die im Rahmen der *Lm* Infektion *in vivo* aktiviert wurden, ergaben eine verminderte zytotoxische Funktion, welches durch eine reduzierte CD107a-Oberflächen-expression und eine ineffiziente Perforinproduktion angezeigt ist. Der Verlust von ADAP hatte jedoch keine globalen Auswirkungen auf die NK-Zellmorphologie oder die intrazelluläre Verteilung von CD107a-haltigen Vesikeln. Proteomische Untersuchungen von ADAPko und Wildtyp NK-Zellen ergaben keine offensichtlichen Unterschiede in der Proteinzusammen-setzung. In Übereinstimmung mit Proteinnetzwerkanalysen, die einen veränderten Migrations-phänotyp in naiven ADAPko NK-Zellen nahelegten, zeigten vergleichende *in vitro* Migrationstests eine signifikant reduzierte Migration sowohl von naiven als auch von infektionsaktivierten ADAPko NK-Zellen. Zusammenfassend lässt sich aus diesen Ergebnissen schließen, dass ADAP im Verlauf einer systemischen *Lm* Infektion für eine effiziente zytotoxische Funktion und Migration von NK-Zellen essentiell ist.

Der zweite Teil der Dissertation baut auf früheren, bislang unveröffentlichten Daten unserer Arbeitsgruppe auf, die zeigen, dass ADAPko Mäuse sehr anfällig für Infektionen mit *Lm* sind. Eine verstärkte Immunpathologie in infizierten Geweben und eine insgesamt erhöhte Morbidität sowie Mortalität waren mit einer übermäßigen Infiltration von Neutrophilen und Monozyten verbunden. Trotz hoher Anzahl an Phagozyten kontrollierten ADAPko Mäuse das Pathogenwachstum nur ineffizient, was auf eine funktionale Beeinträchtigung der Phagozyten hindeutet. Tatsächlich zeigten durchflusszytometrische Analyse typischer pro-inflamma-torischer Mediatoren sowie Transkriptiomanalysen von Neutrophilen und inflammatorischen Monozyten molekulare Veränderungen nach Aktivierung im ADAP-defizienten Wirt auf. Bemerkenswerterweise ergab der *ex vivo* Phagozytosetest eine beeinträchtigte Phagozytose-leistung von Neutrophilen, die von *Lm*-infizierten ADAPko-Mäusen stammten.

Zusammengenommen legen diese Daten nahe, dass eine alternative Aktivierung von Phagozyten in ADAP-defizienten Mäusen während einer *Lm* Infektion deutliche Veränderungen im Entzündungsprofil und der Funktionalität von Phagozyten induziert, wodurch die Fähigkeit zur Eliminierung des Pathogens und somit zur Verhinderung des tödlichen Ausganges der Infektion eingeschränkt wird.

List of Abbreviations

% (v/v)	volume percent
%	percent
α	alpha
ACN	acetonitril
ActA	actin assembly-inducing protein
ADAP	adhesion and degranulation-promoting adaptor protein
AKI	acute kidney injury
ALT	alanine transaminase
ACP	antigen presenting cell
β	beta
Bcl10	B-cell CLL-lymphoma 10
BHI	brain heart infusion
BM	bone marrow
BMDM	bone marrow-derived macrophages
bp	base pair(s)
BSA	bovine serum albumin
Btk	bruton tyrosine kinase
CARMA1	caspase recruitment domain-containing membrane-associated guanylate kinase protein 1
CCR	chemokine receptor
CCL	CC chemokine ligand
CFU	colony forming unit(s)
CO_2	carbon dioxide
cond.	conditional
CR	complement receptor
ctr.	control(s)
CXCR	C-X-C motif chemokine receptor
d	day(s)
DAP12	NDAX activation protein of 12 kDa
DCs	dendritic cells
DEPC	diethyl pyrocarbonate
DMSO	dimethylsulfoxide
DMEM	Dulbecco's modified Eagle's medium
DN	double-negative
DNA	desoxyribonucleic acid
DP	double-positive
d. p. i.	days post infection
DTT	dithiotreitol
EAE	experimental autoimmune encephalomyelitis
EDTA	ethylenediaminetetraacetic acid
EVH1	Ena/vasodilator-stimulated phosphoprotein (VASP) homology 1
ex vivo	*latin*: "out of the living"
FA	formic acid
FACS	fluorescent activated cell sorting
FC	fold change
FCRγ	gamma chain of immunoglobulin Fc receptor
FCS	fetal calf serum
FDR	false discovery rate
fl	floxed
FMO	fluorescence minus one (control)
FRT	flippase recognition target
FSC	forward scatter

Fyb	Fyn-binding protein
Fyn	fibroblast yes-related non-receptor kinase
g	gram(s)
γ	gamma
G-CSF	granulocyte-colony stimulating factor
GM-CSF	granulocyte-macrophage colony-stimulating factor
GrzB	granzyme B
h	hour (s)
het	heterozygous
H&E	hematoxylin and eosin stain
HGF-Rc	hepatocyte growth factor
HIER	heat-induced epitope retrieval
hSH3	SH3 domain with an N-terminal alpha-helix
ICAM	intercellular adhesion molecule
IFN	Interferon
IFNAR	interferon-alpha/beta receptor
IKK	IκB kinase
IL	interleukin
ILC	innate lymphoid cell
iNK	immature NK cells
Inl	internalin
iNOS/NOS2	inducible nitrogen oxide synthase
in vitro	*latin*: "in the glass"
in vivo	*latin*: "within the living"
Iono	ionomycin
IRF	interferon regulating factor
ITAMs	immunoreceptor tyrosine-based activation motif
i. v.	intravenous
KCl	potassium chloride
kDa	dalton (atomic mass)
Kindlin-3	fermitin family homolog 3
KLR	killer cell lectin-like receptor
KMC	k-means cluster
ko/KO	knockout
LAMP-1/CD107a	lysosomal-associated membrane protein-1
LAT	linker of activated T cells
Lck	lymphocyte kinase
LFA-1	lymphocyte function-associated antigen-1
Lm	*Listeria monocytogenes*
LLO	listeriolysin O
loxP	locus of X-over P1
Ly6C	lymphocyte antigen 6C
Ly6G	lymphocyte antigen 6 complex locus G6D
M	molar mass
mM	millimolar
MACS	magnetic activated cell sorting
MALT1	mucosa-associated lymphoid tissue lymphoma translocation gene 1
MAPK	mitogen-activated protein kinase
MFI	mean fluorescence intensity
µg	microgram
$MgCl_2$	magnesium chloride
MHC	major histocompatibility complex
MilliQ	purified, deionized water
min	minute(s)

mNK	mature NK cell
mL	milliliter
µL	microliter
MLN	mesenteric lymph nodes
µm	micrometer
MMP9	matrix metalloproteinase 9
MPO	myeloperoxidase
MS	mass spectrometry
Mst1	mammalian Ste20-like kinase
MTOC	microtubule-organizing center
MyD88	myeloid differentiation primary response gene 88
NaCl	sodium chloride
Nck	non-catalytic region of the tyrosine kinase adaptor protein 1
n. d.	not detectable
NE	neutrophil elastase
NET	neutrophil extracellular trap(s)
NFκB	nuclear factor kappa-light-chain-enhancer of activated B cells
NK cell	Natural killer cell
NKP	NK cell progenitor
NKT cell	Natural killer T cell
nL	nanoliter
nmol	nanomolar
NO	nitric oxide
n. s.	not significant
PAD4	peptidyl arginine deiminase
PAMPs	pathogen-associated molecular patterns
PBS	phosphate buffered saline
PCR	polymerase chain reaction
PFA	paraformaldehyde
pg	picogram(s)
PH	pleckstrin homology
p. i.	post infection
PI3K	phosphoinositide 3-kinase
PKCθ	protein kinase C theta
PLCγ	phospholipase C gamma
PMA	phorbol 12-myristate 13-acetate
PMN	polymorphonuclear leukocytes
PMT	photomultipliers
Post	*latin*: "after an infection"
PRR	pattern recognition receptor
Pro	proline-rich sequences
PSGL-1	P-selectin glycoprotein ligand 1
qRT-PCR	quantitative real time PCR
RAPL	regulator for cell adhesion and polarization enriched in lymphoid tissues
RIAM	Rap1 interacting adaptor molecule
RNA	ribonucleic acid
rpm	rounds per minute
RT	room temperature
SDF-1	stromal cell-derived factor 1
SDS	sodium dodecyl sulfate
sec	second(s)
SEM	standard error of the mean
SH	Src homology
SKAP-55/SKAP1	Src kinase-associated phosphoprotein of 55 kDa

SKAP-HOM/SKAP2	SKAP55/SKAP1 homologue
SLP-76	SH2-domain-containing leukocyte protein of 76 kDa
SLAP-130	SH2-domain-containing leukocyte protein of 76 kDa-associated phosphoprotein of 130 kDa
SSC	side scatter
Syk	spleen tyrosine kinase
TAC	Transcriptome Analysis Console
TAK1	transforming growth factor beta (TGF-β)-activated protein kinase 1
TCR	T cell receptor
TE	buffer solution
TGF	transforming growth factor
TipDC	TNF- and iNOS-producing dendritic cell
TLR	toll-like receptor
Tmp	tyrosine phosphorylated motif
TNF	tumor necrosis factor
TRAF6	TNF receptor associated factor 6
TRAIL	TNF-related apoptosis inducing ligand
Tris	tris(hydroxymethyl)aminomethane
U	Unit(s)
VASP	Ena/vasodilator-stimulated phosphoprotein
WASP	Wiskott-Aldrich Syndrome Protein
WT	wild type
ZAP-70	zeta-chain-associated protein kinase 70

Note: Standard SI units and abbreviations of chemical elements were used.

List of Figures

List of Tables

Appendix

1 Introduction

We are constantly exposed to a plethora of different microorganism surrounding ourselves and that we inhale, swallow or that are in close contact to our skin. Nevertheless, whether or not these microbes cause infections and diseases depends on a complex interplay of the microorganism and the antimicrobial defense mechanisms of the host. The immune system represents a complex and interactive network of different cell types, tissues, lymphoid organs and numerous cytokines as well as chemokines. Its fundamental role is to protect the host against invading pathogens and immunological dysfunctions can result in severe infections. The immune system can be largely divided into the unspecific innate and the specific adaptive immunity. The former takes effects as soon as the invasion occurs. With this, it represents the first line of defense against pathogens by limiting their entry into the host and at the same time initiating antimicrobial defense by different cellular subsets and chemical substances. The adaptive immune system can be further subdivided into humoral and cellular immunity. In contrast to the innate immune response, the adaptive immune system requires more time to take effect and operates in a pathogen-specific manner. This system is able to give rise to the so-called immunological memory, which in case of a re-infection with the same pathogen confers faster and more effective protection of the host.

In the case of infection, a multitude of signaling cascades within the innate and adaptive immune system becomes activated. Adapter proteins mediate the coupling of transmembrane receptors to intracellular signaling pathways. Hence, adaptor proteins are central players in innate and adaptive immune activation and are involved in a number of cellular processes. Cellular signaling cascades usually result in the activation and nuclear translocation of specific transcription factors that regulate the expression of a specific set of target genes.

1.1 Adaptor proteins

The different signaling activities taking place in immune cells are dependent on adaptor proteins. By definition, adaptor proteins do not have an enzymatic or transcriptional activity, but they serve as scaffolds for molecular signaling complexes. They function by localizing or de-localizing of proteins. Adapter proteins contain specialized protein-lipid as well as protein-

protein interaction domains, which are necessary to bind to other parts of the cellular signaling machinery[1–3].

1.1.1 ADAP - Adhesion and degranulation-promoting adaptor protein

The adhesion and degranulation-promoting adaptor protein (ADAP) was first described in human as well as mouse T cells and belongs to the group of cytosolic adaptor proteins. ADAP was discovered as an interaction partner for the T cell signaling proteins SH2-domain-containing leukocyte protein of 76 kDa (SLP-76) and fibroblast yes-related non-receptor kinase (Fyn)[4,5]. The gene encoding for ADAP was identified independently by two different research groups and published under the synonyms Fyn-binding protein (Fyb) and SH2-domain-containing leukocyte protein of 76 kDa-associated phosphoprotein of 130 kDa (SLAP-130)[6,7]. Two isoforms of 120 and 130 kDa have been identified. The splice variants differ by an insertion of 46 amino acids. ADAP is expressed in cells of the hematopoietic lineage, including T cells[5], natural killer (NK) cells[8], platelets[9], myeloid cells[10] such as neutrophils and monocytes as well as pre B cells, while mature splenic B cells lack ADAP[10]. In T cells, the adaptor protein is involved in intracellular signaling cascades leading to cell activation, adhesion and motility as well as proliferation, migration and NFκB activation[11,12]. ADAP was the first adaptor protein identified to link T cell receptor- and chemokine-mediated signaling to integrin activation. With this, ADAP is involved in inside-out signaling[11,13].

To understand the function of ADAP in different signaling pathways, its contribution to different cellular functions as well as its overall impact on the immune system, a closer look at the molecular structure of ADAP is required.

1.1.2 ADAP - Structure, domains and interaction partners

ADAP consists of numerous structural features that enable it to fulfill its function as a molecular scaffold. No specific sequence information are described for to the first third of the N-terminal half of the 120 kDa splice variant of ADAP. Nevertheless, in the middle third of ADAP several proline-rich sequences are located (**Figure 1**). The immunologically important interaction takes place through the binding of the Src kinase-associated phosphoprotein of 55 kDa (SKAP55 or SKAP1) and its homologue SKAP-HOM (SKAP2) to the Src Homology 3 (SH3) proline-rich sequence in ADAP[7,14,15]. Of note, SH3 domains represent adaptable scaffolds by targeting proline-rich sequences inside of proteins[14].
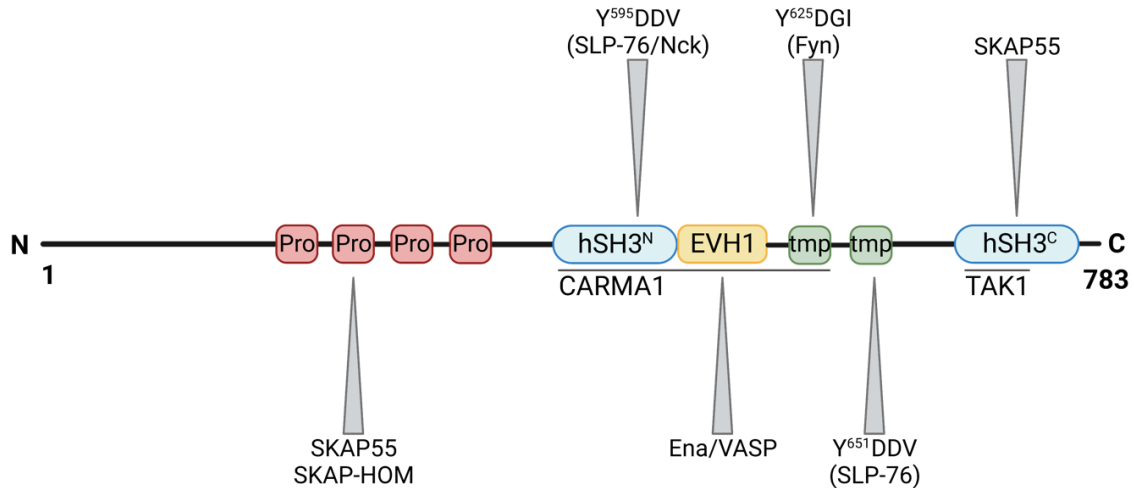
Figure 1 | Schematic representation of the structure of ADAP. The N-terminus of ADAP does not contain any known structural elements except proline-rich sequences (Pro, colored in red) in the middle third. The C-terminally located helical extended SH3 domains (hSH3) are colored in blue. The interaction partners and their binding domains are shown above and below the schematic structure of ADAP. Interactions are furthermore described with their marked tyrosine phosphorylated motif (tmp, colored in green). For the sake of simplicity, potential binding partners and the sites of interaction are not depicted. Figure is not scaled. The scheme was adapted from references [5,16,17] and created with BioRender.com (2021).

In contrast to the N-terminal region of ADAP, hSH3 domains and several interaction partners are known for the C-terminal region. Two unusual Src Homology 3 domains have been described for ADAP[16]. Due to a tryptophan to lysine replacement, both the N-terminal hSH3^N as well as the C-terminal hSH3^C domain, show no binding to proline-rich sequences, which is typical for SH3 domains[14,18]. Depending on the phosphorylation of the interaction partners, they bind between the hSH3 domains to phosphotyrosin or to proline-rich motives with their own Src homology 2 (SH2) sequences[5,15].

ADAP has been identified as an interaction partner of Fyn, which binds at position 625-628 (YDGI; tyrosine-aspartate-glycine-isoleucine) via its SH2 domain. Moreover, Fyn phosphorylates tyrosine of the YDDV (tyrosine-aspartate-aspartate-valine) motif at positions 595-598 and 651-654. These are subsequently bound by the SH2 domain of SLP-76. With this, Y^{595}DDV and Y^{651}DDV are known to bind to SLP-76, whereas Y^{595}DDV has a dual function and mediates as well the binding to a non-catalytic region of the tyrosine kinase adaptor protein 1 (Nck)[7,19–21]. Between the two C-terminally located helically extended SH3 domains a binding site for Ena/vasodilator-stimulated phosphoprotein (VASP) homology 1 (EVH1) is located (**Figure 1**)[22]. Proteins from the Ena/VASP family are important for the regulation of the cell adhesion as well as the shape of the cell and migration by modulating the cytoskeleton[23].

Proteins from the before mentioned family are thought to bind to the proline-rich sequences in ADAP through a EVH1 domain, together with SLP-76, Nck and Wiskott-Aldrich Syndrome Protein (WASP)[10,22]. The functional interaction between Nck and ADAP enhances the actin rearrangement by stabilizing the interaction between WASP and SLP-76[24]. Of note, no changes were observed regarding the F-actin in ADAP knockout mice[11].

Moreover, ADAP consists of a binding site for the interaction with the caspase recruitment domain-containing membrane-associated guanylate kinase protein 1 (CARMA1) as well as another binding site for the transforming growth factor beta (TGF-β)-activated protein kinase 1 (TAK1)[12,25]. Of note, 30 % of ADAP molecules are associated to this module, serving an important role in the NF-κB activation (**Figure 2**). NF-κB is a central transcription factor for the activation as well as the proliferation of T cells[26]. Usually, NF-κB is retained inactive in the cytoplasm by binding to its inhibitor IκB-α.
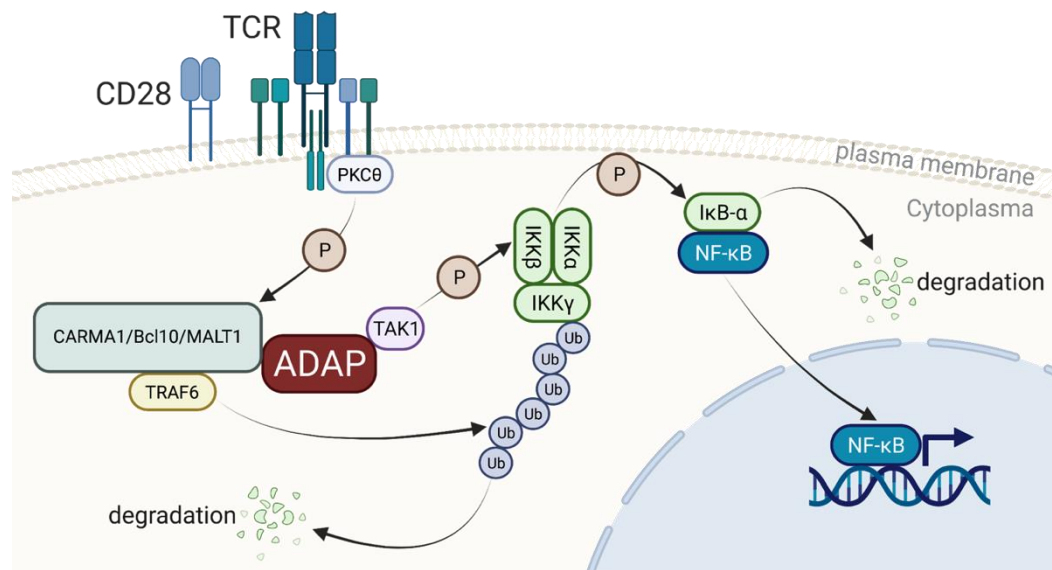
Figure 2 | ADAP is involved in the NF-κB signaling pathway. TCR/CD28 co-stimulation CARMA1 is phosphorylated by the PKCθ and recruited to the plasma membrane. In turn, CARMA1 binds Bcl10 and MALT1, forming the CBM complex, which controls IKK mediated NF-κB activation by promoting the activation of the IKK complex. Within this complex, MALT1-bound TRAF6 is thought to mediate polyubiquitination of the inhibitory γ-subunit of IKK, leading to its degradation. TRAF6-mediated ubiquitination of IKKγ may contribute to IKK activation. ADAP has an essential role in stabilizing the CBM complex, but also recruits TAK1, a kinase needed for the phosphorylation of IKKβ and IKKγ, rendering this complex functional subsequently leading to the release of NF-κB. The scheme was adapted from references [27,28] and created with BioRender.com (2021).

A complex consisting of IκB kinase alpha (IKKα), IKKβ and IKKγ, is needed to phosphorylate IκBα. Upon co-stimulation of the T cell receptor (TCR)/CD28, CARMA1 is phosphorylated by the protein kinase C theta (PKCθ) and recruited to the plasma membrane. Afterwards,

CARMA1 binds to the B-cell CLL-lymphoma 10 (Bcl10) and mucosa-associated lymphoid tissue lymphoma translocation gene 1 (MALT1), together forming the CARMA1/Bcl10/ MALT1 complex, which is necessary for TNF receptor associated factor 6 (TRAF6) mobilization. TRAF6 in combination with the CBM complex is necessary to polyubiquitinate the inhibitory γ-subunit of IKK, leading to its degradation and subsequent activation of the NF-κB signaling pathway[27]. ADAP has a central role in stabilizing the CBM complex, but also recruits TAK1, a kinase needed for the phosphorylation of IKKβ, rendering the IKK kinase functional, subsequently leading to the release of NF-κB. The released NF-κB translocates into the nucleus and initiates transcription of target genes[29,30]. This clearly demonstrates that the complex formation of a PKCθ/CBM/TRAF6/ADAP/TAK1 signalosome promotes the activation of NF-κB.

Medeiros et al. suggested the existence of two ADAP "populations" that differ in terms of their molecular function, with one having a regulatory effect on gene transcription by association with the CBM complex and one playing a pivotal role in the activation of integrins together with SKAP55[12]. Furthermore Burbach et al. suggested a model in which cytoplasmic ADAP can activate the transcription factor NF-κB via the CBM complex. A chimera from the Pleckstrin homology (PH) domain of SKAP55 and the C-terminus of ADAP is generally located on the plasma membrane and thus enables integrin activation. However, if this molecular chimera is mutated within the SKAP55 PH domain, it is constitutively present in the cytoplasm and activates the NF-κB signaling pathway[28]. Thus, approximately 70 % of the ADAP molecules are constitutively bound to SKAP55 while 100 % of the SKAP55 molecules are associated with ADAP[31]. SKAP55 was identified as a protein that interacts with the SH2 domain of the Src kinase Fyn and contains three known phosphorylation sites[4]. Of note, ADAP is needed for the expression of the proteins SKAP55/SKAP-HOM[32–34]. ADAP-deficiency results in the absence of the SKAP55/SKAP-HOM dimer on the protein level, whereas mRNA level were not affected[35]. This indicates, that ADAP is needed for a stable expression of these proteins[32–34].

T cells express a specific TCR, which consists of an α- and a β-chain. Because the cytoplasmic ends of these chains are very short, the signal needs to be transmitted through the cytoplasmic tails of the CD3 complex, containing immunoreceptor tyrosine-based activation motif (ITAMs). After TCR activation, ITAMs are phosphorylated by different Src kinases such as

lymphocyte kinase (Lck) and Fyn[36,37] (**Figure 3**). Lck together with Fyn phosphorylates CD3 receptor molecule after TCR-CD3 stimulation.

Additionally, the ζ-associated protein 70 kDa (ZAP-70) kinase becomes phosphorylated and activated by Lck. Furthermore, the ADAP/SKAP55 module as well as SLP-76 are recruited to linker of activated T cells (LAT)[38–40], whereas SLP-76 is phosphorylated after the recruitment of ZAP-70[38,40,41].
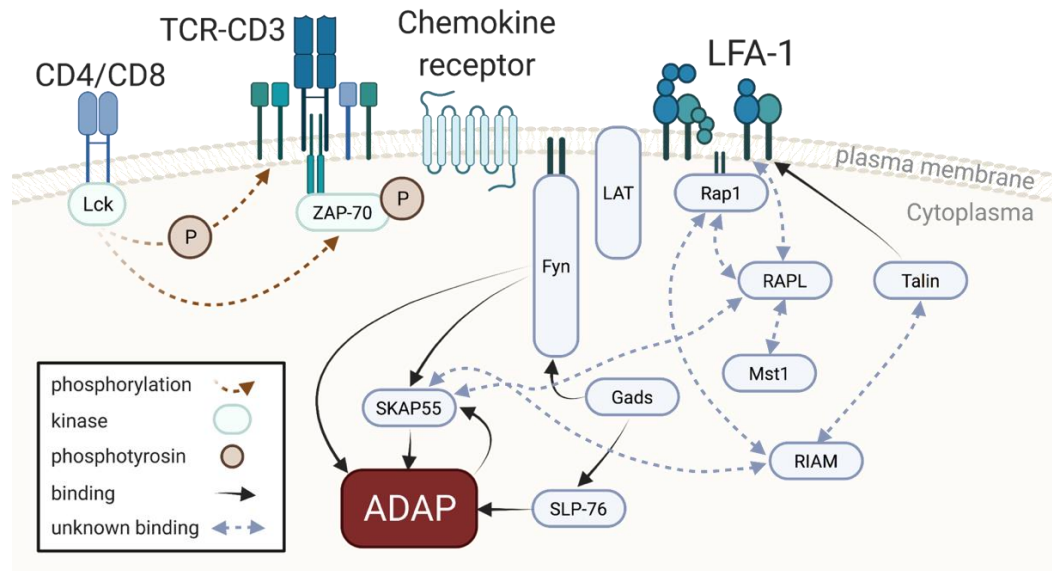
Figure 3 | The role of ADAP in the activation of integrins following TCR-CD3 complex or chemokine receptor stimulation in T cells. Following TCR stimulation, the phosphorylation of LAT mediates the recruitment of ADAP and SKAP55 to the membrane by Gads and SLP-76. SKAP55 interacts with RAPL and RIAM. RAPL and RIAM bind active Rap1, and are directly or indirectly via Talin associated with the cytoplasmic regions of the integrin $α_L$- or $ß_2$-chain (LFA-1). The ADAP/SKAP55 module forms two distinct complexes that each exclusively interact with one of the chains of the integrin LFA-1. Together with RAPL/Rap1/Mst1 it is responsible for the interaction with the $α_L$-chain, while in complex with the RIAM/Rap1/Mst1/Kindlin-3/Talin ADAP/SKAP55 binds to the $β_2$-chain. This interaction leads to a change in the integrin structure, which leads to its activation. For the chemokine receptor induced activation of the integrin the modules are basically the same, nevertheless the direct interaction partners between the chemokine receptor and ADAP remain elusive to date. The scheme was adapted from references [38–40,42] and created with BioRender.com (2021).

The ADAP/SKAP55 module binds and interacts with the two Rap1 proteins Rap1 interacting adaptor molecule (RIAM) and the regulator for cell adhesion and polarization enriched in lymphoid tissues (RAPL)[42–44]. RIAM and RAPL associated with the cytoplasmic domains of the integrin via Talin. RIAM interacts with Rap1, Mst1 and Kindlin-3, which is important for the binding and activation of CD18 (β2-integrin), the second subunit of lymphocyte function-associated antigen-1 (LFA-1)[45]. Of note, these complexes that are involved in the activation of integrin LFA-1 in response to chemokine ligation require the ADAP/SKAP55 module[42].

1.1.3 *The role of ADAP in NK cells*

NK cells develop in the bone marrow from the same common lymphoid precursor as T cells[46]. Furthermore, both cell types share hallmark features like effector cytokine secretion and cytotoxicity. Due to the essential role of ADAP in T cells and the usage of comparable signaling pathways in T cells and NK cells, Fostel et al. proposed a comparable requirement for ADAP in the development and function of NK cells. In contrast to their expectation, ADAP-deficiency in NK cells did not affect NK cell development and function, as well as cytotoxicity, interferon-gamma (IFN-γ) production, anti-tumor response, and LFA-1-dependent conjugate formation with target cells[8].

Using different experimental settings, May et al. showed that NK cell activation relies on ADAP[47], which is in direct contrast to the previously published data by Fostel and colleagues. Based on *in vitro* activation using anti-Ly-49D they found that NK cells lacking ADAP showed impaired IFN-γ production and cytotoxicity as indicated by reduced, expression of the degranulation marker CD107a[47]. Furthermore, they demonstrated that the proliferation of NK cells was not affected by the ADAP-deficiency[47].

Shortly after the publications by Fostel et al. and May et al., Rajasekaran et al. discovered a striking uncoupling of NK cell cytotoxicity and cytokine secretion that was dependent on ADAP (**Figure 4**)[48–50]. The authors used an experimental model system based on *in vitro* stimulation of NK cells with CD137 and NKG2D in combination with a comprehensive analysis of the underlying molecular signaling machinery utilized following NK cell activation. They demonstrated that after *in vitro* NK cell stimulation with NKG2D or CD137 the adaptor protein ADAP is associated to the CBM complex, the so-called signalosome. This ADAP-CBM signalosome was crucial for the production of chemokines (CCL3, CCL4 and CCL5) and cytokines (IFN-γ and granulocyte-macrophage colony-stimulating factor; GM-CSF), but strikingly not for the cytotoxicity of murine as well as human NK cells[48].
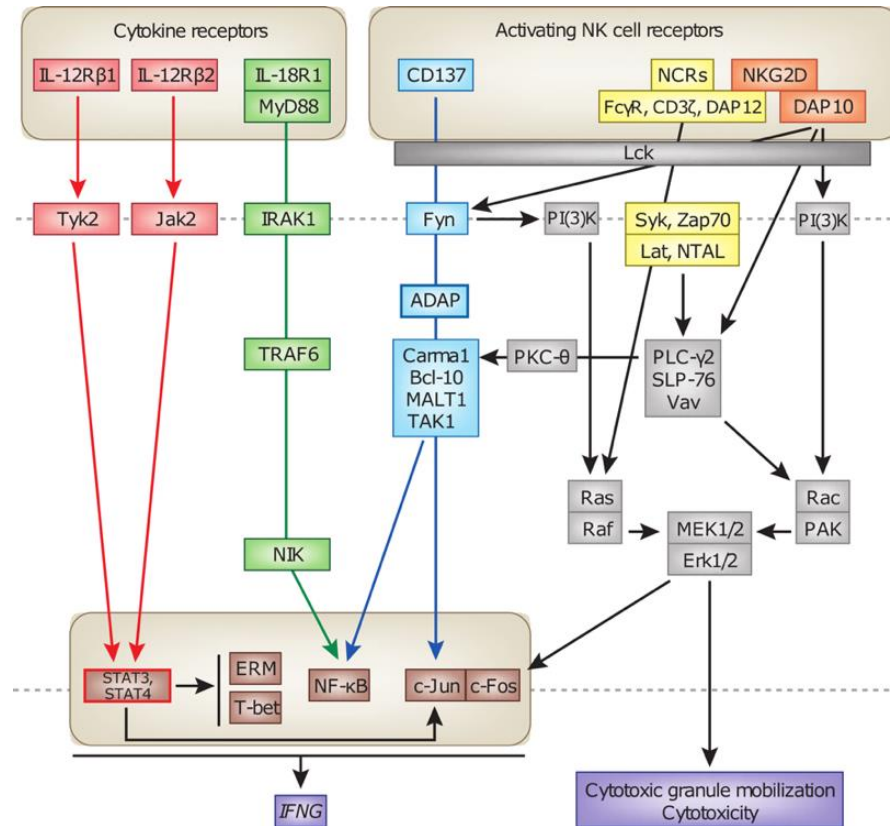
Figure 4 | Proposed model for the induction of cytotoxicity in NK cells being independent of ADAP. The signaling via the Lck → Fyn → ADAP → CARMA1/Bcl10/MALT1/TAK1 pathway that is required for the production of inflammatory cytokines like IFN-γ. Additionally, the pathway triggered by IL-12 and IL-18 can lead to the secretion of IFN-γ, independently of cytotoxicity. Selectively, also CD137 and NKG2D are able to induce IFN-γ transcription, leading to the IFN-γ production via the ADAP-CBM complex. Signaling through the Lck → Fyn → PI(3)K pathway mainly results in cell-mediated cytotoxicity. Lack of ADAP significantly reduces pro-inflammatory cytokine production without affecting cell-mediated cytotoxicity. Due to the complexity, only some of the key signaling elements are presented in this simplified model of NK cell-activation pathways. The scheme was adapted from references [49,51].

Taken together, current data regarding the role of ADAP in NK cells are conflicting. They range from a crucial role of ADAP in both, pro-inflammatory cytokine production and cytotoxicity[47], an uncoupling of cytokine production and cytotoxicity with only cytokine production being dependent on ADAP[48] and the statement, that ADAP is entirely dispensable for NK cell function[8]. While the above mentioned studies utilized different experimental settings and NK cell stimulating ligands, they all have in common that ADAP-dependency of principal NK cell functions was largely characterized either in primary or interleukin (IL)-2-activated NK cells following *in vitro* stimulation of selected NK cell activating receptors.

1.1.4 *The role of ADAP in myeloid cells*

To date, very limited data exist regarding the immunological functions of ADAP in myeloid cells. Using an ischemia-reperfusion induced acute kidney injury (AKI) Block et al. were the first who described a role of ADAP in neutrophil-mediated inflammation. They showed that the interaction between SLP-76 and ADAP is involved for the activation of the integrin LFA-1 on neutrophils and thus for their E-selectin-mediated slow rolling and extravasation into the inflamed tissue. As a consequence, ADAP-dependent impaired rolling and adhesion of neutrophils resulted in reduced susceptibility of ADAPko to AKI[52]. In the same line, conditional ADAP knockout mice lacking ADAP specifically in myeloid cells including neutrophils and monocytes (ADAP$^{fl/fl}$ × LysM-Cre^{het}) developed a significantly milder course of experimental autoimmune encephalitis (EAE), indicating that ADAP in myeloid cells partially contributes to the pathogenesis of EAE[53].

Next to neutrophils, there is some experimental evidence for the role of ADAP in macrophages. Alenghat et al showed, that the ADAP interaction partner SKAP-HOM is required for the integrin-stimulated cytoskeletal rearrangement in macrophages and that phosphorylation of ADAP is dependent on this molecule[54]. Moreover, Yang et al. recently showed, that ADAP plays a crucial role in toll-like receptors (TLR)4-mediated macrophage polarization via modulation of STAT3 activity[55]. More specifically, bone marrow-derived macrophages (BMDM) from ADAP-deficient mice displayed improved polarization towards an M1 macrophage phenotype and enhanced expression of pro-inflammatory cytokines while at the same time the level of anti-inflammatory cytokines released by ADAPko BMDM in response to lipopolysaccharide-induced TLR4 activation was decreased[55].

1.2 *Listeria monocytogenes* - an infection model

The bacterium *Listeria monocytogenes* (*Lm*) was first described in 1926 by Murray, Webb and Swan[56]. They isolated the gram-positive and facultative intracellular microorganism, initially named *Bacterium monocytogenes*, from the ascitic fluid in guinea pigs and smears from the omentum of rabbits that suffered from epidemic infection. The official name of the bacterium *Listeria monocytogenes* was finally adopted in 1940[56]. Listeriosis, i.e. the disease caused by the bacterium, was first reported in humans in 1929[57]. Listeriosis is an opportunistic and systemic infection with a potentially fatal outcome. During the 1980s, the number of reported cases increased and established Listeriosis as a well-recognized foodborne disease[58].

Lm is found widely spread in nature and prevalent in feces of mammals. Due to its capacity to persist and even grow within a wide range of pH conditions, high salt concentration as well as temperatures between 2 and 42 °C, the pathogen represents a serious problem for the food industry. Clinical manifestations caused by *Lm* include gastroenteritis, abortions in pregnant women, meningitis and encephalitis[59–61]. In healthy individuals, *Lm* generally causes asymptomatic infections or self-limited febrile diarrhea. However in the elderly, immune-compromised patients as well as neonates and pregnant women, *Lm* infection can cause severe complications[62].

Of note, the bacterium was already used in the 1960s to study cellular immune responses[63]. Since then *Lm* has been further developed to an established model to study various aspects of the immune system. The natural infection route is typically its oral uptake by contaminated food. Here, a high proportion of the pathogen is already eliminated in the stomach while the remaining bacteria can spread systemically (**Figure 5**)[64]. The murine listeria infection model is generally based on intravenous (i. v.) injection of the pathogen followed by its rapid dissemination to the spleen and the liver[64]. Noteworthy, mice are largely resistant to oral *Lm* infections, since the binding of the bacterial surface protein internalin A (InlA) to E-cadherin in the intestine is weak due to a single base pair exchange in murine compared to human E-cadherin[65].
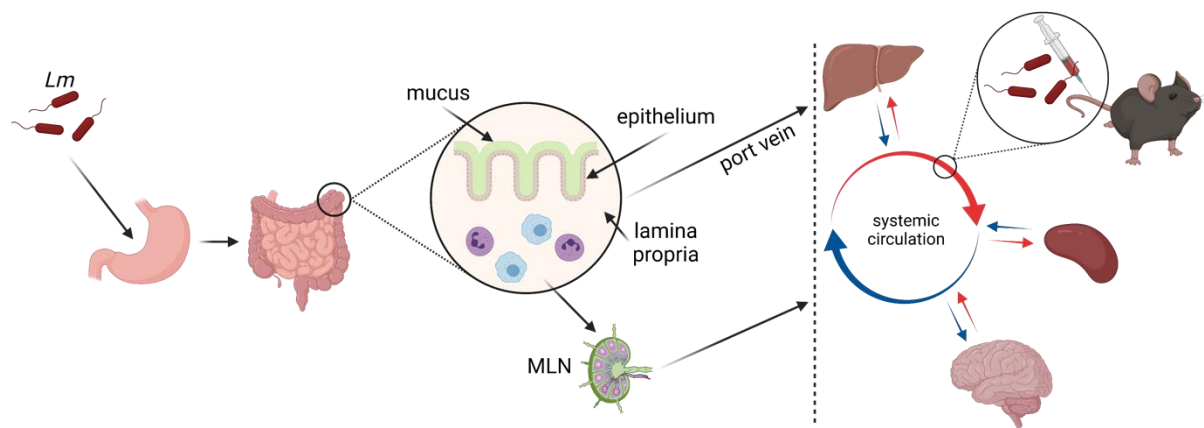
Figure 5 | Infection routes of *Listeria monocytogenes*. In most cases, the pathogen is taken up by contaminated food. Once the bacterium arrived in the small intestine, it can rapidly spread into mesenteric lymph nodes (MLN) and the blood stream. It mainly replicates in the spleen and liver. In severe cases, the bacteria can migrate to the brain via the bloodstream and is furthermore able to cross the placenta, infecting the fetus. Listeria that are injected i. v. seed to the spleen and the liver, directly through the blood circulation. The scheme was adapted from reference [64] and created with BioRender.com (2021).

Introduction

1.2.1 *Pathophysiology and cell biology of Listeria monocytogenes infection*

The life cycle of the bacterium reflects the remarkable adaptation of the microbe to survive within the host. *Lm* is able to induce its own phagocytosis even in non-phagocytic cells and is able to proliferate in various cell types[66]. Host cell invasion is mediated by the two virulence factors internalin A (InlA) and InlB[67], which interact with surface receptors on the host cells. The listeria uptake mechanism is also known as the 'zipper' mechanism, through which the pathogen can also spread to neighboring cells[68]. InlA binds to the transmembrane adhesion protein E-cadherin, which is a host cell adhesion molecule. InlB on the other side binds to the hepatocyte growth factor (HGF-Rc) Met. This interaction activates a signal cascade within cholesterol-rich microdomains, which leads to the internalization of the bacterium. Upon this receptor-mediated internalization of *Lm*, the pathogen enters the host cell (**Figure 6**) and is consequently enclosed by a phagocytic vacuole[69].
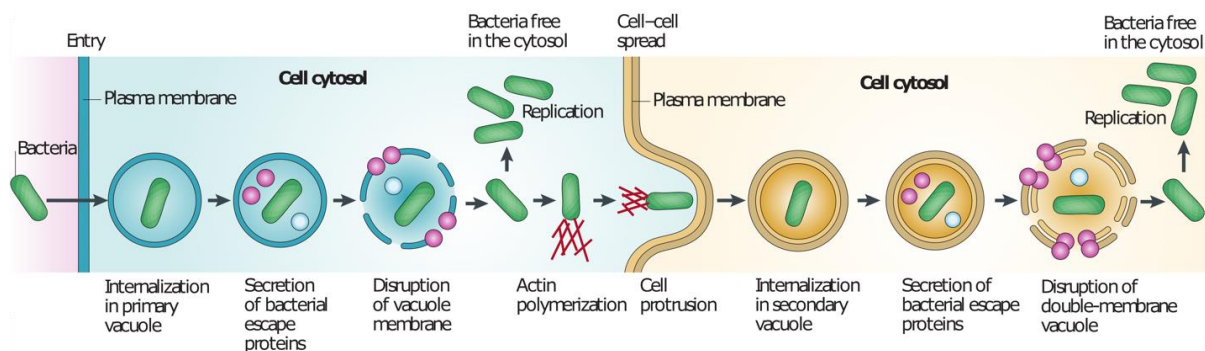
Figure 6 | Different steps of the infectious live cycle of the intracellular pathogen *Listeria monocytogenes*. After a receptor-mediated internalization, the bacterium gets engulfed in a primary vacuole. By the secretion of bacterial proteins like the phospholipases, PI-PLC and PC-PLC, besides the pore-forming toxin listeriolysin O, the bacterium can disrupt the vacuole membrane and escape the vacuole, entering the cytosol were it can replicate. Here, *Lm* can start to polymerize actin at the bacterial pole for cell-to-cell spread, which is induced by ActA. Invading a neighboring cell, the intracellular bacterium is enclosed in a secondary double-membrane vacuole. The scheme was adapted from reference [70].

The pathogen lyses the phagosomal membrane with the help of two different phospholipases (PI-PLC and PC-PLC) and the pore-forming toxin listeriolysin O (LLO) and thus reaches the cytosol of the host cell were it starts to replicate[71]. The bacterium forms a large number of actin filaments, induced by the actin assembly-inducing protein (ActA), which are arranged at the pole of the bacterial cell. This complex then moves to the host cell surface and forms a microvillus at the tip of *Lm* were it forms contact with a neighboring cell, which then phagocytizes the apical end of the microvillus. The bacterium lyses the membrane of the newly

formed phagocytotic vesicle and thus reaches the cytoplasm of the neighboring host cell. By this so-called cell-to-cell spread, *Lm* is able to move from one cell to another without entering the extracellular space[72].

1.2.2   *Immune responses to Listeria monocytogenes*

Since the 1960s, *Listeria monocytogenes* has been intensively used as a model pathogen to study different aspects of innate and adaptive immunity in mice. Together, these studies revealed a highly complex interplay of innate and adaptive immune cells in anti-listerial immunity with the cellular immune response being crucial for pathogen elimination[63].

1.2.2.1   *Adaptive immunity*

The adaptive immune system consists of T and B lymphocytes. Due to its intracellular live cycle and its capability of cell-to-cell spreading without leaving the intracellular space, *Lm* largely escapes antibody-mediated immunity. Thus, cellular immunity against *Lm* is primarily mediated by cytotoxic $CD8^+$ T cells[71].

Dendritic cells (DCs) and macrophages are professional antigen-presenting cells that are able to present proteolytically generated peptide antigens from lysed bacteria via major histocompatibility complex (MHC)-I and MHC-II molecules to naïve T cells[73]. With this, they play an important role in inducing the adaptive immune responses. DCs are constantly sampling antigens from the periphery. In case of their infection-induced activation, they migrate into the draining lymph nodes to prime T cell responses.

Degradation of antigens derived from cytosolic *Lm* mainly occurs in the cytosol followed by MHC class I presentation to $CD8^+$ T cells[74]. During the expansion phase, T cells acquire effector functions and the cytokine IL-12 plays a crucial role in the induction of $CD8^+$ T cells expansion during infection with the intracellular pathogen[75]. Activated $CD8^+$ T cells lyse infected antigen-presenting cells (APCs) via perforin and granzyme secretion or by inducing programmed cell death through Fas/FasL interaction in addition to the secretion of tumor necrosis factor (TNF)-α and IFN-γ[76,77]. Generally, *Lm* infection also induces a strong Th_1 response and Th_1 cell-produced IFN-γ in turn empowers macrophages to kill phagocytosed bacteria[73]. Though $CD4^+$ T helper cells play a minor role during the primary immune response against *Lm*, their function is important during the memory response. In the absence of $CD4^+$ T cells, protective immunity mediated by $CD8^+$ memory T cells is severely impaired[78].

1.2.2.2   Innate immunity

Although T cell-mediated immunity is essential for clearing *Lm*, an effective innate immune response must precede to activate lymphocytes[79]. Of note, the innate immune response is essential for the early control of a *Lm* infection and with that for controlling the bacterial growth[80]. Thus, the innate immune system serves as the first defense mechanism against Listeria infection. In addition to the virulence factors already mentioned above, such as LLO and ActA, *Lm* expresses numerous pathogen-associated molecular patterns (PAMPs) on its surface[81]. Host cells recognize PAMPs on the surface of the pathogen by so-called pattern recognition receptors (PRRs) such as the membrane-bound TLR. Of note, TLR2 signaling plays an important role for an effective early control of Listeria infection and mice lacking TLR2 are more susceptible to systemic *Lm* infection[82]. TLR2 is able to oligomerize with other receptors such as TLR1 or TLR6 and to recognize a variety of PAMPs. Following ligand binding, the conformation of TLR changes enabling the intracellular domain of the TLR to interact with various adaptor molecules like myeloid differentiation primary response gene 88 (MyD88), the mitogen-activated protein kinase (MAPK) or interferon regulating factor 3 (IRF3). Ultimately, this leads to the activation of intracellular signal transduction pathways such as the NF-κB path[81] resulting in the induction of genes involved in host defense, cytokine and chemokine production[83].

Cellular components of the innate immunity include among others DCs, macrophages and natural killer cells as well as eosinophils, basophils, mast cells and neutrophils[84]. The latter along with infiltrating monocytes are important in the initial control of bacterial growth due to their antimicrobial activities[85–87]. Neutrophils are able to kill bacteria by phagocytosis, the generation of reactive oxygen species (ROS) and the formation of neutrophil extracellular traps (NETs)[86,87]. Furthermore, neutrophils release different chemokines thus further promoting antibacterial immunity and recruitment of innate immune cells to the infection site[87–89].

Macrophages are primary targets for Listeria infection, i.e. the pathogen replicates within these cells once it has entered the blood stream[90]. Besides this, tissue resident macrophages, especially Kupffer cells in the liver that are as well efficiently infected by *Lm*, are very important since they are able to clear a large proportion of the bacteria already during the early phase of infection[90]. Macrophages produce among others IL-12 and tumor necrosis factor (TNF)-α in response to a Listeria infection, inducing the release of the pro-inflammatory

cytokine IFN-γ by natural killer cells. The release of cytokines in turn recruits additional immune cells and a rapid local anti-microbial response is induced[90,91].

1.3   NK cells - Natural Killer cells

The term "NK" cell was initially introduced in 1975 in the context of their ability to kill target cells without former immunization to these targets which is in direct contrast to cytolytic T cells[92,93]. At this time, NK cells were characterized as *»[...] small lymphocytes of undefined nature exerting spontaneous selective cytotoxic activity against Moloney leukemia cells [...]«*, a capability considered as "natural cytotoxicity"[93]. Later on, NK cells were characterized as large granular cells, defined by the absence of a T-cell receptor (CD3), representing a further subpopulation of lymphocytes in addition to T cells and B cells[93]. Because of their ability to eliminate target cells without prior sensitization, they were originally assigned to the innate immune system. Of note, recent work has shown that NK cells display some characteristics of specific immunity and thus may be also considered as a bridge between the innate and adaptive immune system[94].

However, NK cells are cytotoxic effectors that play a significant role in protection against different pathogens as well as transformed host cells[95]. NK cells occur widespread throughout the body[96], being present in the circulation and in many tissues, including the bone marrow (BM), the spleen, the lymph nodes, the liver as well as the lung, the intestine and the placenta[97]. In inbred laboratory mice, the frequency of NK cells among lymphocytes ranges from 2-5 % in the spleens and BM[98].

NK cells belong to the family of innate lymphoid cell (ILC), known to produce type I cytokines upon stimulation, primarily IFN-γ and TNF-α[99,100]. Their development is dependent on the cytokines IL-7 and IL-15. ILCs are generally divided into three groups: the ILC type 1, ILC2 and ILC3. NK cells belong to the group of ILC1 and their effector functions largely mirrors those of CD8$^+$ cytotoxic T cells[95,99].

NK cells are usually identified by the expression of specific surface markers that may vary between different mouse strains. NK cells derived from the C57BL/6 background express surface markers like NK1.1 (NKR-P1C), NKp46 (NCR1/ CD335) as well as CD49b (DX5/ Integrin VLA-2α)[101]. The absence of the marker CD3 is important to distinguish them from T cells and natural killer T (NKT) cells that as well express NK1.1 and NKp46[102].

Following activation, NK cells secrete IFN-γ which aids the activation and subsequent differentiation of naïve T cells[103]. Thus, by secretion of cytokines and chemokines, NK cells represent an important link between the innate and acquired immune system[97]. As mentioned above and in contrast to NKT, γδ T cells and conventional T cells, NK cells do not express a T cell receptor or any other antigen-specific receptor[97,104]. MHC class I molecules represent ligands for inhibitory NK cell receptors like Ly49C, Ly49I or NKG2A, forming the basis for the so-called "missing self" mode of action. Cells from healthy hosts generally express MHCI molecules, which bind to inhibitory ligands, thus preventing the activation of NK cells via their activating receptors, such as Ly49H, NKG2D and NCR1. Infected cells however down-regulate the expression of MHCI molecules, thus allowing their activation[97]. Thus, upon infection, NK cells are recruited very early to the site of pathogen entry and replication were they become activated to kill infected target cells and as such play fundamental roles in immediate host response[105].

1.3.1 *Functional maturation of murine NK cells*

Compared to the well-characterized mechanisms of T and B cell development, the knowledge regarding the development of NK cell is rather limited. Nevertheless, over the years a consensus model had been developed[106]. According to this, NK cell development can be subdivided into three phases: the early phase (NK cell progenitors; NKPs), an intermediate phase of differentiation (immature NK cells; iNKs), followed by a late maturation phase (mature NKs; mNKs)[95,98].

Like T cells, NK cells derive from a common lymphoid progenitor (CLP) in the bone marrow[107]. Even though, the bone marrow is the primary location of NK cell development[108], they may also develop in the liver as well as the thymus[109]. Of note, much of our current understanding of murine NK cell development is built on studies on bone marrow-derived NK cells, which represent the majority of NK cells[110]. During their maturation and development, NK cells express different surface receptors in a certain order, which can be used to identify the individual stages of NK cell development[106].

NK cell progenitors (NKP) are identified by lacking different T cell lineage markers, such as CD3, CD4, CD8, CD19 and B220, whereas they are NKG2D- and CD122-positive, the latter known as a subunit of interleukin (IL)-2/IL-15 receptor. Furthermore, these NKPs lack NK1.1 and CD49b[111]. IL-15 drives the differentiation from NKPs to iNKs[112] and additionally the

acquisition of NK1.1 and NKp46 occurs at the iNKs stage[113,114]. Subsequently, a lack of different cytolytic properties as well as regulatory functions leads to the next stage. Here, iNKs further characterized by the differential expression of CD27 and the absence of CD11b expression, become mNK cells. Mature NK cells are defined by an increase in CD49b expression[114]. The development from iNKs to mNKs is a process called NK cell differentiation and further correlates with an increasing CD11b and a decreasing of CD27 expression[114,115] according to different stages (**Figure 7**). Thus, murine mNKs undergo a functional classification based on CD27 and CD11b expression, which help to identify the different NK cell subsets[98,110]. The level of CD11b expression divides NK cells into immature and mature NK cell subsets[114]. The expression of the surface marker CD27 distinguishes the mature NK cells into CD27+ (M1) and CD27- (M2) subsets[115,116]. NK cells expressing both, CD27 and CD11b, are also called double-positive (DP) NK cells[115].
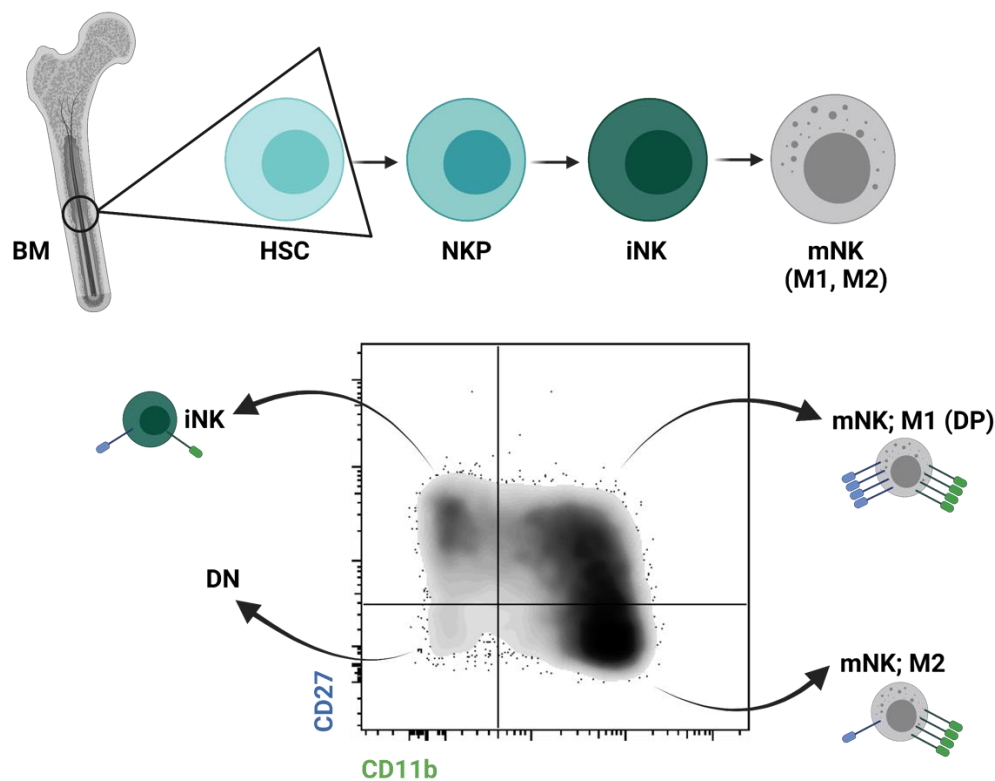
Figure 7 | NK cell development and subsets. Linear developmental pathway (top panel) from haematopoetic stem cells (HSCs) in the bone marrow (BM) to fully functional NK cells via NKP (NK cell progenitors), immature NK (iNK) and mature NK cells (mNK; M1 and M2). Schematic representation of a FACS plot (bottom panel) from spleen-derived NK cells of ADAP wild type mice 3 days p. i. (own data). Late mNK cells mature from an immature subsets with CD27+ CD11b- expression via the expression of the cell surface markers CD27+ and CD11b+ (M1; DP) to a CD27- and CD11b+ (M2) subset. Expression of CD27 is colored in blue, whereas CD11b expression is colored in green. The scheme was adapted from references [95,115–117] and created with BioRender.com (2021).

All of these three subsets differ in their ability to proliferate as well as in their cytotoxic capacity. Of note, during the development and maturation process, the potential of NK cell for homeostatic expansion is reduces whereas the ability to kill target cells as well as the susceptibility to apoptosis is increasing over time. Furthermore they produce fewer cytokines, but develop a higher capability to kill, and with this become more cytotoxic against different target cells as they mature[114–116]. Generally, it has been shown that with proceeding maturation NK cells lose the potential for effective proliferation in response to IL-2, reviewed in [117]. Aside from the two markers CD27 and CD11b, mNKs are furthermore divided into several phenotypic subsets depending on different other markers. Of note, the correlation between these markers is not known in detail yet, the phenotypic subsets remains unclear[110]. NK cells that went through all maturation stages are terminally functional. However, there is still evidence that their functionality with regard to cytotoxicity and cytokine production may not be developed equally[116,118].

1.3.2 *NK cell cytotoxicity*

Once activated via their activation receptors, NK cells achieve cytotoxicity mediated through the release of lytic granules containing granzyme B (GrzB) and perforin[119–121]. The whole procedure is known as degranulation and is used as a correlate of NK cell cytotoxic activity[122]. Stimulation of NK cell activating receptors, such as NCRs or NKG2D, leads to a cytoskeletal re-arrangement, with lytic granules trafficking to the contact zone. The formation of the immunological synapse is followed by secretion of cytolytic granules[123,124].

The release of perforin towards the target cell induces pore formation, enabling various granzymes to enter the target cell. Granzymes belong to the group of serine proteases, leading to an activation of caspase molecules inducing the apoptotic cell death of the target cell[121,122,125]. The process of NK cell degranulation results in the surface expression of the lysosomal-associated membrane protein-1 (LAMP-1 or CD107a) on the NK cell and as such LAMP-1/CD107a serve as markers for NK cell cytotoxic function[126,127].

Next to the killing via lytic granule release, NK cells are able to eliminate different target cells upon contact also by the perforin-independent death-receptor pathway. This involves the TNF or TNF-related apoptosis inducing ligand (TRAIL) and the receptor Fas (FasR)[95,128]. The ligation of these receptors mediates the activation of pro-caspases, resulting in proteolysis of target cells[129].

1.3.3   *The role of NK cells in immunity to Listeria monocytogenes*

The general role of NK cells during *Lm* infection is controversially discussed and it is yet not clear, whether NK cells exhibit a beneficial or detrimental role in immunity to *Lm*. On the one hand, Teixeira and Kaufmann showed, that NK cell-deficiency results in a reduced bacterial load[130], which implies a negative role for NK cells in listeriosis. In the same line, Viegas et al. documented the survival of an otherwise lethal *Lm* infection in mice lacking NK cells. As an underlying mechanism for this protection they identified a high amount of NK cell-released IFN-γ leading to a chemokine receptor 2 (CXCR2) downregulation on neutrophils, thus impairing the recruitment of these cells to the site of infection[131]. On the other hand, NK cells are also considered to exhibit protective functions during Listeria infection. NK cells are activated by DCs and IL-18 that is induced during *Lm* infection[132]. A proof for the activation of NK cells by DCs has been provided in studies where CD11c⁺ cells were depleted, resulting in a severe impairment of NK cell activation during *Lm* infection[133].

The *Lm* virulence factor p60 indirectly supports the activation of NK cells and thus IFN-γ production[134] as it stimulates the cytokine secretion by DCs[135]. However, *in vivo* infection of mice with *Lm* generally induces efficient NK cell activation[134,136], a process that involves a multifaceted cellular network including macrophages, neutrophils, and dendritic cells as well as different mediators derived from these cells[105,137]. In respect to the IFN-γ production by NK cells, type I interferons might be able to suppress the activity of macrophages by IFN-γ[138]. This effect could explain why interferon-α/β receptor (IFNAR)-deficient mice are more resistant to infection with *Lm*[138,139]. Additionally, NK cells have been shown to serve immune-suppressive roles during neuroinflammation, which leads to the speculation that they also might serve regulatory roles during systemic *Lm* infection[140].

Indeed, NK cells were shown to exert important regulatory functions during infection with *Lm* or other pathogens that cause systemic disease. Using IL-10 reporter mice, Perona-Wright et al. found that approximately 80 % of the NK cells circulating in peripheral blood expressed the immunosuppressive cytokine IL-10 on day 4 post infection. They argued that IL-10 production was triggered by high serum concentration of IL-12 and suggested that this might represent a negative feed-back loop to prevent extended inflammation and tissue damage during systemic infection[141]. Clark et al. confirmed these findings showing that NK cells switch from IFN-γ production to the secretion of IL-10[136]. Depletion of NK cells in IL-10-deficient mice had no effect on the bacterial load, suggesting that NK-mediated susceptibility was due

to secretion of this immune suppressive cytokine rather than a lack of immune stimulatory IFN-γ. Mice lacking NK cells exhibit significantly lower serum levels of IFN-γ 24 hours post infection[136]. However, there is a wide variety of other cell types that can be induced to secrete IFN-γ during the first few days of infection. NK cell-deficient mice showed improved pathogen clearance in the affected organs. This again suggests that activated NK cells do not have a major protective role during Listeria infection[142].

As shortly mentioned before, type I interferons interestingly appear to interfere with the generation of an efficient host immune response controlling Listeria infection. This was particularly evident in mice that exhibited a deficit in the type I interferon signaling pathway. The deficient animals showed both improved survival and reduced bacterial loads compared to the wild type controls. Since NK cells are activated by type I interferons, it was suggested that NK cells may worsen the outcome of the infection[143,144]. In summary, the overall function of NK cells in murine listeriosis remains unclear and deserves further investigation.

1.4   Neutrophils

Neutrophils are also known as polymorphonuclear leukocytes (PMNs). They have been described as one of the main players during inflammation. Of note, neutrophils are recruited early on to the site of infection and exhibit different effector functions using multiple effector mechanisms. The number of neutrophils in infected tissues drastically increases and after fulfilling their antimicrobial functions, dying cells are removed by macrophages and DCs[145].

Neutrophils constitute up to 10-25 % of the circulating leukocyte population in mice[145]. Neutrophils share common precursors with other myeloid cells of the innate immune system, such as monocytes[146]. Upon activation, neutrophils release various enzymes and toxic proteins from their granules in order to kill bacteria[147]. In the mouse model, neutrophils can be best identified by their surface expression of the protein lymphocyte antigen 6 complex locus G6D (Ly6G), which is exclusively and abundantly expressed by fully matured neutrophils[148].

Neutrophils are very short-lived cells. After maturation, their extravasation from the bone marrow (BM) into the blood occurs. Via the blood circulation they enter the tissues were they undergo phenotypic as well as morphological changes[149]. Release of neutrophils from the BM into the circulation is tightly regulated. The chemokine receptor 4 (CXCR4), which is expressed on the surface of neutrophils, plays a crucial role for maintaining neutrophils in the BM. Osteoblasts as well as other BM cells produce the C-X-C-motif ligand 12 (CXCL12 or

stromal cell-derived factor 1; SDF-1), which binds to CXCR4 and retains neutrophils in the BM[150]. Retention and the release of neutrophils is coordinated by the balanced expression of CXCR4 (retention) and CXCR2 (release)[151]. The granulocyte-colony stimulating factor (G-CSF) induces down-regulation of CXCL12 on osteoblasts, and induces the production of the chemoattractants CXCL1 (keratinocytes-derived chemokine; KC) and CXCL2 (macrophage inflammatory protein-2; MIP-2). G-CSF furthermore reduces the expression of CXCR4 on neutrophils themselves[152] and stimulates cytokine expression by neutrophils[151].

Once in the circulation, neutrophil extravasation into tissues involves the following steps: tethering, rolling, adhesion, crawling and transmigration (**Figure 8**). The recruitment of neutrophils to the side of infection is initiated by different infection-triggered alterations at the endothelial surface.
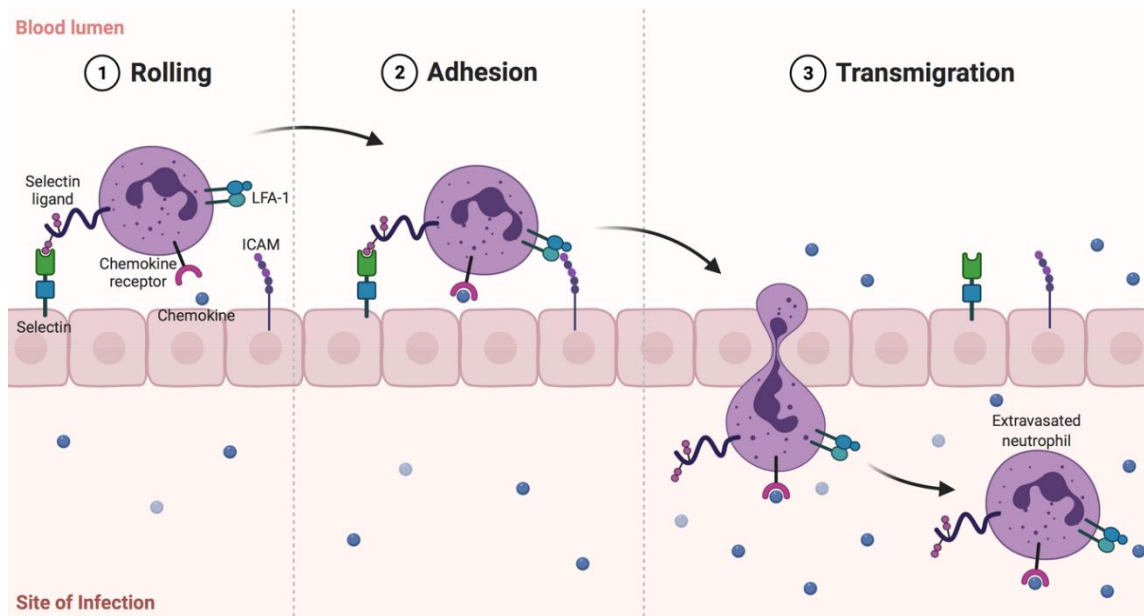
Figure 8 | Classical neutrophil recruitment cascade. Serial steps of the recruitment of neutrophils from the vasculature into the tissue are visualized here. These cascade steps are: tethering, rolling, adhesion, crawling and, finally, transmigration. The rolling is mainly selectin-dependent, however, adhesion, crawling and final transmigration depends on integrin interactions. Chemokines on the luminal part of the endothelium are important for the activation of neutrophils rolling, at the same time inducing conformational changes of integrins on neutrophil surface. This allows for later events. Following along a chemokine gradient, crawling neutrophils are guided and able to transmigration. Regarding the transmigration of neutrophils there are two possible methods, of which the paracellular way is shown here. Not shown is the transcellular transmigration via individual cells and the required dome formation. The scheme was adapted from reference [145] and adapted from "Leukocyte Migration at Sites of Infection", by BioRender.com (2021). Retrieved from https://app.biorender.com/biorender-templatesand created with BioRender.com.

However, efficient neutrophil chemotaxis is dependent on chemoattractive molecules that induce signaling pathways and lead to the upregulation of surface adhesion molecules. More specifically, the migration from the bloodstream into the tissue is mediated by the adhesion molecules P-selectin and E-selectin, which have overlapping functions. Both selectins bind glycoproteins on the surface of neutrophils, including the P-selectin glycoprotein ligand 1 (PSGL1), facilitating the tethering (capturing) of floating neutrophils and allow them to roll along the endothelium[153]. The subsequent tighter adhesion of the neutrophil is mediated by the interaction of the neutrophil expressed integrin LFA-1 with endothelial intercellular adhesion molecules (ICAM)[154]. Of note, LFA-1 is the primary adhesion molecule on neutrophils, mediating the transition from rolling to adhesion on the endothelial cell surface[155].

Upon integrin activation, the cytoskeletal protein Talin-1 binds to the integrin β-subunit. This binding stimulates the LFA-1 extension, and furthermore promotes slower rolling of neutrophils along the endothelium. However, dual activation of Talin-1 and Kindlin-3 induces LFA-1, which also promotes neutrophil arrest[156]. Nevertheless, in the context of inflammation, PSGL1 and CXCR2 regulate LFA-1 activation[157], leading to signaling pathways inside the neutrophil, known as outside-in signaling. Together, these events stabilize neutrophil adhesion to the endothelium and contribute to neutrophil recruitment by initiating cell motility[153,158]. After adhesion, neutrophils transmigrate through the endothelial cell layer to leave the blood stream and enter the underlying tissue. Neutrophils are then attracted to the injured site by different chemokines.

Upon engagement of PSGL-1 with E-selectin, Src-family kinases are recruited and phosphorylate adapter proteins like γ chain of immunoglobulin Fc receptors (FcRγ) or NDAX activation protein of 12 kDa (DAP12)[159], subsequently leading to the phosphorylation of spleen tyrosine kinase (Syk)[160], which then recruits the complex of SLP-76 together with ADAP[52]. In addition, Bruton tyrosine kinase (Btk) is activated, and phosphorylates PI3K (Phosphoinositide 3-kinase), phospholipase C γ (PLCγ) and p38-mitogen-activated protein kinase (p38-MAPK), resulting in integrin activation and cytoskeletal rearrangements within the neutrophil[153,161].

After migrating through the endothelium, neutrophils cross the basal membrane, by breaking down the membrane collagens via proteases such as elastases[162], however it is not clear whether these proteases really contribute to the neutrophil migration[163].

1.4.1 *Neutrophil effector functions during Listeria monocytogenes infection*

Neutrophils eliminate pathogens utilizing three major mechanisms as illustrated in **Figure 9**: phagocytosis of invading bacteria, degranulation as well as the release of so-called neutrophil extracellular traps (NETs)[145].
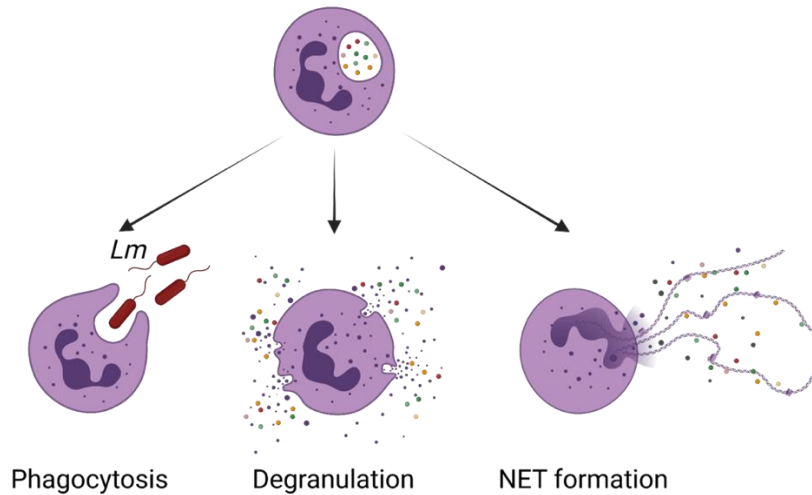
Figure 9 | **Antimicrobial killing mechanisms of neutrophils.** There are three known ways in which neutrophils can eliminate pathogens: phagocytosis of pathogens such as *Lm*, degranulation of antibacterial substances and formation of NETs. The scheme was adapted from reference [145] and created with BioRender.com (2021).

A recent study based on antibody-mediated depletion of Ly6G-positive neutrophils underlined the importance of neutrophils in controlling bacterial growth during murine listeriosis[164]. Neutrophils produce substantial amounts of TNF-α that play a key role in immunity to infections. Consequently, neutrophil depletion in *Lm* infected mice leads to decreased TNF-α levels and increased bacterial burden[164]. In the same line, the deletion of the TNF-α encoding gene or the absence of the TNFR1 resulted in an increased susceptibility to *Lm* infection in mice[165]. Another cytokine that is produced by phagocytes including neutrophils early on during bacterial infection is IL-1. Immediately after *Lm* infection, IL-1α as well as IL-1β are produced in liver and spleen and exogenous IL-1α is known to decrease the bacterial burden by promoting neutrophil recruitment to the infection sites[166,167]. In case the receptor for IL-1α and IL-1β is blocked, the susceptibility to *Lm* infection is increased[168].

Within the tissues, neutrophils follow various chemoattractive substances guiding them to the site of inflammation. Neutrophil recruiting chemokines like CXCL1 and CXCL2[169] are produced in the liver after *Lm* infection. It has been shown that CXCL2 depletion reduces neutrophil recruitment into the *Lm* infected liver, and blockage of CXCR2 entirely stops their

recruitment[170]. Additionally, cytokines such as IL-6 and IL-8 take part in recruiting neutrophils to the sites of inflammation, where they are able to secrete different pro-inflammatory mediators and chemokines[71] and as such contribute to the development of immuno-pathology[171]. Activated neutrophils themselves secrete chemokines including CXCL1, CCL3, CXCL8 and MCP-1 and thus further boost the recruitment of additional neutrophils, monocytes and NK cells to the infection site[89].

1.4.1.1 Phagocytosis

Phagocytosis is the ingestion of a pathogen followed by its intracellular digestion, a function mostly related to neutrophils and macrophages. Phagocytosis and consequently the intracellular killing of pathogens is, among others, induced by pro-inflammatory cytokines like IFN-γ[172] and TNF-α[173]. Pathogens are often coated with a number of opsonins which mark them for efficient recognition by phagocytes[174]. Among them, IgG or iC3b bind to the surface of the pathogen and mediate binding to the FcγReceptors FcγRIIA (CD32) and FcγRIIIB (CD16), as well as the complement receptor 1 (CR1 or CD35) and CR3 (CD11b/CD18 integrin) on phagocytes[174,175]. The pathogen is taken up into the cell, where it is located within a phagosome. Once being encapsulated, neutrophils kill pathogens using NADPH oxygenase-dependent mechanisms as well as antibacterial proteins (see **section 1.4.1.2**) released from granules. Of note, the role of SKAP2 in this process has been described recently. In detail the authors showed, that murine neutrophils showed an impaired phagocytosis of *E. coli* particles in SKAP2-deficient neutrophils[176].

1.4.1.2 Degranulation

Neutrophils, as well as monocytes, secrete proteases and other substances at the site of inflammation. Next to their microbicidal activities, these components can induce considerable tissue damage. The granules containing pre-stored antimicrobial proteins that are able to destroy pathogens are a hallmark of neutrophils. During their maturation, neutrophils form three types of granules that are packed inter alia with pro-inflammatory proteins[177]. These granules are the azurophilic granules containing myeloperoxidase (MPO), defensins and neutrophil elastase (NE), the secondary specific granules containing lactoferrin, lysozyme and collagenases next to the tertiary gelatinase granules containing the matrix metalloproteinase 9 (MMP9 or gelatinase B)[145]. Together, these substances mediate antimicrobial defense by degrading engulfed bacteria[147].

Reactive oxygen species (ROS) increase the activity of the membrane-bound NADPH oxidase, the key enzyme in the formation of oxygen radicals in granulocytes. This enzyme catalyzes the reduction of molecular oxygen (O_2) to the hyperoxide anion (O_2^-). Subsequently, the toxic radical hydroxyl (OH•) or the peroxide anion (OH^-) are formed. Both are highly reactive radicals with antibacterial properties, able to oxidize enzymes or membrane components, thus functionally inactivating them[175]. It has been reviewed, that the phosphorylation of the tyrosine kinase Syk introduces the guanine factor Vav1/3 phosphorylation in neutrophils involving ADAP/SLP-76 and the PLCγ2 complex, which furthermore promotes the oxidative burst[178]. In addition to ROS, neutrophils generate reactive nitrogen species through the expression of an inducible nitrogen oxide synthase (iNOS or NOS2), an enzyme that converts O_2 and L-arginine into nitric oxide (NO^-) and that is encoded by the *Nos2* gene. Of note, mice lacking *Nos2* showed increased susceptibility to bacterial infection[179], indicating that iNOS-mediated microbicidal activity is crucial for anti-bacterial defense.

1.4.1.3   NETs - Neutrophil extracellular traps

Activated neutrophils are able to eliminate pathogens by the release of neutrophil extracellular traps (NETs). NETs are fiber structures consisting of decondensed chromatin and antimicrobial factors in addition to histones, proteins and enzymes, e.g. myeloperoxidase and NE, with the latter components being attached during the ETs release from neutrophils[180]. Noteworthy, NETs entrap microbes, thereby preventing their spread and at the same time facilitating phagocytosis of caught bacteria, fungi and parasite. Those fiber structures are furthermore thought to directly kill bacteria by antimicrobial histones and proteases[181]. On the one hand, the neutrophil-specific serine protease NE degrades bacterial virulence factors[182]. On the other hand, MPO which is one of the most abundant protein in neutrophils catalyzes the oxidation of halide ions in the presence of hydrogen peroxide[183]. Consequently, NE- and MPO-knockout mice are more susceptible to infections with bacteria[184]. Interestingly, there is a marked variability in the general capacity of NET formation by neutrophils across species and different mouse strains[185].

As described earlier in **section 1.4.1.2**, MPO and NE are stored in primary azurophilic granules of neutrophils (**Figure 10**)[145,186]. After neutrophil activation, ROS is induced via MEK/ERK signaling which triggers the MPO pathway. Stimulated MPO activates and triggers NE release from azurophilic granules, which in turn is translocated to the nucleus. Of note, NE is required

for the degradation of the actin cytoskeleton in order to block phagocytosis[187]. Located in the nucleus, NE proteolytically processes histones after synergizing with MPO, a complex known as azurosome, leading to the decondensation of chromatin[188]. This decondensation, which is essential for NET formation, is associated with citrullination of histone H3 by the peptidyl arginine deiminase 4 (PAD4)[188,189]. Together, the formation of NETs is tightly regulated in order to prevent pathology.
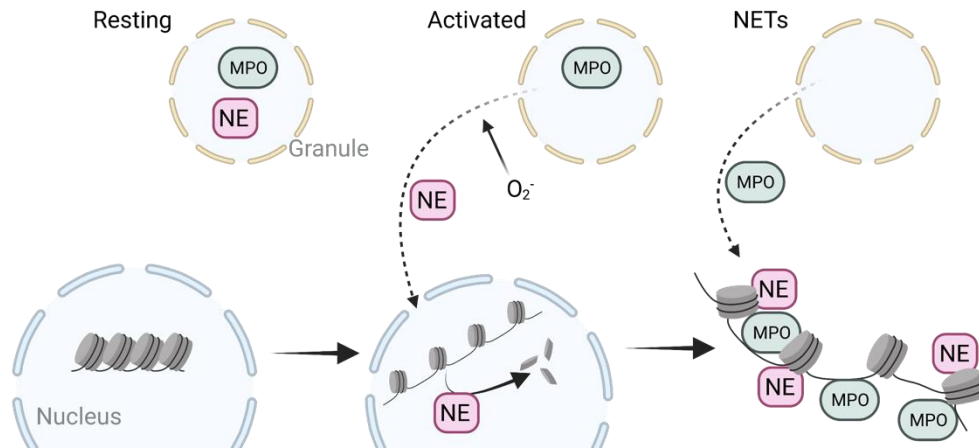
Figure 10 | NET formation - a model. Naïve neutrophils store NE and MPO in azurophilic granules (resting). Following the activation of neutrophils and ROS production (O_2^-), NE translocates from the azurophilic granules to the nucleus. Here, NE cleaves histones and promotes the decondensation of chromatin (activated). MPO binds to chromatin in the late stages of the process whereas binding of MPO promotes further decondensation. NE and MPO cooperatively enhance chromatin decondensation, leading to cell rupture and NET release (NETs). Of note, details of the molecular mechanism are still subjects for further investigations. The scheme was adapted from [188] and created with BioRender.com (2021).

1.5   Monocytes - Introduction and the role post *Listeria monocytogenes* infection

Monocytes are a type of circulating blood leukocytes, classified as mononuclear phagocytes. They are originated in the bone marrow from the same common myeloid progenitor as neutrophils, and can further differentiate into macrophages and DCs[190,191].

As neutrophils, monocytes are rapidly recruited to the sites of infection, were they are activated and exert central antimicrobial functions[192]. As such, they represent a critical component of the innate immune response during inflammation. Consequently, targeted depletion of these cells enhances susceptibility to *Lm* infection in mice[59], indicating their importance and crucial role for protection against listeriosis[193]. In mice, the expression of the chemokine receptor CCR2 is typically used to distinguish between monocytes subsets[194]. Of note, mice deficient for CCR2 or its ligand are highly susceptible to *Lm*, succumbing early on during infection[195]. Peripheral monocytes can be roughly subdivided into two main subsets, based on their lymphocyte

antigen 6C (Ly6C) expression. These include the CX3CR1[low]CCR2^{+}Ly6C^{high} inflammatory and CX3CR1[high]CCR2^{-}Ly6C^{low} patrolling monocytes[194]. The CX3CR1[low]CCR2^{+}Ly6C^{high} inflammatory monocytes are characterized by trafficking to the sites of inflammation and infection[190]. Lack of Ly6C^{high} monocytes is associated with a rapid death of *Lm* infected mice, indicating their central role during listeriosis[196]. The CX3CR1[high]CCR2^{-}Ly6C^{low} patrolling monocytes are thought to differentiate into monocyte-derived tissue-resident macrophages once they have entered the tissue[197]. The role of these Ly6C^{low} monocytes during infection is less well defined. However, they are considered to contribute to the very early immune response to *Lm* infection[190]. Interestingly, a monocyte-derived dendritic cell population that is recruited to the spleen and produces considerable amounts of TNF-α and iNOS has been described as so-called TNF- and iNOS-producing dendritic cells (TipDCs). The recruitment of these TipDCs is dependent on CCR2/CCL2 signaling and these cells are vital for the early control of bacterial pathogen[196].

During inflammation, monocytes circulate through the bloodstream and migrate into infected tissues. The recruitment of inflammatory monocyte to the infection site is mediated by stimulation of the chemokine receptor CCR2 via its ligands CCL2 (MCP-1) and CCL7 (monocyte chemo attractant protein-3; MCP-3)[198], suggesting that monocytes follow a CCL2 gradient from the bloodstream to the infected foci. CCL7 might also play a role in recruiting Ly6C^{high} monocytes[198]. Besides this, it had been shown that during *Lm* infection Ly6C^{high} monocytes are localized in the liver, and moreover these monocytes express TNF and iNOS[199], which in turn stimulates NK cells to produce considerable amounts of IFN-γ. Moreover they contribute to phagocytosis and as such exert important effector functions for an effective immune response during *Lm* infection[91,200].

1.6 Basis for this thesis

Since murine listeriosis represents an excellent model for examining various aspects of innate and adaptive immune responses *in vivo*, it has been used before in the laboratory of Prof. Dunja Bruder to study the role of ADAP in immunity against *Listeria monocytogenes*. In frame of his doctoral thesis, Dr. Gerald P. Parzmair successfully used the *Lm* infection model to clarify in very much detail the role of ADAP in different pathogen-specific T cell subsets during infection[201,202]. Moreover, so far unpublished data from his thesis impressively demonstrated a remarkably enhanced and at this time unknown susceptibility of ADAPko mice to listeriosis.

Introduction

Since these data build the basis for this present thesis, part of them is depicted here in consultation with Dr. Gerald P. Parzmair. Note, that **Figure 11** is modified from the doctoral thesis "Parzmair, Gerald P. The Role of the Adaptor Protein ADAP in different T cell subsets and Pathogen-specific Immune Responses against *Listeria monocytogenes*. PhD thesis. Faculty of Natural Sciences, Otto-von-Guericke University Magdeburg, May 2016"[201].
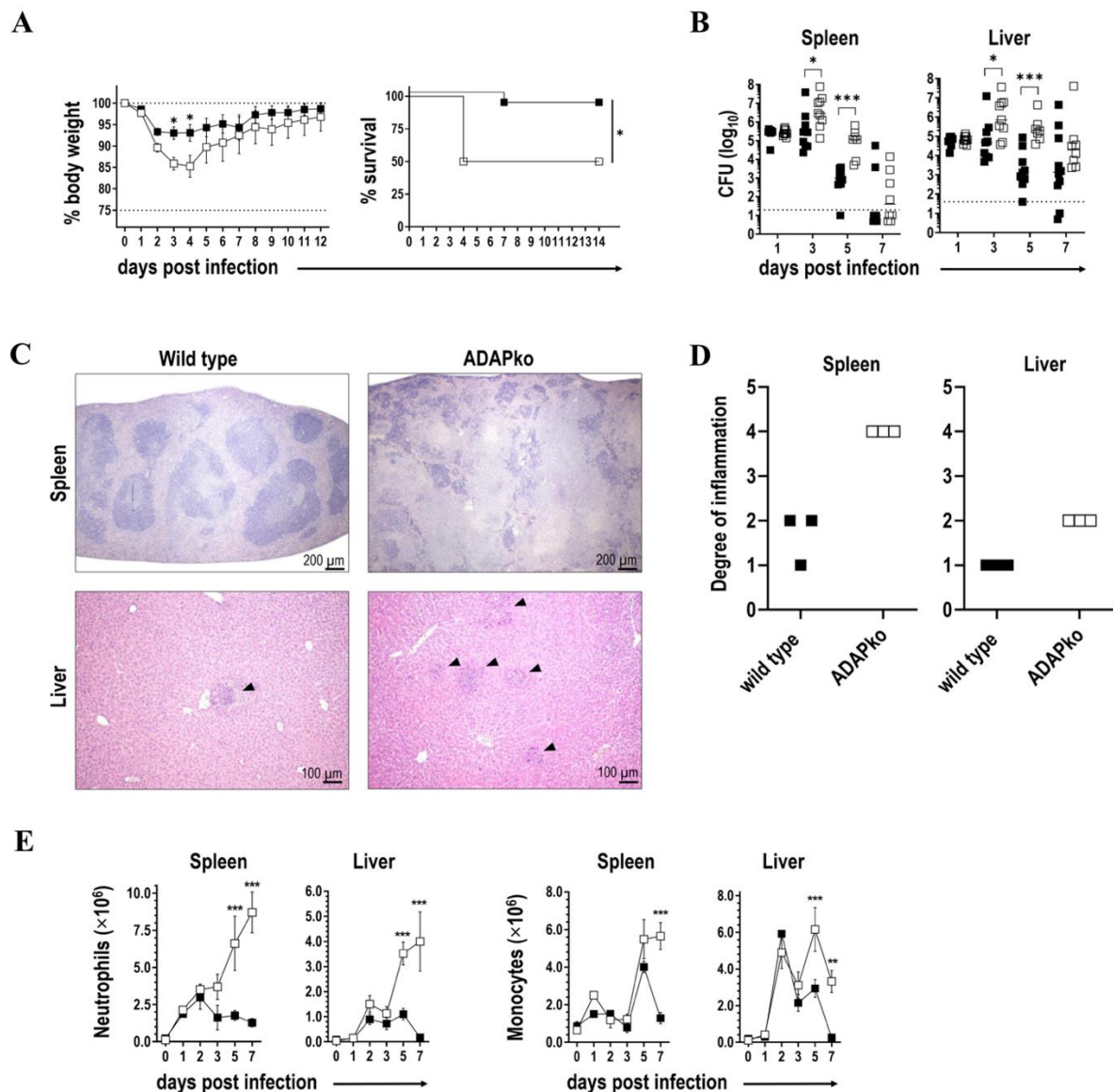
Figure 11 | ADAP-deficiency renders mice highly susceptible for infection with the intracellular pathogen *Listeria monocytogenes*. Wild type (■) and ADAPko (□) mice were either infected i. v. with (A) 5×10^4 CFU or (B-E) 2.5×10^4 CFU *Lm* or left untreated (uninfected control mice, day 0) and were sacrificed at the indicated times post infection. **(A)** Infected mice were weighed and monitored daily and the survival was reported. Data are depicted as mean $\pm$ SEM for n = 8-14 individually analyzed mice. Statistical analyses were performed using two-way ANOVA with Bonferroni's *post hoc* test for the weight loss data and Mantel-Cox log-rank test for the survival data. **(B)** Bacterial loads in spleen and liver after *Lm* infection. The dashed line represents the limit of detection. Data are depicted as medians for n = 8-10 individually analyzed mice. Statistical analyses were performed after

| **27**

log$_{10}$-transformation using two-way ANOVA with Bonferroni's *post hoc* test. **(C)** H&E histology of infected spleens and livers 3 days post infection. Organs were stored in 4 mL 4 % paraformaldehyde and later sectioned for histology and analyzed by H&E staining. The black bar at the bottom right corner of each panel represents a distance of 200 µm for the spleen sections and 100 µm for the liver sections. **(D)** Scoring of degree of inflammation in spleens and livers. **(E)** Neutrophil (left panels), and monocyte (right panels) absolute numbers in spleens and livers. Leukocytes were isolated from spleen and liver, stained against cell specific markers and their frequencies were determined by flow cytometry. From these frequencies the absolute numbers of the cells were calculated. Data are depicted as mean ± SEM for n = 4-5 individually analyzed mice and statistical analyses were performed using two-way ANOVA with Bonferroni's *post hoc* test.. *p < 0.05, **p < 0.01, ***p < 0.001. Modified from reference [201].

As summarized in **Figure 11**, ADAPko mice lost significantly more weight during the course of the *Lm* infection and their survival rate was significantly reduced compared to wild type mice (**Figure 11 A**). Evaluation of the bacterial burden in spleen and liver revealed delayed bacterial elimination in ADAP-deficient mice (**Figure 11 B**). Histopathological examination uncovered that in comparison to wild type mice, ADAPko animals exhibited an overall increased pathology in spleen and liver 3 days post infection (**Figure 11 C** and **D**). Of note, a higher number of leukocyte foci was observed in the liver of ADAPko mice. As depicted in **Figure 11 E**, subsequent FACS-based quantification of leukocytes in spleen and liver revealed an excessive and sustained infiltration of neutrophils (left panels) and a delayed decline of monocyte numbers (right panels) in spleen and liver of *Lm* infected ADAPko mice.

Together, these unpublished observations clearly indicate that ADAPko mice are highly susceptible to infection with *Lm*. Despite excessive infiltration of phagocytes that might contribute to the pronounced immunopathology, ADAPko mice failed to control early bacterial growth. This, together with the fact that differences in morbidity and survival became evident very early after infection, implies that ADAP-deficiency negatively affects innate immune responses against *Lm*. To experimentally prove this hypothesis by the examination of different aspects of anti-listerial innate immunity was the overall aim of this thesis.

1.7   Aims of the thesis

Since NK cells and phagocytes are well known to become activated early after *Listeria monocytogenes* (*Lm*) infection and exhibit crucial functions in innate immune response to the pathogen, the potential roles of ADAP in the activation and acquisition of effector functions during listeriosis was studied in these cellular subsets.

The first part aimed to extend existing knowledge regarding the role of ADAP in NK cells. To achieve this, naïve ADAPko and wild type NK cells will be stimulated *in vitro* with antibody and/or cytokines followed by flow cytometry-based analysis of cytokine production and their capacity to degranulate. In order to allow NK cell priming within their natural environment and to adapt the experimental set-up to a more physiological stimulation, splenic NK cells from *in vivo Lm*-infected ADAPko and wild type mice will be re-stimulated *in vitro* with YAC-1 target cells and degranulation will be assessed by flow cytometry. To gain additional insight regarding a potential effect of ADAP on NK cell morphology, microtubule network structures and vesicle distribution, FACS-sorted naïve and NK cells from infected mice will be analyzed by confocal microscopy and will be applied to unbiased high-resolution mass spectrometry in order to identify possible ADAP-dependent alterations in the NK cell proteome. To rule out any effect of ADAP-deficiency in immune cells other than NK cells, conditional ADAPko mice lacking ADAP specifically in NK cells will be used to study the specific impact of ADAP in NK cells on the outcome of *Lm* infection. Moreover, *in vitro* NK cell migration towards a chemokine gradient comparing naïve and infection-primed NK cells from conditional ko mice and wild type counterparts will be assessed.

In summary, the first part of this thesis will provide profound novel insight into the role of ADAP in NK cells during systemic *Lm* infection.

To date, very limited data exist regarding the immunological function of ADAP in myeloid cells. To gain further insight into the potential contributions of ADAP to the activation and acquisition of effector function in relevant phagocytes, *Lm* infections will be performed in ADAPko and wild type controls followed by in-depth characterization of neutrophils and inflammatory monocytes. This will include quantification of the recruitment of these cellular subsets to the site of infection, characterization of their cytokine and effector molecule profile, their unbiased transcriptional profiling as well as their functional characterization with regard to the formation of neutrophil extracellular traps and their phagocytic capacity.

Together, the second part of the thesis will provide detailed knowledge regarding the potential impact of ADAP on immune responses mediated by neutrophils and inflammatory monocytes during *Lm* infection.

2 Materials

2.1 Conventional ADAP knockout

ADAP wild type and knockout (ADAPko) mice have been created and first described as SLAP-130/Fyb$^{-/-}$ by Peterson et al. in 2001[11]. Peterson et al generated these mice by inserting a neomycin cassette (pPNT.neo) into the animals' ADAP gene locus, in order to switch off its functionality. This leads to the inactivation of the SLAP-130 gene which codes for the ADAP protein in all cells. Mice were on C57BL/6J genetic background. Initial analysis of immune cellularity in these conventional ADAPko mice showed reduced number of CD4$^+$ and CD8$^+$ T cells whereas the number of B220$^+$ B cells was increased. Of note, the number of DX-5$^+$ NK cells was analogous with those in the wild type littermate controls. Furthermore the number of thymocytes and platelets was significantly reduced in ADAPko mice. Overall, the animals show no pathological phenotype, as investigated by Peterson and colleagues in 2001[11]. ADAPko mice therefore have a normal birth rate, are viable, fertile and show normal growth. The respective control mice are the ADAP wild type mice with two intact ADAP alleles. ADAPko and ADAP wild type mice used in this study were littermates derived from the same breeding. Mice were bred in the animal facility at the Helmholtz Center for Infection Research in Braunschweig (Germany) or in the animal facility of the Medical Faculty of the Otto-von-Guericke University Magdeburg (Germany). Mice were kept under specific pathogen-free conditions in environmentally-controlled clean rooms and were used at 8-24 weeks of age. Experiments were approved by the local government agencies of the Niedersächsisches Landesamt für Verbraucherschutz und Lebensmittelsicherheit and Landesamt für Verbraucherschutz, Sachsen-Anhalt under File ID 42502-2-1603 UniMD.

2.2 Conditional ADAP knockout mice

2.2.1 *ADAP$^{fl/fl}$ × NKp46-Cre^{het}*

The ADAP^{fl} × NKp46-Cre^{het} mouse lacks ADAP expression in cells with an active NKp46 promoter, as usually found in NK cells. To generate this mouse line, mice containing the so called "knockout first allele" C57BL/6N-Fyb$^{tm1a(EUCOMM) Hmgu}$/Cnrm^{203} were sourced from the EUCOMM project and purchased from the European Mouse Mutant Archive EMMA. By means of the so-called "knockout-first strategy", the ADAP allele is modified up- and downstream of its largest and critical exon 2. The lacZ and neomycin-resistance cassettes were

both removed by breeding with further transgenic mice, expressing a Flp recombinase resulting in floxed ADAP exon 2 alleles (flanking *loxP* sites) and formal restoration the wild type phenotype[204]. To generate conditional knockout mice with deletion of ADAP in the NK cell lineage, mice with floxed alleles were crossed with NKp46-iCre knock in mice kindly provided by Prof. Eric Vivier[205]. The presence or absence of the *FRT* sites, the *loxP* sites, the gene of interest and the respective Cre transgene were checked routinely by PCR using genomic DNA isolated from ear tissue. To investigate specific effects of ADAP deletion and to exclude off-target effects of Cre recombinase, ADAP$^{wt/wt}$ × Cre^{het} and ADAP$^{fl/fl}$ × Cre^{het} were always used as littermates. Transgenic mice of this mouse model, are used in this thesis, and are named ADAP$^{wt/wt}$ × NKp46-Cre^{het} (wild type littermates) and ADAP$^{fl/fl}$ × NKp46-Cre^{het} (NKp46-conditional ADAP knockout). Of note, NK cell maturation in the bone marrow as well as distribution of mature NK cells in spleen and peripheral blood was similar in both genotypes[204].

2.2.2 *ADAP$^{fl/fl}$ × LysM-Cre^{het}*

To create this mouse line, the above-mentioned conditional ADAP$^{fl/fl}$ mouse was mated with the LysM-Cre^{het} mouse. LysM is the gene product of the Lyz2 gene, which is expressed in all myeloid phagocytes, like neutrophil granulocytes, monocytes, macrophages and DCs. Analogous to the NKp46-Cre^{het} mouse, the LysM-Cre^{het} mouse is a heterozygous deletion mutant for the Lyz2 gene in which one allele of Lyz2 has been replaced by the gene of the Cre recombinase. By mating the two mouse strains, the ADAP$^{fl/fl}$ and LysM-Cre^{het}, the ADAP$^{fl/fl}$ × LysM-Cre^{het} mouse is created, whose phagocytes are no longer able to express ADAP. The corresponding control mouse line is the ADAP$^{wt/wt}$ × LysM-Cre^{het}.

2.3 Consumables

All consumables, technical devices, buffer and media from cooperation experiments are stated in the methods part (Manufacturer, # Cat number).

Table 1 | Chemicals

Product	Cat number	Manufacturer
β-Mercaptoethanol	1001090202	Sigma-Aldrich
Bacto^{TM} Agar	214010	BD Bioscience
Bacto^{TM} Brain Heart Infusion	237200	BD Bioscience
BD FACS^{TM} Clean	340345	BD Bioscience
BD FACS^{TM} Flow	342003	BD Bioscience
BD FACS^{TM} Rinse	340346	BD Bioscience

Materials

BD FACS^{TM} Shutdown	334224	BD Bioscience
Brefeldin A	420601	BioLegend
Brefeldin A	B7651	Sigma-Aldrich
BSA	A7906	Sigma-Aldrich
DMSO	A9941	Carl Roth
Ethanol, absolute	2246.1000	CHEMSOLUTE®
Ethanol, 100 %	8025	Baker
EDTA	E6758-500G	Sigma-Aldrich
FCS	P4047500	PAN Biotech
Fixable Viability Dye eFlour® 780	65-0865-14	eBioscience
Gentamycin	P11-004	PAA
IGEPAL® CA-630	18896	Sigma-Aldrich
IMDM (GlutaMAX-I)	31980-022	Gibco
Ionomycin	I0634	Sigma-Aldrich
MilliQ	-	-
Monensin	M5273	Sigma-Aldrich
NaCl	3975.2	Carl Roth
PFA	252549-1L	Sigma-Aldrich
PFA	158127	Sigma-Aldrich
PBS	14190-169	Gibco
PBS tablets	18912-014	Gibco
Penicillin-Streptomycin	15070-063	Gibco/Invitrogen
PMA	P1585	Sigma-Aldrich
Percoll	17-0891-01	GE Healthcare
RLT buffer	79214	Qiagen
RNAlater	76106	Qiagen
RPMI 1640 medium (+ L-glutamine)	21875034	Gibco
Triton-X100	X100	Sigma-Aldrich
TWEEN-20	A1379-100mL	Sigma-Aldrich
Trypan blue	15250-061	Gibco
TRIS-hydrochlorid	9090.3	Carl Roth

Table 2 | Kits

Product	Cat number	Manufacturer
CD4⁺ T cell isolation Kit, mouse	130-104-454	Miltenyi Biotech
Cytofix/Cytoperm Kit	00-5123-43	BD Bioscience
Cytofix/Cytoperm Kit	554714	BD Bioscience
Fast-Start Essential DNA Green Master	06402712001	Roche
Liver Dissociation Kit + C-tubes	130-105-807	Miltenyi Biotech
Maxima First Strand cDNA Synthesis Kit	00408695	Thermo Fisher Scientific
NK cell isolation Kit, mouse	130-115-818	Miltenyi Biotech
RNeasy Mini Kit	74104	Qiagen

2.4 Technical devices

Table 3 | Technical devices

Product	Model	Manufacturer
autoMACS	ProSeparator	Miltenyi Biotech
Centrifuge	Allegra® X-15R	Beckman Coulter
Centrifuge	Multifuge® 1S-R	Heraeus
Centrifuge	Centrifuge 5417-R	Eppendorf
Clean bench	HERAsafe® KS	Heraeus
CO_2 incubator	NU-8500E	Integra Bioscience
CO_2 incubator (Heracell)	50116047	Thermo Fisher Scientific
Counting chamber	Neubauer	Marienfeld Superior
Homogenizer	POLYTRON® PT 3100 D	KINEMATICA AG
Flow Cytometer	BD FACS Canto™ II	BD Bioscience
Flow Cytometer	BD LSRFortessa™	BD Bioscience
Flow Cytometer	Attune NxT	Thermo Fisher Scientific
gentleMACS	dissociator	Miltenyi Biotech
Incubation shaker	Ecotron	INFORS HT
Laboratory balance	Pioneer®	Ohaus
Magnetic stirrer	C-MAG HS7	IKA
Megafuge 40R	50126358	Thermo Fisher Scientific
Microscope	CX21	Olympus
Multifuge X3 FR	10325804	Thermo Fisher Scientific
pH measuring instrument	EL20	Mettler Toledo
Roller mixer	SRT9	Stuart
Shaker	DOS-10L	neolab
Spectrophotometer	GeneQuant™ pro	Amershan Bioscience
Spectrophotometer	ND-1000	NanoDrop Technologies
Suction pump	Vacusafe	Integra Bioscience
Thermocycler	LightCycler®480 II	Roche
Thermomixer	Thermomixer comfort	Eppendorf
Vacuum dryer	RVC 2-18 CDplus	Christ
Vortex	Vortex Genie 2	Scientific Industries
Water bath	WNE 7	Memmert

2.5 Antibodies - FACS Panels

In the following section, all antibodies that have been used for different analyses are listed. Each antibody was titrated before the usage.

Table 4 | *In vitro* NK cell stimulation

Antibody	Conjugation	Clone	Manufacturer
Fixable Viability Dye	eFlour780	-	eBioscience
CD16/CD32	-	93	BioLegend
CD3ε	FITC	145-2C11	BioLegend

CD107a	Biotin	1D4B	BioLegend
CD49b	APC	DX5	BioLegend
CD11b	PerCP-Cy5.5	M1/70	BioLegend
IFN-γ	BV421	XMG1.2	BioLegend
Streptavidin	PE-Cy7	-	BioLegend

Table 5 | FACS sorting of NK cells

Antibody	Conjugation	Clone	Manufacturer
Fixable Viability Dye	eFlour780	-	eBioscience
CD16/CD32	-	93	BioLegend
CD3ε	FITC	145-2C11	BioLegend
Ly6G	BV510	1A8	BioLegend
CD11b	BV421	M1/70	BioLegend
NK1.1	Biotin	PK136	BioLegend
CD49b	APC	DX5	BioLegend
CD27	PE	LG.3A10	BioLegend
Streptavidin	PE-Cy7	-	BioLegend

Table 6 | IL-10 expression

Antibody	Conjugation	Clone	Manufacturer
Fixable Viability Dye	eFlour780	-	eBioscience
CD16/CD32	-	93	BioLegend
B220	FITC	RA3-6B2	BioLegend
CD4	FITC	RM4-5	BioLegend
CD8	FITC	53-6.7	BioLegend
CD3	BV510	17A2	BioLegend
NK1.1	PE	PK136	BD Pharmingen
NKp46	eFlour660	29A1.4	Invitrogen
IL-10	BV421	JES5-16E3	BioLegend

Table 7 | Integrin expression

Antibody	Conjugation	Clone	Manufacturer
CD16/CD32	-	93	BioLegend
CD3ε	FITC	145-2C11	BioLegend
CD4	FITC	GK1.5	BioLegend
CD8	FITC	53-6.7	BioLegend
CD19	FITC	6D5	BioLegend
TER-119	FITC	TER-119	eBioscience
NK1.1	APC-Cy7	PK136	BioLegend
NKp46	V450	29A1.4	BD Bioscience
CD122	PE-Cy7	TM-β1	BioLegend
CD11b	BV510	M1/70	BioLegend
CD18	Alexa Fluor 647	M18/2	BioLegend
CD29	PE	HMβ1-1	BioLegend
CD11a	PE	2D7	BD Pharmingen

| **34**

| CXCR4 | C450 | 29A1.4 | BioLegend |

Table 8 | Degranulation

Antibody	Conjugation	Clone	Manufacturer
CD3ε	BUV395	17A2	BD Bioscience
NK1.1	APC	PK136	eBiosciences
Perforin	PE	S16009B	BioLegend
Granzyme B	FITC	NGZB	eBiosciences
IFN-γ	BV785	XMG1.2	BioLegend

Table 9 | Migration

Antibody	Conjugation	Clone	Manufacturer
CD16/CD32	-	2.4G2	BD Pharmingen
CD3ε	FITC	145-2C11	BD Pharmingen
NK1.1	APC-Cy7	PK136	BioLegend
NKp46	BV450	29A1.4	BD Bioscience

Table 10 | Phagocytes infiltration and cytokine measurement

Antibody	Conjugation	Clone	Manufacturer
Fixable Viability Dye	eFlour780	-	eBioscience
CD16/CD32	-	2.4G2	BD Pharmingen
CD4	FITC	RM4-4	BioLegend
CD8a	FITC	53-6.7	BioLegend
B220	FITC	RA3-6B2	BioLegend
CD45	PerCP-Cy5.5	30-F11	BioLegend
Ly6G	PE-Cy5	1A8-Ly6g	Invitrogen
CD11b	BV605	M1/70	BioLegend
CX3CR1	BV510	SA011F11	BioLegend
Ly6C	APC	HK1.4	BioLegend
IL-1α	PE	ALF-161	BioLegend
TNF-α	PE-eFlour610	MP6-XT22	Invitrogen
NOS2	PE-Cy7	CXNFT	Invitrogen

Table 11 | FACS sorting of phagocytes and phagocytosis assay

Antibody	Conjugation	Clone	Manufacturer
Fixable Viability Dye	eFlour780	-	eBioscience
CD16/CD32	-	2.4G2	BD Pharmingen
Fluospheres™	FITC	-	Fisher Scientific
CD3ε	APC	145-2C11	BioLegend
CD4	APC	RM4-5	BioLegend
CD8	APC	53-6.7	BioLegend
B220	APC	RA3-6B2	BioLegend
CD45	PerCP-Cy5.5	30-F11	BioLegend
Ly6G	PE-Cy5	1A8-Ly6g	Invitrogen

CD11b	PE-Cy7	M1/70	BioLegend
CX3CR1	BV421	SA011F11	BioLegend
Ly6C	BV711	HK1.4	BioLegend

2.6   Buffer and media composition

Table 12 | General Culture media

Media	Composition	Solvents
BHI-Media	18.5 g Bacto^{TM} Brain Heart Infusion	in 500 mL MilliQ
BHI Agar	18.5 g Bacto^{TM} Brain Heart Infusion 7.5 g Bacto^{TM} Agar	in 500 mL MilliQ

Table 13 | IMDM complete

Component	Final concentration
IMDM with GlutaMAX-I	500 mL
FCS	10 % (v/v)
Penicillin/ Streptomycin	1 % (v/v)
Gentamycin	0.1 % (v/v)
β-Mercaptoethanol	0.1 % (v/v)

Table 14 | FACS buffer

Component	Final concentration
PBS, pH 7.4	-
FCS	2 % (v/v)
EDTA	2 mM

Table 15 | Buffer for NK cell isolation

Component	Final concentration
PBS, pH 7.4	-
BSA	0.5% (v/v)
EDTA	2 mM

Table 16 | Lysis buffer

Component	Final concentration
PBS, pH 7.4	-
IGEPAL CA-630	0.2 %

3 Methods

3.1 Microbiological techniques

3.1.1 *Cultivation of bacteria*

To initially grow *Listeria monocytogenes* (*Lm*), two bacteria bearing polystyrene beads from a cryo glycerol stock were placed in 5 mL BHI medium and were cultured at 37 °C with overnight shaking. On the next day 100 µL were pipetted onto a BHI agar plate and spread over the entire plate. The plate with the bacterial suspension was then cultivated at 37 °C, and afterwards stored in the refrigerator for later use. A day before mouse infection, a pre-culture was prepared by transferring *Lm* cells with an inoculation loop from the initial overgrown agar plate into 5 mL of fresh BHI medium. The preculture was then incubated over night at 37 °C and 180 rpm shaking speed. To prepare the main culture, 1 mL was removed from the incubated preculture and added to 4 mL of fresh BHI medium, followed by incubation for about 4 h in the incubator at 37 °C and 180 rpm to ensure that the bacteria were in the metabolically active growth phase.

3.1.2 *Infection of mice with Listeria monocytogenes*

The *Lm* strain 10403S (kindly provided by Dirk Busch (Germany) and described before in references [202,206]) was used for infection experiments. *Lm* culture in the metabolically active phase were prepared as described above (see **section 3.1.1**) and bacterial numbers were determined by measuring OD_{600} using a spectrophoto-meter. PBS served as a blank. Based on a previously established OD/cell-density correlation curve the suspension was further diluted in sterile PBS to an OD_{600} corresponding to the desired infection dose per mouse and per experiment.

If not stated otherwise, mice were infected by intravenous (i. v.) injection into the tail vein with the calculated dose of 2.5×10^4 bacteria suspended in 100 µL of PBS. To determine the effective infectious dose, serial dilutions of the inoculum were plated on BHI agar plates followed by an overnight incubation of the plates at 37 °C. The colonies were counted on the next day. Effective number of bacteria that had been applied to the mice was calculated based on the serial dilution with the highest countable CFU count.

3.1.3 *Determination of the bacterial burden*

The bacterial burden in organs of *Lm* infected mice was determined from organ homogenates as colony forming units (CFU). Organs of interest from mice were collected at different time points post *Lm* infection and transferred into sterile tubes with 1 mL for the spleen and 2 mL for the liver of PBS with 0.2 % (v/v) IGEPAL CA-630 (NP-40) for lysis of eukaryotic cells and homogenized using a mechanic homogenizer device. The lysis buffer was required to make sure that also intracellular bacteria are released from their host cell. Five 10-fold serial dilutions of the homogenized organs were prepared and 10 µL was plated on BHI agar plates. The plates were incubated over night at 37 °C. Colonies on the agar plates were than counted the next day and the CFU was calculated in respect to the according dilution factor.

3.2 Cell biological techniques

3.2.1 *Organ isolation and preparation of single-cell suspension*

Mice were euthanized with CO_2 inhalation and exitus was proven by reflex control of the legs. Before the organs of interest were collected a transcardial perfusion with 10 mL ice-cold PBS was carried out in order to flush out as many blood components as possible from the organs, which would interfere with the subsequent processing. Subsequently, the organs were removed and stored in PBS on ice until further cell isolation. If blood and serum was required, prior to transcardial perfusion, heart blood was obtained by puncturing the heart with a 1 mL disposable fine-dose syringe and treated as described (see **section 3.2.3**).

For cell isolation, the spleens were weighted, placed in a petri dish and flushed with 10 mL ice-cold PBS with the help of a syringe or were directly meshed through a 100 µm cell strainer into a 6-well plate. After transfer into a 15 mL falcon tube, the dish was flushed with additional 5 mL PBS and this volume was also transferred into the falcon tube. The cells were centrifuged at 300 ×g at 4 °C for 10 min and the supernatant was discarded. Next, erythrocyte lysis was performed using 0.2 % NaCl/MilliQ as well as 1.6 % NaCl/MilliQ. The cell pellet was first resuspended in 5 mL 0.2 % NaCl and after approximately 20 sec 5 mL of 1.6 % NaCl was added, bringing the suspension back to a physiological osmolarity. Finally 5 mL PBS was added. Cells were centrifuged as described before and the supernatant was discarded. The cell pellet was resuspended in PBS and stored on ice until further usage.

Before processing livers, the gallbladder was excised. Liver samples were meshed through a 70 µm cell strainer directly into a 50 mL falcon tube and the strainer was flushed with about

30 mL PBS. Supernatant was discarded after a centrifugation at 300 ×g at 4 °C for 10 min. Erythrocytes lysis was performed as described for spleen samples, however 10 mL of all buffers was used. The cell suspension was centrifuged as defined before and the supernatant was aspirated. Leukocytes from liver samples were obtained by a density gradient centrifugation using Percoll (density of stock solution: 1.124 g/mL). To this end, cells were resuspended in 10 mL Percoll/0.15 M NaCl solution (density: 1.041 g/mL). Cell suspension was then centrifuged at 1800 rpm at RT for 20 min without using the brake of the centrifuge. The density centrifugation resulted in a pellet of total liver leukocytes in the bottom of the falcon tube, whereas the hepatocytes and other remaining organ material stays in the Percoll layer. Next, the supernatant was aspired and the pellet was washed with 10 mL PBS and centrifuged again at 300 ×g at 4 °C for 10 min. Finally, the cells were resuspended in PBS and stored on ice until further analysis.

3.2.2 *Liver dissociation*

For higher cellular yields of single-cell suspensions of liver leucocytes, a liver dissociation procedure was applied. To this end, the Liver Dissociation Kit from Miltenyi Biotech company was used. This procedure combines mechanical dissociation and enzymic degradation of the extracellular matrix, thereby efficiently releasing intercellular and interstitial leucocytes. After isolating the liver and removing the gallbladder, liver was digested according to the protocol of the kit manufacturer's. Briefly, the liver was rinsed with DMEM and transferred into a C-tube (Miltenyi Biotech) with 4.7 mL of prewarmed dissociation mix (200 µL Enzyme D solution, 100 µL enzyme R solution and 20 µL enzyme A solution in DMEM). The C-tube was inserted upside down into the gentleMACS Dissociater device (Miltenyi Biotech) and the gentleMACS program m_liver_03 was run. After termination of the program, C-tube was detached from the device and incubated for 30 min at 37 °C under continuous tube rotation. Subsequently, C-tube was again inserted into the gentleMACS Dissociater and the gentleMACS program m_liver_04 was applied. After termination of the program, cell suspension was filtered through a 100 µm strainer, which was washed with 5 mL DMEM. The tube with the cell suspension was filled up with DMEM medium and centrifuged at 300 ×g for 10 min at 4 °C. The supernatant was completely aspirated and the cells were resuspended in an appropriate volume of PBS. Until further use the cell suspension was stored on ice. To

isolate total leukocytes from the cell suspension, Percoll density gradient centrifugation (see **section 3.2.1**) was used.

3.2.3 *Serum preparation, cytokine analyses and ALT measurement*

Mice were sacrificed and blood was obtained by puncture of the heart. Blood samples in 1.5 mL Eppendorf Tubes were incubated for 30 min at RT and for another additionally 30 min at 4 °C. After a short 5 min centrifugation at 14000 rpm the serum supernatant was collected and stored at -80 °C.

For the detection of different cytokines in serum samples a flow cytometry-based multi-analyte assay (LegendPlex; custom mouse panel) or a pre-defined cytometric bead array (Mouse Inflammation cytokine panel; 13-plex) both from BioLegend was used according to the manufacturer's recommendations.

For the analysis of the serum alanine transaminase (ALT) concentration, a commonly used diagnostic indicator for liver pathology, 32 µL serum was applied on a Refloton® test stripe (Roche). Measurement of the test stripe took place on Reflovet Plus spectrophotometer from Roche.

3.3 Molecular techniques

3.3.1 *Genotyping of mice from in-house breeding*

The mouse-individual genotypes of in-house breed ADAPko ADAP wild type and ADAP het mice were determined by conventional endpoint PCR using a piece of ear biopsy and the KAPA Mouse Genotyping Hot Start Kit (Sigma).

Thus, ear biopsy was digested by adding 2 µL Express Extract Enzyme (1 U/µL) and 10 µL of 10× KAPA Express Extract Buffer. The biopsy preparation was filled up with 100 µL molecular biology grade water and subsequently heated up for 10 min at 75 °C, followed by heating for 5 min at 95 °C. After mixing and centrifuging the solution for 1 min at full speed, the DNA extract was transferred into a new tube. The composition of the genotyping PCR reaction mix can be found in **Table 17**. Genotyping primer combinations used for the according mouse line are presented in **Table 18**.

For PCR amplification 1 µL of the previously prepared template DNA was added to the PCR reaction mix. The PCR program for the Thermocycler is presented in **Table** 19. After the thermocycler program was complete the samples were applied to a 1.5 % agarose gel which

ran for about 35 min at 160 volts in a electrophoresis system. Lengths of PCR amplicon products defined the according genotype. ADAP wild type mice show an amplicon at around 350 bp and ADAPko mice at approx. 550 bp. Heterozygous mice showed both bands.
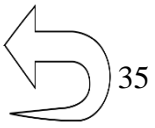
Table 17 | PCR mix components for the reaction of amplification

Component	Volume [µL]
Genotyping mix	12.5
$MgCl_2$ (25 mM)	0.5
Primer forward	1.25
Primer reverse	1.25
DMSO	1.5
water	8.5
Template	1.0

Table 18 | Oligonucleotides primers for mice genotyping

Oligonucleotide	Sequence 5' → 3' (length)
ADAP_neo	GCGCTACCGGTGGATGTGGAATGT (24)
ADAP_fwd	CCGTGGGGCCAAAGTCAGGAGAA (23)
ADAP_rev	CCCACCCCAAGGTCCTTTCTTAC (23)

Table 19 | Cycler program used for genotyping PCR

Cycle	Temperature [°C]	Time	Number of cycles
Initiation Denaturation	95	3 min	
Denaturation	95	15 sec	
Annealing	60	15 sec	35
Elongation	72	15 sec	
Terminal Elongation	72	10 min	

3.3.2 *RNA isolation and reverse transcription*

Mouse organs and tissue material was submerged in RNAlater solution (Qiagen) for 24 h at 4 °C and subsequently stored at -80 °C until RNA isolation. Tissue samples were removed from RNAlater solution and homogenized in RLT buffer containing 1 % (v/v) β-Mercaptoethanol. The homogenate was centrifuged for 10 min at 3000 ×g at RT and 500 µL of the supernatant was used for the RNA isolation. RNA was isolated according to the manufacturer's instructions of the RNeasy Mini Kit (Qiagen). RNA was eluted in 100 µL nuclease-free water. Contaminating DNA within isolated total RNA was digested using the RNase-free DNase set (Ambion). RNA content was determined with the NanoDrop ND-1000 spectrophotometer.

For cDNA synthesis in a reverse transcription reaction, equal amounts of RNA per experiment were transcribed using the Maxima First Strand cDNA Synthesis Kit (Thermo Fisher Scientific) according to the manufacturer's instructions (see **Table 20**). The resulting single-stranded cDNA can be used as a template for the quantification of specific transcripts by means of quantitative real-time RT polymerase chain reaction (qRT-PCR).

Table 20 | Mixture for cDNA synthesis in a reverse transcription reaction

Component	Volume [µL]
Template RNA	1 pg - 5 µg
Maxima Enzyme Mix	2.0
$5 \times$ Reaction Mix	4.0
DEPC-water	ad 20.0

This mixture was mixed and centrifuged. Afterwards the mixture was placed into a thermocycler and was run with the following program, summarized in **Table 21**. Subsequently 8 µL TE 10/1 buffer (Tris-EDTA; 1:10 with MilliQ) per 1 µg reversely transcribed RNA were added to the samples.

Table 21 | Thermal program for reverse transcription reaction

Temperature	Time [min]
25 °C	10
50 °C	15
85 °C	5

3.3.3 *DNase treatment to remove DNA contamination from total RNA*

For the digestion with the RNase-free DNase Kit, 5 µL total RNA was used. After adding 0.5 µL volume of $10 \times$ DNase buffer and 1 µL of DNase enzyme to the RNA, the mixture was gently mixed and incubated at 37 °C for 20-30 min. Next, resuspended DNase Inactivation Reagent (0.5 µL volume) was added, reaction was mixed well and incubated for 5 min at RT with occasional flick mixing. Afterwards, the samples were centrifuged (10000 ×g for 1 min) and the supernatant, containing the RNA, was carefully transferred to a fresh tube. RNA concentration was determined with the NanoDrop ND-1000 spectrophotometer.

3.3.4   *Quantitative real-time Polymerase chain reaction (qRT-PCR)*

Quantitative qRT-PCR can be used to measure the level of expression of a specific gene of interest. The expression level of the gene of interest is typically normalized to the expression of a so-called housekeeping gene, that signifies solid and ubiquitous expression in most cell types. Here, the ribosomal protein 9 (Rps9) was generally used for gene level normalization. Real-time PCR was performed on a Roche Light Cycler II device in 96-well format using SybrGreen-based Fast-Start Essential DNA Green Master Mix and the thermal program, stated in **Table 22**. The device internal Light Cycler II Software was used to determine threshold cycle (C_t) values from amplification curves by the second-derivate maximum method. Relative quantification of gene of interest expression normalized to *Rps9* was calculated with the ΔΔCt method[207] with efficiency correction. All reactions were performed in duplicates and averaged C_t values were used in ΔΔCt calculation. Per sample and PCR reaction, 1 µL cDNA was used as template material. Reaction mix is given in **Table 23**. All primers, see **Table 24**, had a stock concentration of 100 µmol/L and were used in a final concentration of 500 nmol/L. Annealing temperature of all primers were designed to be at about 60 °C.

Table 22 | Thermal program for qRT-PCR
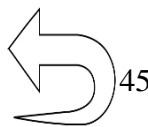
Cycle	Temperature [°C]	Time	Number of cycles
Incubation	95	5 min	
Amplification	95	10 sec	
	60	10 sec	45
	72	10 sec	
Cooling	4	stored	

Table 23 | Components for the qRT-PCR reaction

Component	Volume [µL]
forward Primer (2000 nmol/L)	5.0
reverse Primer (2000 nmol/L)	5.0
cDNA	1.0
Fast-Start Essential DNA Green Master Mix	10.0
Molecular biology grade water	4.0

Table 24 | Primer sequences for qRT-PCR

Gene	Forward primer sequence (length)*	Reverse primer sequence (length)*
Il-2	CAAGCAGGCCACAGAATTGAAA (22)	GGCACTCAAATGTGTTGTCAGA (22)
Il-12p40	GTAACCAGAAAGGTGCGTTCC (21)	GAACACATGCCCACTTGCTG (20)
Il-15	GGTCCTCCTGCAAGTCTCTC (20)	GGTGGATTCTTTCCTGACCTCTC (23)
Il-18	GAAAGCCGCCTCAAACCTTC (20)	CCAGGTCTCCATTTTCTTCAGG (22)

Il-21	ATCTTCTTGGGGACAGTGGC (20)	AGTGCCCCTTTACATCTTGTGG (22)
Rps9	CTGGACGAGGGCAAGATGAAGC (22)	TGACGTTGGCGGATGAGCACA (21)

* Sequences are given in 5'- 3' orientation.

The mRNA sequences and identifiers of genes of interest, used for primer design, were derived from NCBI's RefSeq database and intron spanning qRT-PCR primers were designed using the web based assay design center tool from Roche company. To determine effective qRT-PCR efficiency of all primers, C_t values of 4 serial dilutions, corresponding to 3, 1, 0.1 and 0.01 µL template mix, which contained a mixture of all cDNA samples from one given experiment, were determined. PCR efficiency for each primer pair was calculated by the Light cycler software and was used for relative expression quantification with efficiency correction.

3.4   Immunological techniques

3.4.1   *Fluorescence-activated cell sorting (FACS)*

Single cell suspensions of leucocyte samples in PBS or FACS buffer were transferred and stained in 96-well round-bottom plates and centrifuged (1200 rpm, 5 min, 4 °C) to pellet the cells, the supernatant was discarded.

Cells were incubated (10 min, 4 °C, dark) in 100 µL PBS containing anti-CD16/CD32 antibody and fixable live/dead discrimination dye (eFluor780). CD16/CD32 antibody binds specifically to Fcγ III/II receptors, predominantly present on phagocytes, to prevent unspecific binding of subsequently used fluorescently labeled FACS antibodies. The live/dead discrimination dye only stains dead cells that have impaired membrane integrity, thereby enabling cell entry of the dye and thus allowing exclusion of dead cells in later data analysis. After a washing step with 150 µL the plate was again centrifuged, the supernatant was decanted and the plate gently tapped and vortexed to loosen the cell pellet.

Depending on the purpose of analysis, different combinations of FACS antibodies were used to stain the cells (see **Table 4**, **Table 5**, **Table 6**, **Table 7**, **Table 8**, **Table 9**, **Table 10** and **Table 11**). Antibody staining procedure was done as described before.

If biotinylated antibodies were used, secondary Streptavidin counter-staining was carried out for 10 min at 4 °C protected from light (100 µL FACS buffer with labeled Streptavidin per well). After a finalizing washing step, cell pellets were resuspended in 200 µL FACS buffer and transferred to FACS sample tubes. Samples were either acquired on a BD FACS Canto II (BD Bioscience), Attune NxT Flow Cytometer (Thermo Fisher Scientific) or a BD LSR

Methods

Fortessa (BD Bioscience) and FACS data were analyzed using a FlowJo software (Version 9.6.4, Tristar).

In cases where the intracellular production of cytokines was to be analyzed, the cells were *in vitro* stimulated prior FACS staining procedure, if not stated otherwise. To this end, leukocytes were transferred to 15 mL tubes, resuspended in 1 mL stimulation medium (IMDM complete medium with phorbol-12-myristat-13-acetate (PMA; final concentration: 1:100.000 = 10 pg/mL) and Ionomycin (final concentration: 1:1000 = 1 ng/mL) and initially incubated for one hour at 37 °C. The combination of PMA and Ionomycin enhances the current phenotypic state of the cells, thereby boosting also *in vivo* established inflammatory properties like cytokine production. After 1 h, Brefeldin A (stock concentration: 10 mg/mL, finale concentration: 5 μL/mL) and Monensin (stock concentration: 2 mM, dilution factor: 1000) was added to the medium, while the incubation was continued for additional three hours. Brefeldin A and Monensin prevent cytokine secretion by inhibiting the Golgi apparatus and vesicle merging with the outer plasma membrane and thus ensure accumulation of produced cytokines with the cell. This greatly improves their detection by intracellular cytokine-antibodies. After incubation time was over, live dead discrimination as well as the surface marker staining was done as described above. For intracellular antibody staining Fixation/Permeabilization Kit (BD Bioscience) according to the manufacturer's protocol was used, as described in **section 3.4.1**. In detail, cells were incubated overnight in 100 μL/well Fix/Perm buffer in the dark. On the next day, the 96-well plate was centrifuged (1200 rpm, 5 min, 4 °C) and the supernatant was decanted. Cells were washed with 100 μL/well of 1 × permeabilization buffer, plate was centrifuged, supernatant was decanted, and the cells were stained with 100 μL/well of the intracellular antibody staining mix (in 1 × permeabilization buffer) for 30 min at 4 °C in the dark. The cells were washed with permeabilization buffer. Stained cells were taken up in 200 μL FACS buffer and transferred to FACS tubes. For compensation of fluorochrome spillover during data analysis, each fluorescently labeled antibody within a staining panel was stained separately on excessive splenocyte cell material. PMT voltages of the flow cytometer's detection channels were adjusted to the according cell material based on unstained, but equally treated sample material. In case of cytokine staining, negative cells were defined with the corresponding fluorescence-minus-one (FMO) controls.

NK cells were gated as displayed in **Figure 12**, whereas a representative gating scheme to identify neutrophils and inflammatory monocytes can be found in **Figure 13**.
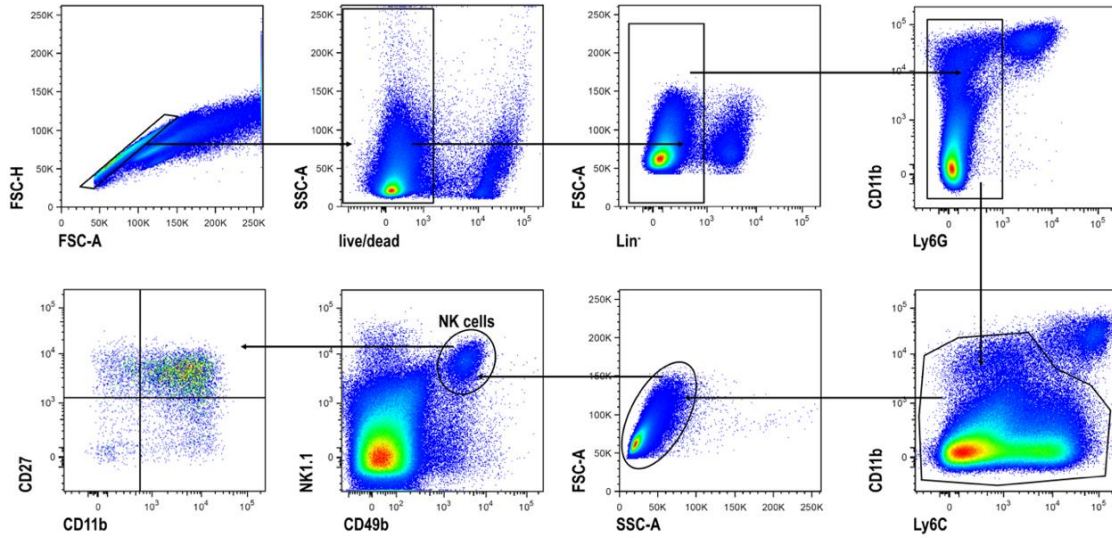
Figure 12 | Representative gating scheme to define NK cells from *Listeria monocytogenes*. Cells, here shown for infected spleens 3 days post infection, were pre-gated on leukocytes by FSC *versus* SSC (pre-gating not shown) and doublets were excluded by FSC-A *versus* FSC-H gating. Dead cells were eliminated by staining with live/dead marker and only CD45+ cells were further characterized. Based on the expression intensity of indicated surface markers, NK cells were defined and divided in subsets, according to **Table 5**.
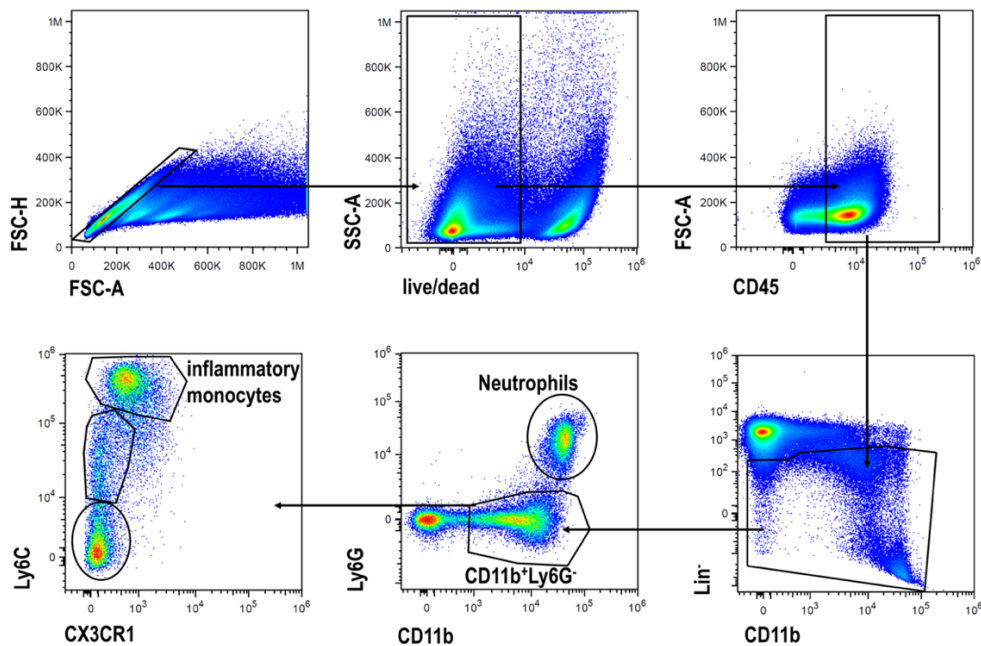
Figure 13 | Representative gating scheme to define neutrophils and inflammatory monocytes from *Listeria monocytogenes*. Cells, here shown for infected spleens 3 days post infection, were pre-gated on leukocytes by FSC *versus* SSC (pre-gating not shown) and doublets were excluded by FSC-A *versus* FSC-H gating. Dead cells were eliminated by staining with live/dead marker and only CD45+ cells were further characterized. Based on the expression intensity of indicated surface markers, neutrophils and inflammatory monocytes were defined, according to **Table 10** and **Table 11**.

3.4.2 *NK cell isolation and in vitro stimulation*

In order to isolate NK cells from the spleen, magnetic activated cell sorting (MACS) followed by FACS sorting technology was used. One day prior to stimulation of isolated NK cells, a 96-well U-bottom plate was pre-coated with anti-NK1.1 (clone: PK139, BioLegend, stock concentration: 0.5 mg/mL) in a final concentration of 1 µg/mL (dilution factor: 500), which was diluted in PBS and incubated overnight at 4 °C. On the next day, this plate was washed with 150 µL PBS to remove unbound NK1.1 antibody and centrifuged (1200 rpm, 5 min, 4 °C) and stored until further use.

For MACS sorting spleens were harvested and processed into single cell suspension. Initially lymphocytes from all spleen samples were collected as described (see **section 3.2.1**). Splenocytes were incubated in PBS containing anti-CD16/CD32 antibody as described in **section 3.4.1**, and subsequently washed with NK cell buffer (containing 0.5 g BSA, 0.5 M EDTA ad 100 mL PBS) and consequently the mouse NK cell isolation Kit (Miltenyi Biotech) was used according to the manufacturer's instructions without erythrocyte lyses of splenocytes in respect to the autoMACS program Depletes. For *in vitro* stimulation untouched NK cells were added to the pre-coated well plate.

If indicated, either recombinant mouse IL-2 (stock concentration: 0.2 mg/mL, final concentration: 3000 Units/mL; dilution factor: 200) and recombinant mouse IL-12 (stock concentration: 0.1 mg/mL, final concentration: 1 ng/mL; dilution factor: 100.000) or PMA (20 ng/mL) and ionomycin (1 µg/mL) were added to the wells and NK cells were stimulated for 4 h at 37 °C in an incubator with 7.5 % CO_2. Control cells were cultured in IMDM-complete medium without any stimulation. After the first 2 h, Brefeldin A was added to all wells including the control wells. After the full 4 h of *in vitro* stimulation, NK cells were incubated with antibodies according to **section 3.4.1** and **Table 4**, whereas Biotin stained samples were counterstained with streptavidin. Intracellular staining done as described before (see **section 3.4.1**). Cells were analysed using an Attune NxT Flow Cytometer (Thermo Fisher Scientific). The purity of autoMACS isolated NK cells was > 86 %.

3.4.3 *FACS-sorting*

For Proteome analyses of NK cells (see **section 3.5.1**), Microarray analyses (see **section 3.5.2**) and microscopy of NK cells (see **section 3.6.1**), NK cells were sorted using a FACS cell sorter. For this purpose, leukocytes from spleens and livers were isolated as described before (see

sections **3.2.1** and **3.2.2**). Subsequently, a T cell and B cell depletion, using the autoMACS device (Miltenyi Biotech) was carried out. Briefly, cell pellets were incubated with biotinylated antibodies for CD3 (dilution factor: 250) and B220 (dilution factor: 120) diluted in PBS and incubated for 5 min (4 °C, dark). Afterwards, cells were resuspended in FACS buffer and anti-Biotin MicroBeads from the CD4$^+$ T cell isolation Kit (mouse) were used according to the manufacturer's instructions (Manual magnetic labeling; Miltenyi Biotech) and incubated for 10 min (4 °C, dark) before proceeded to the magnetic cell separation (program: DEPLETE). Resulting cell suspension was centrifuged and the cell pellet was stained with antibodies according to **Table 5** and **Table 11**.

3.4.4   *IL-10 Expression on NK cells*

For IL-10 expression on NK cells, total leukocytes from spleen and liver were processed into single cell suspension as described in **sections 3.2.1** and **3.2.2** and suspensions were treated with anti-CD16/32 (see **section 3.4.1**). Cell suspensions were furthermore stimulated for 4 h with PMA/Ionomycin (see **section 3.4.1**) and later surface stained with antibodies according to **Table 6**. Cells were fixed (Fixation/Permeabilization Kit) overnight and intracellular staining was done as described before (see **section 3.4.1**). Cells were analysed with a Attune NxT Flow Cytometer (Thermo Fisher Scientific). Flow cytometric data were analysed using the BD FACS Diva v6.1.3 software.

3.4.5   *Integrin expression on NK cells*

For Integrin expression on NK cells, total leukocytes from spleen were processed into single cell suspension as described in **section 3.2.1** and suspensions were treated with anti-CD16/32 (see **section 3.4.1**). Cell suspensions were furthermore surface stained with antibodies according to **Table 7**. Cells were analysed with a BD LSR Fortessa (BD Bioscience). Flow cytometric data were analysed using the BD FACS Diva v6.1.3 software.

3.4.6   *Degranulation*

NK cells mediate cell killing action following cell-to-cell contact with an appropriate target cell and subsequent local secretion of cytotoxic mediators by degranulation. A major trigger of NK cell cytotoxicity is the absence of MHC class I on the target cell. The MHC I-deficient YAC-1 cell line is thus commonly used to provide standardized target cells for NK cell degranulation assays *in vitro,* since it is known to be sensitive to NK cell-mediated cytotoxicity,

representing a great tool to assess the NK cell cytotoxic capacity. NK cells that underwent degranulation express the lysosomal-associated membrane protein-1 (CD107a) protein on their surface, thereby allowing discrimination of degranulated from resting NK cells[126]. Thus, the degranulation assay was used to evaluate the cytotoxic capacity.

For the functional assessment of NK cells, splenocytes were co-incubated with YAC-1 target cells at an effector:target ratio of 10:1 for a total incubation time of 6 h at 37 °C and 5 % CO_2 in complete RPMI 1640 medium (Gibco), containing 10 % FCS, 100 U7mL penicillin, 50 µg/mL streptomycin, 1 mM L-glutamine (Gibco, #25030081). To detect CD107a expression, the medium contained anti-CD107a antibody (concentration: 1:200). After 1 h of incubation, the co-culture was supplemented with Monensin and Brefeldin A (Sigma) to prevent receptor internalization and cytokine secretion, respectively, at a final concentration of 5 µg/mL. Subsequently, the cells were surface-stained for the identification of NK cells (CD3$^-$ NK1.1$^+$) and intracellularly for perforin, granzyme B (GrzB) and IFN-γ using the antibodies, mentioned in **Table 8**. For intracellular staining of perforin, GrzB and IFN-γ, cells were permeabilized and fixed using the Cytofix/Cytoperm buffer (BD Bioscience) according to the manufacturer's protocol, as described in **section 3.4.1**.

3.4.7 *Migration*

The experimental evaluation of the chemotactic ability of immune cells towards certain chemo-attractants of interest is highly useful to understand migratory behavior of those immune subsets *in vivo*. Technically, this can be achieved by using *in vitro* transwell systems. Those consist of a plastic well with a pores bottom, harboring tiny pores with defined diameter. Transwell inlays sit inside wells of conventional cell culture plates, e.g. 12-well plate. This generates two cell-culture-medium containing chambers. Cells are seeded in the upper chamber and the chemoattractant is provided in the lower chamber. Numbers of initial cells in the upper chamber are compared to numbers of transmigrated cells in the bottom chamber. Here, the NK cell attracting chemokine CXCL12 (250 ng/mL) was added to the lower chamber in a total volume of 600 µL chemotaxis medium (RPMI medium, containing 25 mM HEPES and 0.5 % BSA). Total splenocytes were loaded to the upper chamber at a density of 5×10^5 cells in 100 µL chemotaxis medium. Cells were allowed to migrate across the pores of the transwell inserts (pore size of 5 µm) at 37 °C and 5 % CO_2. After 4 h, transmigrated cells from triplicate wells were harvested by centrifugation for 5 min at 300 ×g, resuspended in 100 µL PBS,

containing 2 mM EDTA, stained with trypan blue and counted using a haemocytometer. The percentage of NK cells before and after transmigration was analysed by flow cytometry as described in **section 3.4.1**. Briefly, cells were first incubated with anti-CD16/CD32 for 10 min on ice, followed by staining with antibodies, mentioned in **Table 9** for 30 min on ice. After washing, analysis was performed on a BD LSRFortessa flow cytometer. NK cells were gated by data analysis and absolute NK cell numbers within the upper and lower chamber was calculated. Assay readout was calculated as follows: number of migrated NK cells / number of input NK cells.

3.4.8 *Staining of NETs in mouse tissue*

Mice were anesthetized by intraperitoneal (i. p.) injection of 100 µL per g of bodyweight of the narcotic solution (10 % ketamine, 2 % xylazine in 0.9 % saline). Proper depth of the terminal anesthesia was determined by testing for the interdigital reflex. The heart was punctured for heart blood collection. Organs were rinsed by perfusion of the heart with 20 mL PBS. Afterwards, the organs were perfused with 10 % formalin via the heart. Spleens and livers had been fixed *in situ* by perfusion with 4 % formalin. Following this, tissues were removed and fixed in 4 % formalin for 15-20 h. Tissues were then stored in 70 % ethanol (dark, 4 °C), paraffin-embedded and subsequently cut into 4 µm sections as described before in reference [208]. Antigen retrieval protocol, described from Becker et al.[208] was run at 50 °C for 90 min. Paraffin sections were dried, followed by dewaxing and rehydration. Subsequently, sections were incubated with HIER buffer (heat-induced epitope retrieval, Aptum) at different temperatures before three rinsing steps with de-ionized water and one time with PBS. After antigen retrieval, sections were permeabilized for 5 min with 0.5 % Triton X-100 (Sigma) in PBS at RT, followed by three rinsing steps with PBS. Sections were treated with blocking buffer, containing 2 % donkey serum, 5 % normal goat, 0.05 % TWEEN20 and 0.05 % Triton X-100, for 30 min to prevent non-specific binding before rinsing steps occurred. Primary antibodies for anti-neutrophil elastase (NE; Abcam) and anti-histone H3 (Thermo Fisher) were diluted in blocking buffer incubated on the sections overnight followed by different rinsing steps. The same procedure was followed for the secondary antibodies conjugated to Alexa Fluor 488 donkey anti-rabbit IgG (Bioss) and Alexa Fluor 647 goat anti-rat IgG (Thermo Fisher) with an incubation of 30 min at RT in the dark. Staining of the nuclei was done using DAPI (CarlRoth) prepared in PBS followed by rinsing steps. Since *Lm* infection might not be

homogeneously distributed throughout the organ, four pictures per slide for all three layers (12 in total) at a magnification of 200-fold were taken. Tissue sections were analyzed with the KEYENCE BZ-X800 microscope. and analysis was done by counting the numbers of histone and NE expression quantified by using Image-Pro Plus 6.

3.4.9 *Phagocytosis assay*

The phagocytosis assay quantifies the ingestion of FITC-labeled latex beads by phagocytes. Isolated splenocytes and liver leukocytes (see **sections 3.2.1** and **3.2.2**) of a mouse were placed in triplicates into a 96-well plate (4×10^5 cells/well) and incubated for 2 h at 37 °C with 5 % CO_2. Samples permanently incubated at 4 °C served as negative controls. After the incubation, cells were set up with a cell to beads ratio of 1:5 with FITC-fluorescent (yellow-green), carboxylated latex beads (Fluospheres[TM], F8823, Fisher Scientific, Germany) in IMDM-complete medium, containing 10 % FCS, 1 % Penicillin/Streptavidin, 0.1 % Gentamycin and 0.1 % 2-Mercaptoethanol. Subsequently, cells were washed and stained using antibodies according to **Table 11**. Flow cytometric analyzes was performed using an Attune NxT Flow Cytometer (Thermo Fisher Scientific). Obtained data were analyzed using FlowJo software (Version 9.9.6.). Phagocytosis of latex beads was evaluated by the median fluorescence intensity (MFI) of the positive population in the FITC-fluorescence channel. Within a gated cell subset the percentage of cells that phagocytosed 1, 2, 3 or more than 3 latex beads (FITC-positive cells) were calculated, according to references [209,210].

3.5 Omics techniques

3.5.1 *Proteome analyses*

FACS-sorted NKp46^{+} NK cells (see **section 3.4.3**) were lysed in buffer (1 % SDS (Carl Roth, # 4360.2), 1× Complete protease inhibitor cocktail (Roche, 1# 1697498001), 50 mM HEPES, pH 8.5 (Carl Roth, # 9105.3) and 10 mM DTT (Sigma-Aldrich, # D-0632)) for 5 min at 95 °C, after resting 5 min on ice. Benzonase (MERCK, # 1.016915.0001) was added and samples were incubated (37 °C, 30 min). Afterwards, different chemicals were added to reduce and protect cysteine residues, respectively. Protein purification, protein digestion and peptide purification was performed according to a slightly adapted Single-Pot Solid-Phase-enhanced Sample Preparation (SP3) protocol[211,212]. Sequencing grade trypsin was added at a ratio of 1:20 weight per weight in 50 mM HEPES with pH 8. After < 14 h incubation at 37 °C, samples

were slightly acidified using formic acid (FA; Biosolve, # 01934125 and # 0023244101BS), shaken and incubated overnight at RT after raising the acetonitrile concentration to at least 95 %. Beads containing the adsorbed peptides were washed once with pure acetonitrile and were air dried. Peptides were eluted in a first step with 20 µL 2 % DMSO (Sigma-Aldrich, # D-0632) for 30 min, and in a second step with 20 µL 0.065 % FA, 500 mM KCl (Carl Roth, # 6781.1) in 30 % acetonitrile (ACN; Baker, # 901) for 30 min. Peptides were vacuum dried and dissolved in 0.2 % trifluoroacetic acid + 3 % ACN for subsequent ultracentrifugation (model: Sorvall Discovery M120 SE, Hitachi) (50000 ×g, 30 min, RT). LC-MS/MS analyses of purified and desalted peptides were performed on a Dionex UltiMate 3000 n-RSLC system connected to an Orbitrap Fusion^{TM} Tribrid^{TM} mass spectrometer (model: Tribrid^{TM}, Thermo Fisher Scientific). Peptides of each sample were loaded onto a C18 precolumn (model: 3 µm RP18 beads, Acclaim), washed for 3 min at a flow rate of 6 µL/min and separated on a C18 analytical column (model: 3 mm PepMap RSLC, Dionex) at a flow rate of 200 nL/min via a linear 120 min gradient from 97 % MS buffer A to 25 % MS buffer B, followed by a 30 min gradient from 25 % MS buffer B to 62 % MS buffer B. The LC system was operated with the Chromeleon software embedded in the Xcalibur software suite. The effluent was electro-sprayed by a stainless-steel emitter. Using the Xcalibur software, the mass spectrometer was controlled and operated in the "top speed" mode, allowing the automatic selection of as many doubly and triply charged peptides in a 3 sec time window as possible and the subsequent fragmentation of these peptides. Peptide fragmentation was carried out using the higher energy collisional dissociation mode and peptides were measured in the ion trap (HCD/IT). MS/MS raw data files were processed via the Proteome Discoverer program using Mascot as search machine and fasta files from the Swiss-Prot/UniProt database from January 2018. Used Mascot search parameters were: maximum missed cleavage site: 1, precursor mass tolerance: 10 ppm, fragment mass tolerance: 0.05 Da. Oxidation of methionine was set as a variable modification whereas modification of cysteine by MMTS was set as fixed modification. Filters used in Proteome Discoverer were peptide confidence: high, search engine rank: 1 and false discovery rate: 1 %. The entire mass spectrometry proteomics data have been deposited to the ProteomeXchange Consortium via the PRIDE partner repository with the data set identifier PXD016305.

3.5.2   *Microarray analyses*

RNA of neutrophils and inflammatory monocytes, FACS-sorted from spleen and liver leukocytes of day 3 *Lm* infected wild type and ADAPko mice, were purified using the RNeasy Mini Kit, as described above (see **sections 3.3.2** and **3.3.3**). To acquire a representative mix of all individual, and thus variable samples (n = 6 mice/genotype), a pool within the sorted cells (n = 3 mice/genotype; triplicate, n = 2 for neutrophils of liver wild type; duplicate). The preparation of RNA samples for microarray analysis, including amplification, fragmentation, microarray hybridization, staining as well as scanning was performed at the Genome Analytics Group at Helmholtz Centre for Infection (HZI) Research in Braunschweig, Germany. Samples were analyzed with the Affymetrix Clariom S mouse microarray resulting in 23 microarrays: Microarray raw data were initially analyzed using the Transcriptome Analysis Console (TAC) software (Thermo Fisher Scientific). Briefly, data were summarized, $\log_2$-transformed and quantile-normalized with SST-RMA algorithm. A percentile filter, to decimate lowly abundant transcripts, was applied to the microarray data, removing transcripts with signal intensities consistently below the 20th percentile of the average signal intensity distribution in all microarrays of a given cell subset. Differential expression between ADAPko and wild type cells was calculated based on ANOVA method with FDR < 0.05 and applying a fold change (FC) cutoff of: - 3 < FC > + 3. Volcano plots were generated in Python using Matplotlib library and the Spyder programming environment. K-means clustering of z-score transformed normalized $\log_2$ signal intensities of differentially regulated genes was calculated and plotted using Genesis software[213]. Gene Ontology (GO) enrichment analysis was performed with Cytoscape software and the ClueGO plugin[214], using two-sided hypergeometric test with Bonferroni-step-down multiple-hypothesis-testing correction and GO-term fusion/grouping options applied. Only GO-terms with FDR < 0.05 and GO-level above ≥ 8 were considered. Enriched GO-terms were mapped to previously determined k-means clusters and the percentages of transcripts in each cluster affiliating to significantly enriched GO-terms were color-coded and hierarchically clustered in the Genesis software. Microarray data were deposited in NCBI's Gene Expression Omnibus and are accessible through the GEO series accession number GSE175993.

3.6   Imaging techniques

3.6.1   *Microscopy*

FACS-sorted NK cells (see **section 3.4.3**) were seeded onto poly-L-lysine (Sigma-Aldrich, #P8920) coated coverslips and allowed to adhere for 30 min. Cells were fixed for 20 min, followed by washing with PBS. Cells were permeabilized using 0.15 % Triton-X100 in PBS for 5 min followed by blocking with 1 % BSA in PBS containing 0.05 % TWEEN-20 (Carl Roth, # 9127.1) for 1 h. Antibodies were applied in blocking solution and staining was performed for 2 h at RT. Cells were washed three times with PBS containing 0.05 % Tween-20 followed by dehydration using first 70 % and 100 % ethanol. Samples were dried by air and mounted using Mowiol (Carl Roth, # 9 127.1). Light microscopy was carried out on an inverted microscope (model: ECLIPSE Ti-E, Nikon) with standard epifluorescence illumination. Images were acquired with a back-illuminated, cooled charge-coupled-device camera (model: DS2-Qi2, Nikon). Data acquisition was performed in NIS-Elements.

3.6.2   *Histopathology analyses*

To evaluate structure and organ pathology of spleen and liver of infected and uninfected control mice, histopathological preparations were generated and systematically scored. Mice were euthanatized by inhalation of CO_2. Subsequently, spleen and liver were removed, washed in PBS and fixed with 4 % paraformaldehyde (PFA). Organs were embedded in paraffin, sectioned at 4 µm thickness and Hematoxylin and eosin (H&E) staining was done by the veterinary pathologist Dr. Olivia Kershaw, from the Freie University Berlin. Blinded histological evaluations were performed by the veterinary pathologist Dr. Olivia Kershaw, according to literature Telieps et al.[215]. The number of foci of inflammation was mainly assessed by the grade of affected tissues (grade 1: mild; grade 2: moderate) through microscopy. To measure the characteristic of pathology, samples were microscopically scored in a blinded manner by measuring necrotic areas.

3.7   Statistics

All statistical analyses were performed using the GraphPad Prism Software v9 (GraphPad Software, Inc, La Jolla, USA). The type of the statistic test is indicated in each single figure legend. Where indicated, z-scores of a dataset were calculated by subtraction of the mean of the dataset from each individual data entry and division by the standard deviation of the dataset.

4 Results

To date the adaptor protein ADAP has largely been studied in the context of effector functions in and activation of T cells. CD8$^+$ T cells and NK cell develop from the same common lymphoid precursor and share hallmark features like effector cytokine secretion and cytotoxicity. Apart from T cells, a vital role for ADAP in regulating cell adhesion by integrins has been described for neutrophils. Only limited data is available for the function of ADAP in other immune cells including monocytes.

As described earlier in the introduction, available data regarding the immunological function of ADAP in NK cells are conflicting. They vary from a crucial role of ADAP in the production of pro-inflammatory cytokines like IFN-γ and cytotoxicity to an ADAP-dependent uncoupling of cytokine production and cytotoxicity, with only cytokine production being dependent on ADAP, up to the finding that ADAP in NK cells is entirely dispensable for their function. So far, no data existed concerning the role of ADAP for the function of NK cells in an *in vivo* infection setting. NK cell activation *in vivo* is certainly far more multifaceted than their activation under artificial *in vitro* conditions. Thus, the first part of this thesis aimed at extending existing knowledge regarding the impact of ADAP on NK cell function using *in vivo* infection of wild type and ADAPko mice with *Lm,* a pathogen well-known to effectively induce the activation of NK cells.

While an important contribution of ADAP in integrin-associated adhesion as well as for the recruitment of leukocytes has been demonstrated, its role in pathogen-specific immunity during *in vivo* infection remains largely elusive. Neutrophils and monocytes are rapidly recruited to sites of infection, were they are activated and exert various central antimicrobial functions. The second part of this thesis will therefore elucidate the role of ADAP in phagocyte-mediated anti-bacterial immunity utilizing the *in vivo Lm* infection model in conventional ADAPko mice and mice lacking ADAP exclusively in phagocytes.

Part 1

4.1   Role of ADAP in NK cells during *Listeria monocytogenes* infection in mice

Note: Results of this part of the thesis (pages 57-83) have been published in:

Böning, M. A. L.; Trittel, S.; Riese, P.; van Ham, M.; Heyner, M.; Voss, M.; Parzmair, G. P.; Klawonn, F.; Jeron, A.; Guzman, C. A.; Lothar, J.; Schraven, B.; Reinhold, A. and Bruder, D. ADAP promotes degranulation and migration of NK cells primed during *in vivo Listeria monocytogenes* infection in mice. *Front. Immunol.*, **2020**, *10*, 3144. https://doi.org/10.3389/fimmu.2019.03144.

4.1.1 *Cytotoxic capacity of in vivo Lm infection primed NK cells requires ADAP*

As mentioned in the introduction, NK cells exhibit the capacity to produce effector cytokines, with IFN-γ being the principal NK cell cytokine produced early on during infection[100,216]. Importantly, IFN-γ plays a vital role for the activation of additional immune cells needed for an effective immunity to pathogens[217,218].

To first address the role of ADAP in cytokine production by naïve as well as infection primed NK cells, ADAPko and wild type mice were infected intravenously with a sublethal dose of *Lm*. On day 1 and 3 post infection, spleens were harvested and processed into single cell suspensions. Uninfected mice served as internal control (day 0). NK cells were isolated by negative selection and afterwards stimulated *in vitro* with anti-NK1.1 alone or together with IL-2/IL-12 or PMA/ionomycin known to activate several intracellular signaling pathways, and moreover resulting in the activation and production of a variety of cytokines[219]. Following *in vitro* stimulation, flow cytometric analysis of IFN-γ production by NK cells was performed. As depicted in **Figure 14**, no genotype-dependent differences regarding the percentage of IFN-γ producing NK cells and the level of IFN-γ production (MFI) were observed in unstimulated NK cells isolated from naïve or infected mice. However, ADAP-dependent differences in NK cell activation became evident following their *in vitro* stimulation. NK cell stimulation with anti-NK1.1 revealed a significantly lower frequency of IFN-γ secreting NK cells and in part, a significantly reduced amount of the effector cytokine IFN-γ produced by NK cells from naïve ADAPko mice compared to ADAP sufficient mice (**Figure 14 B**). This held also true for infection-primed NK cells day 1 and, in tendency, day 3 post *Lm* infection. Both IL-2 and IL-12 are known to enhance the cytolytic activity and IFN-γ production by NK cells. In line with this, the combined stimulation with anti-NK1.1 and IL2/IL-12 revealed the most prominent genotype-dependent differences in this setting with a strikingly reduced number of IFN-γ producing NK cells in ADAPko mice that moreover produced significantly lower quantities of the cytokine as indicated by the MFI (**Figure 14 B**).

A

B
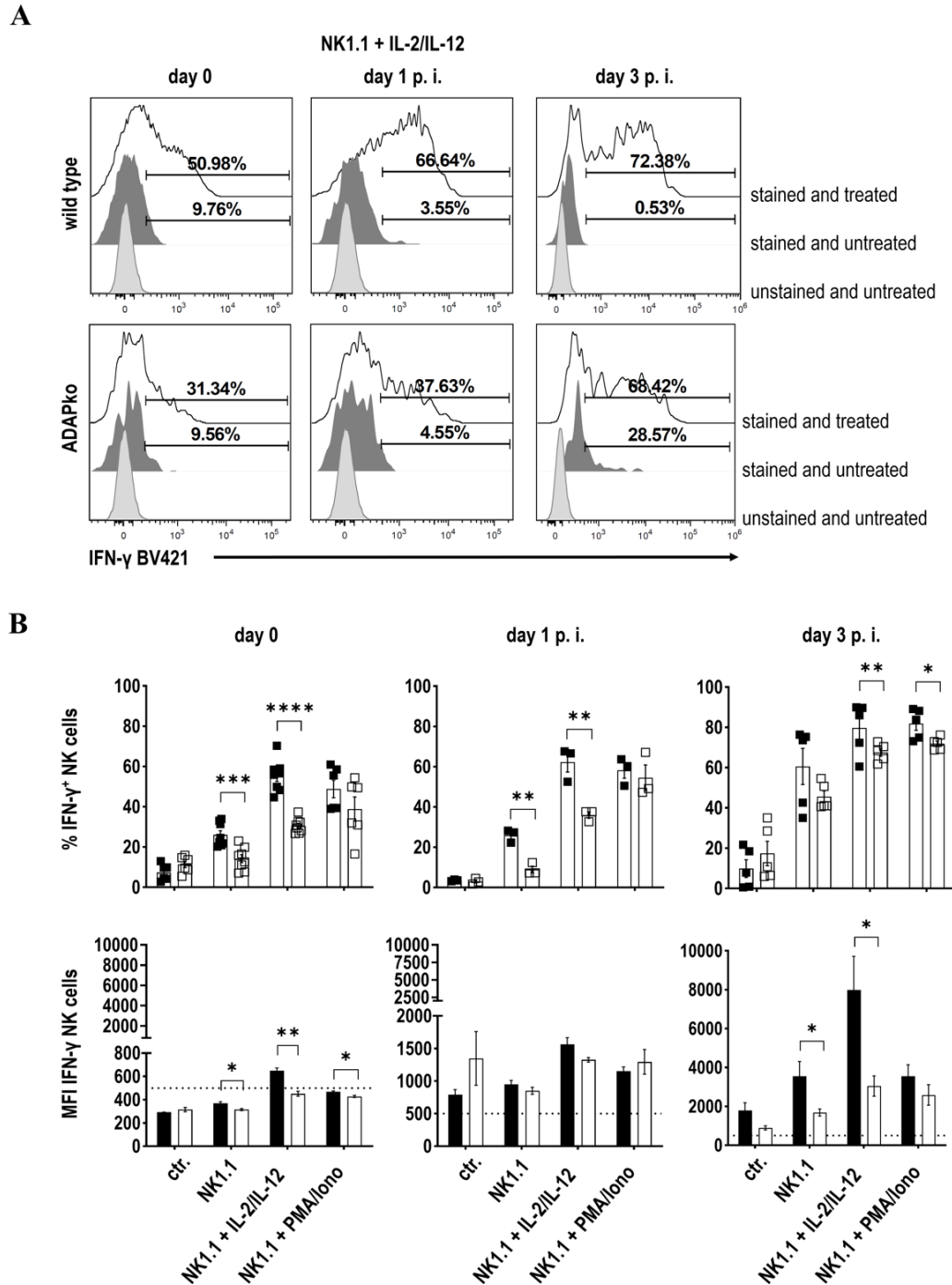
Figure 14 | Production of IFN-γ in naïve and *Listeria monocytogenes* infection-primed NK cells is dependent on ADAP. Wild type (■) and ADAPko (□) mice (age: 10-24 weeks) were either infected *i.v.* with 2.5 × 10⁴ CFU *Lm* or left untreated (uninfected control mice, day 0) and were sacrificed at the indicated times post infection. Leukocytes were isolated from the spleen. Untouched naïve NK cells from the spleen were either stimulated *in vitro* with anti-NK1.1 (plate bound) alone or in combination with IL-2/IL-12 or PMA/ionomycin for 4 h or were left unstimulated (ctr.). Controls were cultured in medium without further stimulation. After 2 h brefeldin A was supplemented to all wells including the control wells to prevent receptor internalization and cytokine secretion, respectively. Subsequently, frequency of IFN-γ producing NK cells was analyzed by flow cytometry. **(A)** Representative histograms (left panels) are shown for re-stimulation with anti-NK1.1 in

| 58

combination with IL-2 and IL-12 (■ unstained and untreated; ■ stained and untreated; □ stained and treated). Numbers in the histograms represent percentage of positive and ctr. cells. **(B)** Summary plots are depicted as mean ± SEM of CD3⁻CD49⁺IFN-γ⁺ NK cells (top panels) and mean fluorescence intensity (MFI, bottom panels) of IFN-γ in NK cells is shown with n = 3-8 individually analyzed mice per group out of three independent experiments. Dashed line indicates MFI of 500 for orientation. Statistical analyses were performed using two-tailed, unpaired *t*-test with Welch's correction (*p < 0.05, **p < 0.01, ***p < 0.001, ****p < 0.0001). Parts of the modified figure have already been published in reference [220].

The fact that the wild type mice exhibit higher frequencies of IFN-γ⁺ NK cells is also visible in the representative histogram shown for the re-stimulation with anti-NK1.1. in combination with IL-2/IL-12 (**Figure 14 A**) for the indicated times post *Lm* infection. Combined stimulation of the NK cells with NK1.1 and PMA/Ionomycin revealed no genotype-dependent differences, except for day 3 post infection with a reduced frequency of IFN-γ producing ADAPko NK cells compared to the NK cells from wild type animals. Taken together, cytokine production by naïve as well as infection-primed NK cells from mice deficient in ADAP is reduced compared to those of the wild type counterparts in different stimulation settings. The significant reduction in IFN-γ production by naïve as well as *Lm* infection-primed NK cells from ADAP-deficient mice raised the question whether NK cell activation in general would be impaired in the absence of ADAP. To test this, the activation status of NK cells was assessed by means of the surface expression of the activation marker CD69 using the same experimental setting as described before.

Figure 15 shows the frequencies of CD69 expression by as well as the MFI of CD69 expression on naïve and infection-primed NK cells from wild type and ADAPko mice. This analysis did not reveal any differences among the different stimulation settings during the course of *Lm* infection. Nevertheless, independent from the genotype the percentage of CD69⁺ NK cells increased from day 0 to day 3 post infection (wild type: 70.9 ± 13.6 %, ADAPko: 93.5 ± 1.6 %). This increase was detectable for all stimulation conditions, even *ex vivo* without further restimulation. Moreover, the level of CD69 expression on NK cells increased over time and notably, on day 3 post infection ADAPko mice expressed significantly more CD69 following NK1.1 stimulation in comparison to the wild type counterparts. Taken together, in contrast to IFN-γ, surface expression of the activation marker CD69 by naïve as well as infection-primed NK cells appears not to depend on ADAP.

A

B
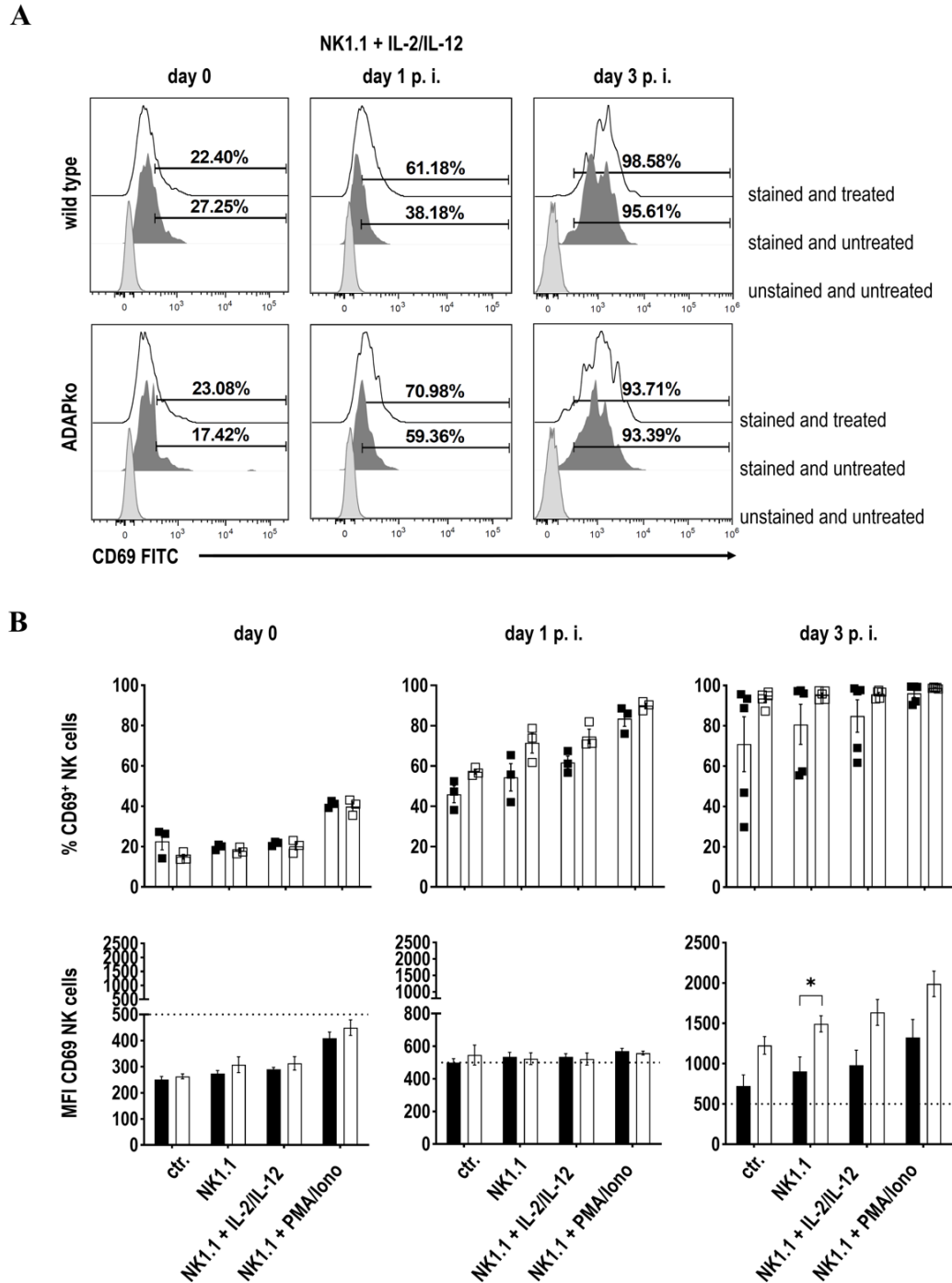
Figure 15 | Expression of the activation marker CD69 of naïve and *Listeria monocytogenes* infection-primed NK cells is independent on ADAP. Wild type (■) and ADAPko (□) mice (age: 10-24 weeks) were either infected i. v. with 2.5×10^4 CFU *Lm* or left untreated (uninfected control mice, day 0) and were sacrificed at the indicated times post infection. Leukocytes were isolated from the spleen. Untouched naïve NK cells from the spleen were either stimulated *in vitro* with anti-NK1.1 (plate bound) alone or in combination with IL-2/IL-12 or PMA/ionomycin for 4 h or were left unstimulated (ctr.). Controls were cultured in medium without further stimulation. After 2 h brefeldin A was supplemented to all wells including the control wells to prevent receptor internalization and cytokine secretion, respectively. Subsequently, frequency of CD69 expressing NK cells was analyzed by flow cytometry. **(A)** Representative histograms (left panels) are shown for re-stimulation with anti-NK1.1 in combination with IL-2 and IL-12 (▨ unstained and untreated; ■ stained and untreated; □ stained and

| 60

treated). Numbers in the histograms represent percentage of positive and ctr. cells. (**B**) Summary plots are depicted as mean ± SEM of CD3$^-$CD49$^+$CD69$^+$ NK cells (top panels) and mean fluorescence intensity (MFI, bottom panels) of CD69 on NK cells is shown with n = 3-5 individually analyzed mice per group out of two independent experiments. Dashed line indicates MFI of 500 for orientation. Statistical analyses were performed using two-tailed, unpaired *t*-test with Welch's correction (*p < 0.05).

As stated above, *in vivo* NK cell activation is far more complex than the activation induced under *in vitro* conditions. Taken this into account, studies were extended to an experimental setting based on NK cell priming within their natural environment during *in vivo* infection, followed by a more physiological *in vitro* stimulation using the MHC class I-deficient NK cell target cell line YAC-1. This cell line is sensitive to NK cell-mediated cytotoxicity[93] that can be indirectly measured by CD107a surface expression on NK cells[126]. For *in vivo* NK cell priming, wild type and ADAPko mice were sublethally infected with *Lm*. Afterwards, NK cells were isolated from the spleen of wild type and ADAPko mice on day 3 post *Lm* infection, as well as from uninfected controls (day 0). Splenocytes were co-cultured for 6 h with or without YAC-1 target cells, followed by NK cells staining for surface CD107a expression and intracellular perforin content. In the absence of YAC-1 target cells, no genotype-dependent difference in CD107a expression and perforin content was detectable, neither in naïve not in the *Lm* infection-primed NK cells (**Figure 16 A**, top panels and **B**). Moreover, for naïve NK cells (day 0), the overall percentage of CD107a$^+$ NK cells increased during co-culture with YAC-1 target cells for both genotypes (no target: wild type: 5.0 % ± 0.3 %, ADAPko: 3.9 ± 0.3 %; (+) YAC-1: wild type: 13.7 ± 1.6 %, ADAPko: 7.2 ± 0.5 %). This effect was as well observed in infection-primed wild type NK cells on day 3 post *Lm* infection (no target: wild type: 12.8 ± 0.9 %; (+) YAC-1: wild type: 32.0 ± 1.3 %) indicating that *in vitro* re-stimulation of NK cells with YAC-1 target cells stimulated significantly more cells to degranulate. Strikingly though, YAC-1 cells did not induce any further degranulation of *in vivo* primed ADAPko NK cells. Taken together, YAC-1-mediated stimulation of naïve NK cells revealed a striking and highly significant ADAP-dependent degranulation defect indicated by reduced numbers of CD107a expressing ADAPko compared to wild type NK cells.

A

B

C
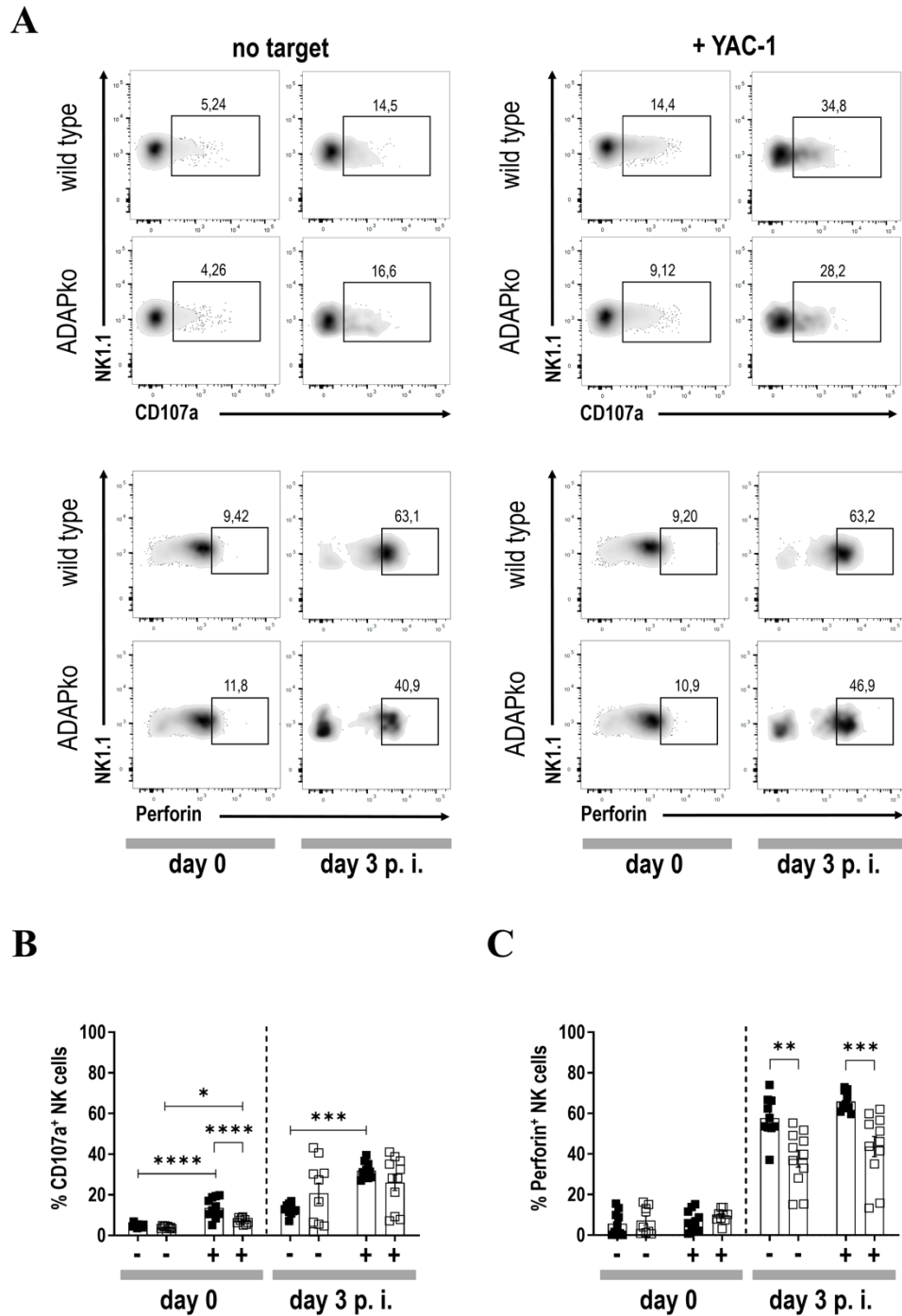
Figure 16 | Degranulation capacity and perforin production by *Listeria monocytogenes* infection-primed NK cells depends on ADAP. Wild type (■) and ADAPko (□) mice (age: 9-18 weeks) were either infected i. v. with 2.5×10^4 CFU *Lm* or left untreated (uninfected control mice, day 0) and were sacrificed at the indicated times post infection. Leukocytes were isolated from the spleen. Splenocytes were isolated and co-incubated *in vitro* without targets (-) or with YAC-1 target cells (+) for a total incubation time of 6 h. After 1 h of incubation, the co-culture was supplemented with brefeldin A and monensin to prevent receptor internalization and cytokine secretion, respectively. **(A)** Representative density dot plots with smoothing and outliers showing surface CD107a or intracellular perforin *versus* NK1.1 expression on wild type and ADAPko splenocytes from naïve mice (day 0) as well as on day 3 post *Lm* infection in the presence or

absence of YAC-1 target cells. Numbers in the density dot plots represent percentage of positive cells. Frequency of summary plots for **(B)** surface CD107a$^+$ and **(C)** perforin^{high} CD3$^-$NK1.1$^+$ NK cells in the spleen of uninfected mice (day 0) and day 3 post *Lm* infection after *in vitro* co-incubation with YAC-1 target cells. Data are depicted as mean ± SEM of n = 10-11 individually analyzed mice per group out of two independent experiments. Statistical analyses were performed using two-way ANOVA with Bonferroni correction for multiple hypothesis testing (*p < 0.05, **p < 0.01, ***p < 0.001, ****p < 0.0001). Figure has already been published in reference [220]. Note: In cooperation with Prof. Carlos A. Guzmán, Dr. P. Riese and Dr. S. Trittel (Helmholtz Centre for Infection Research Braunschweig, Research Group Vaccinology and Applied Microbiology).

Cytotoxicity of NK cells is, among others, mediated by the release of granules containing perforin and granzyme B[119]. The observed ADAP-dependent degranulation defect raised the obvious question if ADAP-deficiency would have an additionally impact on the intracellular perforin level as well as on the GrB and IFN-γ secretion by NK cells. Thus, wild type and ADAPko mice were analyzed as well for these markers by flow cytometry.

As depicted in **Figure 16 A** and **C** bottom panels, for naïve NK cells (day 0) no genotype-dependent changes were observed regarding perforin production, independent of the re-stimulation of NK cells with YAC-1 target cells (no target: wild type: 5.6 ± 1.9 %, ADAPko: 7.2 ± 2.2 %; (+) YAC-1: wild type: 7.1 ± 1.6 %, ADAPko: 9.5 ± 1.1 %). However, well in line with the increased degranulation capacity, *Lm* infection primed NK cells to produce higher levels of perforin. Strikingly, this acquisition of NK cell effector function was significantly impaired in infection-primed NK cell from mice lacking ADAP, as indicated by the decreased frequency of perforin^{high} ADAPko NK cells (no target: wild type: 57.7 ± 3.2 %, ADAPko: 37.6 ± 4.1 %; (+) YAC-1: wild type: 65.8 ± 1.5 %, ADAPko: 43.6 ± 5.0 %).

As for CD107a and perforin, significantly more infection-primed NK cells produced IFN-γ and granzyme B (**Figure 17 A**, **B** and **C**) following co-cultivation with YAC-1 target cells, with the frequency of IFN-γ-producing cells raising from 0.4 ± 0.07 % (day 0) to 5.9 ± 0.9 % (d 3 p. i.) for the wild type and from 0.23 ± 0.04 % (day 0) to 9.9 ± 3.0 % (d 3 p. i.) for the ADAPko NK cells. A similar picture was found for the percentage of GrB$^+$ NK cells. These data are indicative for an efficient *in vivo* priming, however no genotype-dependent alterations were observed. Taken together, the more physiological stimulation of naïve or infection-primed NK cells with YAC-1 target cells uncovered no ADAP-dependent effect with regard to their capacity to produce IFN-γ as well as GrB.
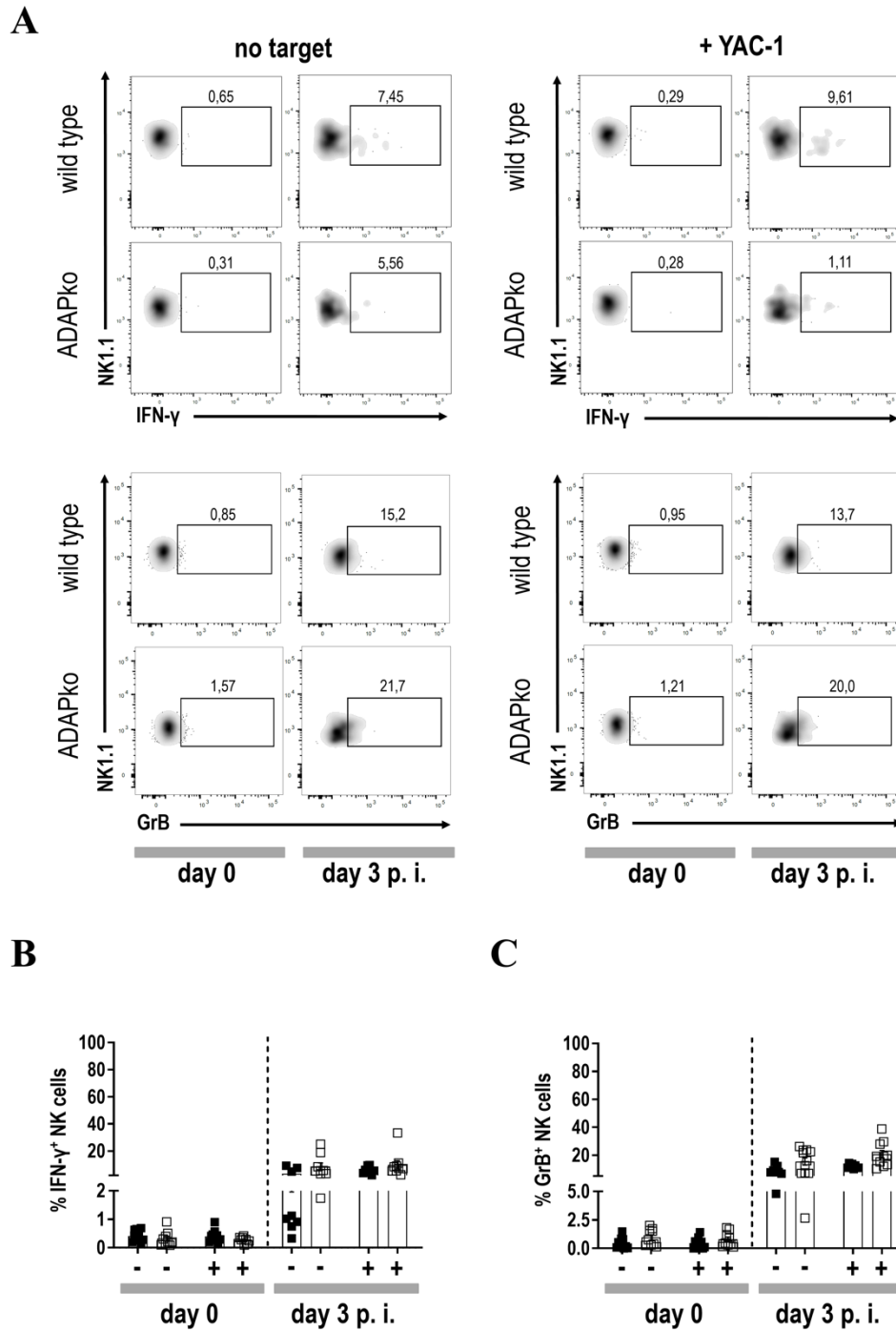
Figure 17 | Production of IFN-γ and granzyme B by *Listeria monocytogenes* infection-primed and YAC-1 re-stimulated NK cells is independent of ADAP. Wild type (■) and ADAPko (□) mice (age: 9-18 weeks) were either infected i. v. with 2.5×10^4 CFU *Lm* or left untreated (uninfected control mice, day 0) and were sacrificed at the indicated times post infection. Leukocytes were isolated from the spleen. Splenocytes were isolated and co-incubated *in vitro* without targets (-) or with YAC-1 target cells (+) for a total incubation time of 6 h. After 1 h of incubation, the co-culture was supplemented with brefeldin A and monensin to prevent receptor internalization and cytokine secretion, respectively. **(A)** Representative density dot plots with smoothing and outliers showing IFN-γ or granzyme B (GrB) *versus* NK1.1 expression on wild type and ADAPko splenocytes from naïve mice (day 0) as well as on day 3 post *Lm* infection in the presence or absence of YAC-1 target cells. Numbers in the

| 64

density dot plots represent percentage of positive cells. Frequency of summary plots for **(B)** IFN-γ⁺ and **(C)** GrB⁺ CD3⁻NK1.1⁺ NK cells in the spleen of uninfected mice (day 0) and day 3 post *Lm* infection after *in vitro* co-incubation with YAC-1 target cells. Data are depicted as mean ± SEM of n = 10-11 individually analyzed mice per group out of two independent experiments. Statistical analyses were performed using two-way ANOVA with Bonferroni correction for multiple hypothesis testing. Parts of the modified figure have already been published in reference [220]. Note: In cooperation with Prof. Carlos A. Guzmán, Dr. P. Riese and Dr. S. Trittel (Helmholtz Centre for Infection Research Braunschweig, Research Group Vaccinology and Applied Microbiology).

We next asked whether the observed striking differences in NK cell degranulation and perforin production were the result of an inefficient NK cell priming in the ADAPko animals during *Lm* infection or rather an intrinsic effect of ADAP-deficiency in NK cells. It is well-known, that in order to successfully fulfill their immunological functions, cytokines secreted by other immune cells are needed to prime NK cell activation, proliferation and their differentiation into fully activated effector cells[221,222]. Thus, a comparative quantification of the serum cytokines that have been described in the context of NK cell activation[98,133,223,224] was performed. Wild type and ADAPko mice were *Lm* infected and sacrificed at the indicated times post infection. Heart blood was taken and the concentration of altogether 13 cytokines in the serum was analyzed by flow cytometry-based multi-analyte assay (custom mouse panel). As depicted in **Figure 18**, the serum cytokine levels for IL-1β, IL-10, IFN-β and IFN-γ on day 1 post *Lm* infection were equivalent in wild type and ADAPko mice. However, although generally low abundant, the IL-1α level was significantly reduced in ADAPko mice (wild type: 12.5 ± 1.7 pg/mL, ADAPko: 5.1 ± 0.6 pg/mL) whereas the TNF-α concentration was slightly higher (wild type: 38.6 ± 6.6 pg/mL, ADAPko: 67.0 ± 13.0 pg/mL) compared to the wild type animals on day 1 post infection. While analysis of IL-2, IL-4, IL12p70, IL-15 and IL-18 did not reveal genotype-dependent differences, the IL-12p40 serum level was reduced in ADAPko mice on day 1 p. i. compared to the wild type mice. Of note, IL-21 was not detectable (data not shown). Interestingly, serum levels of IFN-β, IFN-γ, as well as IL-1α and in tendency TNF-α, which are all known to stimulate cytotoxic priming in NK cells [225–227], were even higher 3 days post infection in ADAP-deficient compared to wild type mice.
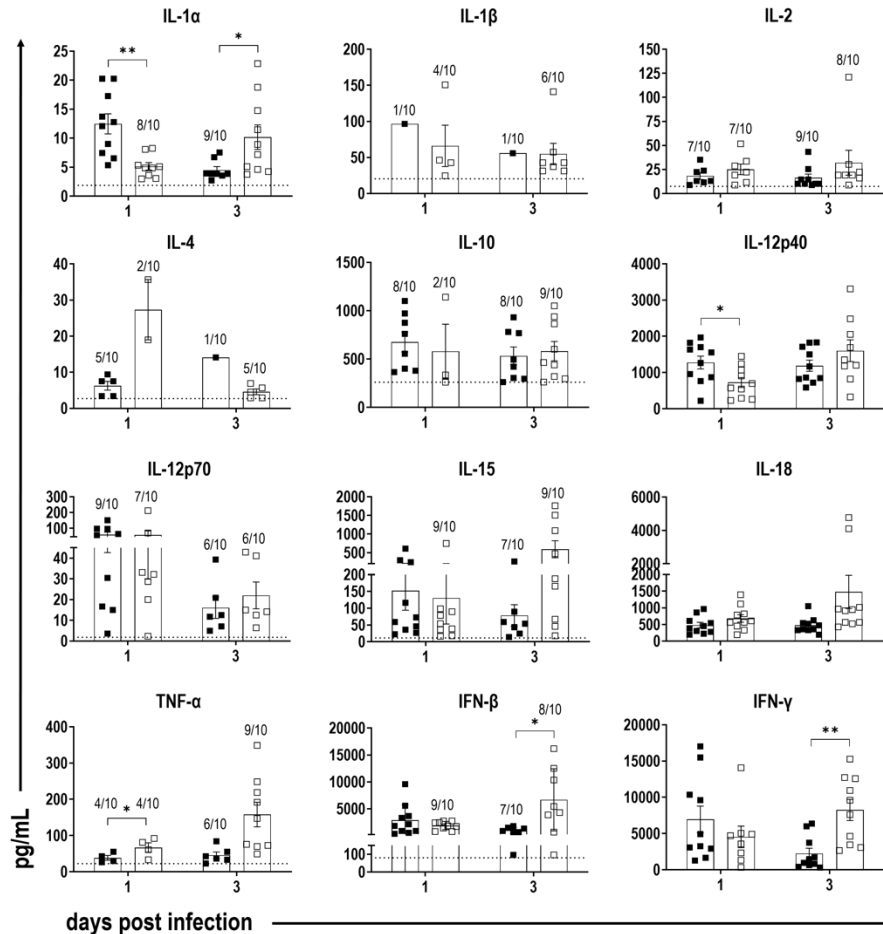
Figure 18 | ADAPko and wild type mice exhibit distinct differences in serum levels of NK cell activating cytokines day 1 and day 3 post *Listeria monocytogenes* infection. Wild type (■) and ADAPko (□) mice (age: 8-24 weeks) were infected i. v. with 2.5×10^4 CFU *Lm* and sacrificed at the indicated times post infection. Blood was obtained by puncture of the heart, after centrifugation the supernatant was collected. Cytokine concentration (pg/mL) in serum of *Lm* infected mice was analyzed via a flow cytometry-based multi-analyte assay (custom mouse panel). Summary plots present the average concentration of the analytes calculated from two replicates. Data are depicted as mean ± SEM for n = 5-10 individually analyzed mice per group out of two independent experiments. Horizontal dotted lines show the limit of detection. Protein concentrations under the detection line were considered undetectable and hence were not included into statistics; numbers represent the detectable samples out of the total number of samples, if not stated otherwise all samples were detectable. Statistical analyses were performed using two-tailed, unpaired *t*-test with Welch's correction (*p < 0.05, **p < 0.01). Modified figure has already been published as a Supplement figure in reference [220].

To further validate serum cytokine data on the transcriptional level, quantitative gene expression analyses for the major NK cell activating cytokines were performed in splenocytes obtained from mice 1 and 3 days post *Lm*-infection.

As depicted in **Figure 19**, this analysis did not reveal any genotype-dependent differences with regard to mRNA expression levels in splenocytes.
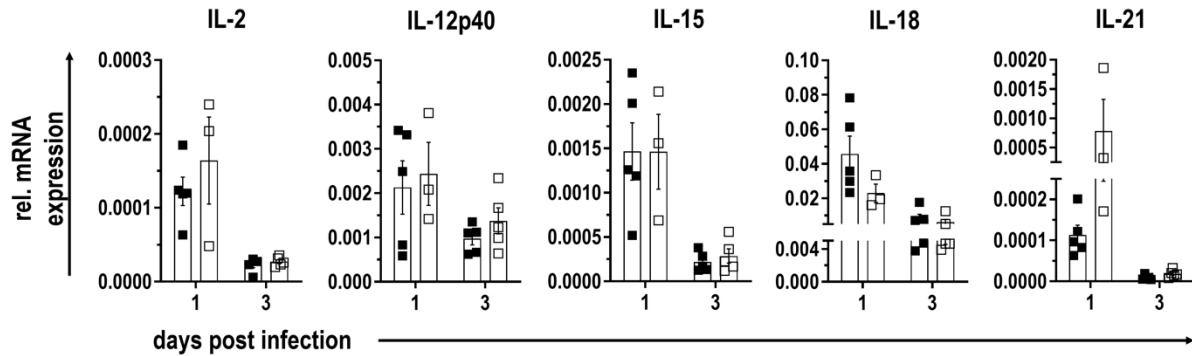
Figure 19 | Wild type and ADAPko mice exhibit equal expression levels of NK cell activating cytokines in splenocytes on day 1 and day 3 post *Listeria monocytogenes* infection. Wild type (■) and ADAPko (□) mice (age: 12-15 weeks) were infected i. v. with 2.5×10^4 CFU *Lm* and sacrificed at the indicated times post infection. Leukocytes were isolated from the spleen and subsequently re-suspended in RLT buffer. RNA was isolated from splenocytes. For cDNA synthesis RNA was transcribed, whereas cDNA was used as a template for quantitative real-time PCR. mRNA sequences were derived from ncbi gene database and intron spanning real time PCR primers were designed accordingly using the web based assay design center tool from Roche company. The relative expression of the investigated target genes was calculated with the aid of the ΔΔCt method. Quantitative RT-PCRs were run in duplicates in the LightCycler 480 system II. Shown are the relative mRNA expressions for the chemokines Il-2, Il-12p40, Il-15, Il-18 and Il-21 in wild type and ADAPko splenocytes on day 1 and day 3 post *Lm* infection normalized to the house keeping gene Rps9. Summary plots are depicted as mean ± SEM for n = 3-5 individually analyzed mice per group out of one experiment. Statistical analyses were performed using two-tailed, unpaired *t*-test with Welch's correction. Modified figure has already been published as a Supplement figure in reference [220].

Taken together, ADAPko animals did not exhibit an overall defect in mounting a pro-inflammatory cytokine response. At least in part, they even showed a more pronounced cytokine response to *Lm* infection than their wild type counterparts. This implies that the observed impaired effector function in ADAPko NK cells is not the consequence of their insufficient priming in the ADAP-deficient animals, but is more likely an intrinsic effect due to ADAP-deficiency in the NK cells itself.

4.1.2 *Morphology, vesicle distribution and the overall pattern of protein abundances is not affected in NK cells deficient for ADAP during Lm infection*

The stimulation of splenocytes with YAC-1 target cells uncovered an unequivocal role of ADAP in the degranulation of NK cells. Since it has been reported that ADAP-deficiency impairs the translocation of the microtubule-organizing center (MTOC) following T cell activation[228], we next analyzed whether ADAP-deficiency would equally affect NK cell morphology, microtubule network structures and distribution of vesicles. To this end, NK1.1$^+$ NK cells were FACS-sorted from the spleen of wild type and ADAPko mice 1 day post *Lm* infection and analyzed by confocal light microscopy without any further *in vitro* stimulation.

As illustrated in **Figure 20 A**, NK cells showed a well-structured and genotype-independent microtubule network with single microtubules originating from the MTOC, indicated with a white arrow. Remarkably, the staining for CD107a identified CD107a$^+$ vesicles (colored in green) spread in the periphery of the MTOC, as well as the α-tubulin itself (colored in red), but with no observable alterations in NK cells from wild type and ADAPko mice. Additionally, the quantification of the polarized MTOC-oriented CD107a distribution in NK cells from *Lm* infected mice did not reveal any differences (**Figure 20 B**). For both genotypes around 65 % to approximately 90 % of the sorted NK cells exhibited a MTOC-oriented distribution of CD107a (wild type: 75.2 ± 4.0 %, ADAPko: 75.0 ± 5.4 %). Analogously, NK cells from naïve wild type and ADAPko mice showed no differences in CD107a distribution (data not shown). Thus, the *ex vivo* analysis of NK cells at an early phase of *Lm* infection did not uncover obvious ADAP-dependent differences regarding the cellular morphology as well as the localization of CD107a in vesicle-like structures.

In order to identify potential ADAP-dependent alterations of infected and naïve wild type and ADAPko mice, the molecular phenotyping was extended by NK cell proteome profiling by unbiased high-resolution mass spectrometry. For this purpose, splenic NK cells from wild type as well as ADAPko mice were isolated on day 1 post *Lm* infection and analyzed without further stimulation in comparison to NK cells from naïve wild type and ADAPko mice. This was done using a label-free quantitative proteomics approach (LC-MS). The box plots are showing the distribution of abundances ($\log_{10}$) of all proteins detected in each individual sample. The numbers of the detected proteins in each single sample are given in red in the top of the respective plots. In total, the relative abundance of 4.131 proteins was quantified in NK cells. Within the individual samples of wild type and ADAPko mice, 3.365-3.705 proteins were identified that showed a normal distribution in protein abundances, indicating the robustness of the analytical workflow (**Figure 20 C**). Of note, the obtained data did not distinguish wild type from ADAPko mice rather than separated the abundances of detectable proteins into infected and non-infected mice.
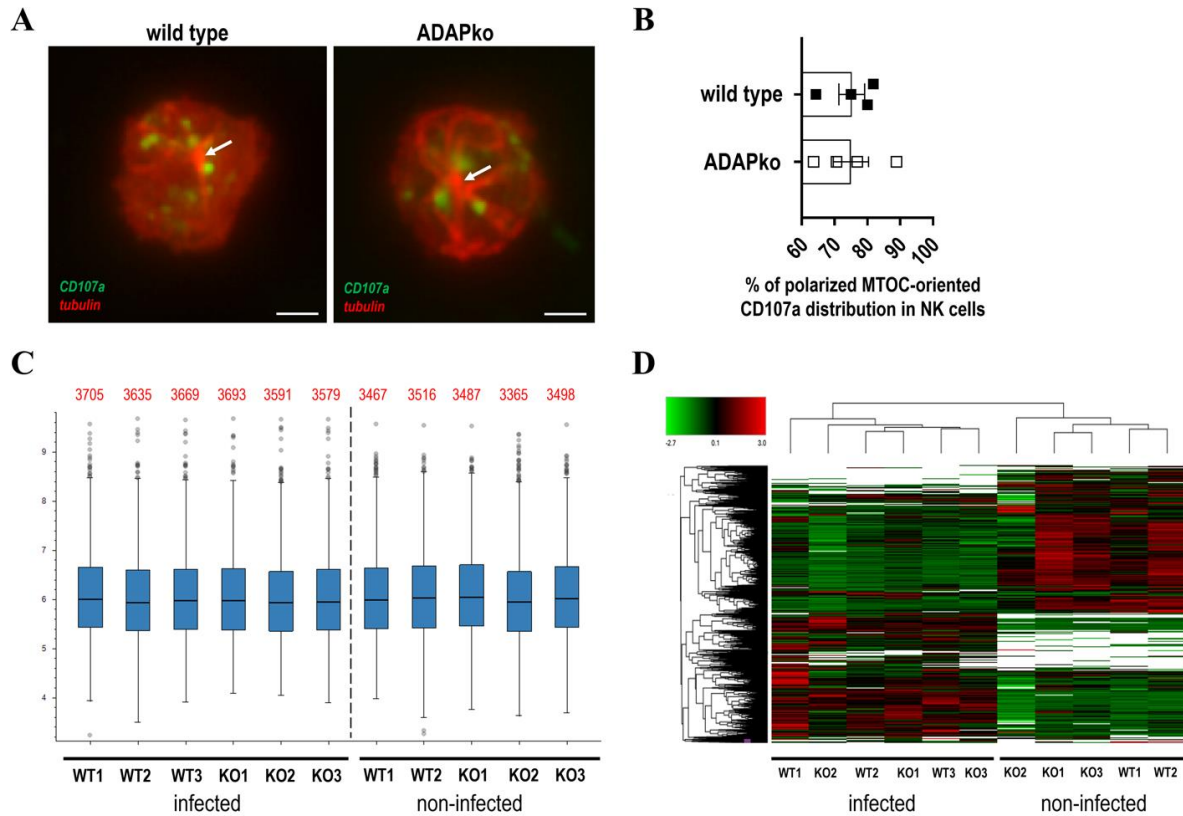
Figure 20 | Similar distribution of CD107a and proteomic characterization of naïve and *Listeria monocytogenes* infection-primed NK cells in wild type and ADAPko mice. Wild type (WT; ■) and ADAPko (KO; □) mice (age: 11-17 weeks) were either infected i. v. with 2.5×10^4 CFU *Lm* or left untreated (uninfected control mice, day 0) and were sacrificed one day post infection. Leukocytes were isolated from the spleen. **(A-B)** Flow cytometry sorted splenic NK cells were gated as alive singlets stained CD3$^-$NK1.1$^+$ cells. Sorted NK cells were prepared for microscopy or mass spectrometry. **(A)** NK cells were seeded onto poly-L-lysine coated coverslips and stained for CD107a (green) and α-tubulin (red). Representative images of NK cells from *Lm* infected mice are given as stacked images. Scale bars are 2 μm. **(B)** Quantification of CD107a distribution toward the MTOC in wild type and ADAPko in NK cells from *Lm* infected mice (n = 4; up to 25 cells per animal were analyzed). **(C-D)** Flow cytometry sorted splenic NK cells were gated as alive singlets stained CD3$^-$NK1.1$^+$ cells. Sorted NK cells were lysed and analyzed by high-resolution mass spectrometry after tryptic digestion. **(C)** Box plots showing the distribution of abundances (log$_{10}$) of all proteins detected in each sample. Numbers of detected proteins in each single sample are given in red. Wild type n = 5, ADAPko n = 6. **(D)** Cluster analysis by using Proteome Discoverer™ revealing two main clusters, i.e. infected mice and non-infected mice. The color code is showing the relative enrichment of proteins; green: less present, red: more present. The different proteins were clustered on the basis of the color code pattern. Modified figure has already been published, partially as a Supplement figure, in reference [220]. Note: In cooperation with Prof. Lothar Jänsch and Dr. M. van Ham (Helmholtz Centre for Infection Research Braunschweig, Research Group Cellular Proteomics).

Moreover, computational clustering analysis of the total NK cell proteomes distinguished again NK cells from infected and non-infected mice, but did not discriminate between NK cells from wild type and ADAPko mice, as indicated by the color code showing the relative enrichment of the proteins (**Figure 20 D**).

To next address whether the overall pattern of protein abundances in NK cells differs in wild type compared to ADAPko mice, flow cytometry sorted splenic NK cells were analyzed by high-resolution mass spectrometry. The scatter plots in **Figure 21 A** summarize the mean abundances (log$_{10}$) of all detected NK cell proteins and selected proteins that are associated with NK cell function are highlighted in colored circles and squares. Dot plots presented in **Figure 21 A** depict the absolute abundances of eight selected NK cell proteins for each individually analyzed mouse for all four experimental conditions.
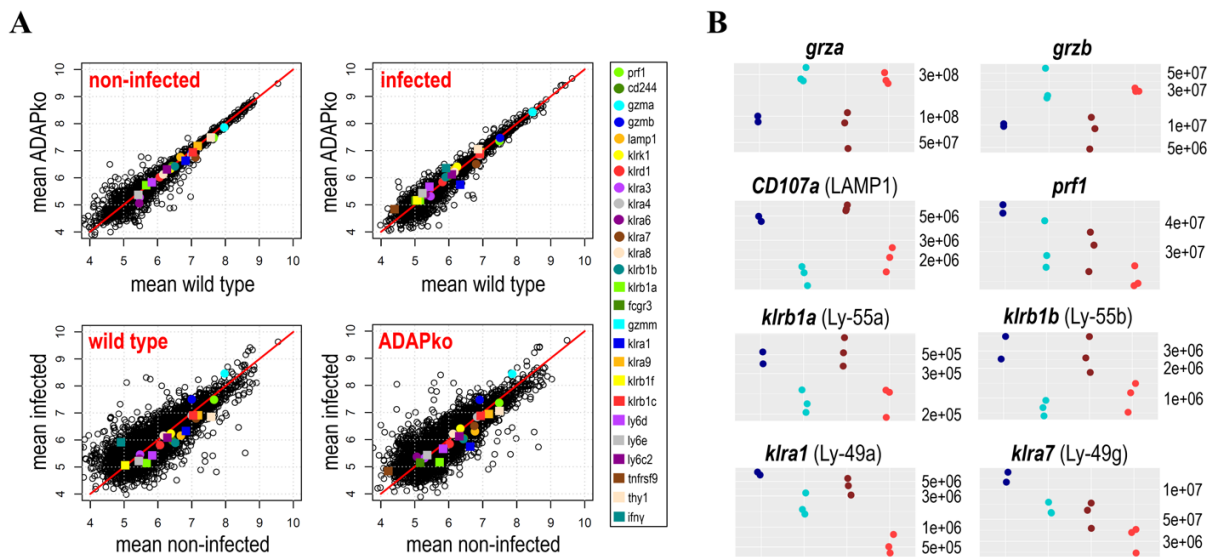
Figure 21 | Global NK cell protein composition is similar in naïve and *Listeria monocytogenes* infection-primed NK cells in wild type and ADAPko mice. Wild type and ADAPko mice (age: 11-17 weeks) were either infected i. v. with 2.5×10^4 CFU *Lm* or left untreated (uninfected control mice; non-infected, day 0) and were sacrificed at the indicated times post infection. Leukocytes were isolated from the spleen. Flow cytometry sorted splenic NK cells were gated as alive singlets stained CD3$^-$NK1.1$^+$ cells. Sorted NK cells were prepared for mass spectrometry. NK cells were lysed and analyzed by high-resolution mass spectrometry after tryptic digestion. **(A)** Scatter plots depicting mean log$_{10}$ abundances (n = 3; for wild type day 0: n = 2) of all detected proteins (circles and squares) and selected NK cell proteins are marked in colors (color code given in the right panel). **(B)** Dot plots depicting absolute abundances of selected NK cell proteins for each individual mouse in all four conditions (■ wild type non-infected, ■ wild type infected, ■ ADAPko non-infected, ■ ADAPko infected). Modified figure has already been published in reference [220]. Note: In cooperation with Prof. Lothar Jänsch and Dr. M. van Ham (Helmholtz Centre for Infection Research Braunschweig, Research Group Cellular Proteomics).

As demonstrated in **Figure 21 A** (top panel), computational cluster analysis of total NK cell proteomes clearly discriminated NK cells from infected and non-infected mice, but did not differentiate between NK cells from wild type and ADAPko mice. Besides this, it presents the variation of NK cell proteins from infected *versus* non-infected mice in the two different genotypes (lower panel). As depicted in **Figure 21 A**, the comparison of protein abundancies revealed higher variation in NK cells from infected *versus* non-infected mice (lower panel).

This definitively underscores that the infection-related *in vivo* priming of NK cells, but not the presence or absence of ADAP, is decisive for the global changes observed in the proteome composition of NK cells (lower panel). This was the case for a number of NK cell proteins that were identified with a comparable abundance in NK cells from naïve wild type and ADAPko mice (**Figure 21 B**). For instance, the abundance of granzyme A (grza) and grzb in NK cells increased after *Lm* infection, but to the same extend in both genotypes. Other proteins related to NK cell functions including CD107a, perforin and the Killer cell lectin-like receptor (KLR) subfamily members Ly-49a, Ly-49g, Ly-55a and Ly-55b were less abundant in NK cells from infected mice, this was however as well independent of the genotype (**Figure 21 B**).

Taken together, unbiased *ex vivo* proteome profiling of splenic naïve and infection-primed NK cells clearly revealed *in vivo* responsiveness of NK cells to the infection but did not uncover any obvious ADAP-dependent alterations in the effector molecule inventory involved in this process.

4.1.3 *NK cell migration, but not IL-10 production, is dependent on ADAP during Lm infection*

Since the proteome analyses of naïve and infection-primed splenic NK cells did not uncover obvious global ADAP-dependent alterations in the effector molecule inventory, the question raised, if and how ADAP-deficiency in NK cells would affect the overall course of *Listeria monocytogenes* infection. To rule out effects of ADAP-deficiency in immune cells other than NK cells, conditional knockout mice (ADAP$^{fl/fl}$ × NKp46-Cre^{het}) were used that lack ADAP specifically in NK cells. Importantly, the maturation of NK cells in the bone marrow and the distribution of mature NK cells in the spleen and peripheral blood were shown before to be normal in these mice[53].

To get a first impression regarding the role of ADAP in NK cells for the immune response towards *Lm*, conditional ADAPko mice and littermate controls were infected with a sublethal dose of *Lm*, followed by monitoring of the body weight loss as an indicator for disease severity. Strikingly, as depicted in **Figure 22 A**, the conditional ADAPko mice lost significantly more weight from day 2 until day 5 post *Lm* infection (day 2 p. i.: 93.6 ± 1.0 %; day 5 p. i.: 89.4 ± 3.0 %) compared to the littermates (day 2 p. i.: 96.7 ± 0.8 %; day 5 p. i.: 98.8 ± 1.4 %). At the chosen infection dose, none of the mice succumbed to the infection (data not shown). Taken

together, these data gave a first hint that ADAP in NK cells might be involved in the regulation of inflammatory pathways especially during the early innate immune response towards *Lm*.
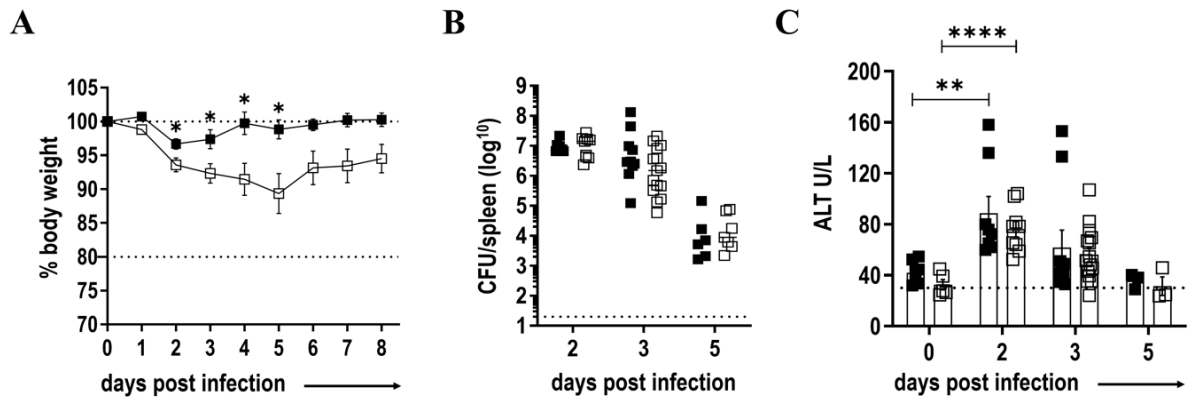
Figure 22 | Enhanced susceptibility of conditional ADAPko mice to *Listeria monocytogenes* infection is not associated with altered bacterial burden in the spleen. ADAP$^{fl/fl}$ × NKp46-Cre^{het} (□) mice (age: 10-24 weeks) lacking ADAP specifically in NK cells and respective littermate controls (ADAP$^{wt/wt}$ × NKp46-Cre^{het}, ■) were either infected i. v. with **(A)** 5×10^4 CFU or **(B, C)** 2.5×10^4 CFU *Lm* or left untreated (uninfected control mice, day 0) and were sacrificed at the indicated times post infection. **(A)** Body weight loss of ADAP$^{wt/wt}$ × NKp46-Cre^{het} control and conditional ADAP$^{fl/fl}$ × NKp46-Cre^{het} mice during the course of *Lm* infection over a period of 8 days. **(B)** CFU was quantified in the spleen as a measure for the bacterial load. **(C)** Serum ALT levels were determined. The dashed line indicates the threshold of $30 \text{ IU} \times \text{L}^{-1}$. Levels higher than this are considered elevated and indicative of a liver damage. Data are depicted as mean ± SEM for n = 6-15 individually analyzed mice per group out of three independent experiments. Statistical analyses were performed using two-tailed, unpaired *t*-test with Welch's correction (*p < 0.05, **p < 0.01, ****p < 0.0001). Parts of the modified figure have already been published in reference [220].

Given the aforementioned finding of an enhanced susceptibility of conditional ADAPko mice to *Lm* infection, we next evaluated their capacity to control bacterial growth at the site of *Lm* infection. For this purpose, spleens from both genotypes were collected at the indicated times post *Lm* infection. The organ homogenates were plated on BHI agar plates and the bacterial burden was determined after 24 h incubation. As presented in **Figure 22 B**, the bacterial load was identical in both genotypes during the course of *Lm* infection indicating that ADAP-deficiency in NK cell does not affect anti-bacterial immunity.

Since impaired pathogen control was excluded as underlying mechanism for enhanced disease severity in conditional ADAPko mice, serum alanine aminotransferase (ALT) levels as a reliable clinical biomarker indicative for liver damage were quantified. To this end, cardiac blood of Listeria-infected conditional ADAPko and wild type mice was collected from naïve mice (day 0) as well as on day 2, 3 and 5 post infection and the ALT level in the serum was determined. As depicted in **Figure 22 C**, ALT serum levels were equally low in the absence of infection (day 0) in both genotypes (wild type: 42.1 ± 3.5 IU/mL, cond. ADAPko: 32.6 ±

4.0 IU/mL). While the ALT levels significantly increased from day 0 to day 2 post infection (wild type: 88.6 ± 13.1 IU/mL, cond. ADAPko: 76.1 ± 6.0 IU/mL) in both genotypes, no statistically significant differences were observed between wild type and conditional ADAPko mice. Five days post infection the ALT concentration went back to baseline level in both genotypes (wild type: 36.0 ± 3.5 IU/mL, cond. ADAPko: 31.4 ± 7.2 IU/mL). Together, this analysis did as well not reveal an explanation for the increased disease severity in conditional ADAPko mice following Listeria infection.

It is well-known that *Lm* infection is accompanied by the expression of a plethora of pro- and anti-inflammatory cytokines[229,230]. Cytokines such as TNF-α[229] and IFN-γ[229,231] are described to play a central role in protective immunity against a *Lm* infection. In contrast, IL-10 was shown to have a detrimental role in listeriosis[232]. The downstream consequences of IL-10 expression differ depending on the phase of infection the cytokine is secreted[229]. Potential differences in the serum concentrations of these cytokines during *Lm* infection in wild type and conditional ADAPko mice might hint at potential changes in the inflammatory response and thus might help explaining the enhanced disease severity in mice lacking ADAP in NK cells. Thus, serum cytokines were analyzed by flow cytometry-based multi-analyte assay (custom mouse panel, **Figure 23**).

While for most individually analyzed mice IL-1β and IL-10 serum concentrations remained under the detection limit up to day 3 post *Lm* infection, TNF-α (day 2 p. i. wild type: 51.2 ± 4.3 pg/mL, cond. ADAPko: 54.7 ± 11.7 pg/mL; day 3 p. i. wild type: 70.3 ± 21.3 pg/mL, cond. ADAPko: 62.1 ± 6.1 pg/mL) and IL-1α (day 2 p. i. wild type: 8.6 ± 1.7 pg/mL, cond. ADAPko: 10.3 ± 2.7 pg/mL; day 3 p. i. wild type: 18.3 ± 6.4 pg/mL, cond. ADAPko: 30.0 ± 5.4 pg/mL) concentrations slightly rose over time (**Figure 23**). This was however independent of ADAP expression in NK cells. Moreover, while the serum concentration of IFN-β (wild type: 2846.1 ± 1356.5 pg/mL, cond. ADAPko: 1140.4 ± 279.1 pg/mL) and IFN-γ (wild type: 16329.5 ± 2549.7 pg/mL, cond. ADAPko: 17667.1 ± 4212.3 pg/mL) were comparable on day 2 post infection in conditional ADAP-deficient and wild type mice, conditional ADAPko mice exhibited significantly higher levels of IFN-β (wild type: 1082.5 ± 132.0 pg/mL, cond. ADAPko: 2484.0 ± 471.3 pg/mL) compared to the wild type counterparts on day 3 post *Lm* infection. This ADAP-dependent difference was not observed for IFN-γ serum levels, which declined equally in both genotypes after a peak on day 2 post infection. For IL-2, IL-4,

IL12p40, IL12p70 IL-15 and IL-18 no statistically significant genotype-dependent differences were found (data not shown). Of note, IL-21 was not detectable (data not shown).
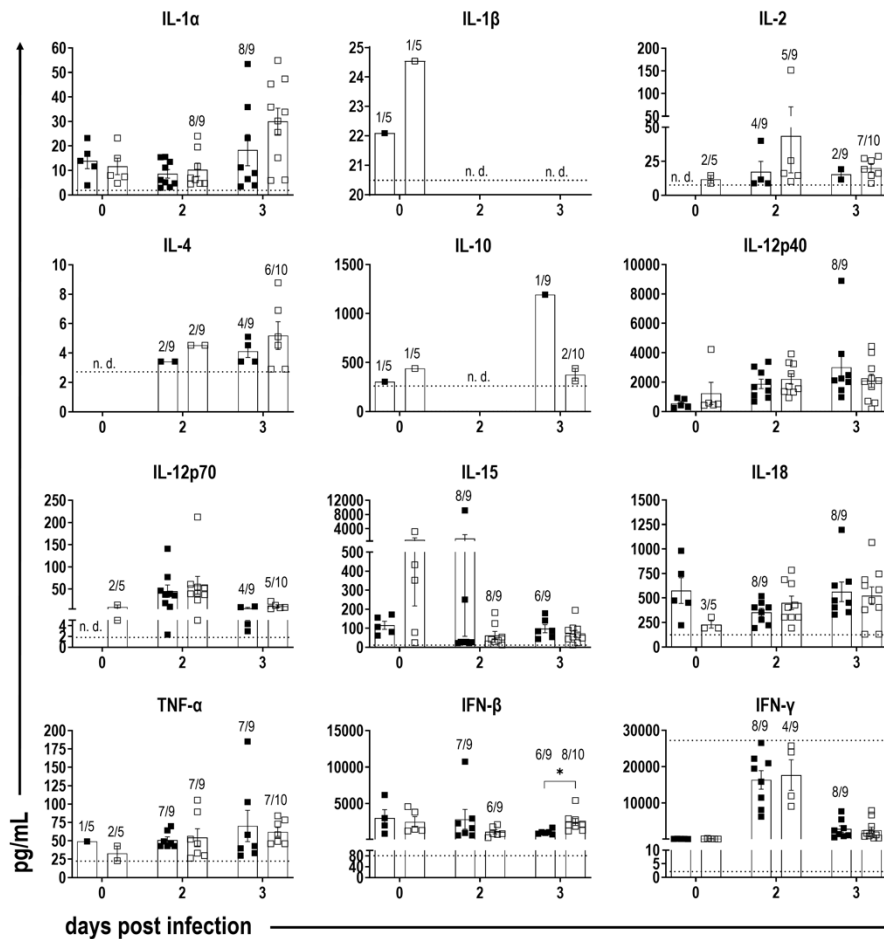
Figure 23 | Conditional ADAPko and wild type mice exhibit equivalent serum levels of NK cell activating cytokines on day 1 and day 3 post *Listeria monocytogenes* infection as well as in an naïve state. ADAP$^{fl/fl}$ × NKp46-Cre^{het} (□) mice (age: 10-24 weeks) lacking ADAP specifically in NK cells and respective littermate controls (ADAP$^{wt/wt}$ × NKp46-Cre^{het}, ■) were either infected i. v. with $2.5 × 10^4$ CFU *Lm* or were left untreated (uninfected control, day 0) and were sacrificed at the indicated times post infection. Blood was obtained by puncture of the heart, after centrifugation the supernatant was collected. Cytokine concentration (pg/mL) in serum of *Lm* infected mice was analyzed via a flow cytometry-based multi-analyte assay (custom mouse panel). Summary plots present the average concentration of the analytes calculated from two replicates. Data are depicted as mean ± SEM for n = 5-10 individually analyzed mice per group out of three independent experiments. Horizontal dotted lines show the limit of detection. Protein concentrations under the detection line were considered undetectable and hence were not included into statistics; numbers represent the detectable samples out of the total number of samples, if not stated otherwise all samples were detectable. n. d.; not detectable. Statistical analyses were performed using two-tailed, unpaired *t*-test with Welch's correction (*p < 0.05).

During the later stages of a *Lm* infection, IL-10 confers central regulatory functions[229]. Since it has been recently shown, that IL-10 produced by NK cells enhances the susceptibility of mice to *Lm* infection[136] the question raised whether ADAP-deficiency would affect the

capacity of NK cells to produce IL-10. To experimentally address this, $ADAP^{fl/fl} \times$ NKp46-Cre^{het} and respective littermates were either infected or were left untreated, leukocytes were isolated from the spleen and the liver, and afterwards cells were re-stimulated, intracellularly stained for IL-10 and analyzed by flow cytometry.

As depicted in **Figure 24**, NK cells from the spleen (wild type: 0.02 ± 0.01 %, cond. ADAPko: 0.01 ± 0.006 %) and the liver (wild type: 0.8 ± 0.3 %, cond. ADAPko: 0.4 ± 0.05 %) of naïve mice did not produce relevant amounts of IL-10 (**Figure 24 A**, **B** and **C**).

A
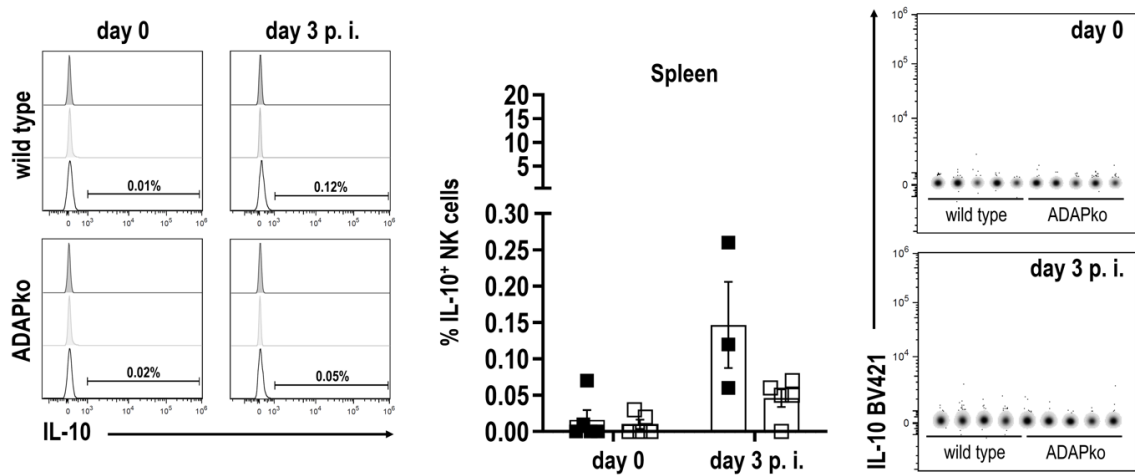
B
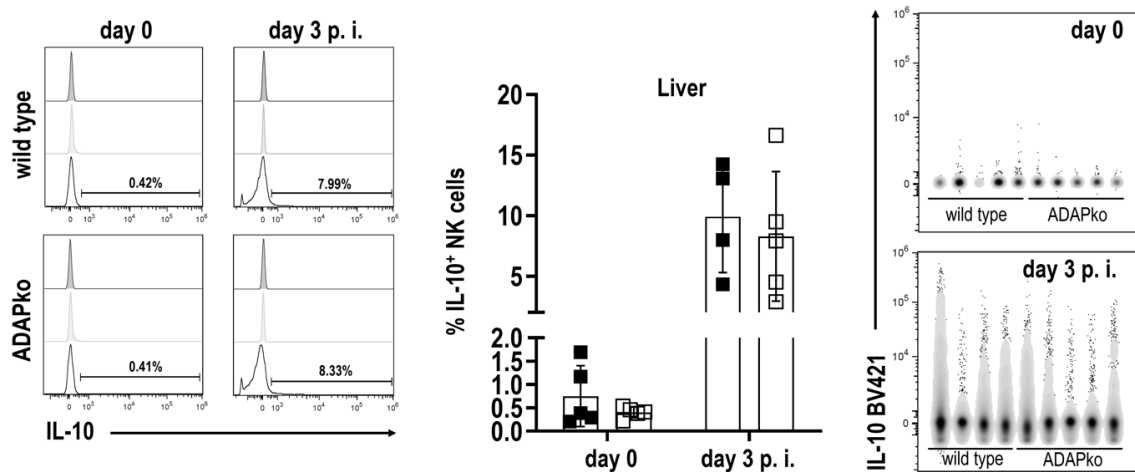
Figure 24 | IL-10 production by NK cells from conditional ADAPko mice after *Listeria monocytogenes* infection is independent of ADAP. $ADAP^{fl/fl} \times$ NKp46-Cre^{het} (□) mice (age: 12-20 weeks) lacking ADAP specifically in NK cells and respective littermate controls ($ADAP^{wt/wt} \times$ NKp46-Cre^{het}, ■) were either infected i. v. with 2.5×10^4 CFU *Lm* or were left untreated (uninfected control, day 0) and were sacrificed at the indicated times post infection. Leukocytes were isolated from the spleen and the liver. Subsequently cells were re-stimulated *in vitro* with PMA/ionomycin for 4 h. After 1 h brefeldin A and Monensin were added. Flow cytometry analyzed splenic and hepatic NK cells were gated as alive singlets stained $Lin^-CD3^-NK1.1^+NKp46^+$ cells. Negative cells

| **75**

were defined with the corresponding FMO for IL-10 whereas positive cells were gated. Representative histograms (left panels) are shown for **(A)** splenic and **(B)** hepatic CD3$^-$NK1.1$^+$NKp46$^+$ IL-10 producing NK cells (■ respective stained fluorescence minus one control, ▦ unstained and untreated, □ stained) whereas numbers represent percentage of positive NK cells on day 0 (female mice) and day 3 post *Lm* infection. Summary plots show percentage of IL-10 producing NK cells (middle panel) in **(A)** spleen and **(B)** liver. Data are presented as mean ± SEM for n = 4-5 individually analyzed mice per group out of one experiment. Data were constrained to alive singlet NK cells and are shown in columns side-by-side in a concatenated qualitative dot plot (right panels) in which each column represents data of an individual mouse. Statistical analyses were performed using two-tailed, unpaired *t*-test with Welch's correction. Parts of the modified figure have already been published in reference [220].

Three days post *Lm* infection, the IL-10 production in NK cells was induced in both organs, however this was independent of the genotype (spleen: wild type: 0.2 ± 0.06 %, cond. ADAPko: 0.05 ± 0.01 %; liver: wild type: 10.0 ± 2.3 %, cond. ADAPko: 8.3 ± 2.4 %). Of note, there was generally a stronger increase in the percentage of IL-10$^+$ NK cells in the liver.

Together, these data largely excluded the possibility that the enhanced morbidity of conditional ADAPko mice lacking ADAP in NK cells (**Figure 22**) was due to an altered IL-10 production by ADAP-deficient NK cells.

We next asked whether ADAP-deficiency in NK cells would affect their recruitment to sites of infection. To this end, a closer look was taken to the absolute number of the NK cells in spleen and liver of *Lm* infected mice. For the calculation of the absolute NK cell numbers during the course of *Lm* infection leukocytes where isolated from the organs, stained for different specific cell markers and the frequency was than quantified by flow cytometry. As depicted in **Figure 25 A** and **B**, ADAP-deficiency exclusively in NK cells was accompanied by a significant reduction in absolute NK cell numbers in the spleen and in the liver post *Lm* infection.
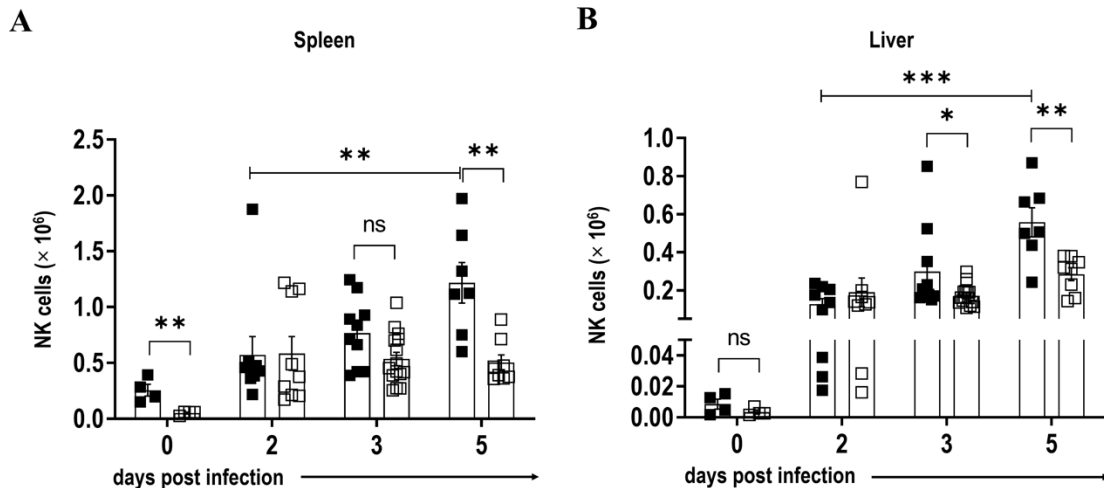
Figure 25 | Reduced accumulation of ADAP-deficient NK cells in the spleen and the liver of *Listeria monocytogenes* infected conditional ADAPko mice. ADAP$^{fl/fl}$ × NKp46-Cre^{het} (□) mice (age: 10-24 weeks) lacking ADAP specifically in NK cells and respective littermate controls (ADAP$^{wt/wt}$ × NKp46-Cre^{het}, ■) were either infected i. v. with $2.5 × 10^4$ CFU *Lm* or left untreated (uninfected control mice, day 0) and were sacrificed at the indicated times post infection. Leukocytes were isolated from **(A)** the spleen and **(B)** the liver. **(A, B)** Flow cytometry analyzed splenic and hepatic NK cells were gated as alive singlets stained Lin$^-$CD49b$^+$NK1.1$^+$ cells. Negative cells were defined with the corresponding FMO whereas positive cells were gated. Summary plots show the absolute NK cell numbers, calculated from the NK cell frequencies assessed by flow cytometry referred to the absolute leukocyte numbers as well as the frequencies of live cells. Data are depicted as mean ± SEM for n = 4-15 individually analyzed mice per group out of three independent experiments. Statistical analyses were performed using two-tailed, unpaired *t*-test with Welch's correction (*p < 0.05, **p < 0.01, ***p < 0.001). ns; not significant. Parts of the modified figure have already been published in reference [220].

Notably, this was evident already in the spleen of naïve mice (**Figure 25 A**), but not in the liver (**Figure 25 B**). In the spleen of wild type animals the absolute number of NK cells steadily rose until day 5 post *Lm* infection, with the increase from day 2 to day 5 post infection being significant (spleen day 2 p. i.: wild type: 0.6 ± 0.2 %, day 5 p. i.: wild type: 1.2 ± 0.2 %). The same pattern was observed for the absolute NK cell number in the liver (liver day 2 p. i.: wild type: 0.1 ± 0.03 %, day 5 p. i.: wild type: 0.6 ± 0.1 %) (**Figure 25 B**). In contrast, the number of ADAPko NK cells in the spleen as well as in the liver rose to a far lesser extent, reaching the plateau already by day 2 post *Lm* infection in the spleen. In the liver, the absolute number of ADAPko NK cells remained almost the same for day 2, 3 and 5 post infection. For the liver, but not for the spleen, the conditional ADAPko mice exhibited less NK cells on day 3 post infection (spleen day 3 p. i.: wild type: 0.8 ± 0.1 %, cond. ADAPko: 0.5 ± 0.1 %; liver day 3 p. i.: wild type: 0.3 ± 0.1 %, cond. ADAPko: 0.2 ± 0.01 %). This hold true for both organs on day 5 post infection (spleen day 5 p. i.: wild type: 1.2 ± 0.2 %, cond. ADAPko: 0.5 ± 0.1 %; liver day 5 p. i.: wild type: 0.6 ± 0.1 %, cond. ADAPko: 0.3 ± 0.03 %).

Results

Taken together, there was a significantly reduced accumulation of ADAP-deficient NK cells in the spleen as well as in the liver during *L. monocytogenes* infection. This raised the question, whether this was due to an ADAP-dependent impaired migration or rather an altered NK cell maturation. Of note, flow cytometric analysis of NK cell maturation markers revealed only slight though in part significant differences in the maturation of ADAP-sufficient and -deficient NK cells in the spleen and the liver of *Lm* infected mice during the course of infection (**Figure 26** and **Figure 27**). However, the frequency of NK cells that reached the different maturation stages was the same by day 5 post *Lm* infection in the spleen and as such, impaired NK cell maturation was largely excluded as a reason for the pronounced ADAP-dependent differences in NK cell abundance in the spleen and the liver of *Lm* infected mice.
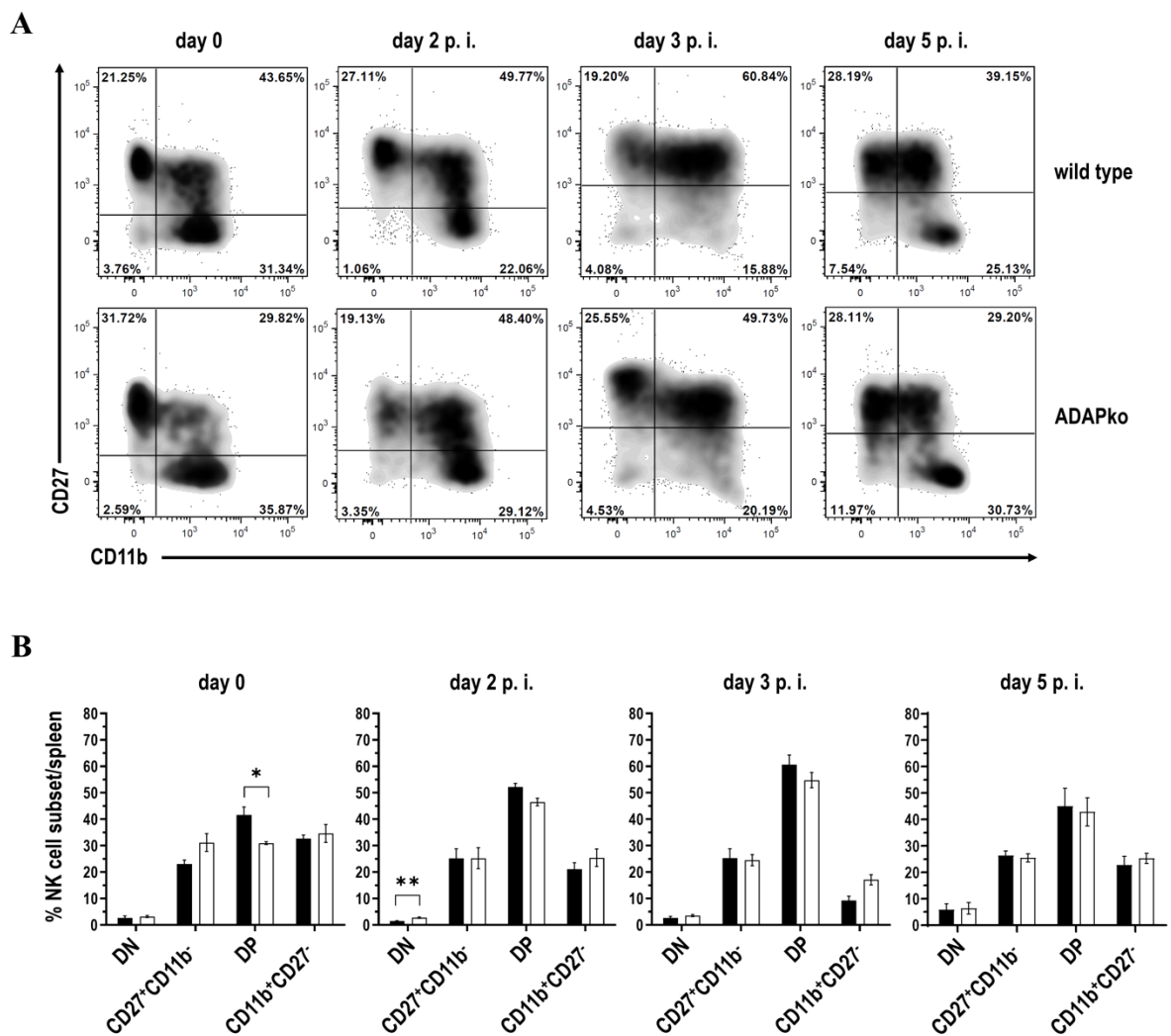
Figure 26 | ADAP-deficiency in NK cells only marginally affects NK cell maturation in spleen of *Listeria monocytogenes* infected conditional ADAPko mice. ADAP$^{fl/fl}$ × NKp46-Cre^{het} (□) mice (age: 10-24) lacking ADAP specifically in NK cells and respective littermate controls (ADAP$^{wt/wt}$ × NKp46-Cre^{het}, ■) were either

infected i. v. with 2.5×10^4 CFU *Lm* or left untreated (uninfected control mice, day 0) and were sacrificed at the indicated times post *Lm* infection. Leukocytes were isolated from the spleen. Flow cytometry analyzed splenic NK cells were gated as alive singlets stained Lin⁻CD49b⁺NK1.1⁺ cells. Negative cells were defined with the corresponding FMOs whereas positive cells were gated. For classification of the different maturation stages NK cells were stained for CD27 and CD11b. NK cell subsets are shown as double negative (DN; CD27⁻CD11b⁻), CD27⁺CD11b⁻, double positive (DP; CD27⁺CD11b⁺) and CD11b⁺CD27⁻. **(A)** Representative density dot plots with outliers showing surface expression of CD27 and CD11b and **(B)** summary plots show the percentages of NK cell subsets in the spleen. Data are depicted as mean ± SEM for n = 4-15 individually analyzed mice per group out of three independent experiments. Statistical analyses were performed using two-tailed, unpaired *t*-test with Welch's correction (*p < 0.05, **p < 0.01). Modified figure has already been published in reference [220].
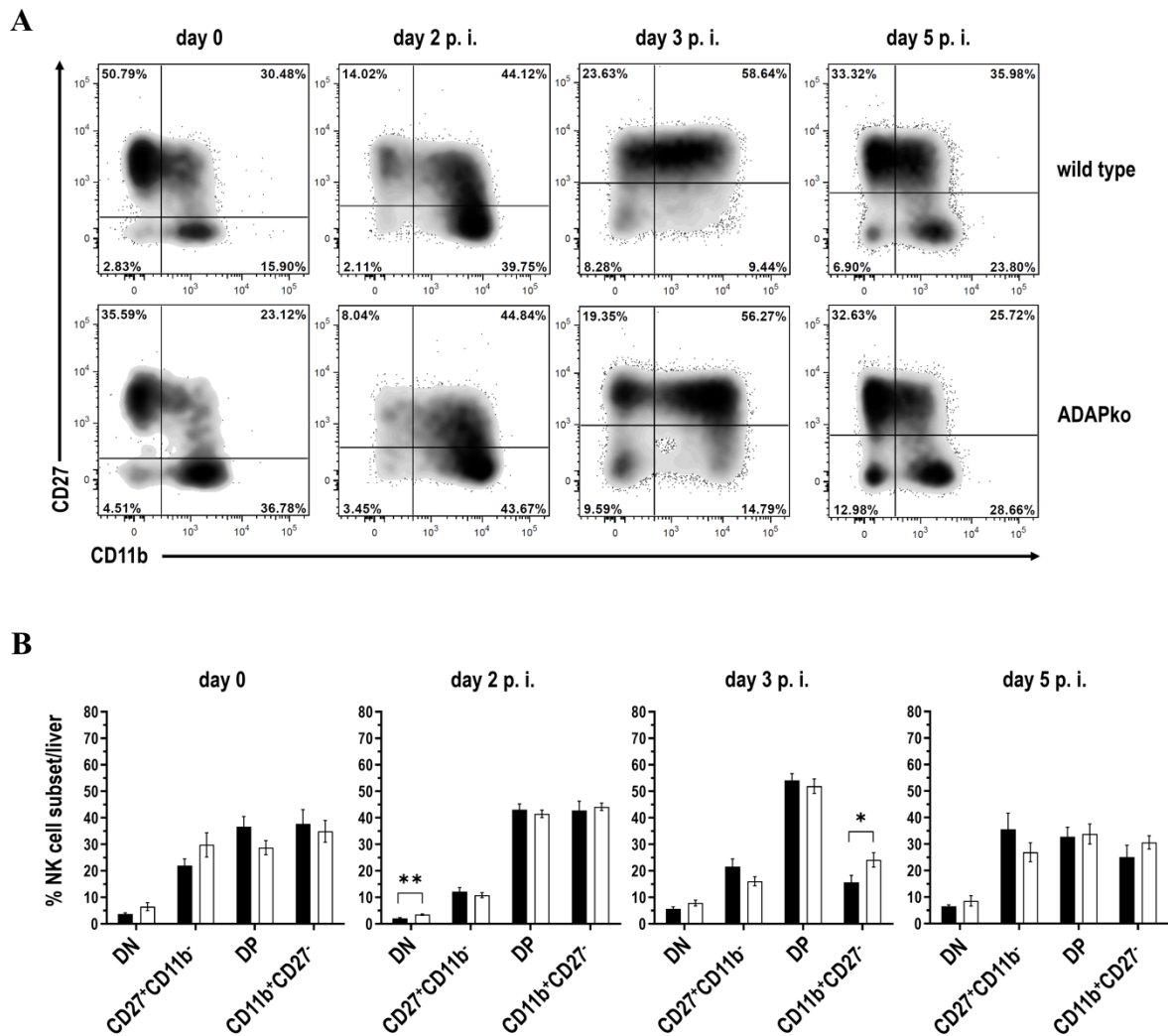
Figure 27 | ADAP-deficiency in NK cells only marginally affects NK cell maturation in liver of *Listeria monocytogenes* infected conditional ADAPko mice. ADAP^fl/fl × NKp46-Cre^het (□) mice (age: 10-24) lacking ADAP specifically in NK cells and respective littermate controls (ADAP^wt/wt × NKp46-Cre^het, ■) were either infected i. v. with 2.5×10^4 CFU *Lm* or left untreated (uninfected control mice, day 0) and were sacrificed at the indicated times post infection. Leukocytes were isolated from the liver. Flow cytometry analyzed hepatic NK cells were gated as alive singlets stained Lin⁻CD49b⁺NK1.1⁺ cells. Negative cells were defined with the corresponding FMOs whereas positive cells were gated. For classification of the different maturation stages NK cells were stained for CD27 and CD11b. NK cell subsets are shown as double negative (DN, CD27⁻CD11b⁻), CD27⁺CD11b⁻, double positive (DP, CD27⁺CD11b⁺) and CD11b⁺CD27⁻. **(A)** Representative density dot plots

with outliers showing surface expression of CD27 and CD11b and **(B)** summary plots show the percentages of NK cell subsets in the liver. Data are depicted as mean ± SEM for n = 4-15 individually analyzed mice per group out of three independent experiments. Statistical analyses were performed using two-tailed, unpaired *t*-test with Welch's correction (*p < 0.05, **p < 0.01). Modified figure has already been published in reference [220].

It has been shown before that ADAP is involved in the migration of other immune cells[11,13] and moreover, protein network analyses of NK cell proteomes identified three pathways related to cell migration that were potentially affected by ADAP-deficiency in NK cells (data not shown). Moreover, it is well-described, that the activation of integrins, upon stimulation of the T cell- or CCR7 chemokine receptor, induces inside-out signaling[42] and recent findings show that the migration of both, CD4$^+$ and CD8$^+$ T cells, is dependent on ADAP[202]. Moreover the integrin-dependent stimulation of NK cells is important for their migration and cytotoxicity[233]. Considering this, the observed phenotype (**Figure 25**) might at least in part be the outcome of an impaired migration of ADAP-deficient NK cell to sites of *Lm* infection. To experimentally address this hypothesis, *in vitro* NK cell migration assays using an artificial CXCL12 gradient were performed using splenocytes from naïve and *Lm*-infected mice 1 and 3 days after the infection.

As depicted in **Figure 28 A** the migration of naïve NK cells (day 0) from conditional ADAPko mice was indeed reduced compared to the wild type animals (wild type: 5.2 ± 0.3 %, cond. ADAPko: 3.6 ± 0.2 %).
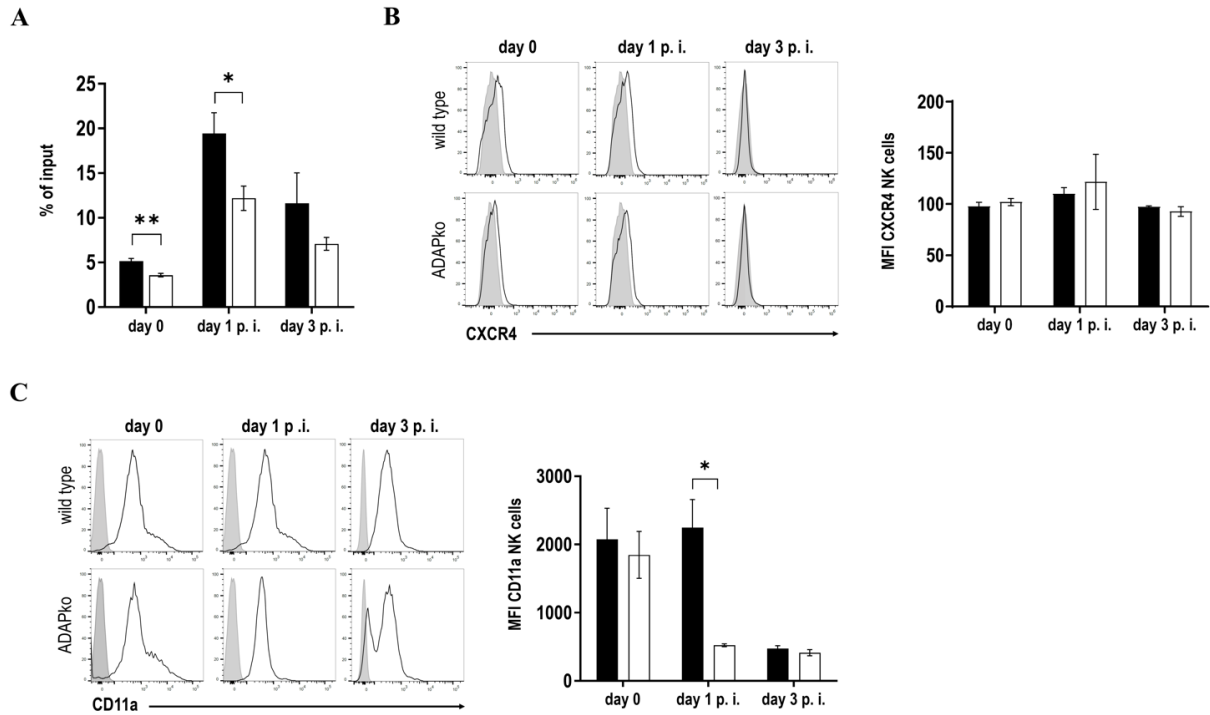
Figure 28 | Impaired migratory capacity of splenic ADAP-deficient NK cells from *Listeria monocytogenes*-infected mice. ADAP^{fl/fl} × NKp46-Cre[het] (□) mice (age: 12-20 weeks) lacking ADAP specifically in NK cells and respective littermate controls (ADAP[wt/wt] × NKp46-Cre[het], ■) were either infected i. v. with 2.5×10^4 CFU *Lm* or left untreated (uninfected control mice, day 0) and were sacrificed at the indicated times post infection. Leukocytes were isolated from the spleen. **(A)** Splenocytes were seeded in the upper transwell chamber that was placed in medium containing the chemokine CXCL12 (250 ng/mL). After 4 h cells were recovered from the lower chamber, counted and analyzed by flow cytometry to determine the percentage of migrated NK cells (% of input). **(B)** Level of CXCR4 and **(C)** CD11a surface expression on NK cells. Depicted are representative histograms (■ respective stained fluorescence minus one control FMO, □ stained) and mean fluorescence intensity (MFI) ± SEM of (B) CXCR4 and (C) CD11a on NK1.1^{+} NK cells analyzed day 0 (female mice), day 1 and day 3 post infection. Data are depicted as mean ± SEM for n = 4-5 individually analyzed mice per group out of one to two independent experiments. Statistical analyses were performed using two-tailed, unpaired *t*-test with Welch's correction (*p < 0.05, **p < 0.01, ***p < 0.001). Modified figure has already been published in reference [220]. Note: In cooperation with PD Dr. A. Reinhold and M. Sc. M. Voss (Institute of Molecular and Clinical Immunology Magdeburg).

Despite the overall increased percentage of input, similar results were observed for infection-primed NK cells day 1 post *Lm* infection (wild type: 19.4 ± 2.3 %, cond. ADAPko: 12.2 ± 1.4 %). Although not reaching statistical significance, reduced migration of ADAPko NK cells was also evident day 3 post *Lm* infection. Together and well in line with our expectation, *in vitro* NK cell migration towards a chemokine gradient was significantly impaired both in naïve

as well as in *in vivo* pre-activated ADAP-deficient NK cells. This lead to the question if the expression of the CXCL12 receptor CXCR4 on the surface of NK cells would be affected by ADAP-deficiency. As depicted in **Figure 28 B**, naïve NK cells as well as day 1 and day 3 infection-primed NK cells, did not show any ADAP-dependent differences in CXCR4 expression levels. Therefore, the reduced *in vitro* migration of ADAPko NK cells towards the NK cell attracting chemokine CXCL12 was not the consequence of altered surface expression of the CXCL12 receptor CXCR4.

The adhesion molecule LFA-1, consisting of CD18 and CD11a, interacts with its ligand ICAM on endothelial cells, promoting the entry of leukocytes into tissues. Notably, LFA-1 was shown to be important for the adhesion and migration of NK cells through the vascular endothelium[234]. Of note, the intracellular domain of CD11a is linked to the signaling complex involving the adaptor protein ADAP, at least in T cells[235,236]. Due to this, the surface expression of different integrins on NK cells was next analyzed. For this purpose, splenic NK cells from *Lm* infected wild type and conditional ADAPko mice were stained for selected integrins and analyzed by FACS. While ADAP-deficiency had no impact on the expression levels of CD18, CD29 and CD11b (**Figure 29**), a significant drop in CD11a surface expression was observed on ADAPko compared to wild type NK cells on day 1 post *Lm* infection (wild type: 2245.5 ± 413.6 %, cond. ADAPko: 523.0 ± 21.9 %) (**Figure 28 C**).
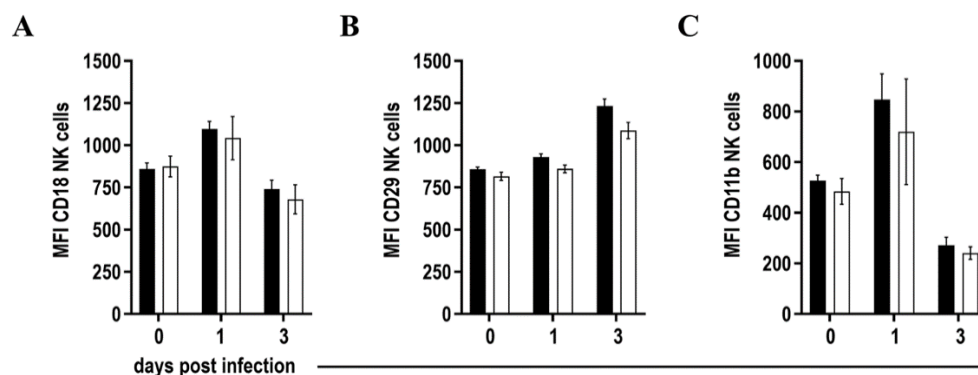
Figure 29 | ADAP-deficiency has no impact on CD18, CD29 and CD11b expression levels on NK cells in conditional ADAPko mice during *Listeria monocytogenes* infection. ADAP$^{fl/fl}$ × NKp46-Cre^{het} (□) mice (age: 12-20) lacking ADAP specifically in NK cells and respective littermate controls (ADAP$^{wt/wt}$ × NKp46-Cre^{het}, ■) were either infected i. v. with 2.5×10^4 CFU *Lm* or left untreated (uninfected control mice, day 0) and were sacrificed at the indicated times post infection. Leukocytes were isolated from the spleen. Level of **(A)** CD18, **(B)** CD29 and **(C)** CD11b surface expression on NK cells. Depicted is the mean fluorescence intensity (MFI) of (A) CD18, (B) CD29 and (C) CD11b on NK1.1$^+$ NK cells analyzed day 0 (female mice), day 1 and day 3 post *Lm* infection. Data are depicted as mean ± SEM for n = 4-5 individually analyzed mice per group out of one to two independent experiments. Statistical analyses were performed using two-tailed, unpaired *t*-test with Welch's correction. Note: In cooperation with PD Dr. A. Reinhold and M. Sc. M. Voss (Institute of Molecular and Clinical Immunology Magdeburg).

These data indicate that ADAP is crucial for efficient migration of NK cells both *in vitro* and *in vivo* and that reduced NK cell cellularity in infected tissue of conditional ADAPko mice might be, at least in part, the consequence of reduced CD11a surface expression on ADAP-deficient NK cells.

As summarized in **Figure 30**, data generated within the first part of this thesis clearly show that the *in vitro* stimulation of naïve NK cells from ADAPko mice with anti-NK1.1 alone or in combination with IL-2/IL-12 induces a normal degranulation as measured by CD107a surface expression in addition to a decreased IFN-γ production (**Figure 30**, highlighted in blue). However, ADAPko NK cells are impaired in their migration, both in a naïve state (day 0) as well as following their *in vivo* activation (day 1 p. i.) which might be the result of a decreased CD11a surface expression on these NK cells (**Figure 30**, highlighted in red). Moreover, *Lm* infection-primed NK cells exhibit reduced levels of perforin, suggesting that ADAP-deficiency negatively affects the generation and/or intracellular storage of this cytotoxic effector molecule. In addition to that, reduced CD107a expression is indicative for a potential degranulation defect in ADAP-deficient NK cells.
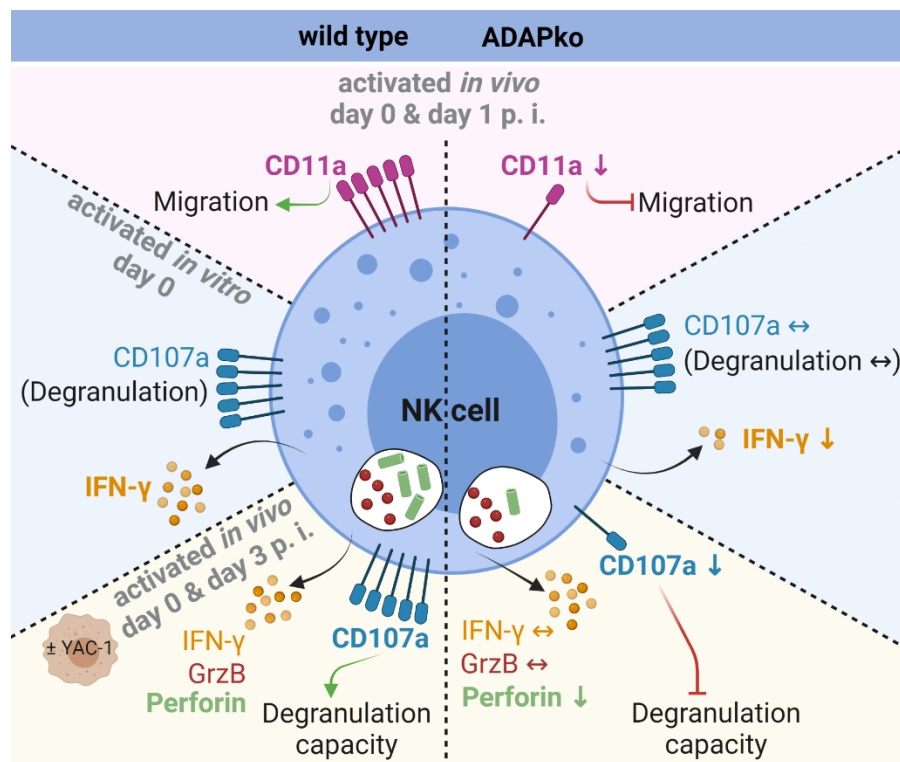
Figure 30 | Summary - NK cells. This figure summarizes major differences observed in surface marker expression (CD11a; migration, CD107a; degranulation), effector molecule inventory (perforin, granzyme B; GrzB) and IFN-γ release by NK cells from wild type (left side) *versus* ADAPko (right side) mice. Created with BioRender.com (2021).

Part 2

4.2   Role of ADAP in phagocytes during *Listeria monocytogenes* infection in mice

Note: Results from this second part of this thesis (pages 85-110) have been submitted for publication in *Frontiers in Immunology* (status: 25.06.2021):

Böning, M. A. L.; Parzmair, G. P.; Jeron, A., Düsedau, H. P.; Kershaw, O.; Xu, B.; Relja, B.; Schlüter, D.; Dunay, I. R.; Reinhold, A.; Schraven, B. and Bruder, D. Enhanced susceptibility of ADAP-deficient mice to *Listeria monocytogenes* infection is associated with altered phagocyte phenotype and function. Manuscript submitted in *Frontiers in Immunology.*

4.2.1   *Increased infiltration of neutrophils and monocytes into Lm-infected organs of ADAPko mice*

As depicted earlier in **Figure 11**, Parzmair clearly demonstrated that ADAP-deficiency renders mice highly susceptible for infection with the intracellular pathogen *Lm* and that the increased morbidity and mortality of ADAPko mice is associated with failures in pathogen control and enhanced immunopathology in the early phase of the infection compared to the wild type littermates[201]. Furthermore, an exaggerated infiltration of neutrophils and monocytes into *Lm*-infected organs of ADAPko compared to the wild type mice was shown[201]. The pronounced leukocyte aggregates in the liver of ADAPko animals observed on day 3 post *Lm* infection prompted us to have a closer look on the identity and number of leukocytes infiltrating the spleen and the liver at different times post infection. Since ADAPko mice already succumbed by day 4 post infection, innate immune cells were considered the primary targets for the following analysis. Among those cell types, neutrophils and monocytes are rapidly recruited to the sites of infection, were they are activated and exert central antibacterial functions. Therefore, the relative cell numbers of neutrophils and monocytes during the course of *Lm* infection were analyzed in spleen and liver by flow cytometry.

As depicted in **Figure 31 A** (left panel) and well in line with data described before (**Figure 11 E**), the frequency of neutrophils in the spleen of wild type mice reached the highest level 3 days post infection (wild type: 13.6 ± 1.8 %), followed by a slight decrease during the further course of *Lm* infection (day 5 p. i.: wild type: 9.8 ± 1.4 %). In contrast, the frequency of neutrophils in the spleen of ADAPko mice rose faster and remained higher compared to the wild type mice up to day 5 post *Lm* infection (day 3 p. i.: ADAPko: 20.7 ± 2.0 %, day 5 p. i.: ADAPko: 19.6 ± 1.9 %). Analogous results were obtained for the percentage of neutrophils in the liver (**Figure 31 A**, right panel). Here, the frequency of neutrophils in wild type mice rose on day 3 post infection (wild type: 11.7 ± 1.3 %) and remained quite stable until day 5 post infection (wild type: 11.5 ± 1.6 %). A similar pattern was observed in ADAPko animals where the overall frequency of neutrophils was however significantly higher than in wild type mice (day 3 p. i. ADAPko: 19.4 ± 1.9 % and day 5 p. i. ADAPko: 17.4 ± 1.2 %). Taken together, these results show that during the early phase of *Lm* infection higher numbers (**Figure 11 E**) and frequencies (**Figure 31 A**) of neutrophils are found in the spleen and liver of ADAPko mice.

Results
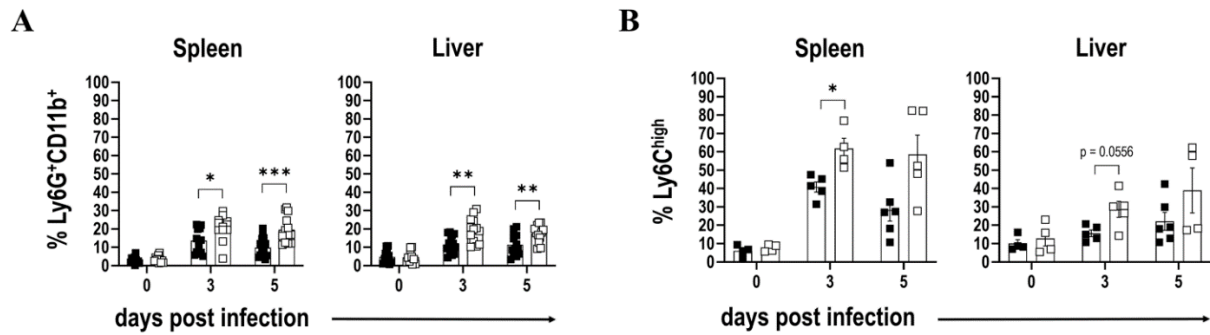
Figure 31 | Increased accumulation of neutrophils and monocytes in spleen and liver of ADAPko mice after *Listeria monocytogenes* **infection.** Wild type (■) and ADAPko (□) mice (age: 10-17 weeks) were either infected i. v. with 2.5×10^4 CFU *Lm* or left untreated (uninfected control mice, day 0) and were sacrificed at the indicated times post infection. Leukocytes were isolated from the spleen and liver. Liver tissue was digested via the gentleMACS dissociator in order to isolate liver leukocytes followed by density centrifugation with 35 % Percoll/PBS. Subsequently cells were re-stimulated *in vitro* with PMA/ionomycin for 4 h. After 1 h brefeldin A and Monensin were added. Flow cytometry analyzed **(A)** $Ly6G^+CD11b^+$ and **(B)** $CD11b^+Ly6G^-$ $CX3CR1^{low}Ly6C^{high}$ leukocytes were gated as alive singlets and stained for $CD45^+Lin^-$ cells. Negative cells were defined with the corresponding FMO whereas positive cells were gated. Data are depicted as mean ± SEM. Data shown are representative of (A) three individual experiments for n = 4-6 individually analyzed mice per group and (B) from one experiment with n = 4-6 individually analyzed mice per group. Statistical analyses were performed using unpaired, nonparametric Mann-Whitney test (*p < 0.05, **p < 0.01, ***p < 0.001). Manuscript submitted in *Frontiers in Immunology* (status: 25.06.2021).

Regarding the percentage of inflammatory monocytes in the spleen, ADAPko mice showed significantly higher frequencies of $Ly6C^{high}$ cells 3 days (wild type: 40.8 ± 2.8 %, ADAPko: 61.8 ± 5.6 %) and (in tendency) 5 days (wild type: 28.3 ± 6.0 %, ADAPko: 58.6 ± 10.6 %) post *Lm* infection (**Figure 31 B**, left panel). Of note, no significant genotype-dependent differences were observed regarding $Ly6C^{high}$ monocytes in the liver following *Lm* infection (**Figure 31 B**, right panel). In summary, these data demonstrate that throughout the early phase of *Lm* infection exaggerated numbers of neutrophils as well as inflammatory monocytes are recruited to the spleen and liver of ADAP-deficient mice. Nevertheless, despite their increased numbers (**Figure 11 E** and **Figure 31**), these phagocytes appeared to be inefficient in controlling pathogen growth in ADAPko mice early following *Lm* infection (**Figure 11 B**).

These date raised the question whether ADAP-deficiency in mice leads to a functional impairment of phagocytes and if so, whether the observed phenotype could be attributed directly to ADAP-deficiency in phagocytes or would depend on an altered activation of phagocytes in the ADAP-deficient host. To experimentally proof this, *Lm* infections were carried out in mice lacking ADAP exclusively in phagocytes ($ADAP^{fl/fl} \times LysM\text{-}Cre^{het}$; conditional ADAPko).

Strikingly, health monitoring of conditional ADAPko and littermate control mice (ADAP$^{wt/wt}$ × LysM-Cre^{het}) revealed no genotype-dependent differences with regard to the overall morbidity and mortality (**Figure 32 A**). In addition, the lack of ADAP in neutrophils and monocytes had no effect on the bacterial burden in spleen and liver of conditional ADAPko compared to control mice early during *Lm* infection (**Figure 32 B**). As expected, the histological analyzes of the spleen and the liver revealed acute and necrotizing inflammatory changes on day 3 post *Lm* infection. In more detail, the spleens showed multifocal to almost diffuse, acute and necrotizing splenitis, while the livers showed multifocal, acute and randomly distributed, necrotizing hepatitis. However, all histological changes as well as the overall degree of inflammation in spleens and livers were genotype-independent (**Figure 32 C** and **D**). In line with this, the serum ALT levels of conditional ADAPko mice were comparable to the control mice following *Lm* infection. Both genotypes reached their peak ALT level on day 3 (wild type: 46.6 ± 5.0 U/L, ADAPko: 61.7 ± 7.8 U/L) post *Lm* infection. On day 5 p. i. the level of ALT returned to normal, independent of the genotype (wild type: 30.8 ± 3.8 U/L, ADAPko: 39.5 ± 5.0 U/L). Of note, the ADAPko mice generally showed a slightly increased ALT level in the serum compared to the wild type mice, however without any statistical significance, overall indicating only minor and genotype-independent liver damage as a consequence to the infection (**Figure 32 E**).
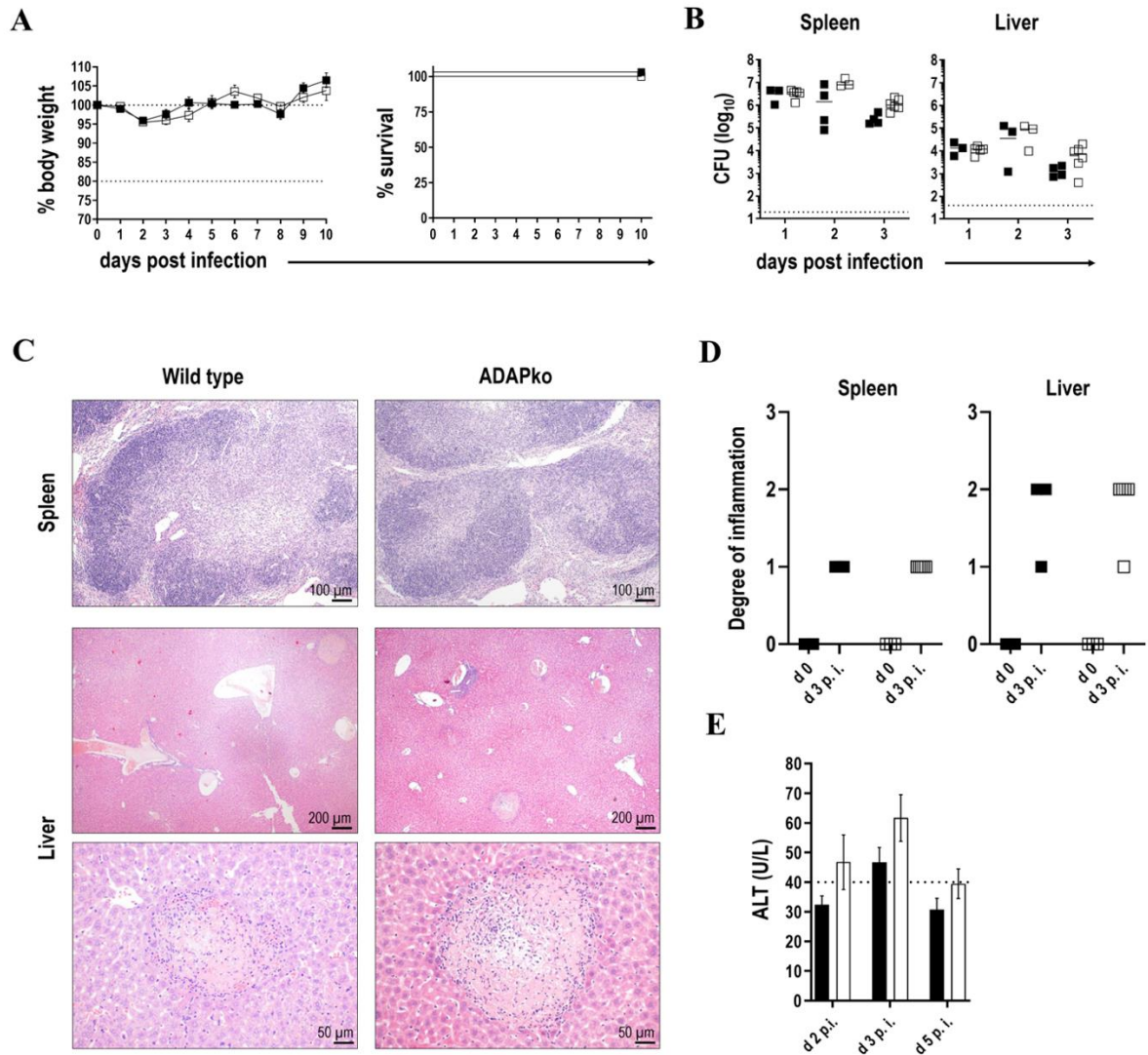
Figure 32 | Disease phenotype of conditional ADAPko mice resembles that of *Listeria monocytogenes*-infected littermate controls. ADAP$^{fl/fl}$ × LysM-Cre^{het} (□) mice (age: 9-14 weeks) lacking ADAP specifically in phagocytes and respective littermate controls (ADAP$^{wt/wt}$ × LysM-Cre^{het}, ■) were infected i. v. with (A) 1×10^5 and (B, C, D, E) 2.5×10^4 *Lm* or left untreated (uninfected control mice, day 0) and sacrificed at the indicated times post infection. **(A)** Infected mice were weighed and monitored daily and the survival was reported. Data are depicted as mean ± SEM for n = 8 individually analyzed mice per group out of two independent experiments. Statistical analyses were performed using two-way ANOVA with Bonferroni's *post hoc* test for the weight loss data and Mantel-Cox log-rank test for the survival data. **(B)** Bacterial loads in spleen and liver after *Lm* infection. The dashed line represents the limit of detection. Data are depicted as medians for n = 3-6 individually analyzed mice. Statistical analyses were performed after log$_{10}$-transformation using two-way ANOVA with Bonferroni's *post hoc* test. **(C)** H&E histology of infected spleens and livers 3 days post infection. Organs were stored in 4 mL 4 % paraformaldehyde and later sectioned for histology and analyzed by H&E staining. The black bar at the bottom right corner of each panel represents a distance of 100 µm for the spleen sections and 200 µm as well as 50 µm for the liver sections. **(D)** Scoring of degree of inflammation in spleens and livers. Data are depicted for n = 2-5. **(E)** Serum ALT levels were determined. The dashed line indicates the threshold. Levels higher than this are considered elevated and indicative of liver damage. Data are depicted as mean ± SEM for n = 3-13 individually analyzed mice per group out of at least two independent experiments. Statistical analyses were performed using two-tailed, unpaired *t*-test with Welch's correction. Note: (C) In cooperation with Prof. Achim Gruber and Dr. O. Kershaw (Department of Veterinary Medicine at the Freie Universität Berlin, Institute of Veterinary Pathology). Manuscript submitted in *Frontiers in Immunology* (status: 25.06.2021).

Additionally, serum cytokine levels in conditional ADAPko and wild type control mice following *Lm* infection was compared. Despite IFN-γ on day 3 p. i., no alterations in the cytokine response in mice lacking ADAP in phagocytes were detectable (**Figure 33**). These data clearly indicate that ADAP-deficiency in phagocytes is not sufficient to mirror the above described phenotype observed in *Lm* infected conventional ADAPko mice.
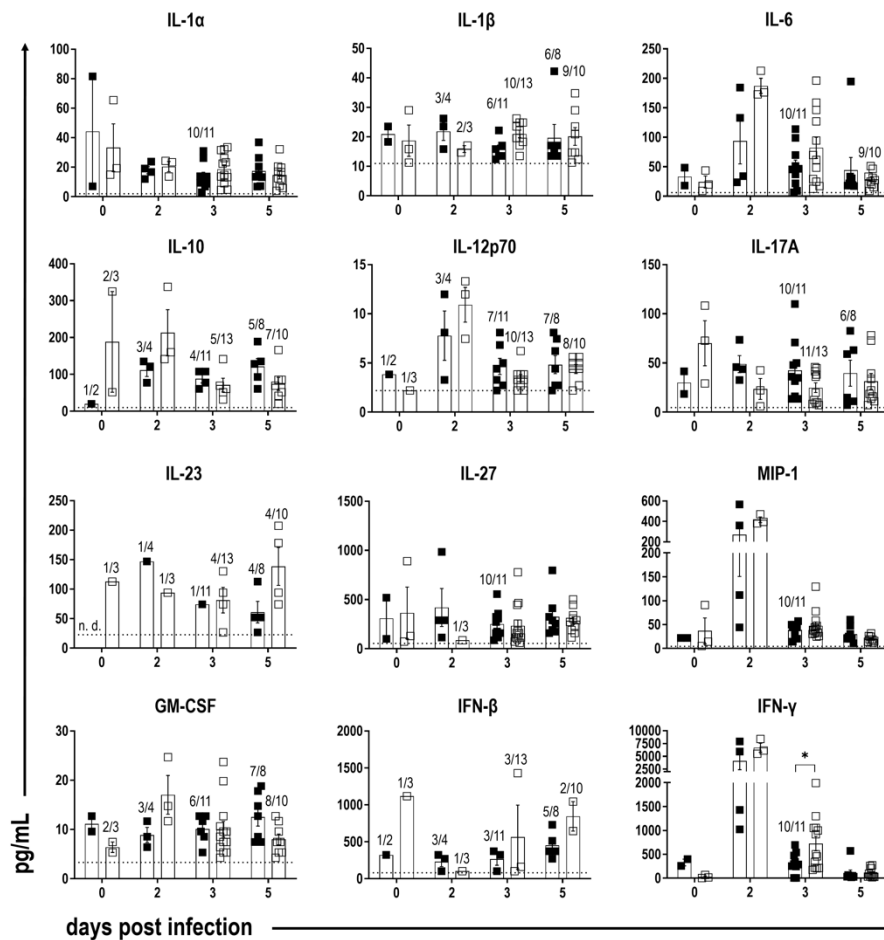
Figure 33 | Conditional ADAPko and littermate controls display similar serum cytokine profile post *Listeria monocytogenes* **infection.** ADAP$^{fl/fl}$ × LysM-Cre^{het} (□) mice (age: 9-16 weeks) lacking ADAP specifically in phagocytes and respective littermate controls (ADAP$^{wt/wt}$ × LysM-Cre^{het}, ■) were infected i. v. with 2.5×10^4 *Lm* or left untreated (uninfected control mice, day 0) and sacrificed at the indicated times post infection. Blood was obtained by puncture of the heart, after centrifugation the supernatant was collected. Cytokine concentration (pg/mL) in serum of infected mice was analyzed via a flow cytometry-based multi-analyte assay (custom mouse panel). Summary plots present the average concentration of the analytes calculated from two replicates. Data are depicted as mean ± SEM for n = 5-10 individually analyzed mice per group out of at least two independent experiments. Horizontal dotted lines show the limit of detection. Protein concentrations under the detection line were considered undetectable and hence were not included into statistics; numbers represent the detectable samples out of the total number of samples, if not stated otherwise all samples were detectable. Statistical analyses were performed using two-tailed, unpaired *t*-test with Welch's correction (*p < 0.05). Manuscript submitted in *Frontiers in Immunology* (status: 25.06.2021).

4.2.2 *Infection-associated priming of phagocytes in an ADAP-deficient host induces an altered phagocyte phenotype*

The striking discrepancy that on the one hand neutrophil and inflammatory monocyte infiltration is significantly increased in ADAPko mice during *Lm* infection (**Figure 11 E** and **Figure 31**) but on the other hand pathogen elimination is significantly delayed (**Figure 11 B**) lead to the question whether the infection-associated activation of phagocytes in ADAPko mice would negatively affect their function. To this end and in order to describe the phenotype of these cells in more detail, wild type and ADAPko mice were infected with *Lm* followed by flow cytometry-based quantification of TNF-α, IL-1α and iNOS. These mediators are known to be secreted by infection-primed phagocytes and play essential roles during the early course of immune response to bacterial pathogens.

As depicted in **Figure 34 A** and **B** (left panels), the release of TNF-α by neutrophils was comparable in ADAPko and wild type mice, both in the spleen (day 3 p. i.: wild type: 183.2 MFI, ADAPko: 324.8 MFI; day 5 p. i.: wild type: 252.8 MFI, ADAPko: 276.9 MFI) and in the liver (day 3 p. i.: wild type: 252.5 MFI, ADAPko: 355.7 MFI; day 5 p. i.: wild type: 231.1 MFI, ADAPko: 257.6 MFI). Interestingly though, neutrophils from ADAPko mice produced significantly more IL-1α on day 3 p. i. in the spleen (wild type: 365.3 MFI, ADAPko: 710.4 MFI) and on day 3 and day 5 p. i. in the liver (day 3 p. i.: wild type: 519.2 MFI, ADAPko: 756.8 MFI; day 5 p. i.: wild type: 551.1 MFI, ADAPko: 708.8 MFI) compared to the wild type counterparts (**Figure 34 A** and **B**, middle panels). Of note, increased IL-1α production was already evident in the spleen of naïve ADAP-deficient mice (day 0).
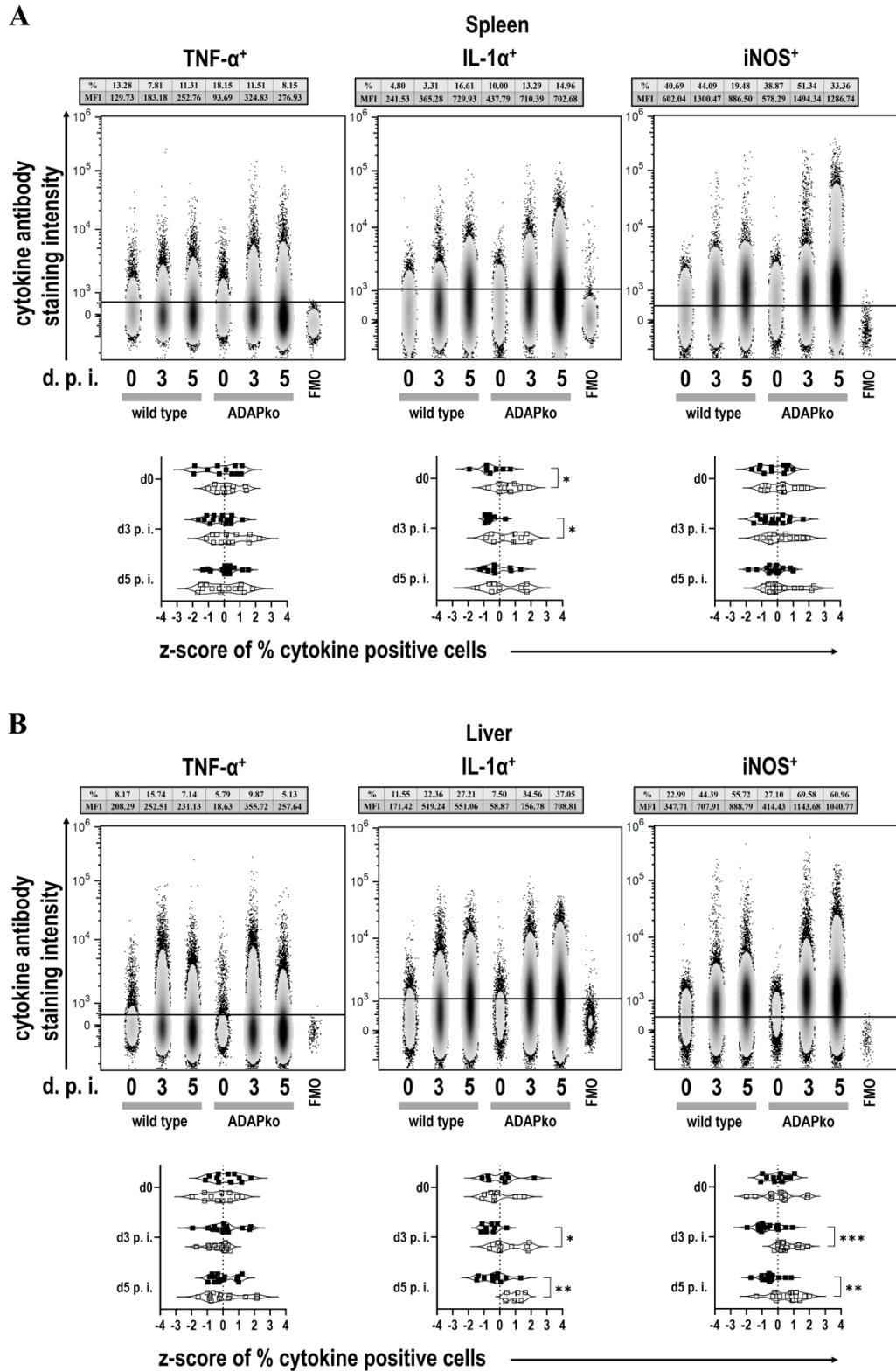
Figure 34 | Neutrophils from ADAPko mice show an altered inflammatory profile during *in vivo Listeria monocytogenes* infection. Wild type (■) and ADAPko (□) mice (age: 10-17 weeks) were infected i. v. with 2.5 × 10⁴ CFU *Lm* or left untreated (uninfected control mice, day 0) and were sacrificed at the indicated times post infection. Leukocytes were isolated from (A) spleen and (B) liver. Liver tissue was digested via the gentleMACS

dissociator in order to isolate liver leukocytes followed by density centrifugation with 35 % Percoll/PBS. Subsequently all cells were re-stimulated *in vitro* with PMA/ionomycin for 4 h. After 1 h brefeldin A and Monensin were added. Cells were stained for Ly6G$^+$CD11b$^+$ cells in reference to CD45$^+$Lin$^-$ leukocytes. **(A, B)** Representative data (top panels) from one experiment with n = 4-6 individually analyzed mice per group were constrained to alive singlet Ly6G$^+$CD11b$^+$ neutrophils and are shown in columns side-by-side in a concatenated qualitative density plot (with outliers) in which each column represents data of all pooled mice from one genotype to a given time. Shown is the mean of cytokine positive neutrophils (in %) and the MFI (geometric mean) of all pooled mice per genotype in the top of the data. Summary plots (bottom panels) present the percent of cytokine (TNF-α, IL-1α and iNOS)-positive neutrophils, determined in reference to the corresponding FMO controls in a violin plot with all data points. Results from each independent experiment with n = 8-14 individually analyzed mice per group were normalized over all mice on a given day post infection by z-score calculation. Resulting z-scores from 2-3 independent experiments are shown. Statistical analyses were performed using unpaired, nonparametric Mann-Whitney test (*p < 0.05, **p < 0.01, ***p < 0.001). Manuscript submitted in *Frontiers in Immunology* (status: 25.06.2021).

In addition to IL-1α, hepatic but not splenic neutrophils from ADAP-deficient mice produced considerably more iNOS compared to littermate controls during the course of *Lm* infection (day 3 p. i.: wild type: 707.9 MFI, ADAPko: 1143.9 MFI; day 5 p. i.: wild type: 888.8 MFI, ADAPko: 1040.8 MFI) (**Figure 34 B**).

Similar cytokine production patterns were observed for inflammatory monocytes in the spleen and the liver of ADAPko compared to the wild type control animals. Of note, genotype-dependent differences in the TNF-α production of Ly6C^{high} monocytes from ADAPko mice in spleen and liver were observed already in naïve mice (day 0) (**Figure 35 A**, left panels). Following *Lm* infection, Ly6C^{high} monocytes derived from the spleen of ADAPko mice produced more TNF-α compared to the wild type littermates (day 3 p. i.: wild type: 351.9 MFI, ADAPko: 622.3 MFI). As shown in **Figure 35 B** (left panels), decreased TNF-α production by Ly6C^{high} monocytes was observed on day 5 post infection in the liver of ADAPko mice (day 5 p. i.: wild type: 520.0 MFI, ADAPko: 99.7 MFI).

As for the neutrophils, Ly6C^{high} monocytes from ADAPko mice produced higher amounts of IL-1α on day 3 p. i. in the spleen (wild type: 1121.8 MFI, ADAPko: 1377.7 MFI) and the liver (wild type: 1150.6 MFI, ADAPko: 1939.9 MFI), depicted in **Figure 35 A** and **B** (middle panels). Moreover, while iNOS production in neutrophils from ADAPko mice was increased only in the liver, Ly6C^{high} monocytes derived from both, the spleen (day 3 p. i.: wild type: 1798.0 MFI, ADAPko: 3391.3 MFI; day 5 p. i.: wild type: 1951.3 MFI, ADAPko: 2513.1 MFI) and the liver (day 3 p. i.: wild type: 1653.6 MFI, ADAPko: 4249.6 MFI; day 5 p. i.: wild type: 1894.6 MFI, ADAPko: 2918.3 MFI) of ADAPko mice, produced significantly more iNOS during the course of *Lm* infection (**Figure 35 A** and **B**, right panels).

A
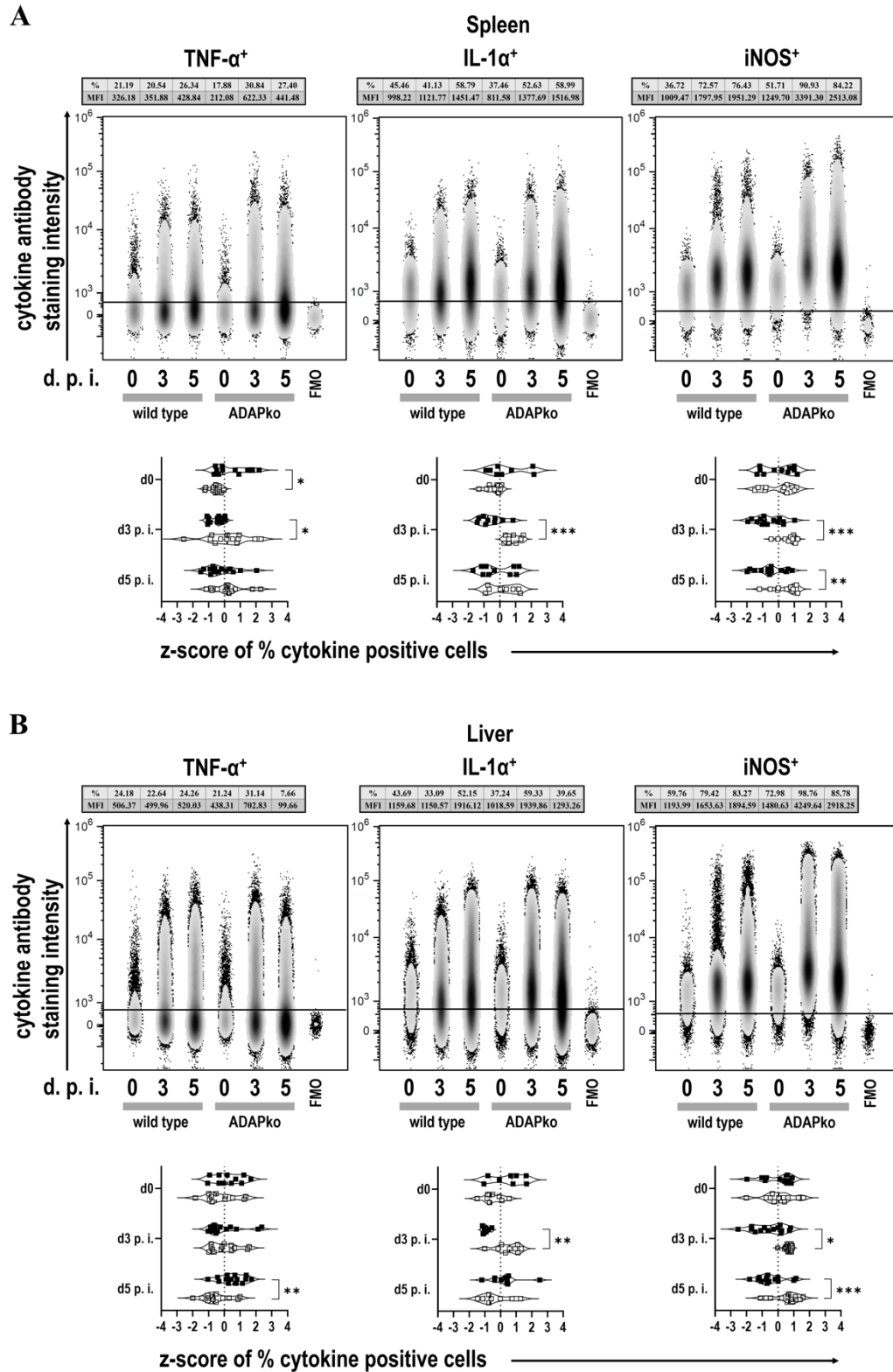
Figure 35 | Inflammatory monocytes derived from ADAPko mice exhibit an altered inflammatory profile during *in vivo Listeria monocytogenes* infection. Wild type (■) and ADAPko (□) mice (age: 10-17) were infected i. v. with 2.5×10^4 CFU *Lm* or left untreated (uninfected control mice, day 0) and were sacrificed at the indicated times post infection. Leukocytes were isolated from (A) spleen and (B) liver. Liver tissue was digested

| 93

via the gentleMACS dissociator in order to isolate liver leukocytes followed by density centrifugation with 35 % Percoll/PBS. Subsequently all cells were re-stimulated *in vitro* with PMA/ionomycin for 4 h. After 1 h brefeldin A and Monensin were added. Cells were stained for CX3CR1^{low}Ly6C^{high} cells in reference to CD45^{+}Lin^{-}Ly6G^{-}CD11b^{+} leukocytes. (**A**, **B**) Representative data (top panels) from one experiment with n = 4-6 individually analyzed mice per group were constrained to alive singlet CX3CR1^{low}Ly6C^{high} inflammatory monocytes and are shown in columns side-by-side in a concatenated qualitative density plot (with outliers) in which each column represents data of all pooled mice from one genotype to a given time. Shown is the mean of cytokine positive inflammatory monocytes (in %) and the MFI (geometric mean) of all pooled mice per genotype in the top of the data. Summary plots (bottom panels) present the percent of cytokine (TNF-α, IL-1α and iNOS)-positive inflammatory monocytes, determined in reference to the corresponding FMO controls in a violin plot with all data points. Results from each independent experiment with n = 8-14 individually analyzed mice per group were normalized over all mice on a given day post infection by z-score calculation. Resulting z-scores from 2-3 independent experiments are shown. Statistical analyses were performed using unpaired, nonparametric Mann-Whitney test (*p < 0.05, **p < 0.01, ***p < 0.001). Manuscript submitted in *Frontiers in Immunology* (status: 25.06.2021).

Taken together, data depicted in **Figure 34** and **Figure 35** very much support the hypothesis that phagocytes like neutrophils and inflammatory monocytes, which were primed during Listeria infection within an ADAP-deficient environment, develop an altered phenotype.

4.2.3   *Broad changes in the gene expression profile of neutrophils and monocytes from ADAPko mice during Lm infection*

Enhanced production of pro-inflammatory cytokines such as IL-1α and bactericidal mediators such as iNOS by phagocytes is well in line with the observed increased immunopathology in ADAPko mice, but are in contrast to our observation that the bacteria are poorly controlled in mice lacking ADAP. Thus, in order to further characterize potential alterations in phagocyte phenotype and function on the genetic level, unbiased *ex vivo* transcriptional profiling of neutrophils and inflammatory monocytes derived from spleen and liver of *Lm*-infected mice was performed.

To this end, neutrophils and inflammatory monocytes from total leukocyte preparations from livers and spleens day 3 post infection were sorted by FACS. Per genotype, organ and cell type, 3 independent sample sets, each consisting of cells pooled from 2 mice per replicate, were generated. Of note, due to limitations in cell numbers, neutrophils from livers of day 3 infected wild type mice were analyzed only in duplicates. Together, transcriptomes of 23 samples were assessed by Clariom S microarray analysis. For both cell subsets, lists of differentially expressed genes were compiled (see **Table 25** and **Table 26**), comparing ADAPko *versus* wild type genotype and applying a fold change (FC) cutoff of ± 3-fold with False Discovery Rate (FDR) < 0.05, as shown in the volcano plots in **Figure 36 A** for neutrophils and **Figure 37 A** for inflammatory monocytes.

As depicted in **Figure 36 A**, spleen- and liver-derived neutrophils from *Lm* infected ADAPko mice show more genes which are up- rather than downregulated based on their expression in wild type mice (spleen: up: 200, down: 129; liver: up: 229, down: 170). Compared to neutrophils, the transcriptional influence of ADAP-deficiency in inflammatory monocytes is less pronounced, with 70 upregulated and 63 downregulated transcripts in spleen-derived inflammatory monocytes, and 110 upregulated and 100 downregulated transcripts in their liver-derived counterparts (**Figure 37 A**).

Highly affected transcripts in neutrophils from both organs are e.g. *Ffar2*, *Qsox1*, *Lipg*, *Batf2*, *Ggt1*, *Prok2* and *Nos2*, all being intensely upregulated in the ADAPko genotype with some of them known for being functionally involved in neutrophil recruitment and their induction under inflammatory conditions. Highly affected transcripts, similarly regulated in inflammatory monocytes from both organs are *Gmppb*, *Ms4a3*, *Nos2*, *S100a9* and *Saa3*. As expected for the ADAPko genotype, expression of the ADAP encoding gene (*Fyb* transcript) is reduced compared to the wild type genotype in all comparisons for both cell subsets derived from both organs, thereby confirming ADAP-deficiency (FC in spleen: neutrophils: -4.74, inflammatory monocytes: -5.88; FC in liver: neutrophils: -2.88, inflammatory monocytes: -5.43).

To describe the organ-specific alterations induced by ADAP-deficiency in more detail, genes differentially regulated in phagocytes from spleen or liver were merged. This approach resulted in a total of 604 annotated transcripts differentially regulated in neutrophils from spleen or liver and 290 transcripts generally regulated in inflammatory monocytes. Out of the 604 transcripts generally regulated in neutrophils, only 124 core transcripts were found to be regulated in neutrophils from both spleen and liver (**Figure 36 B**). Interestingly, 205 transcripts were found to be regulated exclusively in spleen-derived neutrophils and 275 transcripts specifically in liver-derived neutrophils. Similarly, in inflammatory monocytes, out of 290 generally regulated transcripts only 53 core transcripts show differential expression in both spleen and liver. Moreover, 80 transcripts were specific for spleen-derived monocytes, and a majority of 157 transcripts was found to be specific for liver-derived inflammatory monocytes (**Figure 37 B**), suggesting a tissue-specific, *Lm*-induced transcriptional patterns within neutrophils as well as inflammatory monocytes. Interestingly, the lack of ADAP seems to have greater influence on expression levels of neutrophils and inflammatory monocytes derived from the liver rather than from the spleen.
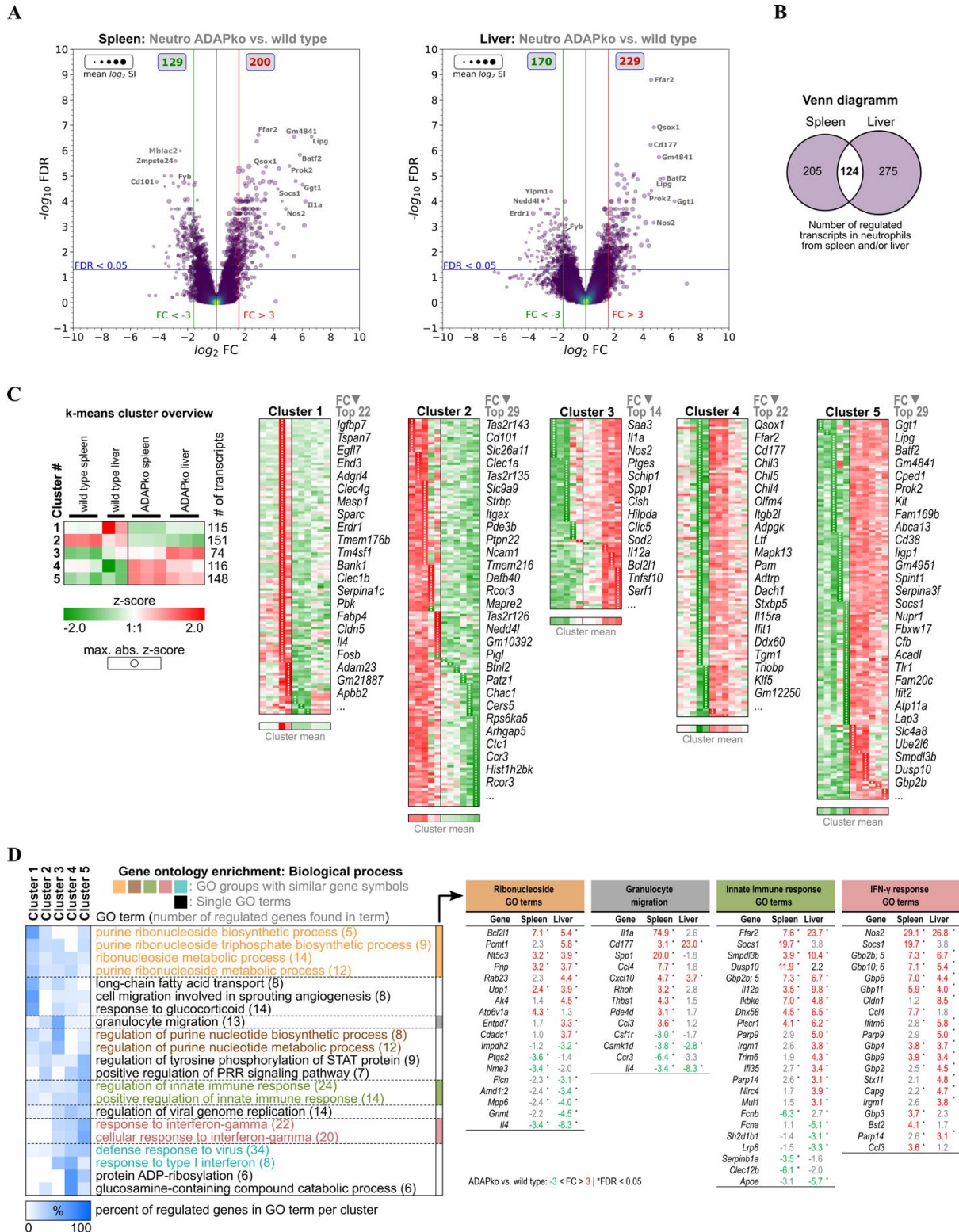
Figure 36 | Microarray analysis of neutrophils from spleen and liver of wild type and ADAPko mice 3 days post *Listeria monocytogenes* infection. Wild type and ADAPko mice (age: 9-15 weeks) were infected i. v. with 2.5×10^4 CFU *Lm* and sacrificed on day 3 post infection. Neutrophils (Neutro; Ly6G⁺CD11b⁺ cells) were FACS-sorted from spleen and liver. Per genotype and organ, neutrophils from 6 mice were isolated and cells from 2 mice each were pooled, resulting in n = 3 independent replicate sample pools per organ and genotype (n for wild type

Results

liver = 2). Total RNA was isolated and analyzed by Clariom S microarray (23 samples in total). Differentially expressed transcripts in spleen/liver-derived neutrophils were determined comparing ADAPko *versus* wild type condition (fold change > ± 3-fold, FDR < 0.05). **(A)** Volcano plots of validly detected transcripts from indicated microarray comparisons, plotting $-\log_{10}$ FDR *versus* $\log_2$ fold change. Point sizes refer to mean $\log_2$ signal intensities (SI) of transcripts calculated across all microarrays. Point color code reflects point density. FC (red/green vertical lines) and FDR (blue horizontal lines) criteria for differential gene expression are indicated. Grey boxes show numbers of significantly up (red) and down (green) regulated transcripts. Gene symbols of selected transcripts are stated. **(B)** Venn diagram of 604 transcripts, differentially regulated in neutrophils isolated from spleen or liver comparing ADAPko *versus* wild type condition, respectively. **(C)** $\log_2$ SI data of the 604 transcripts were z-score transformed, k-means clustered (k = 5) and transcripts in resulting clusters were descendingly sorted by maximal absolute z-score (marked by withe point indicators). Data represent color-coded z-scores. Stated gene symbols in each cluster are descendingly ranked by average absolute FC, showing the top n symbols. Top left subfigure: Averaged representation of k-means clusters. Sample type, cluster ID and numbers of genes per cluster are indicated. **(D)** Gene Ontology (GO) enrichment analysis for GO category "Biological Process" (FDR < 0.05, GO-level ≥ 8). GO term groups with highest significance and numbers over over-represented genes for ADAPko *versus* wild type are shown. Data represent hierarchically clustered percentages of enriched genes (color code), that fall into indicated k-means clusters. Numbers in brackets represent number of enriched genes per GO-term. Note: In cooperation with Dr. Robert Geffers (Helmholtz Centre for Infection Research Braunschweig, Research Group Genome Analytics) and Dr. A. Jeron (Institute for Medical Microbiology and Hospital Hygiene Magdeburg, Research Group Infection Immunology). Manuscript submitted in *Frontiers in Immunology* (status: 25.06.2021).

In order to dissect expressional differences in ADAPko *versus* wild type neutrophils and inflammatory monocytes in more detail, $\log_2$ signal intensities of the 604 and 290, respectively identified transcripts were z-score transformed and subjected to k-means cluster algorithm (KMC, with k = 5).

Cluster numbering was based on averaged mean expression profiles of each cluster and ascendingly sorting them according to the ADAPko conditions. Next, gene clusters were evaluated by Gene Ontology (GO) enrichment analysis for statistically overrepresented GO-terms in the "Biological process" GO category (FDR < 0.05, GO-level ≥ 8). The following section will concentrate on the description of clustering and GO-enrichment results for neutrophils followed by the description of the data for inflammatory monocytes.

Clustering of neutrophil data (**Figure 36 C**) resulted in 115 (cluster 1), 151 (cluster 2), 74 (cluster 3), 116 (cluster 4) and 148 (cluster 5) groups of genes, respectively. Cluster 1 signifies low to moderate z-scores in most conditions (see k-means cluster overview), except for liver-derived neutrophils from wild type mice on day 3 post infection. Here, a strong gene induction with high positive z-scores was observed. Functional enrichment of genes in cluster 1 attributes to GO-terms like response to glucocorticoid (14 transcripts), cell migration, long-chain fatty acid transport and purine ribonucleoside biosynthetic process (**Figure 36 D**).

Cluster 2 (151 transcripts) is, next to cluster 5, one of the largest clusters. It shows genotype-related differences in the expression profiles. However, these differences are largely not organ-

specific. In more detail, cluster 2 transcripts show high z-scores in spleen-derived neutrophils from wild type mice, with moderate to high z-scores also in the wild type liver condition. Consequently, cluster 2 transcripts are generally not induced in neutrophils from both organs of ADAPko mice and hence can be regarded as ADAP-dependent. Functional attributions reveal GO-enriched terms related to positive regulation of the PRR signaling pathway (7 transcripts), granulocyte migration (13 transcripts) and regulation of purine nucleotide metabolic process (12 transcripts).

With 74 transcripts, cluster 3 represents the smallest cluster containing transcripts with moderate to high z-scores especially in the ADAPko liver condition. Neutrophils derived from wild type mice show minimal z-scores with the remaining two conditions mainly showing moderate z-scores of cluster 3 transcripts. Thus, cluster 3 transcripts are most relevant for neutrophils derived from the liver of ADAPko mice, being consistently upregulated in this condition. Noteworthy and in line with FACS data presented in **Figure 34**, top-regulated transcripts are *Il1α* (interleukin 1 alpha; fold change ADAPko *versus* wild type: 2.6-fold in liver and 75-fold in spleen) and *Nos2* (inducible nitric oxide synthase 2; fold change: 26.8-fold in liver and 29.1-fold in spleen), both being involved in hallmark innate inflammatory and bactericidal processes. Further functional attributions show GO-enrichment in granulocyte migration, purine ribonucleoside biosynthetic process as well as purine nucleotide metabolic process.

Cluster 4 (116 transcripts) shows a largely different expression profile compared to cluster 1. In cluster 4, transcripts of neutrophils from both organs of ADAPko mice are generally upregulated, indicated by a higher z-score. The functional attributions show very strong enrichment of glucosamine-containing compound catabolic process, protein ADP-ribosylation and response to type 1 interferon (8 transcripts). Of note, *Qsox1* which is known for resolution and protective response during acute stress in mice[237] is strongly upregulated in spleen- and liver-derived neutrophils form ADAPko mice.

Cluster 5 (148 transcripts) is most interesting when it comes to ADAP genotype-dependent differences, as transcripts in this cluster are highly induced only in neutrophils from ADAP-deficient mice, both in spleen and liver. Functional GO annotation enrichment clearly demonstrates involvement of cluster 5 transcripts in IFN-γ response. Interestingly, numerous cluster 5 genes relate to the family of guanylate-binding proteins (Gbp; e.g.: *Gbp2b; Gbp5, Gbp3*, *Gbp4*, *Gbp8*, *Gbp10; Gbp6* and *Gbp11*), known to function as IFN-γ-induced GTPases.

They play a central role in protective immunity against microbial as well as viral pathogens[238]. Since these guanylate-binding proteins are known to be induced by IFN-γ-signaling, it is worth to note that we indeed observed that ADAPko mice exhibit significantly elevated serum levels of IFN-γ 3 days post *Lm* infection (**Figure 18**). Likely in consequence of the enhanced IFN-γ response, production of reactive oxygen species in neutrophils from ADAPko mice by the nitric oxide synthetase 2 (*Nos2*) might be enhanced, considering *Nos2* fold changes of 29.1 (spleen) and 26.8 (liver).

The k-means clustering for spleen- and liver-derived inflammatory monocytes from wild type and ADAPko mice 3 day post *Lm* infection (**Figure 37 C**) categorized the total number of 290 transcripts into 5 clusters as well: 97 (cluster 1), 48 (cluster 2), 15 (cluster 3), 59 (cluster 4) and 71 (cluster 5) genes.

Cluster 1 clearly shows an ADAP-dependent expression profile, with impaired transcriptional induction in ADAPko, compared to strong expression in inflammatory monocytes isolated from both, spleen and liver of wild type animals. GO-enrichment revealed few significantly enriched transcripts involved in liver regeneration (3 transcripts) as well as animal organ regeneration (5 transcripts) and regulation of vascular associated smooth muscle cell proliferation (**Figure 37 D**). Interesting genes in this cluster are e.g. *Cx3cr1*[239,240] and *Ace*[241].

Cluster 2 (48 transcripts) represents average transcript induction in all settings except for the inflammatory monocytes derived from liver of wild type mice 3 days post *Lm* infection. The maximal absolute z-scores in this compartment clearly indicates the highest regulation of genes compared to the ADAPko mice. Functional attributions show pronounced enrichments regarding regulation of interleukin-10 production, T-helper cell differentiation next to the CD4$^+$, αβT cell differentiation.

Cluster 3 comprises of 15 transcripts and thus is the smallest gene profile cluster in respect to inflammatory monocytes. Nevertheless, it is of interest since it contains upregulated gene transcripts like *Il1r2* (fold change: 3.62 in liver, fold change: 33.06 in spleen ADAPko *versus* wild type) and *Dmkn* (dermokine, fold change: 3.88 in liver, fold change: 9.95 in spleen ADAPko *versus* wild type). Of note, dermokine expression is known to be induced in inflammatory diseases[242].

Results
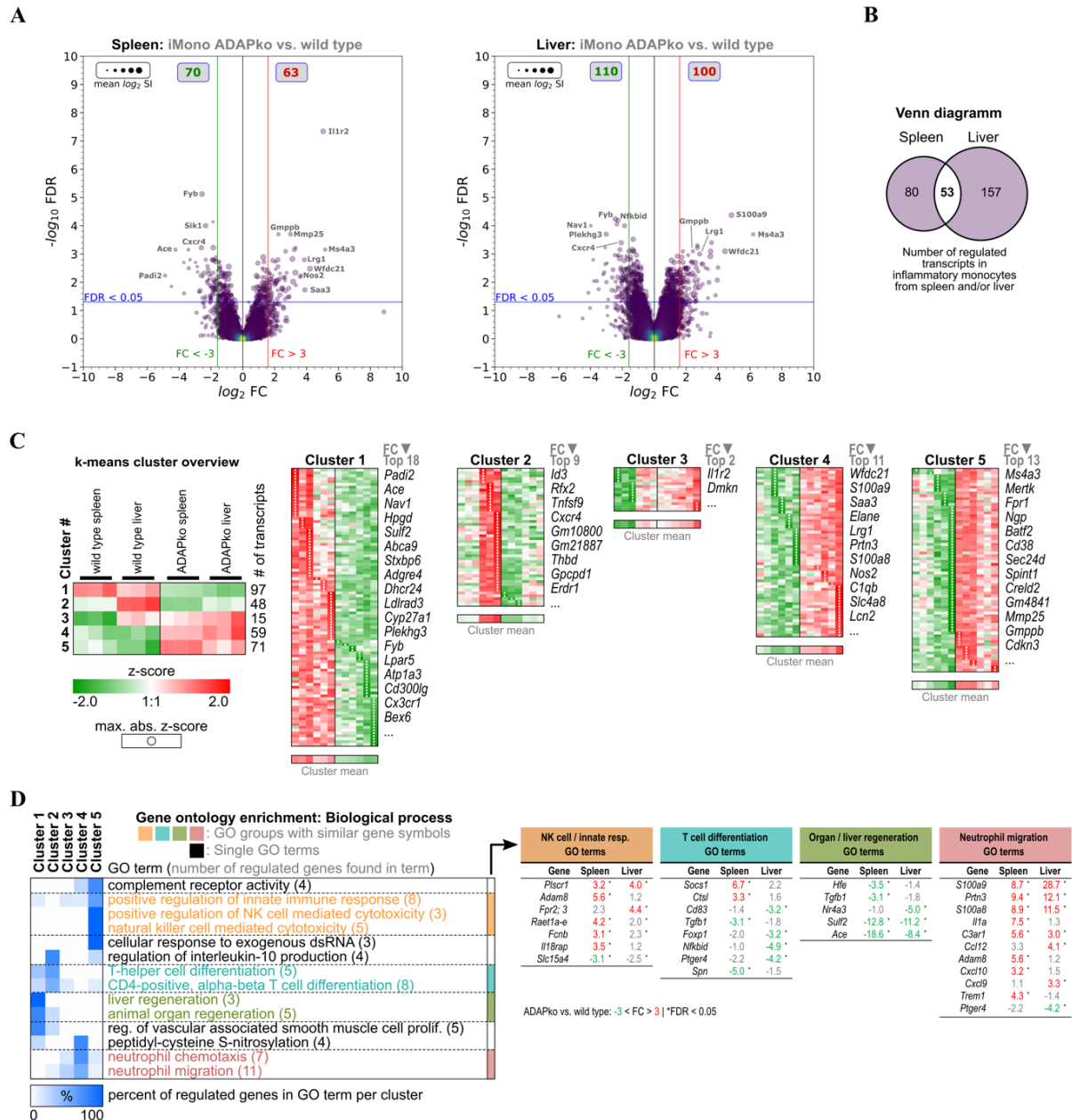
Figure 37 | Microarray analysis of inflammatory monocytes from spleen and liver of wild type and ADAPko mice 3 days post *Listeria monocytogenes* infection. Wild type and ADAPko mice (age: 9-15 weeks) were infected i. v. with 2.5×10^4 CFU *Lm* and sacrificed on day 3 post infection. Inflammatory monocytes (iMono; Ly6G⁻CD11b⁺Ly6C⁺CX3CR1⁺ cells) were FACS-sorted from spleen and liver. Per genotype and organ, inflammatory monocytes from 6 mice were isolated and cells from 3 mice each were pooled, resulting in n = 3 independent replicate sample pools per organ and genotype. Total RNA was isolated and analyzed by Clariom S microarray (23 samples in total). Differentially expressed transcripts in spleen-/liver-derived inflammatory monocytes were determined comparing ADAPko *versus* wild type condition (fold change > ± 3-fold, FDR < 0.05). **(A)** Volcano plots of validly detected transcripts from indicated microarray comparisons, plotting -log₁₀ FDR *versus* log₂ fold change. Point sizes refer to mean log₂ signal intensities (SI) of transcripts calculated across all microarrays. Point color code reflects point density. FC (red/green vertical lines) and FDR (blue horizontal lines) criteria for differential gene expression are indicated. Grey boxes show numbers of significantly up (red) and down (green) regulated transcripts. Gene symbols of selected transcripts are stated. **(B)** Venn diagram of 290 transcripts, differentially regulated in inflammatory monocytes isolated from spleen or liver comparing ADAPko

versus wild type condition, respectively. **(C)** Log$_2$ SI data of the 290 transcripts were z-score transformed, k- means clustered (k = 5) and transcripts in resulting clusters were descendingly sorted by maximal absolute z-score (marked by withe point indicators). Data represent color-coded z-scores. Stated gene symbols in each cluster are descendingly ranked by average absolute FC, showing the top n symbols. Top left subfigure: Averaged representation of k-means clusters. Sample type, cluster ID and numbers of genes per cluster are indicated. **(D)** Gene Ontology (GO) enrichment analysis for GO category "Biological Process" (FDR < 0.05, GO-level ≥ 8). GO term groups with highest significance and numbers over over-represented genes for ADAPko *versus* wild type are shown. Data represent hierarchically clustered percentages of enriched genes (color code), that fall into indicated k-means clusters. Numbers in brackets represent number of enriched genes per GO-term. Note: In cooperation with Dr. Robert Geffers (Helmholtz Centre for Infection Research Braunschweig, Research Group Genome Analytics) and Dr. A. Jeron (Institute for Medical Microbiology and Hospital Hygiene Magdeburg, Research Group Infection Immunology). Manuscript submitted in *Frontiers in Immunology* (status: 25.06.2021).

Both, clusters 4 and 5 (59 and 71 transcripts, respectively) show a clear and strong genotype-dependent transcript induction for spleen- and liver-derived inflammatory monocytes from the ADAPko mice, while the gene expression in spleen- and liver-derived inflammatory monocytes of wild type animals is mainly downregulated.

Interestingly, the transcript for *S100a9* (S100 calcium binding protein A9, fold change: 28.68 in liver and 8.66 in spleen) and *S100a8* (fold change: 11.45 in liver and 8.91 in spleen), both belonging to cluster 4, were upregulated in the spleen- and liver-derived inflammatory monocytes. Both factors are known to be involved in neutrophil chemotaxis (7 transcripts) and neutrophil migration (11 transcripts). Furthermore, these proteins play a crucial role in the regulation of inflammatory processes and immune responses. Additionally, they can increase the bactericidal activity of phagocytes by promoting phagocytosis. However, the functional attributes of genes compiled in cluster 5 are quite diverse, and the cluster contains genes involved in complement receptor activity, positive regulation of innate immune responses as well as regulation of natural killer cell mediated cytotoxicity and cellular response to exogenous dsRNA.

A closer look on GO term groups with highest significance and numbers of over-represented genes suggests inflammatory monocytes from ADAP-deficient mice to have an altered phenotype regarding the regulation of NK cell cytotoxicity, T cell differentiation, organ/liver regeneration and neutrophil migration (**Figure 37 D**). Especially, transcripts involved in neutrophil attraction/migration are consistently stronger expressed in inflammatory monocytes derived from ADAPko mice. An interesting observation made in splenic inflammatory monocytes from ADAP-deficient animals is the strong induction of the neutrophil attractant *Il1α* (fold change: 7.5) together with the up-regulation of the IL-1α decoy receptor *Il1r2* (fold

change: 30), potentially antagonizing IL-1α sensing by inflammatory monocytes in the ADAPko environment in an autocrine manner.

Taken together, microarray analyses showed that neutrophils in general are transcriptionally more affected by ADAP-deficiency than inflammatory monocytes, regardless of their tissue origin. Moreover, it seems that the observed ADAP-dependent transcriptional alterations in both cell subsets relate to the ADAP-deficient tissue environment. This notion is based on the large extend of tissue-specific differential gene expression in neutrophils and inflammatory monocytes of splenic or liver origin. As can be expected for a multifaceted signaling adaptor protein like ADAP, consequences of its deficiency in neutrophils and inflammatory monocytes can only be interpreted in the context of relevant inflammatory signaling events the cells are exposed to in a tissue-specific manner. In light of this and given the comparable disease severity in *Lm* infected phagocyte-specific conditional ADAPko and wild type controls, it remains difficult to distinguish cell-intrinsic and tissue-environmental consequences of ADAP-deficiency in the conventional ADAPko mouse model.

Despite the majority of regulated genes in neutrophils and inflammatory monocytes were either regulated in spleen or liver (**Figure 36** and **Figure 37**), there are also common sense genes regulated in cells from both organs that were considered of special interest. Since ADAP is a receptor-associated signaling adapter protein, a mouse receptor/ligand database[243] was used to filter the previously identified ADAP-dependent genes for known receptor/ligand interactions (**Figure 38**).

Receptor encoding common sense genes in neutrophils comprise *Adora2b*, *IL15rα*, *IL18bp*, *Tlr1* and *Tmem67*. Common sense soluble ligands produced by neutrophils are *Cxcl10*, *Il4*, *Il12α*, *Il27*, *Prok2* and *Spint1*, with only *Il4* showing reduced expression in neutrophils from ADAPko mice (**Figure 38**, right hand sided). Microarray analysis shows that common sense receptors up-regulated in inflammatory monocytes from ADAPko mice are *C3ar1*, *Fpr1*, *Il1r2* and *Mertk*, whereas *Atp1a3*, *Cx3cr1*, *Cxcr4* and *Plxnd1* are down-regulated (**Figure 38**, left hand sided).
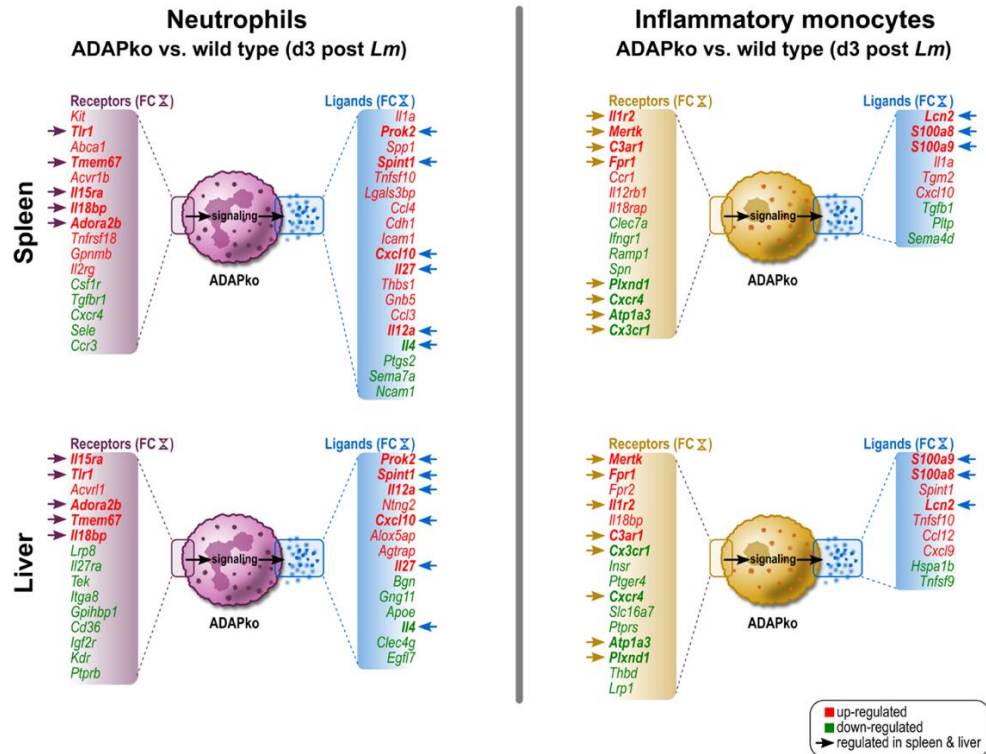
Figure 38 | Receptors and ligands differentially expressed in neutrophils and inflammatory monocytes from spleen and liver of *Listeria monocytogenes* infected ADAPko mice 3 days post infection. Gene symbols of differentially expressed transcripts from microarray analysis in **Figure 36** and **Figure 37** were filtered by a mouse receptor/ligand interaction database according to reference [243] and resulting gene lists were sorted by fold change. Differentially regulated (up: red, down: green) common sense genes found in cells isolated from spleen as well as liver are shown in bold letters and are indicated with an arrow. Note: In cooperation with Dr. Robert Geffers (Helmholtz Centre for Infection Research Braunschweig, Research Group Genome Analytics) and Dr. A. Jeron (Institute for Medical Microbiology and Hospital Hygiene Magdeburg, Research Group Infection Immunology). Manuscript submitted in *Frontiers in Immunology* (status: 25.06.2021).

Notably, these common sense receptors differ from those in neutrophils. In inflammatory monocytes from ADAPko mice, the only up-regulated common sense ligands identified are *Lcn2*, *S100a8* and *S100a9*. Nevertheless, our analyses revealed new clues as to which signaling pathways within neutrophils and inflammatory monocytes may depend on ADAP as a signaling adapter in a naturally orchestrated, innate-driven *in vivo* infection.

In summary, transcriptional profiling of neutrophils and inflammatory monocytes uncovered pronounced alterations in gene expression dependent on their priming in an ADAP-sufficient or -deficient environment. The observed molecular changes imply that phagocytes would as well undergo ADAP-dependent functional adaptations. To directly prove whether ADAP-deficiency would affect hallmark features in phagocytes, *in vivo* NET formation as well as *ex vivo* phagocytosis assays were performed.

4.2.4 *Reduced phagocytotic capacity of neutrophils primed in ADAPko mice during Lm infection*

To next test whether and how phagocyte function in ADAPko mice might be affected, assessments of extracellular traps (NETs) formation and the phagocytic capability of neutrophils were performed. To quantify NET formation, histones in *Lm*-infected spleen and liver tissues were stained. As shown in **Figure 39 A**, no significant differences in the quantity of NETs in spleens of ADAPko animals compared to the wild type counterparts were detected. Interestingly, while the number of detectable NETs in spleens of ADAPko mice was significantly reduced from day 1 to day 3 post *Lm* infection (day 1 p. i.: ADAPko: 65.6 ± 7.6 mean $\pm$ SEM of counts, day 3 p. i.: ADAPko: 31.2 ± 2.9 mean $\pm$ SEM of counts), this effect was not observed in wild type mice (**Figure 39 A**, right panel; day 1 p. i.: wild type: 40.2 ± 6.5 mean $\pm$ SEM of counts, day 3 p. i.: wild type: 30.3 ± 9.7 mean $\pm$ SEM of counts).

NET counts in the liver of infected animals displayed a different picture. While no differences in NET numbers were observed on day 1 post infection, the number of NETs on day 3 post infection was significantly increased in ADAP-deficient animals compared to the wild type counterparts (**Figure 39 B**; wild type: 27.0 ± 2.7 mean $\pm$ SEM of counts, ADAPko: 49.3 ± 6.1 mean $\pm$ SEM of counts). Thus, ADAP-deficiency results in minor but distinct changes in NET formation by neutrophils in *Lm*-infected organs.

A

B
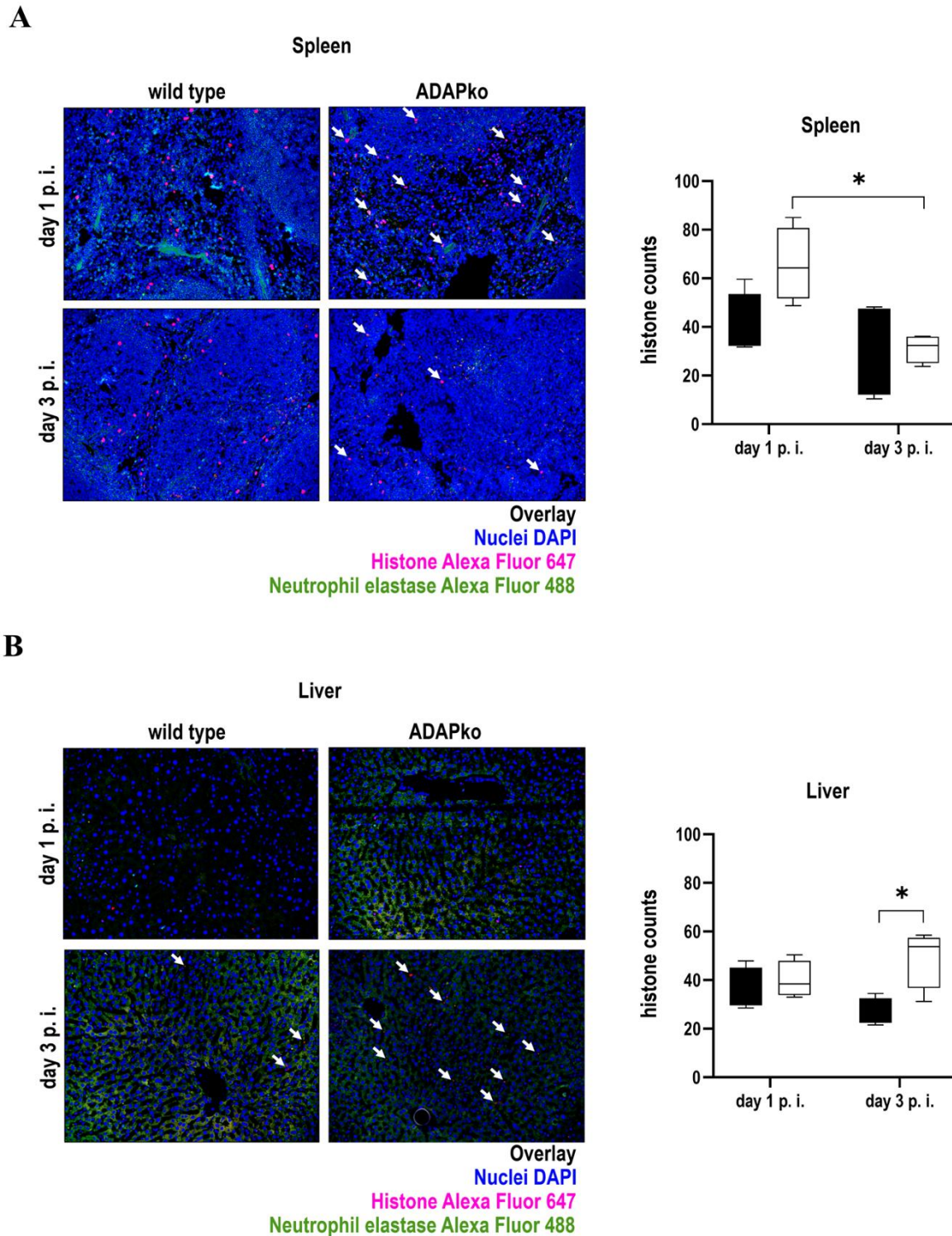
Figure 39 | Distinct changes in NET formation by neutrophils from ADAP-deficient mice in response to *in vivo Listeria monocytogenes* infection. Wild type (■) and ADAPko (□) mice (age: 10-14 weeks) were infected i. v. with 2.5×10^4 CFU *Lm* and sacrificed at the indicated times post infection. Formalin-fixed tissue slices were stained with primary antibody (neutrophil elastase, Histone H3), and subsequently with the secondary antibody (Alexa Fluor 488 donkey anti-rabbit IgG, goat anti-rat IgG Alexa Fluor) as well as DAPI for nuclei staining. Representative pictures show the overlay of the nuclei (colored in blue), histones (colored in pink) and neutrophil elastase (colored in green) in **(A)** spleen and **(B)** liver tissues, whereas white arrows highlight the histones.

| **105**

Results

Summary plots show the mean of counted histones. Four pictures per slide (3 different layers) at a magnification of 200× were taken and histones were counted using Image-Pro Plus 6 (double-blinded). Data are depicted as box and whiskers ± min to max for n = 4 individually analyzed mice per genotype out of one experiment. Statistical analyses were performed using two-way ANOVA with Bonferroni's *post hoc* test (*p < 0.05). Note: In cooperation with Prof. Borna Relja and Dr. B. Xu (Department of Radiology and Nuclear Medicine, Research Group Experimental Radiology). Manuscript submitted in *Frontiers in Immunology* (status: 25.06.2021).

To further define potential functional alterations in phagocytes that might explain the inefficient pathogen control in ADAPko mice (**Figure 11 B**), a closer look was taken at the phagocytic activity of neutrophils and inflammatory monocytes from *Lm*-infected mice. To this end, FACS-based *ex vivo* phagocytosis assays using fluorescence labeled latex microspheres were performed (**Figure 40**).
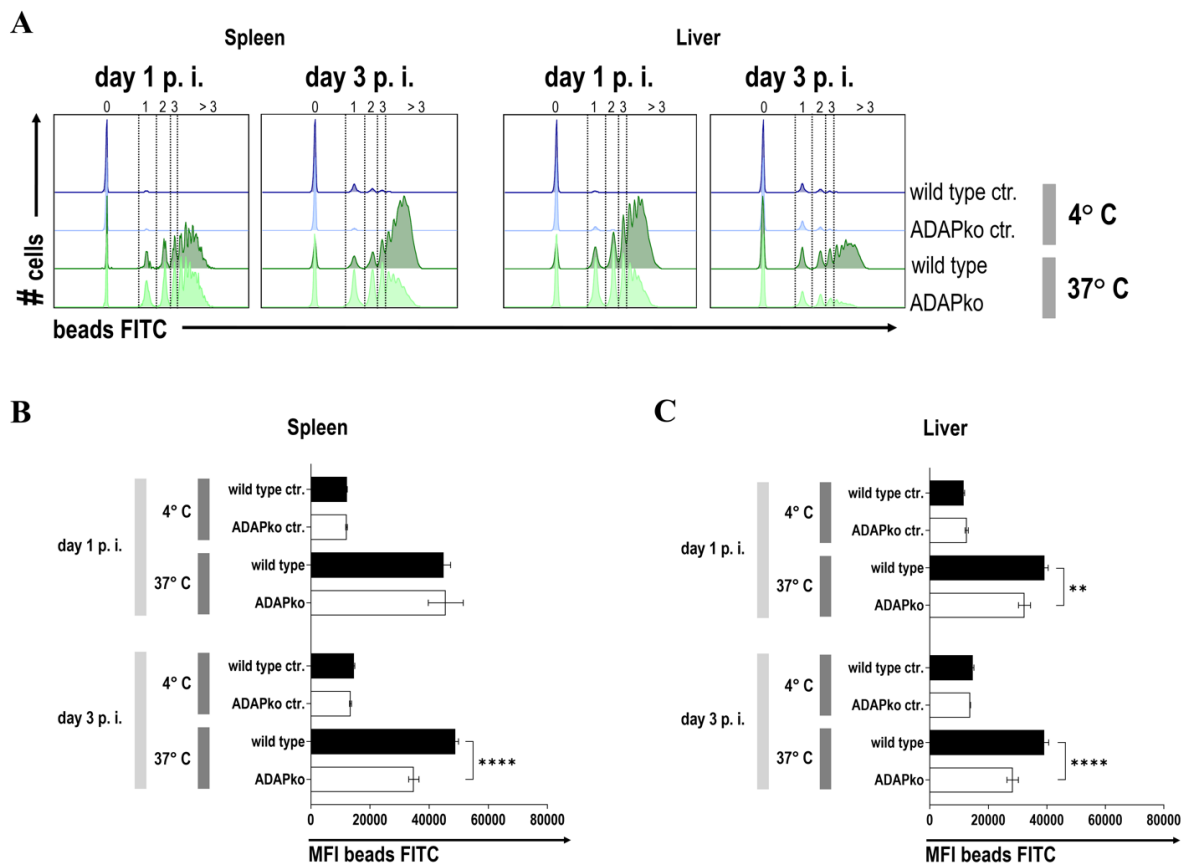
Figure 40 | *In vivo Listeria monocytogenes*-primed neutrophils from ADAP-deficient mice are functionally impaired in their phagocytotic capacity. Male wild type (■) and ADAPko (□) mice (age: 10-17 weeks) were infected i. v. with 2.5×10^4 CFU *Lm* and sacrificed at the indicated times post infection. Leukocytes were either isolated from the spleen respectively liver tissue was digested via the gentleMACS dissociator in order to isolate liver leukocytes followed by density centrifugation with 35 % Percoll/PBS. Leukocytes were from spleen and liver were stained for Ly6G$^+$CD11b$^+$ neutrophils in reference to CD45$^+$Lin$^-$ cells and phagocytosis of Ly6G$^+$CD11b$^+$ cells was assessed by a 2 h incubation of the cells with carboxylate-modified FITC-fluorescent latex microspheres at 37 °C or 4 °C serving as negative controls (ctr.) with a cell to beads ratio of 1:5. **(A)** Representative histograms for spleen (left histograms) and liver (right histograms) for Ly6G$^+$CD11b$^+$ neutrophils in wild type and ADAPko mice in addition to the related negative ctr. 1 and 3 days post infection. Numbers and

dotted lines of the histograms show the fractioned cells according to the amount of incorporated beads. Phagocytic capability of **(B)** spleen and **(C)** liver neutrophils was considered by the MFI of bead positive populations. Data are depicted as mean ± SEM for n = 6-8 individually analyzed mice per group out of two independent experiments. Statistical analyses were performed using two-way ANOVA with Bonferroni's *post hoc* test (**p < 0.01, ****p < 0.0001). Note: In cooperation with Prof. Ildiko Rita Dunay (Center for Behavioral Brain Sciences Magdeburg, Institute of Inflammation and Neurodegeneration Magdeburg) and M. Sc. H. P. Düsedau (Institute of Inflammation and Neurodegeneration Magdeburg). Manuscript submitted in *Frontiers in Immunology* (status: 25.06.2021).

While on day 1 p. i. no genotype-dependent differences were observed for the spleen, neutrophil phagocytic capacity was significantly decreased in ADAPko mice on day 3 p. i. (day 3 p. i.: wild type: 48817.5 ± 1106.8 mean ± SEM, ADAPko: 34812.8 ± 1721.5 mean ± SEM) (**Figure 40 A** and **Figure 40 B**). In the liver, genotype-dependent differences were already detectable on day 1 post *Lm* infection and became even more pronounced by day 3 (**Figure 40 A** and **Figure 40 C**; wild type: 39103.1 ± 1538.8 mean ± SEM, ADAPko: 28320.1 ± 1956.4 mean ± SEM). Interestingly, no ADAP-dependent effects on phagocytosis were observed for inflammatory monocytes, except for day 1 post infection in the liver, were inflammatory monocytes from ADAPko mice showed reduced phagocytic activity compared to the wild type control mice (**Figure 41**; wild type: 26362.9 ± 1081.4 mean ± SEM, ADAPko: 20786.4 ± 1360.0 mean ± SEM).

Analysis of the FITC-fluorescent signal intensity allows to further distinguish the cells according to the absolute number of incorporated beads (**Supplement Figure 1**). Strikingly, this analysis revealed that next to their overall reduced phagocytic capacity, the number of incorporated beads was generally lower in splenic and hepatic neutrophils from ADAPko than in wild type mice (**Supplement Figure 1 A**). Well in line with data depicted in **Figure 41**, this effect was far less pronounced in inflammatory monocytes from the liver and was not observed in these cells derived from the spleen (**Supplement Figure 1 B**).

In conclusion, *ex vivo* phagocytosis assay uncovered functional impairment of neutrophils that were primed in the ADAP-deficient environment. This might explain at least in part the inability of ADAPko mice to limit bacterial growth and, in consequence, the fatal outcome of the infection.
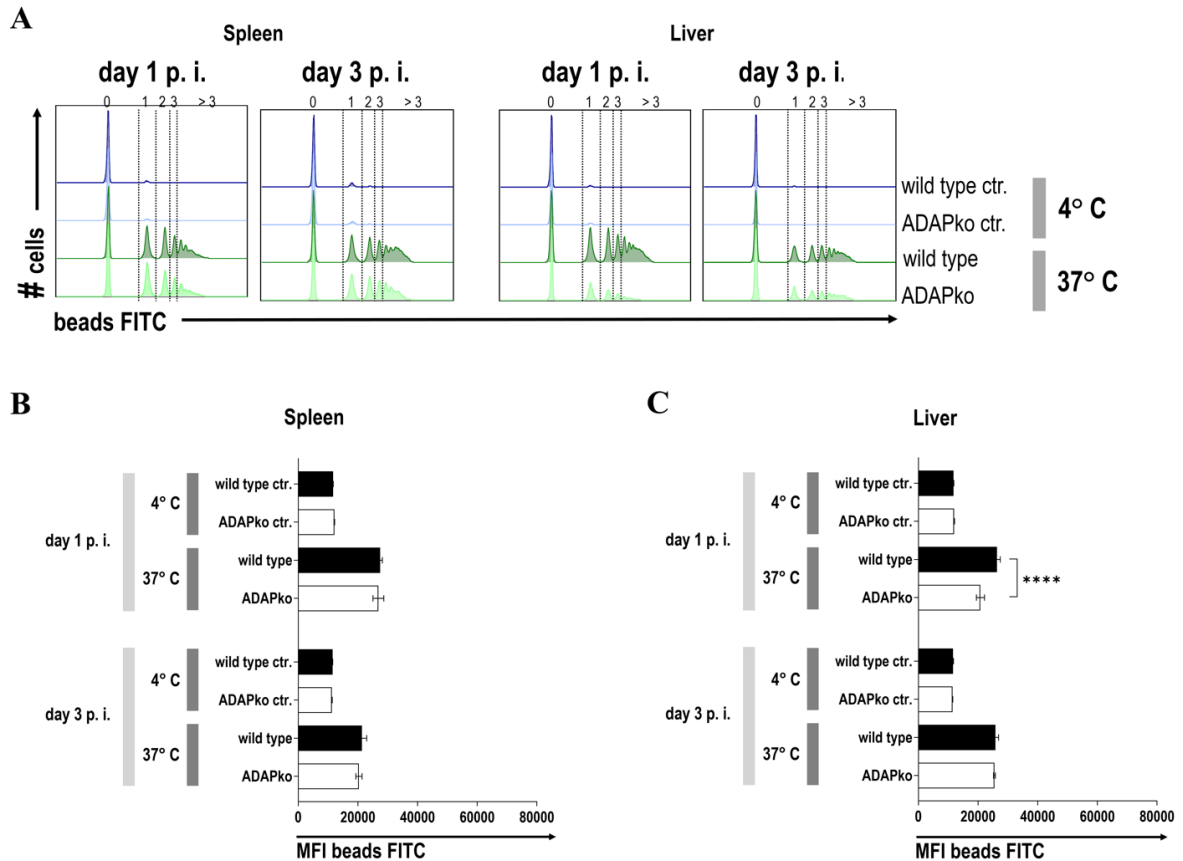
Figure 41 | Phagocytic capacity of inflammatory monocytes following *in vivo Listeria monocytogenes* infection is largely independent of ADAP. Male wild type (■) and ADAPko (□) mice (age: 10-17 weeks) were infected i. v. with 2.5×10^4 CFU *Lm* and sacrificed at the indicated times post infection. Leukocytes were either isolated from the spleen respectively liver tissue was digested via the gentleMACS dissociator in order to isolate liver leukocytes followed by density centrifugation with 35 % Percoll/PBS. Leukocytes were from spleen and liver were stained for CX3CR1^{low}Ly6C^{high} cells in reference to CD45$^+$Lin$^-$CD11b$^+$ cells and phagocytosis was assessed by a 2 h incubation of the cells with carboxylate-modified FITC-fluorescent latex microspheres at 37 °C or 4 °C serving as negative controls (ctr.) with a cell to beads ratio of 1:5. Representative histograms for **(B)** spleen and **(C)** liver CX3CR1^{low}Ly6C^{high} cells in wild type and ADAPko mice in addition to the related negative ctr. 1 and 3 days post infection. Numbers and dotted lines of the histograms show the fractioned cells according to the amount of incorporated beads. Phagocytic capability of **(B)** spleen and **(C)** liver inflammatory monocytes was considered by the MFI of bead positive populations. Data are depicted as mean ± SEM for n = 6-8 individually analyzed mice per group out of two independent experiments. Statistical analyses were performed using two-way ANOVA with Bonferroni's *post hoc* test (****p < 0.0001). Note: In cooperation with Prof. Ildiko Rita Dunay (Center for Behavioral Brain Sciences Magdeburg, Institute of Inflammation and Neurodegeneration Magdeburg) and M. Sc. H. P. Düsedau (Institute of Inflammation and Neurodegeneration Magdeburg). Manuscript submitted in *Frontiers in Immunology* (status: 25.06.2021).

Taken together, data from the second part of this thesis show that during *Lm* infection neutrophils (**Figure 42**) and inflammatory monocytes (**Figure 43**) from ADAPko mice accumulate in the spleen and the liver.
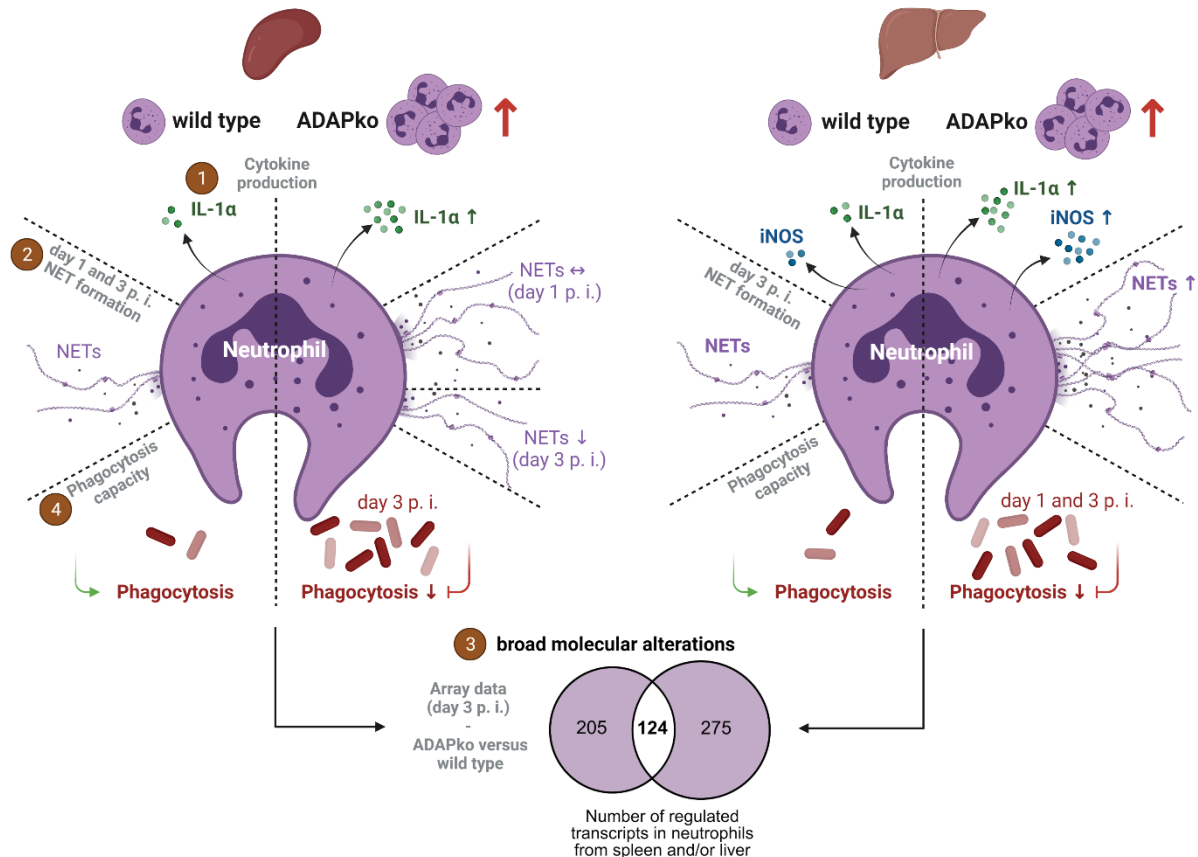
Figure 42 | Summary - Neutrophils. This figure summarizes major differences in terms of neutrophil release of IL-1α and iNOS (1), NET formation (2), transcriptional profile (3) and phagocytosis capacity (4) in spleen (left) and liver (right) from wild type (each left side) *versus* ADAPko (each right side) mice. Created with BioRender.com (2021).

Despite this, the pathogen is only inefficiently controlled in these mice (**Figure 11**), hinting at a functional impairment of infection-primed phagocytes. Of note, quantification of pro-inflammatory mediators such as IL-1α, as well as transcriptional profiling of the whole genome revealed broad molecular alterations following activation of neutrophils and inflammatory monocytes in the ADAP-deficient host. Moreover, while the formation of NETs by neutrophils was only slightly affected in ADAPko, *ex vivo* analyses uncovered a significantly impaired phagocytotic capacity of neutrophils. Together with an altered activation profile, reduced phagocytic function might explain inefficient pathogen control and thus the fatal outcome of the infection in ADAPko mice.
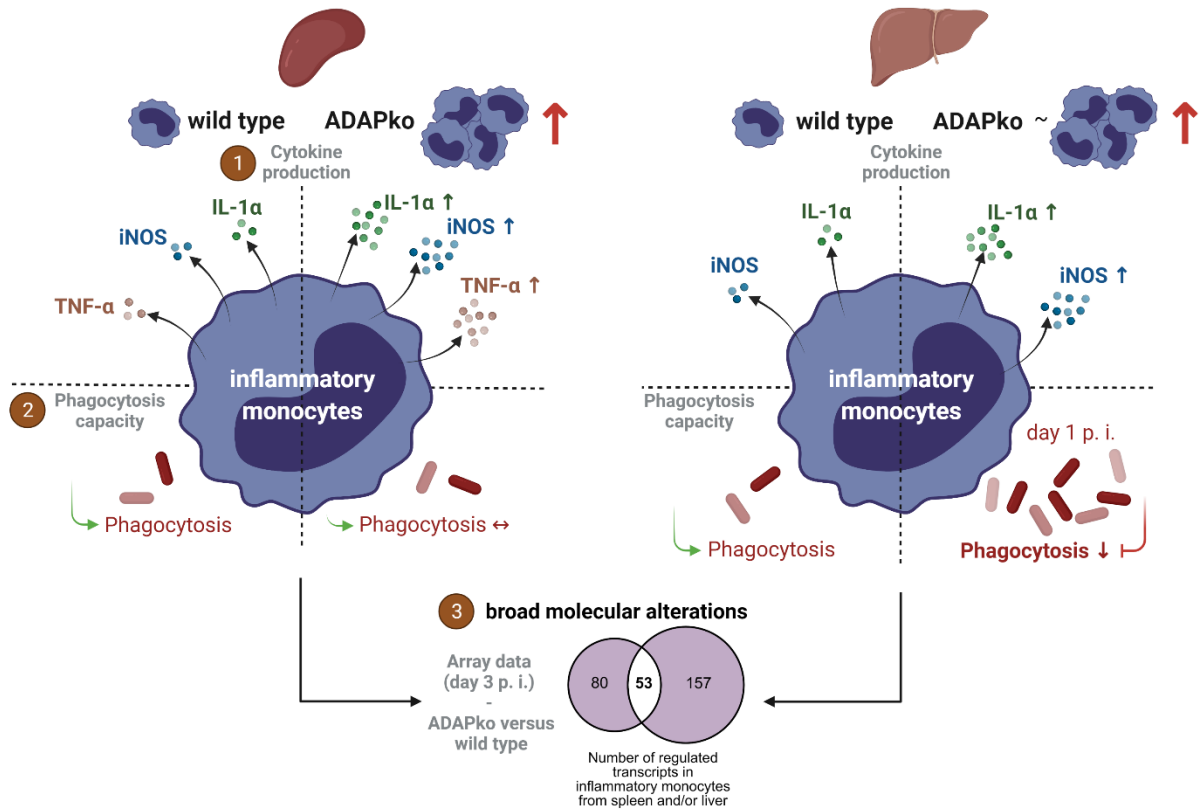
Figure 43 | Summary - Inflammatory monocytes. This figure summarizes major differences in terms of inflammatory monocytes release of IL-1α, iNOS and TNF-α (1), phagocytosis capacity (2) and transcriptional profile (3) in spleen (left) and liver (right) from wild type (each left side) *versus* ADAPko (each right side) mice. Created with BioRender.com (2021).

5 Discussion

5.1   Role of ADAP in NK cell cytotoxicity during *Listeria monocytogenes* in mice

Rajasekaran et al. studied in very much detail signaling pathways that are induced in NK cells following the *in vitro* stimulation of activating receptors such as CD137 and NKG2D. They uncovered an ADAP-dependent signaling pathway that is exclusively involved in inflammatory cytokine production, but not required for cytotoxicity of NK cells[48]. As mechanism underlying this remarkable dichotomy they described a unique interaction between Fyn and ADAP, linking the upstream signaling to the CBM module. Under the chosen experimental conditions, this interaction of ADAP with the CBM complex led to IFN-γ as well as chemokine production, but did not induce cytotoxicity in murine and human NK cells[48]. NK cell function heavily depends on the conditions in which they are activated. Therefore, Vivier and colleagues raised some doubt regarding the transferability of these findings to NK cells that have been activated *in vivo* under more physiological conditions[48]. Well in line with this, antibody/cytokine-mediated *in vitro* stimulation of naïve and infection-primed NK cells confirmed impaired IFN-γ secretion by ADAP-deficient NK cells (**Figure 14**)[220]. However, as shown in this thesis, a more physiological stimulation of NK cells that were either primed in the ADAP-sufficient or -deficient host by YAC-1 target cells indeed did not reveal any negative effect of ADAP-deficiency on IFN-γ production by NK cells. Strikingly though, YAC-1 stimulation of naïve or infection-primed NK cell uncovered an impaired cytotoxic function of ADAPko NK cells (**Figure 16** and **Figure 17**)[220].

An altered ADAPko phenotype was additionally confirmed by *ex vivo* profiling of the NK cell proteome following their *in vivo* activation in the context of *Lm* infection. This revealed an overall decrease of intracellular perforin and CD107a in NK cells, suggesting the release of perforin from CD107a$^+$ granules after their *in vivo* priming. Furthermore, LC-MS/MS analysis revealed a marginal but noticeable reduction in CD107a protein abundance in NK cells from ADAPko compared to wild type control mice following *Lm* infection further confirming a decreased cytolytic activity of ADAPko NK cells (**Figure 21 B**)[220]. Strikingly, independent of the genotype, infection-primed NK cells exhibited an overall decreased abundance of almost all detectable prototypic NK cell proteins with the exception of granzyme A and granzyme B, which were found at even higher abundances (**Figure 21**)[220]. The fact that the priming of NK

cells results in increased granzyme A and B levels but at the same time decreased abundance of CD107a and perforin seems to be counter-intuitive at a first glance, but numerous mechanisms could explain this finding. Heyner et al. showed a co-localization of CD107a and perforin, but not with granzymes (unpublished data, personal communication). Furthermore, it was reported that different cytotoxic vesicles are present within the cell, dependent on the activating signal used to stimulate NK cell function. As an example, the engagement of 2B4 or NKG2D on NK cells induces the co-localization of perforin with Rab27a^{+} but not Munc13-4[+] vesicles. In direct contrast, an antibody-dependent CD16 activation of NK cells leads to localization of perforin to Munc13-4[+] vesicles but not to Rab27a[+][244]. Of note, both, Munc13-4 and Rab27a, are described to be involved in granzyme B polarization to the immunological synapse[245]. Consequently, the observed differences concerning the abundances of granzyme A/B and CD107a/perforin in NK cells might on the one hand be the result of a complex receptor/ligand binding event, which is induced early on during infection and leads to discrete maturation of lytic granules in NK cells[220]. On the other hand, proteins that are newly synthesized as a consequence of infection-triggered gene expression, might also contribute to the differences of cytotoxic protein abundances. Well in line with the proteome data (**Figure 21 B**), Fehniger et al. uncovered that resting NK cells contain high levels of granzyme A but only little granzyme B as well as perforin[246]. Remarkably, Fehniger and colleagues observed a strong discrepancy in terms of protein *versus* mRNA content, with mRNA being detectable in naïve NK cells at high abundance for all three genes. Whereas naïve NK cells were granzyme A-positive, an IL-15-stimulation increased the frequency of granzyme B and perforin expressing NK cells and, of note, only granzyme B abundance was associated with induced mRNA expression[246]. While these data provide evidence for potential differences concerning the regulation of transcription as well as translation for these different cytotoxic mediators, they do not fully explain the inverse pattern of granzyme A and B as well as perforin in infection-primed NK cells. Nevertheless, perforin and granzyme B were shown to be essential for efficient cytotoxicity *in vitro* and *in vivo*[246] and we showed here that the abundance of one of them appears to be reduced in NK cells lacking ADAP (**Figure 16 A**, bottom panels and **C**)[220].

5.2   The impact of ADAP on migration and infiltration of innate immune cells during

    Listeria monocytogenes in mice

During the early phase of *Lm* infection, phagocytes such as neutrophils and monocytes contribute to the initiation of an inflammatory response[247] and furthermore, these cells are critically involved in immune containment of the pathogen[59]. Infiltrating monocytes and especially neutrophils are attracted to the site of infection were they contribute to immunopathology as adverse side effects[85,171].

The *in vivo* infection experiments revealed increased infiltration of neutrophils and monocytes into the spleen and the liver of ADAP-deficient mice (**Figure 11** and **Figure 31**). This is well in line with the observation that NK cells from infection-primed ADAPko mice exhibited a significantly impaired production of the phagocyte attracting chemokines CCL3, CCL4, and CCL5 compared to their wild type counterparts (data not shown)[220]. On the other hand it has been reported that SLP-76-deficient neutrophils are not able to spread following stimulation of the β2-integrin[248]. SLP-76 is an immune cell adaptor that is associated with phosphorylated ADAP via the Src kinase Fyn[5,249]. Of note, SLP-76-deficient neutrophils fail to trigger central downstream regulators following integrin ligation, thus providing convincing evidence for a vital role of SLP-76 in regulating neutrophil function[248]. Further reports showed that ADAP-deficient neutrophils displayed a reduced transmigration behavior into tissues[52]. In more detail, Block et al. studied the recruitment of neutrophils to the kidney in wild type compared to ADAPko mice, using an ischemia-reperfusion induced acute kidney injury (AKI) model. They demonstrated, that ADAP and SLP-76 are both part of the E-selectin-mediated integrin activation. As already mentioned in the introduction, the tyrosines Y112 and Y128 of SLP-76 as well as the interaction of SLP-76 with ADAP are known to be required for the activation of LFA-1 and the E-selectin-mediated slow rolling, and thus for the recruitment of leukocytes into inflamed tissue. Block and colleagues demonstrated that the loss of ADAP indeed resulted in an impaired rolling, adhesion to the endothelium and transmigration and these defects resulted in an increased resistance of ADAPko mice to AKI[52]. Furthermore, it has been suggested that the lack of SLP-76 in myeloid cells affects neutrophil functions *in vivo*[250]. If and how data generated in frame of the present thesis are comparable to the ones mentioned before could be discussed controversially, since Block and colleagues studied neutrophil migration in a setting of sterile inflammation. The *Lm* infection model used in the present work results in direct as well as indirect pathogen-related activation of a variety of different immune

and nonimmune cells, together establishing a multifaceted cellular interaction network, which, at different layers, might be dependent on the adaptor protein ADAP. This might be one explanation for the diverse effects observed regarding the impact of ADAP-deficiency on neutrophil migration.

In addition to the increased neutrophil infiltration in spleen and liver of ADAPko mice following *Lm* infection (**Figure 31**), no differences in the absolute numbers of neutrophils as well as monocytes were detectable in conditional ADAPko mice lacking ADAP exclusively in NK cells (data not shown)[220]. Interestingly, studies performed in frame of this thesis revealed that ADAP-deficiency in NK cells was associated with a more severe course of *Lm* infection (**Figure 22 A**), which was not due to impaired antibacterial immunity (**Figure 22 B**)[220]. Activated NK cells respond to *Lm* infection[132] in a complex process that requires crosstalk with macrophages, neutrophils as well as dendritic cells[105,137]. With this, NK cells are able to shape the immune response by the release of pro-inflammatory cytokines and chemokines as well as due to cell-to-cell contacts[251,252]. Enhanced disease severity might be indicative for a critical role of ADAP in NK cells in the overall innate immune response induced during Listeria infection. Of note, macrophages and neutrophils are considered to be the major source for IL-12 during listeriosis[91,253]. Notably, we found no quantitative differences in serum IL-12 levels (data not shown) between *Lm*-infected conditional ADAPko mice and littermate controls[220], which would have been a potential indicator for altered activation of phagocytes in mice lacking ADAP in NK cell. Together, the observed enhanced body weight loss of *Lm*-infected conditional ADAPko mice (**Figure 22 A**) can most likely not be attributed to an enhanced immunopathology exerted by phagocytes. However, the molecular mechanism by which ADAP-deficiency in NK cells promotes disease severity during *Lm* infection remains elusive.

So far, no data were available regarding the migration of ADAP-deficient NK cells. Utilizing an *in vitro* transwell system we showed for the first time that CXCL12-induced migration of ADAP-deficient NK cells is reduced compared to wild type NK cells[220]. During infection, NK cells are recruited to sites of inflammation in a chemokine-dependent manner. This is well-reflected by the observed increased migratory activity of *Lm* infection-primed compared to naïve NK cells (**Figure 28 A**)[220]. CXCL12 is an important chemokine not only for T cells, but also for the chemoattraction of NK cells[254]. Since *Lm* infection in mice represents a complex disease with different leukocyte subsets being recruited and activated to produce pro-

inflammatory cytokines and chemokines during early innate immune activation, *in vitro* testing of CXCL12-induced migration of NK cells only insufficiently reflects the *in vivo* situation. Nevertheless, impaired migratory activity of ADAP-deficient NK cells might at least in part explain the reduced numbers of NK cells in the spleen of conditional ADAPko mice early after *Lm* infection (**Figure 25 A**)[220]. In T cells, the inside-out signaling pathways leading to integrin activation after chemokine receptor stimulation are well-described[42] and Parzmair et al. have recently shown that migration of both, CD4^{+} and CD8^{+} T cells, depends on ADAP[202]. For NK cells, it is known that integrin-dependent activation is essential for migration and for cytotoxicity[233]. Therefore, it seems likely that similar signaling complexes are formed in T cells and NK cells. Of note, compared to wild type NK cells, CD11a surface expression on infection-primed ADAPko NK cells was markedly reduced on day 1 post *Lm* infection (**Figure 28 C**)[220]. As described in the introduction, CD11a together with CD18 forms the heterodimeric adhesion molecule LFA-1 which upon interaction with its ligand ICAM on endothelial cells promotes entry of leukocytes from the bloodstream into tissues. In fact, an early study by Allavena et al. has shown that LFA-1 is crucial for NK cell adhesion to and migration through the vascular endothelium[234]. Importantly, at least in T cells the intracellular domain of CD11a is directly linked to the signaling complex involving ADAP[235,236]. Thus, it is tempting to speculate that the lack of ADAP in NK cells and the associated reduced surface expression of CD11a on NK cells 1 day post *Lm* infection is mechanistically linked to the reduced accumulation of NK cells in the infected spleen of conditional ADAPko mice (**Figure 25**)[220]. However, since differential CD11a expression on ADAPko *versus* wild type NK cells was only transient and genotype-dependent differences in CD11a surface expression were lost by day 3 post infection, most probably further molecular factors will contribute to the observed phenotype. Yet, further studies are needed to dissect in more detail the molecular mechanism underlying reduced migratory activity of naïve and infection-primed ADAP-deficient NK cells.

However, Parzmair[201] and data generated in frame of this thesis showed, that ADAPko mice display a significantly enhanced pathology in spleen and liver as well as excessive bacterial load, and exaggerated accumulation of neutrophils and monocytes in ADAP-deficient mice compared to wild type counterparts (**Figure 11** and **Figure 31**). Remarkably, these inflammatory changes were not observed in conditional knockout mice, lacking ADAP exclusively in phagocytes (**Figure 32**), hinting at an extrinsic rather than an intrinsic effect of

ADAP in neutrophil and monocyte activation and effector function during *Lm* infection or a combination of both aspects. ADAP-dependent alterations in cytokine and chemokine expression in response to infection might be considered to play a key role in modulating the recruitment as well as priming of these cell types, i.e. neutrophils and inflammatory monocytes.

5.3   Infection-associated priming of innate immune cells in the ADAP-deficient host

During *Lm* infection several cytokines are induced, known to permit NK cell activation[255] and indeed most of the known NK cell-activating cytokines were detectable in sera of both, *Lm*-infected wild type and ADAPko mice (**Figure 18**)[220]. Thus, ADAPko mice did not exhibit a general defect in cytokine response to *Lm* infection[220]. Therefore, it can largely be excluded that impaired effector function in ADAPko NK cells is due to their impaired priming in the ADAP-deficient host rather than an inherent effect due to ADAP-deficiency in NK cells[220]. Apart from the proteome data (**Figure 20** and **Figure 21**), further analyses regarding the influence of *Lm* infection on the expression of activating/inhibitory receptors on NK cells and the expression of the corresponding ligands on target cells[220] lead to the hypothesis that during infection the combination of cytokines and/or receptor-ligand pairs is ideal to prime NK cells for both, cytokine production and cytotoxicity. Thus, under these optimized priming conditions the separation of the ADAP-dependent and -independent signaling pathways in NK cells is abrogated[220]. Still, future studies are needed to clarify the underlying mechanisms on a molecular level.

Independent of the role of ADAP in NK cells during listeriosis it is still not clear whether NK cells have a beneficial or detrimental character in immunity to *Lm* infections. A very early study by Teixeira and Kaufmann revealed an improved pathogen control in mice lacking NK cells[130]. This deleterious role of NK cells in listeriosis was later confirmed by Viegas and colleagues, which demonstrated that even though NK cells are not essential for the elimination of the pathogen, NK cell-deficient mice showed improved survival after *Lm*-infection[131]. However, data from Shtrichman et al. implied that NK cells might rather be protective during *Lm* infection[255]. By secretion of the pro-inflammatory cytokines IL-12, TNF-α, IL-1β, and IL-18 by *Lm*-activated dendritic cells, NK cells are primed to produce IFN-γ, which is known to play a pivotal role in innate and adaptive immunity to intracellular bacteria and indeed mice lacking the IFN-γ receptor are highly susceptible to Listeria infection[256]. Despite comparable IFN-γ production in infection-primed wild type and ADAP-deficient NK cells (**Figure 17 A**,

top panels and **B**), IFN-γ serum concentration was increased by day 3 p. i. in ADAP-deficient mice (**Figure 18**). However, since in conventional ADAPko mice also immune cells other than NK cells are deficient for ADAP, IFN-γ produced by e.g. T cells, NKT cells, macrophages, B cells or dendritic cells may account for the observed difference. This is supported by the finding that in conditional ADAPko mice lacking ADAP exclusively in NK cells the IFN-γ serum concentration markedly increases by day 2 post Listeria infection, while no significant differences in infection-induced IFN-γ levels between wild type and conditional ADAPko mice were observe (**Figure 23**)[220].

It has recently been shown, that independent from their IFN-γ production, NK cells may as well contribute to enhanced susceptibility of mice to Listeria infection[136]. As an underlying mechanism for the detrimental role of NK cells in listeriosis the authors uncovered that NK cells responding to Listeria infection acquire the ability to produce the immunosuppressive cytokine IL-10[136]. In a follow-up study the same group identified that licensing of IL-10 production in NK cells requires IL-18 released by *Lm*-infected Bat3+ DCs[257]. In frame of the current thesis, no effect of ADAP-deficiency in NK cells on their capacity to produce IL-10 was observed (**Figure 24**)[220]. However, since neither the concentration of the immunosuppressive IL-10, nor the levels of the NK cell licensing cytokine IL-18 differed in sera from *Lm*-infected wild type and ADAPko mice (**Figure 18** and **Figure 23**)[220], the possibility that IL-10 produced by NK cells would account for the enhanced morbidity of conditional ADAPko mice to *Lm* infection can largely be excluded.

Phagocytosis by neutrophils and inflammatory monocytes as well as the subsequent killing of pathogens is, among others, induced by pro-inflammatory cytokines such as IFN-γ[172,258] and TNF-α[173,259]. Additionally, next to neutrophils themselves[260], TNF-α is produced by macrophages and monocytes and at the same time stimulates NK cells to produce substantial amounts of IFN-γ, which in turn increases the intracellular killing capacity of these cells. Potential failures in the TNF-α/IFN-γ regulatory network, and consequently reduced bactericidal capacity of macrophages and monocytes, could explain the increased bacterial loads in ADAPko animals. However, while ADAPko NK cells produce lower levels of IFN-γ following *in vitro* stimulation, no effect of ADAP-deficiency on IFN-γ production by NK cells primed during *in vivo Lm* infection was observed[220]. Moreover, data obtained in frame of this thesis revealed that both TNF-α and IFN-γ levels are in fact significantly higher in ADAPko

than in wild type mice during *Lm* infection[220], therefore excluding reduced abundance of these mediators as the underlying mechanism for altered phagocyte priming.

Additionally to TNF-α and IFN-γ, the concentration of IL-1α was increased in sera of *Lm*-infected ADAP-deficient mice[220]. Of note, IL-1α can induce neutrophil recruitment[167], drives immunopathology, and is involved in several pathophysiological processes[166]. Increased serum levels of IL-1α in combination with increased levels of the neutrophil recruiting chemoattractant CXCL1 (KC)[201] might explain in part the massive neutrophil influx in spleen and liver of ADAPko mice depicted in the present thesis. However, ADAPko mice appear to be inefficient in controlling pathogen growth, suggesting that they were not appropriately activated within the ADAP-deficient immune system.

Monocytes are considered to differentiate into iNOS- and TNF-α-producing inflammatory monocytes during *Lm* infection[261]. Okunnu et al. stated that during *Lm* infection monocytes are more efficient than neutrophils in respect to the production of TNF-α and IL-1α[261], which is well in line with data from this thesis (**Figure 34** and **Figure 35**, left and middle panels). The authors stated that the production of TNF-α might enhance the ability of neutrophils to take up and kill *Lm*[261]. Data from this thesis, however, did not reveal any correlation between TNF-α production and antibacterial function of neutrophils.

Most of the published data on ADAP in immune cells were collected from *in vitro* experiments or *in vivo* studies using models for sterile inflammation. As an exception from this, Li et al. reported that ADAPko mice were more susceptible to infection with highly pathogenic influenza A virus, which was most likely due to a severe CD8^{+} T cell-mediated immune pathology. The cytokine storm induced in influenza infected ADAPko animals was explained by impaired TGF-β production by CD8^{+} T cells[262]. Interestingly, while this study focused on adaptive immunity, Parzmair also found TGF-β plasma levels in ADAPko to be reduced already in naïve mice and, moreover, increases in TGF-β were delayed in ADAP-deficient mice early on following *Lm* infection[201]. Platelets might be mechanistically involved in this abnormal response, since they store high amounts of TGF-β[263]. Of note, Rudolph and colleagues demonstrated that the platelet-specific deletion of ADAP increases experimental autoimmune encephalomyelitis (EAE) in mice, leading to the hypothesis that ADAP plays a regulatory role in platelets during EAE[53,204]. One might speculate that dependent on the

inflammatory setting both, innate and adaptive immune responses are insufficiently controlled in ADAP-deficient mice, thus leading to severe immunopathology following *Lm* infection.

5.4 Broad alterations in the gene expression profile of neutrophils and inflammatory monocytes from *Listeria monocytogenes*-infected ADAP-deficient mice

The enhanced expression of common sense receptors in ADAPko neutrophils renders them interesting candidates for future analysis regarding involvement of ADAP in their associated signaling pathways or mechanisms responsible for their increased expression (**Figure 38**). In this context, IL-15 receptor α (IL-15rα) seems of particular interest. Interleukin 15 (IL-15) promotes neutrophil migration, activation and phagocytosis. The multi-subunit IL-15 receptor consists of the IL-15rα, IL-2/15 receptor β (CD122) and common cytokine receptor γ chain (Gammac or CD132) subunits, and is highly expressed on neutrophils[264]. IL-15 receptor engagement in human neutrophils stimulates phagocytosis in dependency of the tyrosine-protein kinase Syk, which physically interacts with IL-15rα and becomes phosphorylated[265]. Importantly, ADAP is known to interact with Syk and together with SLP-76 activates the downstream Bruton tyrosine kinase (Btk)[52]. Btk is considered as a key kinase in many innate immunity signaling networks as reviewed by Weber et al.[266]. Blocking of IL-15rα was shown to reduce phagocytic capacity of human neutrophils by 40 %[265]. Thus, ADAP-deficiency may prevent efficient enhancement of neutrophil phagocytosis by abrogating Btk activation, despite enhanced expression of IL-15rα on ADAPko neutrophils and robust levels of IL-15 in ADAPko sera[220]. Taken together, this proposed mechanism might represent a possible explanation for the significantly reduced phagocytic properties of neutrophils in ADAPko mice.

Furthermore, there is evidence that neutrophils might be dispensable for controlling *Lm* infection and instead inflammatory monocytes are suggested to be of highest importance for innate *Lm* control[267]. In this regard, it is important to note, that the phagocytic capacity of inflammatory monocytes from ADAPko mice is less affected than that of neutrophils. However, ADAPko mice still fail to effectively control early bacterial growth suggesting that inflammatory monocytes from ADAP-deficient animals are functionally impaired in other aspects.

Another gene of interest that is very prominently upregulated in neutrophils from spleen and liver of *Lm*-infected ADAPko mice is *Batf2/Irf1* (Basic leucine zipper transcription factor 2;

interferon regulatory factor 1) (**Figure 36 A**). Strikingly, Batf2-deficiency was shown to increase resistance of mice to high-dose *Lm* infection which was accompanied by reduced tissue pathology and reduced bacterial burden[268]. This matches our findings (**Figure 11** and **Figure 36 A**), since *Batf2* is strongly upregulated in ADAPko mice, which succumb to the infection. Of note, Batf2-knockdown in stimulated macrophages resulted in downregulation of *Tnf*, *Ccl5*, *Il-12b* and *Nos2*, indicating an important role for Batf2 in the innate immune response[269]. Considering this, the observed overexpression of *Batf2* and *Nos2* in phagocytes of ADAPko mice might be linked to the exaggerated immunopathology in these animals. Interestingly, *Cd101* (Immunoglobulin superfamily member 2), which together with CXCR2 is used to distinguish CXCR2$^-$CD101^{low} immature from CXCR2$^+$CD101$^+$ mature neutrophils[247], was down-regulated in neutrophils, thereby possibly indicating compromised maturity of ADAPko neutrophils and at the same time supporting the hypothesis that neutrophils are differentially primed during *Lm* infection in an ADAP-deficient.

Next to these mentioned genes, *Ffar2* (*Gpr43*) encoding a free fatty acid receptor is highly upregulated in splenic and hepatic neutrophils of *Lm*-infected ADAPko mice (**Figure 36 A**). Ffar2 is involved in the modulation of immune cell recruitment during inflammation[270] matching the enhanced infiltration of neutrophils into spleen and liver of ADAPko mice. Interestingly, *Cd177* is upregulated in neutrophils from liver of *Lm*-infected ADAPko mice. CD177 belongs to the Ly6 toxin superfamily[271], and its expression is induced by inflammatory stimuli[272]. Furthermore, CD177 is associated with the β2-integrins CD11b/CD18 (Mac-1)[273]. CD177 expression was shown to be induced during bacterial infections[274] and a recent study has shown that CD177 mediates neutrophil migration through endothelial cells by interacting with serine proteinase-3[275]. Prok2/Bv8 is an inflammatory mediator strongly induced in neutrophils in response to G-CSF[276,277] and, of note, data from this thesis show an increased expression of *Prok2* in splenic neutrophils of infected ADAPko mice (**Figure 36 A**). Zhong et al. demonstrated Prok2/Bv8 to endorse the migration of neutrophils from human blood cells likely via ERK and phosphatidylinositol 3-kinase (PI3K) pathways[278]. Thus, one might speculate that the upregulation of *Cd177* and *Prok2* in neutrophils from ADAPko mice is mechanistically involved in the enhanced infiltration of these cells into *Lm*-infected spleen.

5.5   Reduced phagocytotic capacity of murine neutrophils during *Listeria monocytogenes* infection

Neutrophils and monocytes release proteases and aggressive microbicidal substances at the infection site, causing tissue damage as adverse side effect[147]. Substances like defensins as well as neutrophil elastase, which are contained in neutrophil granules, are involved in antimicrobial defense by degrading engulfed bacteria[147]. Additionally, neutrophils can generate reactive nitrogen species in a mechanism involving the inducible nitrogen oxide synthase (iNOS, NOS2). Noteworthy, transcriptome data from this thesis clearly indicate that preferentially pro-inflammatory pathways are switched on, both in infection-primed neutrophils and monocytes from ADAPko and wild type mice, while at the same time molecular processes involved in tissue regeneration are less active, especially in monocytes (**Figure 36** and **Figure 37**). Thus, it appears that phagocytes from ADAP-deficient mice are potential drivers of inflammation which is well in line with the pronounced immunopathology observed in spleen and liver of *Lm*-infected ADAPko mice.

Neutrophils catch and kill bacteria by releasing extracellular traps (NETs) containing histones as powerful antimicrobials. The formation of NETs is triggered by different agonists such as cytokines, microbial components and by bacteria themselves. Nevertheless, the so-called NETosis requires the formation of ROS. Interestingly, equal numbers of histone counts in infected spleens were observed in ADAPko and wild type mice. However, the number of histone counts declined from day 1 to day 3 post *Lm* infection in ADAPko but not in wild type animals (**Figure 39 A**). In contrast, although in the liver no differences in histone counts were detected on day 1 p. i., significantly more histones were released by neutrophils in ADAP-deficient mice compared to wild type counterparts on day 3 post *Lm* infection (**Figure 39 B**). However, no obvious impairment of NET release in ADAPko mice was observed and further experiments are required to clarify, if and to which extend the distinct differences in NET formation would affect pathogen control.

Next to NETs, neutrophils are capable to control bacterial pathogens by phagocytosis followed by the intracellular killing of ingested pathogens by producing reactive nitrogen and oxygen species[86]. It has been shown, that neutrophils play an important role in the immune response to low dose *Lm* infection in the liver, while in the spleen these cells play a vital role for protection against high dose infections[164]. Additionally, and as mentioned before, neutrophils

are more effective in phagocytosis of *Lm* than inflammatory monocytes[261]. Coppolino and colleagues documented that, among others, SLP-76 is necessary for the formation of phagosomes. Next to the initiation of phagocytosis, a molecular complex of Fyb, SLP-76 and other molecules is formed and the activation of Fcγ receptors leads to signaling events during phagocytosis that regulate actin polymerization, which indeed is indispensable for phagocytosis[10]. Noteworthy, TNF and especially iNOS are essential for clearing a murine *Lm* infection[179,193]. One might speculate that in spleen of *Lm*-infected ADAPko mice neutrophils switch from NETosis on day 1 post infection to phagocytosis on day 3, supported by the significantly reduced number of histones released (**Figure 39 A**) and at the same time the increased phagocytosis on day 3 post infection (**Figure 40 A** and **B**, **Supplement Figure 1 A**, right panel). A functional switch like this has indeed been described before[279–281] and is well in line with the findings of this thesis in livers on day 3 post *Lm* infection. Here, neutrophils from ADAPko mice formed more NETs than the wild type animals (**Figure 39 B**), while in direct contrast the phagocytic capacity of neutrophils from these mice was reduced (**Figure 40 A** and **C**, **Supplement Figure 1 A**, left panel). Taken together, one may consider the ineffective phagocytic capacity together with the observed broad alteration in the transcriptional program of neutrophils and in part inflammatory monocytes to be responsible for impaired pathogen control in ADAPko animals.

It remains largely unclear which of the observed effects regarding phagocyte phenotype and their functionality is most prominently affecting the outcome of listeriosis in ADAP-deficient mice and still there is a puzzling dichotomy between phagocyte accumulations at infection sites and inefficient pathogen control (**Figure 11** and **Figure 31**). It should be further considered that impaired early control of the pathogen and with this uncontrolled bacterial growth might result in continuing attraction of phagocytes that in turn directly contribute to immunopathology in spleen and liver of *Lm*-infected ADAPko mice[171]. During NET formation, histones are released into the surrounding tissues. Noteworthy, histones are toxic for invading pathogens, but additionally can cause tissue damage[282]. The priming of neutrophils results in a rapid as well as effective elimination of several pathogens, but also to the induction of toxic ROS, which can enhance tissue damage[283]. Targeted depletion of neutrophils during infection with *Lm* led to increased susceptibility and mortality especially at higher infection doses[164]. Interestingly, bacterial burden in spleen and liver as well as survival curves in neutrophil-deficient animals closely resemble those observed in ADAPko mice.

Together, these data not only highlight the overall importance of neutrophils during the early phase of listeriosis but at the same time support the findings that ADAP-deficiency negatively affects neutrophil-mediated immunity.

Taken together, in frame of this thesis the role of ADAP in a variety of different innate immune cell types was analyzed in the context of *Listeria monocytogenes* infection in mice. The obvious advantage of the chosen infection model is that it allows an *in vivo* priming of NK cells, neutrophils and inflammatory monocytes under physiological conditions, thereby adding another level of complexity and extending existing knowledge that has been mainly generated in simplified *in vitro* systems. Data obtained within this thesis show that during systemic *Lm* infection in mice ADAP is essential for efficient cytotoxic capacity and migration of NK cells, while an alternative priming of phagocytes during *Lm* infection in the ADAP-deficient host results in broad alterations in their inflammatory profile as well as impaired phagocytic capacity. We propose, that these alterations, together with so far unknown additional effects of ADAP-deficiency on anti-bacterial immune response induced in other innate immune cells, contribute to failures in anti-bacterial defense and ultimately the fatal outcome of listeriosis in mice lacking ADAP.

6 References

(1) Togni, M.; Lindquist, J.; Gerber, A.; Kölsch, U.; Hamm-Baarke, A.; Kliche, S.; Schraven, B. The Role of Adaptor Proteins in Lymphocyte Activation. *Mol. Immunol.* **2004**, *41* (6–7), 615–630. https://doi.org/10.1016/j.molimm.2004.04.009.

(2) Horejsí, V.; Zhang, W.; Schraven, B. Transmembrane Adaptor Proteins: Organizers of Immunoreceptor Signalling. *Nat. Rev. Immunol.* **2004**, *4* (8), 603–616. https://doi.org/10.1038/nri1414.

(3) Jordan, M. S.; Singer, A. L.; Koretzky, G. A. Adaptors as Central Mediators of Signal Transduction in Immune Cells. *Nat. Immunol.* **2003**, *4* (2), 110–116. https://doi.org/10.1038/ni0203-110.

(4) Marie-Cardine, A.; Bruyns, E.; Eckerskorn, C.; Kirchgessner, H.; Meuer, S. C.; Schraven, B. Molecular Cloning of SKAP55, a Novel Protein That Associates with the Protein Tyrosine Kinase P59 Fyn in Human T-Lymphocytes. *J. Biol. Chem.* **1997**, *272* (26), 16077–16080. https://doi.org/10.1074/jbc.272.26.16077.

(5) Veale, M.; Raab, M.; Li, Z.; da Silva, A. J.; Kraeft, S. K.; Weremowicz, S.; Morton, C. C.; Rudd, C. E. Novel Isoform of Lymphoid Adaptor FYN-T-Binding Protein (FYB-130) Interacts with SLP-76 and up-Regulates Interleukin 2 Production. *J. Biol. Chem.* **1999**, *274* (40), 28427–28435. https://doi.org/10.1074/jbc.274.40.28427.

(6) da Silva, A. J.; Li, Z.; de Vera, C.; Canto, E.; Findell, P.; Rudd, C. E. Cloning of a Novel T-Cell Protein FYB That Binds FYN and SH2-Domain-Containing Leukocyte Protein 76 and Modulates Interleukin 2 Production. *Proc. Natl. Acad. Sci. U. S. A.* **1997**, *94* (14), 7493–7498. https://doi.org/10.1073/pnas.94.14.7493.

(7) Musci, M. A.; Hendricks-Taylor, L. R.; Motto, D. G.; Paskind, M.; Kamens, J.; Turck, C. W.; Koretzky, G. A. Molecular Cloning of SLAP-130, an SLP-76-Associated Substrate of the T Cell Antigen Receptor-Stimulated Protein Tyrosine Kinases. *J. Biol. Chem.* **1997**, *272* (18), 11674–11677. https://doi.org/10.1074/jbc.272.18.11674.

(8) Fostel, L. V; Dluzniewska, J.; Shimizu, Y.; Burbach, B. J.; Peterson, E. J. ADAP Is Dispensable for NK Cell Development and Function. *Int. Immunol.* **2006**, *18* (8), 1305–1314. https://doi.org/10.1093/intimm/dxl063.

(9) Kasirer-Friede, A.; Cozzi, M. R.; Mazzucato, M.; De Marco, L.; Ruggeri, Z. M.; Shattil, S. J. Signaling through GP Ib-IX-V Activates Alpha IIb Beta 3 Independently of Other Receptors. *Blood* **2004**, *103* (9), 3403–3411. https://doi.org/10.1182/blood-2003-10-3664.

(10) Coppolino, M. G.; Krause, M.; Hagendorff, P.; Monner, D. A.; Trimble, W.; Grinstein, S.; Wehland, J.; Sechi, A. S. Evidence for a Molecular Complex Consisting of Fyb/SLAP, SLP-76, Nck, VASP and WASP That Links the Actin Cytoskeleton to Fcgamma Receptor Signalling during Phagocytosis. *J. Cell Sci.* **2001**, *114* (Pt 23), 4307–4318.

(11) Peterson, E. J.; Woods, M. L.; Dmowski, S. A.; Derimanov, G.; Jordan, M. S.; Wu, J. N.; Myung, P. S.; Liu, Q. H.; Pribila, J. T.; Freedman, B. D.; Shimizu, Y.; Koretzky, G. A. Coupling of the TCR to Integrin Activation by SLAP-130/Fyb. *Science (80-.).* **2001**, *293* (5538), 2263–2265. https://doi.org/10.1126/science.1063486.

(12) Medeiros, R. B.; Burbach, B. J.; Mueller, K. L.; Srivastava, R.; Moon, J. J.; Highfill, S.; Peterson, E. J.; Shimizu, Y. Regulation of NF-KB Activation in T Cells via Association of the Adapter Proteins ADAP and CARMA1. *Science (80-.).* **2007**, *316* (5825), 754–758. https://doi.org/10.1126/science.1137895.

(13) Griffiths, E. K.; Krawczyk, C.; Kong, Y. Y.; Raab, M.; Hyduk, S. J.; Bouchard, D.; Chan, V. S.; Kozieradzki, I.; Oliveira-Dos-Santos, A. J.; Wakeham, A.; Ohashi, P. S.; Cybulsky, M. I.; Rudd, C. E.; Penninger, J. M. Positive Regulation of T Cell Activation and Integrin Adhesion by the Adapter Fyb/Slap. *Science (80-.).* **2001**, *293* (5538), 2260–2263. https://doi.org/10.1126/science.1063397.

(14) Heuer, K.; Sylvester, M.; Kliche, S.; Pusch, R.; Thiemke, K.; Schraven, B.; Freund, C. Lipid-Binding HSH3 Domains in Immune Cell Adapter Proteins. *J. Mol. Biol.* **2006**, *361* (1), 94–104. https://doi.org/10.1016/j.jmb.2006.06.004.

(15) Sylvester M Lange S, Geithner S, Klemm C, Schlosser A, Grossmann A, K. S.; Stelzl U Krause E, Freund C, S. B. Adhesion and Degranulation Promoting Adapter Protein (ADAP) Is a Central Hub for Phosphotyrosine-Mediated Interactions in T Cells. *PLoS One* **2010**, *Jul 22* (5(7)), e11708. doi: 10.1371/journal.pone.0011708.-e11708.

(16) Heuer, K.; Kofler, M.; Langdon, G.; Thiemke, K.; Freund, C. Structure of a Helically Extended SH3 Domain of the T Cell Adapter Protein ADAP. *Structure* **2004**, *12* (4), 603–610. https://doi.org/10.1016/j.str.2004.02.021.

References

(17) Kuropka, B.; Witte, A.; Sticht, J.; Waldt, N.; Majkut, P.; Hackenberger, C. P. R.; Schraven, B.; Krause, E.; Kliche, S.; Freund, C. Analysis of Phosphorylation-Dependent Protein Interactions of Adhesion and Degranulation Promoting Adaptor Protein (ADAP) Reveals Novel Interaction Partners Required for Chemokine-Directed T Cell Migration. *Mol. Cell. Proteomics* **2015**, *14* (11), 2961–2972. https://doi.org/10.1074/mcp.M115.048249.

(18) Pawson, T.; Scott, J. D. Signaling Through Scaffold, Anchoring, and Adaptor Proteins. *Science (80-.).* **1997**, *278* (5346), 2075–2080. https://doi.org/10.1126/science.278.5346.2075.

(19) Kang, H.; Freund, C.; Duke-Cohan, J. S.; Musacchio, A.; Wagner, G.; Rudd, C. E. SH3 Domain Recognition of a Proline-Independent Tyrosine-Based RKxxYxxY Motif in Immune Cell Adaptor SKAP55. *EMBO J.* **2000**, *19* (12), 2889–2899. https://doi.org/10.1093/emboj/19.12.2889.

(20) Boerth, N. J.; Judd, B. A.; Koretzky, G. A. Functional Association between SLAP-130 and SLP-76 in Jurkat T Cells. *J. Biol. Chem.* **2000**, *275* (7), 5143–5152. https://doi.org/10.1074/jbc.275.7.5143.

(21) Raab, M.; Kang, H.; da Silva, A.; Zhu, X.; Rudd, C. E. FYN-T-FYB-SLP-76 Interactions Define a T-Cell Receptor Zeta/CD3-Mediated Tyrosine Phosphorylation Pathway That up-Regulates Interleukin 2 Transcription in T-Cells. *J. Biol. Chem.* **1999**, *274* (30), 21170–21179. https://doi.org/10.1074/jbc.274.30.21170.

(22) Krause, M.; Sechi, A. S.; Konradt, M.; Monner, D.; Gertler, F. B.; Wehland, J. Fyn-Binding Protein (Fyb)/Slp-76–Associated Protein (Slap), Ena/Vasodilator-Stimulated Phosphoprotein (Vasp) Proteins and the Arp2/3 Complex Link T Cell Receptor (Tcr) Signaling to the Actin Cytoskeleton. *J. Cell Biol.* **2000**, *149* (1), 181–194. https://doi.org/10.1083/jcb.149.1.181.

(23) Krause, M.; Dent, E. W.; Bear, J. E.; Loureiro, J. J.; Gertler, F. B. Ena/VASP Proteins: Regulators of the Actin Cytoskeleton and Cell Migration. *Annu. Rev. Cell Dev. Biol.* **2003**, *19* (1), 541–564. https://doi.org/10.1146/annurev.cellbio.19.050103.103356.

(24) Pauker, M. H.; Reicher, B.; Fried, S.; Perl, O.; Barda-Saad, M. Functional Cooperation between the Proteins Nck and ADAP Is Fundamental for Actin Reorganization. *Mol. Cell. Biol.* **2011**, *31* (13), 2653–2666. https://doi.org/10.1128/MCB.01358-10.

(25) Srivastava, R.; Burbach, B. J.; Mitchell, J. S.; Pagan, A. J.; Shimizu, Y. ADAP Regulates Cell Cycle Progression of T Cells via Control of Cyclin E and Cdk2 Expression through Two Distinct CARMA1-Dependent Signaling Pathways. *Mol. Cell. Biol.* **2012**, *32* (10), 1908–1917. https://doi.org/10.1128/MCB.06541-11.

(26) Blonska, M.; Lin, X. CARMA1-Mediated NF-KB and JNK Activation in Lymphocytes. *Immunol. Rev.* **2009**, *228* (1), 199–211. https://doi.org/10.1111/j.1600-065X.2008.00749.x.

(27) Thome, M.; Charton, J. E.; Pelzer, C.; Hailfinger, S. Antigen Receptor Signaling to NF-KappaB via CARMA1, BCL10, and MALT1. *Cold Spring Harbor perspectives in biology*. 2010. https://doi.org/10.1101/cshperspect.a003004.

(28) Burbach, B. J.; Srivastava, R.; Ingram, M. A.; Mitchell, J. S.; Shimizu, Y. The Pleckstrin Homology Domain in the SKAP55 Adapter Protein Defines the Ability of the Adapter Protein ADAP to Regulate Integrin Function and NF-KappaB Activation. *J. Immunol.* **2011**, *186* (11), 6227–6237. https://doi.org/10.4049/jimmunol.1002950.

(29) Ghosh, S.; Hayden, M. S. New Regulators of NF-KappaB in Inflammation. *Nat. Rev. Immunol.* **2008**, *8* (11), 837–848.

(30) Cheng, J.; Montecalvo, A.; Kane, L. P. Regulation of NF-KB Induction by TCR/CD28. *Immunol. Res.* **2011**, *50* (2–3), 113–117. https://doi.org/10.1007/s12026-011-8216-z.

(31) Marie-Cardine, A.; Ranee Hendricks-Taylor, L.; Boerth, N. J.; Zhao, H.; Schraven, B.; Koretzky, G. A. Molecular Interaction between the Fyn-Associated Protein SKAP55 and the SLP-76-Associated Phosphoprotein SLAP-130. *J. Biol. Chem.* **1998**, *273* (40), 25789–25795. https://doi.org/10.1074/jbc.273.40.25789.

(32) Burbach, B. J.; Srivastava, R.; Medeiros, R. B.; O'Gorman, W. E.; Peterson, E. J.; Shimizu, Y. Distinct Regulation of Integrin-Dependent T Cell Conjugate Formation and NF-Kappa B Activation by the Adapter Protein ADAP. *J. Immunol.* **2008**, *181* (7), 4840–4851. https://doi.org/10.4049/jimmunol.181.7.4840.

(33) Togni, M.; Swanson, K. D.; Reimann, S.; Kliche, S.; Pearce, A. C.; Simeoni, L.; Reinhold, D.; Wienands, J.; Neel, B. G.; Schraven, B.; Gerber, A. Regulation of In Vitro and In Vivo Immune Functions by the Cytosolic Adaptor Protein SKAP-HOM. *Mol. Cell. Biol.* **2005**, *25* (18), 8052–8063. https://doi.org/10.1128/mcb.25.18.8052-8063.2005.

References

(34) Kliche, S.; Breitling, D.; Togni, M.; Pusch, R.; Heuer, K.; Wang, X.; Freund, C.; Kasirer-Friede, A.; Menasche, G.; Koretzky, G. A.; Schraven, B. The ADAP/SKAP55 Signaling Module Regulates T-Cell Receptor-Mediated Integrin Activation through Plasma Membrane Targeting of Rap1. *Mol. Cell. Biol.* **2006**, *26* (19), 7130–7144. https://doi.org/10.1128/mcb.00331-06.

(35) Huang, Y.; Norton, D. D.; Precht, P.; Martindale, J. L.; Burkhardt, J. K.; Wange, R. L. Deficiency of ADAP/Fyb/SLAP-130 Destabilizes SKAP55 in Jurkat T Cells. *J. Biol. Chem.* **2005**, *280* (25), 23576–23583. https://doi.org/10.1074/jbc.M413201200.

(36) Hegedûs, Z.; Chitu, V.; Tóth, G. K.; Finta, C.; Váradi, G.; Andó, I.; Monostori, E. Contribution of Kinases and the CD45 Phosphatase to the Generation of Tyrosine Phosphorylation Patterns in the T-Cell Receptor Complex Zeta Chain. *Immunol. Lett.* **1999**, *67* (1), 31–39. https://doi.org/10.1016/s0165-2478(98)00138-2.

(37) Burkhardt, A. L.; Stealey, B.; Rowley, R. B.; Mahajan, S.; Prendergast, M.; Fargnoli, J.; Bolen, J. B. Temporal Regulation of Non-Transmembrane Protein Tyrosine Kinase Enzyme Activity Following T Cell Antigen Receptor Engagement. *J. Biol. Chem.* **1994**, *269* (38), 23642–23647.

(38) Liu, S. K.; Fang, N.; Koretzky, G. A.; McGlade, C. J. The Hematopoietic-Specific Adaptor Protein Gads Functions in T-Cell Signaling via Interactions with the SLP-76 and LAT Adaptors. *Curr. Biol.* **1999**, *9* (2), 67–75. https://doi.org/10.1016/S0960-9822(99)80017-7.

(39) Acuto, O.; Bartolo, V. Di; Michel, F. Tailoring T-Cell Receptor Signals by Proximal Negative Feedback Mechanisms. *Nature Reviews Immunology*. 2008, pp 699–712. https://doi.org/10.1038/nri2397.

(40) Smith-Garvin, J. E.; Koretzky, G. A.; Jordan, M. S. T Cell Activation. *Annu Rev Immunol* **2009**, *27*, 591–619.

(41) Simeoni, L.; Kliche, S.; Lindquist, J.; Schraven, B. Adaptors and Linkers in T and B Cells. *Curr. Opin. Immunol.* **2004**, *16* (3), 304–313. https://doi.org/10.1016/j.coi.2004.03.001.

(42) Kliche, S.; Worbs, T.; Wang, X.; Degen, J.; Patzak, I.; Meineke, B.; Togni, M.; Moser, M.; Reinhold, A.; Kiefer, F.; Freund, C.; Förster, R.; Schraven, B. CCR7-Mediated LFA-1 Functions in T Cells Are Regulated by 2 Independent ADAP/SKAP55 Modules. *Blood* **2012**, *119* (3), 777–785. https://doi.org/10.1182/blood-2011-06-362269.

(43) Lafuente, E. M.; van Puijenbroek, A. A. F. L.; Krause, M.; Carman, C. V; Freeman, G. J.; Berezovskaya, A.; Constantine, E.; Springer, T. A.; Gertler, F. B.; Boussiotis, V. A. RIAM, an Ena/VASP and Profilin Ligand, Interacts with Rap1-GTP and Mediates Rap1-Induced Adhesion. *Dev. Cell* **2004**, *7* (4), 585–595. https://doi.org/10.1016/j.devcel.2004.07.021.

(44) Katagiri, K.; Maeda, A.; Shimonaka, M.; Kinashi, T. RAPL, a Rap1-Binding Molecule That Mediates Rap1-Induced Adhesion through Spatial Regulation of LFA-1. *Nat. Immunol.* **2003**, *4* (8), 741–748. https://doi.org/10.1038/ni950.

(45) Raab, M.; Wang, H.; Lu, Y.; Smith, X.; Wu, Z.; Strebhardt, K.; Ladbury, J. E.; Rudd, C. E. T Cell Receptor "Inside-Out" Pathway via Signaling Module SKAP1-RapL Regulates T Cell Motility and Interactions in Lymph Nodes. *Immunity* **2010**, *32* (4), 541–556. https://doi.org/10.1016/j.immuni.2010.03.007.

(46) Sánchez, M. J.; Muench, M. O.; Roncarolo, M. G.; Lanier, L. L.; Phillips, J. H. Identification of a Common t/Natural Killer Cell Progenitor in Human Fetal Thymus. *J. Exp. Med.* **1994**, *180* (2), 569–576. https://doi.org/10.1084/jem.180.2.569.

(47) May, R. M.; Okumura, M.; Hsu, C. J.; Bassiri, H.; Yang, E.; Rak, G.; Mace, E. M.; Philip, N. H.; Zhang, W.; Baumgart, T.; Orange, J. S.; Nichols, K. E.; Kambayashi, T. Murine Natural Killer Immunoreceptors Use Distinct Proximal Signaling Complexes to Direct Cell Function. *Blood* **2013**, *121* (16), 3135–3146. https://doi.org/10.1182/blood-2012-12-474361.

(48) Rajasekaran, K.; Kumar, P.; Schuldt, K. M.; Peterson, E. J.; Vanhaesebroeck, B.; Dixit, V.; Thakar, M. S.; Malarkannan, S. Signaling by Fyn-ADAP via the Carma1-Bcl-10-MAP3K7 Signalosome Exclusively Regulates Inflammatory Cytokine Production in NK Cells. *Nat. Immunol.* **2013**, *14* (11), 1127–1136. https://doi.org/10.1038/ni.2708.

(49) Thakar, M. S.; Kearl, T. J.; Malarkannan, S. Controlling Cytokine Release Syndrome to Harness the Full Potential of CAR-Based Cellular Therapy. *Frontiers in Oncology*. Frontiers Media S.A. January 31, 2020. https://doi.org/10.3389/fonc.2019.01529.

(50) Gerbec, Z. J.; Thakar, M. S.; Malarkannan, S. The Fyn-ADAP Axis: Cytotoxicity versus Cytokine Production in Killer Cells. *Frontiers in Immunology*. Frontiers Media S.A. 2015, p 472. https://doi.org/10.3389/fimmu.2015.00472.

(51) Vivier, E.; Ugolini, S.; Nunès, J. A. ADAPted Secretion of Cytokines in NK Cells. *Nature Immunology*. Nature Publishing Group 2013, pp 1108–1110. https://doi.org/10.1038/ni.2737.

References

(52) Block, H.; Herter, J. M.; Rossaint, J.; Stadtmann, A.; Kliche, S.; Lowell, C. A.; Zarbock, A. Crucial Role of SLP-76 and ADAP for Neutrophil Recruitment in Mouse Kidney Ischemia-Reperfusion Injury. *J. Exp. Med.* **2012**, *209* (2), 407–421. https://doi.org/10.1084/jem.20111493.

(53) Rudolph, J.; Meinke, C.; Voss, M.; Guttek, K.; Kliche, S.; Reinhold, D.; Schraven, B.; Reinhold, A. Immune Cell-Type Specific Ablation of Adapter Protein ADAP Differentially Modulates EAE. *Front. Immunol.* **2019**, *10*. https://doi.org/10.3389/fimmu.2019.02343.

(54) Alenghat, F. J.; Baca, Q. J.; Rubin, N. T.; Pao, L. I.; Matozaki, T.; Lowell, C. A.; Golan, D. E.; Neel, B. G.; Swanson, K. D. Macrophages Require Skap2 and Sirpα for Integrin-Stimulated Cytoskeletal Rearrangement. *J. Cell Sci.* **2012**, *125* (22), 5535–5545. https://doi.org/10.1242/jcs.111260.

(55) Yang, N.; Xiong, Y.; Wang, Y.; Yi, Y.; Zhu, J.; Ma, F.; Li, J.; Liu, H. ADAP Y571 Phosphorylation Is Required to Prime STAT3 for Activation in TLR4-Stimulated Macrophages. *J. Immunol.* **2021**, *206* (4), 814–826. https://doi.org/10.4049/jimmunol.2000569.

(56) Murray, E. G. D.; Webb, R. A.; Swann, M. B. R. A Disease of Rabbits Characterised by a Large Mononuclear Leucocytosis, Caused by a Hitherto Undescribed Bacillus Bacterium Monocytogenes (n.Sp.). *J. Pathol.* **1926**, *29* (4), S. 407–439. doi: 10.1002/path.1700290409.

(57) Nyfeldt A. Etiologie de La Mononucleose Infectieuse. *Comptes Rendus des Seances la Soc. Biol.* **1929**, *101* (590–591).

(58) Ueda, F.; Anahara, R.; Yamada, F.; Mochizuki, M.; Ochiai, Y.; Hondo, R. Discrimination of Listeria Monocytogenes Contaminated Commercial Japanese Meats. *Int. J. Food Microbiol.* **2005**, *105* (3), 455-462. doi: 10.1016/j.ijfoodmicro.2005.04.022. https://doi.org/10.1016/j.ijfoodmicro.2005.04.022.

(59) Pamer, E. G. Immune Responses to Listeria Monocytogenes. *Nature Reviews Immunology*. 2004, pp 812–823. https://doi.org/10.1038/nri1461.

(60) Mateus, T.; Silva, J.; Maia, R. L.; Teixeira, P. Listeriosis during Pregnancy: A Public Health Concern. *ISRN Obstet. Gynecol.* **2013**, *2013*, 851712. doi: 10.1155/2013/851712.

(61) Levidiotou, S.; Charalabopoulos, K.; Vrioni, G.; Chaidos, A.; Polysoidis, K.; Bourantas, K.; Stefanou, D. Fatal Meningitis Due to Listeria Monocytogenes in Elderly Patients with Underlying Malignancy. *Int. J. Clin. Pract.* **2004**, *58* (3), 292-6. doi: 10.1111/j.1368-5031.2004.00076.x.

(62) Schuchat, A.; Deaver, K. A.; Wenger, J. D.; Plikaytis, B. D.; Mascola, L.; Pinner, R. W.; Reingold, A. L.; Broome, C. V. Role of Foods in Sporadic Listeriosis. I. Case-Control Study of Dietary Risk Factors. The Listeria Study Group. *JAMA* **1992**, *267* (15), 2041–2045.

(63) Mackaness, G. B. CELLULAR RESISTANCE TO INFECTION. *J. Exp. Med.* **1962**, *116* (3), 381-406. doi: 10.1084/jem.116.3.381.

(64) Pitts, M. G.; D'Orazio, S. E. F. A Comparison of Oral and Intravenous Mouse Models of Listeriosis. *Pathogens*. MDPI AG March 1, 2018. https://doi.org/10.3390/pathogens7010013.

(65) Lecuit, M.; Dramsi, S.; Gottardi, C.; Fedor-Chaiken, M.; Gumbiner, B.; Cossart, P. A Single Amino Acid in E-Cadherin Responsible for Host Specificity towards the Human Pathogen Listeria Monocytogenes. *EMBO J.* **1999**, *18* (14), 3956–3963. https://doi.org/10.1093/emboj/18.14.3956.

(66) Camilli, A.; Tilney, L. G.; Portnoy, D. A. Dual Roles of PlcA in Listeria Monocytogenes Pathogenesis. *Mol. Microbiol.* **1993**, *8* (1), 143–157. https://doi.org/10.1111/j.1365-2958.1993.tb01211.x.

(67) Bierne, H.; Sabet, C.; Personnic, N.; Cossart, P. Internalins: A Complex Family of Leucine-Rich Repeat-Containing Proteins in Listeria Monocytogenes. *Microbes Infect.* **2007**, *9* (10), 1156-66. doi: 10.1016/j.micinf.2007.05.003.

(68) Veiga, E.; Cossart, P. Listeria Hijacks the Clathrin-Dependent Endocytic Machinery to Invade Mammalian Cells. *Nat. Cell Biol.* **2005**, *7* (9), 894–900. https://doi.org/10.1038/ncb1292.

(69) Pizarro-Cerdá, J.; Cossart, P. Subversion of Cellular Functions by Listeria Monocytogenes. *J. Pathol.* **2006**, *208* (2), 215-23. doi: 10.1002/path.1888.

(70) Ray, K.; Marteyn, B.; Sansonetti, P. J.; Tang, C. M. Life on the inside: The Intracellular Lifestyle of Cytosolic Bacteria. *Nature Reviews Microbiology*. Nature Publishing Group 2009, pp 333–340. https://doi.org/10.1038/nrmicro2112.

(71) Stavru, F.; Archambaud, C.; Cossart, P. Cell Biology and Immunology of Listeria Monocytogenes Infections: Novel Insights. *Immunol. Rev.* **2011**, *240* (1), 160-84. doi: 10.1111/j.1600-065X.2010.00993.x.

(72) Welch, M. D.; Iwamatsu, A.; Mitchison, T. J. Actin Polymerization Is Induced by Arp 2/3 Protein Complex at the Surface of Listeria Monocytogenes. *Nature* **1997**, *385* (6613), 265-269. doi: 10.1038/385265a0.

(73) Daugelat, S.; Ladel, C. H.; Schoel, B.; Kaufmann, S. H. Antigen-Specific T-Cell Responses during Primary and Secondary Listeria Monocytogenes Infection. *Infect. Immun.* **1994**, *62* (5), 1881–1888.

References

(74) Finelli, A.; Kerksiek, K. M.; Allen, S. E.; Marshall, N.; Mercado, R.; Pilip, I.; Busch, D. H.; Pamer, E. G. MHC Class I Restricted T Cell Responses to Listeria Monocytogenes, an Intracellular Bacterial Pathogen. *Immunologic Research*. Humana Press 1999, pp 211–223. https://doi.org/10.1007/BF02786489.

(75) Pearce, E. L.; Shen, H. Generation of CD8 T Cell Memory Is Regulated by IL-12. *J. Immunol.* **2007**, *179* (4), 2074–2081. https://doi.org/10.4049/jimmunol.179.4.2074.

(76) Sharma, K.; Wang, R. X.; Zhang, L. Y.; Yin, D. L.; Luo, X. Y.; Solomon, J. C.; Jiang, R. F.; Markos, K.; Davidson, W.; Scott, D. W.; Shi, Y. F. Death the Fas Way: Regulation and Pathophysiology of CD95 and Its Ligand. *Pharmacology and Therapeutics*. Pharmacol Ther 2000, pp 333–347. https://doi.org/10.1016/S0163-7258(00)00096-6.

(77) Harty, J. T.; Badovinac, V. P. Influence of Effector Molecules on the CD8+ T Cell Response to Infection. *Current Opinion in Immunology*. Curr Opin Immunol June 1, 2002, pp 360–365. https://doi.org/10.1016/S0952-7915(02)00333-3.

(78) Sun, J. C.; Bevan, M. J. Defective CD8 T Cell Memory Following Acute Infection without CD4 T Cell Help. *Science (80-.).* **2003**, *300* (5617), 339–342. https://doi.org/10.1126/science.1083317.

(79) Calame, D. G.; Mueller-Ortiz, S. L.; Wetsel, R. A. Innate and Adaptive Immunologic Functions of Complement in the Host Response to Listeria Monocytogenes Infection. *Immunobiology*. Elsevier GmbH December 1, 2016, pp 1407–1417. https://doi.org/10.1016/j.imbio.2016.07.004.

(80) Cheers, C.; McKenzie, I. F.; Pavlov, H.; Waid, C.; York, J. Resistance and Susceptibility of Mice to Bacterial Infection: Course of Listeriosis in Resistant or Susceptible Mice. *Infect. Immun.* **1978**, *19* (3), 763–770.

(81) Akira, S.; Uematsu, S.; Takeuchi, O. Pathogen Recognition and Innate Immunity. *Cell*. February 24, 2006, pp 783–801. https://doi.org/10.1016/j.cell.2006.02.015.

(82) Torres, D.; Barrier, M.; Bihl, F.; Quesniaux, V. J. F.; Maillet, I.; Akira, S.; Ryffel, B.; Erard, F. Toll-like Receptor 2 Is Required for Optimal Control of Listeria Monocytogenes Infection. *Infect. Immun.* **2004**, *72* (4), 2131–2139. https://doi.org/10.1128/iai.72.4.2131-2139.2004.

(83) Corr, S. C.; O'Neill, L. A. J. Listeria Monocytogenes Infection in the Face of Innate Immunity. *Cell. Microbiol.* **2009**, *11* (5), 703–709. https://doi.org/10.1111/j.1462-5822.2009.01294.x.

(84) Medzhitov, R. Recognition of Microorganisms and Activation of the Immune Response. *Nature*. Nature Publishing Group October 18, 2007, pp 819–826. https://doi.org/10.1038/nature06246.

(85) Thaler, B.; Hohensinner, P. J.; Krychtiuk, K. A.; Matzneller, P.; Koller, L.; Brekalo, M.; Maurer, G.; Huber, K.; Zeitlinger, M.; Jilma, B.; Wojta, J.; Speidl, W. S. Differential in Vivo Activation of Monocyte Subsets during Low-Grade Inflammation through Experimental Endotoxemia in Humans. *Sci. Rep.* **2016**, *6*, 30162. https://doi.org/10.1038/srep30162.

(86) Segal, A. W. How Neutrophils Kill Microbes. *Annu. Rev. Immunol.* **2005**, *23* (1), 197–223. https://doi.org/10.1146/annurev.immunol.23.021704.115653.

(87) Witter, A. R.; Okunnu, B. M.; Berg, R. E. The Essential Role of Neutrophils during Infection with the Intracellular Bacterial Pathogen Listeria Monocytogenes. *J. Immunol.* **2016**, *197* (5), 1557–1565. https://doi.org/10.4049/jimmunol.1600599.

(88) Guleria, I.; Pollard, J. W. Aberrant Macrophage and Neutrophil Population Dynamics and Impaired Th1 Response to Listeria Monocytogenes in Colony-Stimulating Factor 1-Deficient Mice. *Infect. Immun.* **2001**, *69* (3), 1795–1807. https://doi.org/10.1128/IAI.69.3.1795-1807.2001.

(89) Tecchio, C.; Micheletti, A.; Cassatella, M. A. Neutrophil-Derived Cytokines: Facts beyond Expression. *Frontiers in Immunology*. Frontiers Media S.A. 2014. https://doi.org/10.3389/fimmu.2014.00508.

(90) Zenewicz, L. A.; Shen, H. Innate and Adaptive Immune Responses to Listeria Monocytogenes: A Short Overview. *Microbes and Infection*. August 2007, pp 1208–1215. https://doi.org/10.1016/j.micinf.2007.05.008.

(91) Tripp, C. S.; Wolf, S. F.; Unanue, E. R. Interleukin 12 and Tumor Necrosis Factor Alpha Are Costimulators of Interferon Gamma Production by Natural Killer Cells in Severe Combined Immunodeficiency Mice with Listeriosis, and Interleukin 10 Is a Physiologic Antagonist. *Proc. Natl. Acad. Sci. U. S. A.* **1993**, *90* (8), 3725–3729. https://doi.org/10.1073/pnas.90.8.3725.

(92) Herberman, R. B.; Nunn, M. E.; Holden, H. T.; Lavrin, D. H. Natural Cytotoxic Reactivity of Mouse Lymphoid Cells against Syngeneic and Allogeneic Tumors. II. Characterization of Effector Cells. *Int. J. Cancer* **1975**, *16* (2), 230–239. https://doi.org/10.1002/ijc.2910160205.

(93) Kiessling, R.; Klein, E.; Pross, H.; Wigzell, H. "Natural" Killer Cells in the Mouse. II. Cytotoxic Cells with Specificity for Mouse Moloney Leukemia Cells. Characteristics of the Killer Cell. *Eur. J. Immunol.* **1975**, *5* (2), 117–121. https://doi.org/10.1002/eji.1830050209.

References

(94) Vivier, E.; Raulet, D. H.; Moretta, A.; Caligiuri, M. A.; Zitvogel, L.; Lanier, L. L.; Yokoyama, W. M.; Ugolini, S. Innate or Adaptive Immunity? The Example of Natural Killer Cells. *Science (80-.).* **2011**, *331* (6013), 44–49. https://doi.org/10.1126/science.1198687.

(95) Held, W.; Jeevan-Raj, B.; Charmoy, M. Transcriptional Regulation of Murine Natural Killer Cell Development, Differentiation and Maturation. *Cellular and Molecular Life Sciences*. Birkhauser Verlag AG 2018, pp 3371–3379. https://doi.org/10.1007/s00018-018-2865-1.

(96) Lanier, L. L.; Phillips, J. H.; Hackett, J.; Tutt, M.; Kumar, V. Natural Killer Cells: Definition of a Cell Type Rather than a Function. *J. Immunol.* **1986**, *137* (9), 2735–2739.

(97) Moretta, A.; Bottino, C.; Mingari, M. C.; Biassoni, R.; Moretta, L. *What Is a Natural Killer Cell?*; 2002.

(98) Abel, A. M.; Yang, C.; Thakar, M. S.; Malarkannan, S. Natural Killer Cells: Development, Maturation, and Clinical Utilization. *Frontiers in Immunology*. Frontiers Media S.A. 2018, p 1869. https://doi.org/10.3389/fimmu.2018.01869.

(99) Vivier, E.; Artis, D.; Colonna, M.; Diefenbach, A.; Di Santo, J. P.; Eberl, G.; Koyasu, S.; Locksley, R. M.; McKenzie, A. N. J.; Mebius, R. E.; Powrie, F.; Spits, H. Innate Lymphoid Cells: 10 Years On. *Cell.* 2018, pp 1054–1066. https://doi.org/10.1016/j.cell.2018.07.017.

(100) Zhang, Y.; Huang, B. The Development and Diversity of ILCs, NK Cells and Their Relevance in Health and Diseases. In *Advances in Experimental Medicine and Biology*; Springer New York LLC, 2017; Vol. 1024, pp 225–244. https://doi.org/10.1007/978-981-10-5987-2_11.

(101) Walzer, T.; Bléry, M.; Chaix, J.; Fuseri, N.; Chasson, L.; Robbins, S. H.; Jaeger, S.; André, P.; Gauthier, L.; Daniel, L.; Chemin, K.; Morel, Y.; Dalod, M.; Imbert, J.; Pierres, M.; Moretta, A.; Romagné, F.; Vivier, E. Identification, Activation, and Selective in Vivo Ablation of Mouse NK Cells via NKp46. *Proc. Natl. Acad. Sci. U. S. A.* **2007**, *104* (9), 3384–3389. https://doi.org/10.1073/pnas.0609692104.

(102) Walzer, T.; Bléry, M.; Chaix, J.; Fuseri, N.; Chasson, L.; Robbins, S. H.; Jaeger, S.; André, P.; Gauthier, L.; Daniel, L.; Chemin, K.; Morel, Y.; Dalod, M.; Imbert, J.; Pierres, M.; Moretta, A.; Romagné, F.; Vivier, E. Identification, Activation, and Selective in Vivo Ablation of Mouse NK Cells via NKp46. *Proc. Natl. Acad. Sci. U. S. A.* **2007**, *104* (9), 3384–3389. https://doi.org/10.1073/pnas.0609692104.

(103) Strowig, T.; Brilot, F.; Münz, C. *Non-Cytotoxic Functions of Natural Killer Cells: Direct Pathogen Restriction and Assistance to Adaptive Immunity 1*.

(104) Sun, J. C.; Lanier, L. L. NK Cell Development, Homeostasis and Function: Parallels with CD8 + T Cells. https://doi.org/10.1038/nri3044.

(105) Vivier, E.; Tomasello, E.; Baratin, M.; Walzer, T.; Ugolini, S. Functions of Natural Killer Cells. *Nature Immunology*. May 2008, pp 503–510. https://doi.org/10.1038/ni1582.

(106) Vosshenrich, C. A. J.; Samson-Villéger, S. I.; Di Santo, J. P. Distinguishing Features of Developing Natural Killer Cells. *Current Opinion in Immunology*. Elsevier Ltd 2005, pp 151–158. https://doi.org/10.1016/j.coi.2005.01.005.

(107) Kondo, M.; Weissman, I. L.; Akashi, K. *Identification of Clonogenic Common Lymphoid Progenitors in Mouse Bone Marrow*; 1997; Vol. 91.

(108) Rosmaraki, E. E.; Douagi, I.; Roth, C.; Colucci, F.; Cumano, A.; Di Santo, J. P. Identification of Committed NK Cell Progenitors in Adult Murine Bone Marrow. *Eur. J. Immunol.* **2001**, *31* (6), 1900–1909. https://doi.org/10.1002/1521-4141(200106)31:6<1900::AID-IMMU1900>3.0.CO;2-M.

(109) Sojka, D. K.; Tian, Z.; Yokoyama, W. M. Tissue-Resident Natural Killer Cells and Their Potential Diversity. *Seminars in Immunology*. 2014, pp 127–131. https://doi.org/10.1016/j.smim.2014.01.010.

(110) Goh, W.; Huntington, N. D. Regulation of Murine Natural Killer Cell Development. *Frontiers in Immunology*. Frontiers Research Foundation 2017, p 130. https://doi.org/10.3389/fimmu.2017.00130.

(111) Fathman, J. W.; Bhattacharya, D.; Inlay, M. A.; Seita, J.; Karsunky, H.; Weissman, I. L. Identification of the Earliest Natural Killer Cell-Committed Progenitor in Murine Bone Marrow. *Blood* **2011**, *118* (20), 5439–5447. https://doi.org/10.1182/blood-2011-04-348912.

(112) Ramirez, K.; Chandler, K. J.; Spaulding, C.; Zandi, S.; Sigvardsson, M.; Graves, B. J.; Kee, B. L. Gene Deregulation and Chronic Activation in Natural Killer Cells Deficient in the Transcription Factor ETS1. *Immunity* **2012**, *36* (6), 921–932. https://doi.org/10.1016/j.immuni.2012.04.006.

(113) Vosshenrich, C. A. J.; Ranson, T.; Samson, S. I.; Corcuff, E.; Colucci, F.; Rosmaraki, E. E.; Di Santo, J. P. Roles for Common Cytokine Receptor γ-Chain-Dependent Cytokines in the Generation, Differentiation, and Maturation of NK Cell Precursors and Peripheral NK Cells in Vivo. *J. Immunol.* **2005**, *174* (3), 1213–1221. https://doi.org/10.4049/jimmunol.174.3.1213.

References

(114)   Kim, S.; Iizuka, K.; Kang, H. S. P.; Dokun, A.; French, A. R.; Greco, S.; Yokoyama, W. M. In Vivo Developmental Stages in Murine Natural Killer Cell Maturation. *Nat. Immunol.* **2002**, *3* (6), 523–528. https://doi.org/10.1038/ni796.

(115)   Chiossone, L.; Chaix, J.; Fuseri, N.; Roth, C.; Vivier, E.; Walzer, T. Maturation of Mouse NK Cells Is a 4-Stage Developmental Program. *Blood* **2009**, *113* (22), 5488–5496. https://doi.org/10.1182/blood-2008-10-187179.

(116)   Hayakawa, Y.; Smyth, M. J. CD27 Dissects Mature NK Cells into Two Subsets with Distinct Responsiveness and Migratory Capacity. *J. Immunol.* **2006**, *176* (3), 1517–1524. https://doi.org/10.4049/jimmunol.176.3.1517.

(117)   Huntington, N. D.; Vosshenrich, C. A. J.; Di Santo, J. P. Developmental Pathways That Generate Natural-Killer-Cell Diversity in Mice and Humans. *Nature Reviews Immunology*. Nat Rev Immunol September 2007, pp 703–714. https://doi.org/10.1038/nri2154.

(118)   Di Santo, J. P. Natural Killer Cell Developmental Pathways: A Question of Balance. *Annu. Rev. Immunol.* **2006**, *24* (1), 257–286. https://doi.org/10.1146/annurev.immunol.24.021605.090700.

(119)   Warren, H. S.; Smyth, M. J. NK Cells and Apoptosis. *Immunology and Cell Biology*. Immunol Cell Biol 1999, pp 64–75. https://doi.org/10.1046/j.1440-1711.1999.00790.x.

(120)   Lee, S. H.; Miyagi, T.; Biron, C. A. Keeping NK Cells in Highly Regulated Antiviral Warfare. *Trends Immunol.* **2007**, *28* (6), 252–259. https://doi.org/10.1016/j.it.2007.04.001.

(121)   Martínez-Lostao, L.; Anel, A.; Pardo, J. How Do Cytotoxic Lymphocytes Kill Cancer Cells? *Clin. Cancer Res.* **2015**, *21* (22), 5047–5056. https://doi.org/10.1158/1078-0432.CCR-15-0685.

(122)   Topham, N. J.; Hewitt, E. W. Natural Killer Cell Cytotoxicity: How Do They Pull the Trigger? *Immunology*. Immunology September 2009, pp 7–15. https://doi.org/10.1111/j.1365-2567.2009.03123.x.

(123)   MacE, E. M.; Dongre, P.; Hsu, H. T.; Sinha, P.; James, A. M.; Mann, S. S.; Forbes, L. R.; Watkin, L. B.; Orange, J. S. Cell Biological Steps and Checkpoints in Accessing NK Cell Cytotoxicity. *Immunology and Cell Biology*. Nature Publishing Group 2014, pp 245–255. https://doi.org/10.1038/icb.2013.96.

(124)   Lopez, J. A.; Jenkins, M. R.; Rudd-Schmidt, J. A.; Brennan, A. J.; Danne, J. C.; Mannering, S. I.; Trapani, J. A.; Voskoboinik, I. Rapid and Unidirectional Perforin Pore Delivery at the Cytotoxic Immune Synapse. *J. Immunol.* **2013**, *191* (5), 2328–2334. https://doi.org/10.4049/jimmunol.1301205.

(125)   Van den Brink, M. R. M.; Burakoff, S. J. Cytolytic Pathways in Haematopoietic Stem-Cell Transplantation. *Nature Reviews Immunology*. European Association for Cardio-Thoracic Surgery 2002, pp 273–281. https://doi.org/10.1038/nri775.

(126)   Alter, G.; Malenfant, J. M.; Altfeld, M. CD107a as a Functional Marker for the Identification of Natural Killer Cell Activity. *J. Immunol. Methods* **2004**, *294* (1–2), 15-22. doi: 10.1016/j.jim.2004.08.008.

(127)   Aktas, E.; Kucuksezer, U. C.; Bilgic, S.; Erten, G.; Deniz, G. Relationship between CD107a Expression and Cytotoxic Activity. *Cell. Immunol.* **2009**, *254* (2), 149–154. https://doi.org/10.1016/j.cellimm.2008.08.007.

(128)   Smyth, M. J.; Cretney, E.; Takeda, K.; Wiltrout, R. H.; Sedger, L. M.; Kayagaki, N.; Yagita, H.; Okumura, K. Tumor Necrosis Factor-Related Apoptosis-Inducing Ligand (TRAIL) Contributes to Interferon γ-Dependent Natural Killer Cell Protection from Tumor Metastasis. *J. Exp. Med.* **2001**, *193* (6), 661–670. https://doi.org/10.1084/jem.193.6.661.

(129)   Reed, J. C. Apoptosis-Based Therapies. *Nature Reviews Drug Discovery*. Nat Rev Drug Discov February 2002, pp 111–121. https://doi.org/10.1038/nrd726.

(130)   Teixeira, H. C. and Kaufmann, S. H. Role of NK1.1+ Cells in Experimental Listeriosis. NK1+ Cells Are Early IFN-Gamma Producers but Impair Resistance to Listeria Monocytogenes Infection. *J Immunol* **1994**, *Feb 15* (152(4)), 1873-82. PMID: 8120395.

(131)   Viegas, N.; Andzinski, L.; Wu, C. F.; Komoll, R. M.; Gekara, N.; Dittmar, K. E.; Weiss, S.; Jablonska, J. IFN-γ Production by CD27+ NK Cells Exacerbates Listeria Monocytogenes Infection in Mice by Inhibiting Granulocyte Mobilization. *Eur. J. Immunol.* **2013**, *43* (10), 2626–2637. https://doi.org/10.1002/eji.201242937.

(132)   Humann, J and Lenz, L. L. Activation of Naive NK Cells in Response to Listeria Monocytogenes Requires IL-18 and Contact with Infected Dendritic Cells. *J. Immunol.* **2010**, *184* (9), 5172–5178. https://doi.org/10.4049/jimmunol.0903759.

(133)   Lucas, M.; Schachterle, W.; Oberle, K.; Aichele, P.; Diefenbach, A. Dendritic Cells Prime Natural Killer Cells by Trans-Presenting Interleukin 15. *Immunity* **2007**, *26* (4), 503–517. https://doi.org/10.1016/j.immuni.2007.03.006.

(134) Humann, J.; Bjordahl, R.; Andreasen, K.; Lenz, L. L. Expression of the P60 Autolysin Enhances NK Cell Activation and Is Required for Listeria Monocytogenes Expansion in IFN-γ-Responsive Mice. *J. Immunol.* **2007**, *178* (4), 2407–2414. https://doi.org/10.4049/jimmunol.178.4.2407.

(135) Schmidt, R. L.; Filak, H. C.; Lemon, J. D.; Potter, T. A.; Lenz, L. L. A LysM and SH3-Domain Containing Region of the Listeria Monocytogenes P60 Protein Stimulates Accessory Cells to Promote Activation of Host NK Cells. *PLoS Pathog.* **2011**, *7* (11). https://doi.org/10.1371/journal.ppat.1002368.

(136) Clark, S. E.; Filak, H. C.; Guthrie, B. S.; Schmidt, R. L.; Jamieson, A.; Merkel, P.; Knight, V.; Cole, C. M.; Raulet, D. H.; Lenz, L. L. Bacterial Manipulation of NK Cell Regulatory Activity Increases Susceptibility to Listeria Monocytogenes Infection. *PLoS Pathog.* **2016**, *12* (6). https://doi.org/10.1371/journal.ppat.1005708.

(137) Newman, K. C.; Riley, E. M. Whatever Turns You on: Accessory-Cell-Dependent Activation of NK Cells by Pathogens. *Nature Reviews Immunology*. Nature Publishing Group April 2007, pp 279–291. https://doi.org/10.1038/nri2057.

(138) Rayamajhi, M.; Humann, J.; Penheiter, K.; Andreasen, K.; Lenz, L. L. Induction of IFN-Aβ Enables Listeria Monocytogenes to Suppress Macrophage Activation by IFN-γ. *J. Exp. Med.* **2010**, *207* (2), 327–337. https://doi.org/10.1084/jem.20091746.

(139) Rayamajhi, M.; Humann, J.; Kearney, S.; Hill, K. K.; Lenz, L. L. Antagonistic Crosstalk between Type I and II Interferons and Increased Host Susceptibility to Bacterial Infections. *Virulence* **2010**, *1* (5), 418–422. https://doi.org/10.4161/viru.1.5.12787.

(140) Williams, M. A.; Schmidt, R. L.; Lenz, L. L. Early Events Regulating Immunity and Pathogenesis during Listeria Monocytogenes Infection. *Trends in Immunology*. Trends Immunol October 2012, pp 488–495. https://doi.org/10.1016/j.it.2012.04.007.

(141) Perona-Wright, G.; Mohrs, K.; Szaba, F. M.; Kummer, L. W.; Madan, R.; Karp, C. L.; Johnson, L. L.; Smiley, S. T.; Mohrs, M. Systemic but Not Local Infections Elicit Immunosuppressive IL-10 Production by Natural Killer Cells. *Cell Host Microbe* **2009**, *6* (6), 503–512. https://doi.org/10.1016/j.chom.2009.11.003.

(142) Takada, H.; Matsuzaki, G.; Hiromatsu, K.; Nomoto, K. Analysis of the Role of Natural Killer Cells in Listeria Monocytogenes Infection: Relation between Natural Killer Cells and T-Cell Receptor Gamma Delta T Cells in the Host Defence Mechanism at the Early Stage of Infection. *Immunology* **1994**, *82* (1), 106–112.

(143) Auerbuch, V.; Brockstedt, D. G.; Meyer-Morse, N.; O'Riordan, M.; Portnoy, D. A. Mice Lacking the Type I Interferon Receptor Are Resistant to Listeria Monocytogenes. *J. Exp. Med.* **2004**, *200* (4), 527–533. https://doi.org/10.1084/jem.20040976.

(144) O'Connell, R. M.; Saha, S. K.; Vaidya, S. A.; Bruhn, K. W.; Miranda, G. A.; Zarnegar, B.; Perry, A. K.; Nguyen, B. O.; Lane, T. F.; Taniguchi, T.; Miller, J. F.; Cheng, G. Type I Interferon Production Enhances Susceptibility to Listeria Monocytogenes Infection. *J. Exp. Med.* **2004**, *200* (4), 437–445. https://doi.org/10.1084/jem.20040712.

(145) Kolaczkowska, E.; Kubes, P. Neutrophil Recruitment and Function in Health and Inflammation. *Nature Reviews Immunology*. Nat Rev Immunol March 2013, pp 159–175. https://doi.org/10.1038/nri3399.

(146) da Silva, F. M.; Massart-Leën, A. M.; Burvenich, C. Development and Maturation of Neutrophils. *The Veterinary quarterly*. Vet Q 1994, pp 220–225. https://doi.org/10.1080/01652176.1994.9694452.

(147) Pham, C. T. N. Neutrophil Serine Proteases: Specific Regulators of Inflammation. *Nature Reviews Immunology*. Nat Rev Immunol July 2006, pp 541–550. https://doi.org/10.1038/nri1841.

(148) Fleming, T. J.; Fleming, M. L.; Malek, T. R. Selective Expression of Ly-6G on Myeloid Lineage Cells in Mouse Bone Marrow. RB6-8C5 MAb to Granulocyte-Differentiation Antigen (Gr-1) Detects Members of the Ly-6 Family. *J. Immunol.* **1993**, *151* (5).

(149) Rosales, C. Neutrophil: A Cell with Many Roles in Inflammation or Several Cell Types? *Frontiers in Physiology*. Frontiers Media S.A. February 20, 2018. https://doi.org/10.3389/fphys.2018.00113.

(150) Lapidot, T.; Kollet, O. The Essential Roles of the Chemokine SDF-1 and Its Receptor CXCR4 in Human Stem Cell Homing and Repopulation of Transplanted Immune-Deficient NOD/SCID and NOD/SCID/B2mnull Mice. *Leukemia*. Nature Publishing Group October 1, 2002, pp 1992–2003. https://doi.org/10.1038/sj.leu.2402684.

(151) Borregaard, N. Neutrophils, from Marrow to Microbes. *Immunity*. Immunity November 24, 2010, pp 657–670. https://doi.org/10.1016/j.immuni.2010.11.011.

(152) Eash, K. J.; Greenbaum, A. M.; Gopalan, P. K.; Link, D. C. CXCR2 and CXCR4 Antagonistically Regulate Neutrophil Trafficking from Murine Bone Marrow. *J. Clin. Invest.* **2010**, *120* (7), 2423–2431. https://doi.org/10.1172/JCI41649.

References

(153) Ley, K.; Laudanna, C.; Cybulsky, M. I.; Nourshargh, S. Getting to the Site of Inflammation: The Leukocyte Adhesion Cascade Updated. *Nature Reviews Immunology*. Nat Rev Immunol September 2007, pp 678–689. https://doi.org/10.1038/nri2156.

(154) Zarbock, A.; Ley, K.; McEver, R. P.; Hidalgo, A. Leukocyte Ligands for Endothelial Selectins: Specialized Glycoconjugates That Mediate Rolling and Signaling under Flow. *Blood*. Blood December 22, 2011, pp 6743–6751. https://doi.org/10.1182/blood-2011-07-343566.

(155) Phillipson, M.; Heit, B.; Colarusso, P.; Liu, L.; Ballantyne, C. M.; Kubes, P. Intraluminal Crawling of Neutrophils to Emigration Sites: A Molecularly Distinct Process from Adhesion in the Recruitment Cascade. *J. Exp. Med.* **2006**, *203* (12), 2569–2575. https://doi.org/10.1084/jem.20060925.

(156) Lefort, C. T.; Rossaint, J.; Moser, M.; Petrich, B. G.; Zarbock, A.; Monkley, S. J.; Critchley, D. R.; Ginsberg, M. H.; Fässler, R.; Ley, K. Distinct Roles for Talin-1 and Kindlin-3 in LFA-1 Extension and Affinity Regulation. *Blood* **2012**, *119* (18), 4275–4282. https://doi.org/10.1182/blood-2011-08-373118.

(157) Lefort, C. T.; Ley, K. Neutrophil Arrest by LFA-1 Activation. *Frontiers in Immunology*. Front Immunol 2012. https://doi.org/10.3389/fimmu.2012.00157.

(158) Cicchetti, G.; Allen, P. G.; Glogauer, M. Chemotactic Signaling Pathways in Neutrophils: From Receptor to Actin Assembly. *Critical Reviews in Oral Biology and Medicine*. Intern. and American Associations for Dental Research 2002, pp 220–228. https://doi.org/10.1177/154411130201300302.

(159) Zarbock, A.; Abram, C. L.; Hundt, M.; Altman, A.; Lowell, C. A.; Ley, K. PSGL-1 Engagement by E-Selectin Signals through Src Kinase Fgr and ITAM Adapters DAP12 and FcRγ to Induce Slow Leukocyte Rolling. *J. Exp. Med.* **2008**, *205* (10), 2339–2347. https://doi.org/10.1084/jem.20072660.

(160) Zarbock, A.; Lowell, C. A.; Ley, K. Spleen Tyrosine Kinase Syk Is Necessary for E-Selectin-Induced ALβ2 Integrin-Mediated Rolling on Intercellular Adhesion Molecule-1. *Immunity* **2007**, *26* (6), 773–783. https://doi.org/10.1016/j.immuni.2007.04.011.

(161) Yago, T.; Shao, B.; Miner, J. J.; Yao, L.; Klopocki, A. G.; Maeda, K.; Coggeshall, K. M.; McEver, R. P. E-Selectin Engages PSGL-1 and CD44 through a Common Signaling Pathway to Induce Integrin ALβ2-Mediated Slow Leukocyte Rolling. *Blood* **2010**, *116* (3), 485–494. https://doi.org/10.1182/blood-2009-12-259556.

(162) Kang, T.; Yi, J.; Guo, A.; Wang, X.; Overall, C. M.; Jiang, W.; Elde, R.; Borregaard, N.; Pei, D. Subcellular Distribution and Cytokine- and Chemokine-Regulated Secretion of Leukolysin/MT6-MMP/MMP-25 in Neutrophils. *J. Biol. Chem.* **2001**, *276* (24), 21960–21968. https://doi.org/10.1074/jbc.M007997200.

(163) Kolaczkowska, E.; Grzybek, W.; van Rooijen, N.; Piccard, H.; Plytycz, B.; Arnold, B.; Opdenakker, G. Neutrophil Elastase Activity Compensates for a Genetic Lack of Matrix Metalloproteinase-9 (MMP-9) in Leukocyte Infiltration in a Model of Experimental Peritonitis. *J. Leukoc. Biol.* **2009**, *85* (3), 374–381. https://doi.org/10.1189/jlb.0808460.

(164) Carr, K. D.; Sieve, A. N.; Indramohan, M.; Break, T. J.; Lee, S.; Berg, R. E. Specific Depletion Reveals a Novel Role for Neutrophil-Mediated Protection in the Liver during Listeria Monocytogenes Infection. *Eur. J. Immunol.* **2011**, *41* (9), 2666–2676. https://doi.org/10.1002/eji.201041363.

(165) Rothe, J.; Lesslauer, W.; Lötscher, H.; Lang, Y.; Koebel, P.; Köntgen, F.; Althage, A.; Zinkernagel, R.; Steinmetz, M.; Bluethmann, H. Mice Lacking the Tumour Necrosis Factor Receptor 1 Are Resistant to IMF-Mediated Toxicity but Highly Susceptible to Infection by Listeria Monocytogenes. *Nature* **1993**, *364* (6440), 798–802. https://doi.org/10.1038/364798a0.

(166) Malik, A.; Kanneganti, T. D. Function and Regulation of IL-1α in Inflammatory Diseases and Cancer. *Immunological Reviews*. Blackwell Publishing Ltd January 1, 2018, pp 124–137. https://doi.org/10.1111/imr.12615.

(167) Czuprynski, C. J.; Brown, J. F.; Young, K. M.; Cooley, A. J.; Kurtz, R. S. Effects of Murine Recombinant Interleukin 1α on the Host Response to Bacterial Infection. *J. Immunol.* **1988**, *140* (3), 962–968.

(168) Havell, E. A.; Moldawer, L. L.; Helfgott, D.; Kilian, P. L.; Sehgal, P. B. Type I IL-1 Receptor Blockade Exacerbates Murine Listeriosis. *J. Immunol.* **1992**, *148* (5), 1486–1492.

(169) Liu, M.; Chen, K.; Yoshimura, T.; Liu, Y.; Gong, W.; Wang, A.; Gao, J. L.; Murphy, P. M.; Wang, J. M. Formylpeptide Receptors Are Critical for Rapid Neutrophil Mobilization in Host Defense against Listeria Monocytogenes. *Sci. Rep.* **2012**, *2*. https://doi.org/10.1038/srep00786.

(170) Ebe, Y.; Hasegawa, G.; Takatsuka, H.; Umezu, H.; Mitsuyama, M.; Arakawa, M.; Mukaida, N.; Naito, M. The Role of Kupffer Cells and Regulation of Neutrophil Migration into the Liver by Macrophage Inflammatory Protein-2 in Primary Listeriosis in Mice. *Pathol. Int.* **1999**, *49* (6), 519–532. https://doi.org/10.1046/j.1440-1827.1999.00910.x.

References

(171) Yang, Q.; Ghose, P.; Ismail, N. Neutrophils Mediate Immunopathology and Negatively Regulate Protective Immune Responses during Fatal Bacterial Infection-Induced Toxic Shock. *Infect. Immun.* **2013**, *81* (5), 1751–1763. https://doi.org/10.1128/IAI.01409-12.

(172) Ellis, T. N.; Beaman, B. L. Interferon-γ Activation of Polymorphonuclear Neutrophil Function. *Immunology*. Immunology May 2004, pp 2–12. https://doi.org/10.1111/j.1365-2567.2004.01849.x.

(173) Rainard, P.; Riollet, C.; Poutrel, B.; Paape, M. J. Phagocytosis and Killing of Staphylococcus Aureus by Bovine Neutrophils after Priming by Tumor Necrosis Factor-α and the Des-Arginine Derivative of C5a. *Am. J. Vet. Res.* **2000**, *61* (8), 951–959. https://doi.org/10.2460/ajvr.2000.61.951.

(174) Rosales, C.; Uribe-Querol, E. Phagocytosis: A Fundamental Process in Immunity. *BioMed Research International*. Hindawi Limited 2017. https://doi.org/10.1155/2017/9042851.

(175) Witko-Sarsat, V.; Rieu, P.; Descamps-Latscha, B.; Lesavre, P.; Halbwachs-Mecarelli, L. Neutrophils: Molecules, Functions and Pathophysiological Aspects. *Lab. Investig.* **2000**, *80* (5), 617–654. https://doi.org/10.1038/labinvest.3780067.

(176) Boras, M.; Volmering, S.; Bokemeyer, A.; Rossaint, J.; Block, H.; Bardel, B.; Van Marck, V.; Heitplatz, B.; Kliche, S.; Reinhold, A.; Lowell, C.; Zarbock, A. Skap2 Is Required for B2 Integrin-Mediated Neutrophil Recruitment and Functions. *J. Exp. Med.* **2017**, *214* (3), 851–874. https://doi.org/10.1084/jem.20160647.

(177) Häger, M.; Cowland, J. B.; Borregaard, N. Neutrophil Granules in Health and Disease. *Journal of Internal Medicine*. J Intern Med July 2010, pp 25–34. https://doi.org/10.1111/j.1365-2796.2010.02237.x.

(178) Bouti, P.; Webbers, S. D. S.; Fagerholm, S. C.; Alon, R.; Moser, M.; Matlung, H. L.; Kuijpers, T. W. B2 Integrin Signaling Cascade in Neutrophils: More Than a Single Function. *Frontiers in Immunology*. Frontiers Media S.A. February 18, 2021. https://doi.org/10.3389/fimmu.2020.619925.

(179) MacMicking, J. D.; Nathan, C.; Hom, G.; Chartrain, N.; Fletcher, D. S.; Trumbauer, M.; Stevens, K.; Xie, Q. wen; Sokol, K.; Hutchinson, N.; Chen, H.; Mudget, J. S. Altered Responses to Bacterial Infection and Endotoxic Shock in Mice Lacking Inducible Nitric Oxide Synthase. *Cell* **1995**, *81* (4), 641–650. https://doi.org/10.1016/0092-8674(95)90085-3.

(180) Brinkmann, V.; Reichard, U.; Goosmann, C.; Fauler, B.; Uhlemann, Y.; Weiss, D. S.; Weinrauch, Y.; Zychlinsky, A. Neutrophil Extracellular Traps Kill Bacteria. *Science (80-.).* **2004**, *303* (5663), 1532–1535. https://doi.org/10.1126/science.1092385.

(181) Papayannopoulos, V.; Zychlinsky, A. NETs: A New Strategy for Using Old Weapons. *Trends in Immunology*. Trends Immunol November 2009, pp 513–521. https://doi.org/10.1016/j.it.2009.07.011.

(182) Weinrauch, Y.; Drujan, D.; Shapiro, S. D.; Weiss, J.; Zychlinsky, A. Neutrophil Elastase Targets Virulence Factors of Enterobacteria. *Nature* **2002**, *417* (6884), 91–94. https://doi.org/10.1038/417091a.

(183) Nauseef, W. M. How Human Neutrophils Kill and Degrade Microbes: An Integrated View. *Immunological Reviews*. Immunol Rev October 2007, pp 88–102. https://doi.org/10.1111/j.1600-065X.2007.00550.x.

(184) Tkalcevic, J.; Novelli, M.; Phylactides, M.; Iredale, J. P.; Segal, A. W.; Roes, J. Impaired Immunity and Enhanced Resistance to Endotoxin in the Absence of Neutrophil Elastase and Cathepsin G. *Immunity* **2000**, *12* (2), 201–210. https://doi.org/10.1016/S1074-7613(00)80173-9.

(185) Ermert, D.; Urban, C. F.; Laube, B.; Goosmann, C.; Zychlinsky, A.; Brinkmann, V. Mouse Neutrophil Extracellular Traps in Microbial Infections. *J. Innate Immun.* **2009**, *1* (3), 181–193. https://doi.org/10.1159/000205281.

(186) Lominadze, G.; Powell, D. W.; Luerman, G. C.; Link, A. J.; Ward, R. A.; McLeish, K. R. Proteomic Analysis of Human Neutrophil Granules. *Mol. Cell. Proteomics* **2005**, *4* (10), 1503–1521. https://doi.org/10.1074/mcp.M500143-MCP200.

(187) Papayannopoulos, V. Neutrophil Extracellular Traps in Immunity and Disease. *Nature Reviews Immunology*. Nature Publishing Group February 1, 2018, pp 134–147. https://doi.org/10.1038/nri.2017.105.

(188) Papayannopoulos, V.; Metzler, K. D.; Hakkim, A.; Zychlinsky, A. Neutrophil Elastase and Myeloperoxidase Regulate the Formation of Neutrophil Extracellular Traps. *J. Cell Biol.* **2010**, *191* (3), 677–691. https://doi.org/10.1083/jcb.201006052.

(189) Wang, Y.; Wysocka, J.; Sayegh, J.; Lee, Y. H.; Pertin, J. R.; Leonelli, L.; Sonbuchner, L. S.; McDonald, C. H.; Cook, R. G.; Dou, Y.; Roeder, R. G.; Clarke, S.; Stallcup, M. R.; Allis, C. D.; Coonrod, S. A. Human PAD4 Regulates Histone Arginine Methylation Levels via Demethylimination. *Science (80-.).* **2004**, *306* (5694), 279–283. https://doi.org/10.1126/science.1101400.

References

(190) Auffray, C.; Sieweke, M. H.; Geissmann, F. Blood Monocytes: Development, Heterogeneity, and Relationship with Dendritic Cells. *Annual Review of Immunology*. Annu Rev Immunol 2009, pp 669–692. https://doi.org/10.1146/annurev.immunol.021908.132557.

(191) Ginhoux, F.; Jung, S. Monocytes and Macrophages: Developmental Pathways and Tissue Homeostasis. *Nature Reviews Immunology*. Nature Publishing Group 2014, pp 392–404. https://doi.org/10.1038/nri3671.

(192) Shi, C.; Pamer, E. G. Monocyte Recruitment during Infection and Inflammation. *Nature Reviews Immunology*. Nat Rev Immunol November 2011, pp 762–774. https://doi.org/10.1038/nri3070.

(193) Serbina, N. V.; Shi, C.; Pamer, E. G. Monocyte-Mediated Immune Defense against Murine Listeria Monocytogenes Infection. In *Advances in Immunology*; Academic Press Inc., 2012; Vol. 113, pp 119–134. https://doi.org/10.1016/B978-0-12-394590-7.00003-8.

(194) Geissmann, F.; Jung, S.; Littman, D. R. Blood Monocytes Consist of Two Principal Subsets with Distinct Migratory Properties. *Immunity* **2003**, *19* (1), 71–82. https://doi.org/10.1016/S1074-7613(03)00174-2.

(195) Kurihara, T.; Warr, G.; Loy, J.; Bravo, R. Defects in Macrophage Recruitment and Host Defense in Mice Lacking the CCR2 Chemokine Receptor. *J. Exp. Med.* **1997**, *186* (10), 1757–1762. https://doi.org/10.1084/jem.186.10.1757.

(196) Serbina, N. V.; Salazar-Mather, T. P.; Biron, C. A.; Kuziel, W. A.; Pamer, E. G. TNF/INOS-Producing Dendritic Cells Mediate Innate Immune Defense against Bacterial Infection. *Immunity* **2003**, *19* (1), 59–70. https://doi.org/10.1016/S1074-7613(03)00171-7.

(197) Yang, J.; Zhang, L.; Yu, C.; Yang, X. F.; Wang, H. Monocyte and Macrophage Differentiation: Circulation Inflammatory Monocyte as Biomarker for Inflammatory Diseases. *Biomarker Research*. BioMed Central Ltd. January 7, 2014. https://doi.org/10.1186/2050-7771-2-1.

(198) Tsou, C. L.; Peters, W.; Si, Y.; Slaymaker, S.; Aslanian, A. M.; Weisberg, S. P.; Mack, M.; Charo, I. F. Critical Roles for CCR2 and MCP-3 in Monocyte Mobilization from Bone Marrow and Recruitment to Inflammatory Sites. *J. Clin. Invest.* **2007**, *117* (4), 902–909. https://doi.org/10.1172/JCI29919.

(199) Shi, C.; Velázquez, P.; Hohl, T. M.; Leiner, I.; Dustin, M. L.; Pamer, E. G. Monocyte Trafficking to Hepatic Sites of Bacterial Infection Is Chemokine Independent and Directed by Focal Intercellular Adhesion Molecule-1 Expression. *J. Immunol.* **2010**, *184* (11), 6266–6274. https://doi.org/10.4049/jimmunol.0904160.

(200) Lauvau, G.; Chorro, L.; Spaulding, E.; Soudja, S. M. H. Inflammatory Monocyte Effector Mechanisms. *Cellular Immunology*. Academic Press Inc. September 1, 2014, pp 32–40. https://doi.org/10.1016/j.cellimm.2014.07.007.

(201) Parzmair, G. P. The Role of the Adaptor Protein ADAP in Different T Cell Subsets and Pathogen-Specific Immune Responses against Listeria Monocytogenes, PhD thesis. Faculty of Natural Sciences, Otto-von-Guericke University Magdeburg., 2016.

(202) Parzmair, G. P.; Gereke, M.; Haberkorn, O.; Annemann, M.; Podlasly, L.; Kliche, S.; Reinhold, A.; Schraven, B.; Bruder, D. ADAP Plays a Pivotal Role in CD4+ T Cell Activation but Is Only Marginally Involved in CD8+ T Cell Activation, Differentiation, and Immunity to Pathogens. *J. Leukoc. Biol.* **2017**, *101* (2), 407-419. doi: 10.1189/jlb.1A0216-090RR.

(203) Skarnes, W. C.; Rosen, B.; West, A. P.; Koutsourakis, M.; Bushell, W.; Iyer, V.; Mujica, A. O.; Thomas, M.; Harrow, J.; Cox, T.; Jackson, D.; Severin, J.; Biggs, P.; Fu, J.; Nefedov, M.; de Jong, P. J.; Stewart, A. F.; Bradley, A. A Conditional Knockout Resource for the Genome-Wide Study of Mouse Gene Function. *Nature* **2011**, *474* (7351), 337-342. doi: 10.1038/nature10163.

(204) Rudolph, J. M.; Guttek, K.; Weitz, G.; Meinke, C. A.; Kliche, S.; Reinhold, D.; Schraven, B.; Reinhold, A. Characterization of Mice with a Platelet-Specific Deletion of the Adapter Molecule ADAP. *Mol. Cell. Biol.* **2019**, *39* (9), doi: 10.1128/MCB.00365-18.

(205) Narni-Mancinelli, E.; Chaix, J.; Fenis, A.; Kerdiles, Y. M.; Yessaad, N.; Reynders, A.; Gregoire, C.; Luche, H.; Ugolini, S.; Tomasello, E.; Walzer, T.; Vivier, E. Fate Mapping Analysis of Lymphoid Cells Expressing the NKp46 Cell Surface Receptor. *Proc. Natl. Acad. Sci.* **2011**, *108* (45), 18324-18329. doi: 10.1073/pnas.1112064108.

(206) Frentzel, S.; Katsoulis-Dimitriou, K.; Jeron, A.; Schmitz, I.; Bruder, D. Essential Role of IκBNS for in Vivo CD4+ T-Cell Activation, Proliferation, and Th1-Cell Differentiation during Listeria Monocytogenes Infection in Mice. *Eur. J. Immunol.* **2019**, *49* (9), 1391–1398. https://doi.org/10.1002/eji.201847961.

References

(207) Rao, X.; Huang, X.; Zhou, Z.; Lin, X. An Improvement of the 2ˆ(-Delta Delta CT) Method for Quantitative Real-Time Polymerase Chain Reaction Data Analysis. *Biostat. Bioinforma. Biomath.* **2013**, *3* (3), 71–85.

(208) Becker, N.; Störmann, P.; Janicova, A.; Köhler, K.; Horst, K.; Dunay, I. R.; Neunaber, C.; Marzi, I.; Vollrath, J. T.; Relja, B. Club Cell Protein 16 Attenuates CD16brightCD62dimImmunosuppressive Neutrophils in Damaged Tissue upon Posttraumatic Sepsis-Induced Lung Injury. *J. Immunol. Res.* **2021**, *2021*. https://doi.org/10.1155/2021/6647753.

(209) Düsedau, H. P.; Kleveman, J.; Figueiredo, C. A.; Biswas, A.; Steffen, J.; Kliche, S.; Haak, S.; Zagrebelsky, M.; Korte, M.; Dunay, I. R. P75 NTR Regulates Brain Mononuclear Cell Function and Neuronal Structure in Toxoplasma Infection-Induced Neuroinflammation. *Glia* **2019**, *67* (1), 193–211. https://doi.org/10.1002/glia.23553.

(210) Figueiredo, C. A.; Düsedau, H. P.; Steffen, J.; Gupta, N.; Dunay, M. P.; Toth, G. K.; Reglodi, D.; Heimesaat, M. M.; Dunay, I. R. Immunomodulatory Effects of the Neuropeptide Pituitary Adenylate Cyclase-Activating Polypeptide in Acute Toxoplasmosis. *Front. Cell. Infect. Microbiol.* **2019**, *9* (MAY). https://doi.org/10.3389/fcimb.2019.00154.

(211) Hughes, C. S.; Foehr, S.; Garfield, D. A.; Furlong, E. E.; Steinmetz, L. M.; Krijgsveld, J. Ultrasensitive Proteome Analysis Using Paramagnetic Bead Technology. *Mol. Syst. Biol.* **2014**, *10* (10), 757. https://doi.org/10.15252/msb.20145625.

(212) Sielaff, M.; Kuharev, J.; Bohn, T.; Hahlbrock, J.; Bopp, T.; Tenzer, S.; Distler, U. Evaluation of FASP, SP3, and IST Protocols for Proteomic Sample Preparation in the Low Microgram Range. *J. Proteome Res.* **2017**, *16* (11), 4060–4072. https://doi.org/10.1021/acs.jproteome.7b00433.

(213) Sturn, A.; Quackenbush, J.; Trajanoski, Z. *Genesis: Cluster Analysis of Microarray Data*; 2002; Vol. 18.

(214) Bindea, G.; Mlecnik, B.; Hackl, H.; Charoentong, P.; Tosolini, M.; Kirilovsky, A.; Fridman, W.-H.; Pagès, F.; Trajanoski, Z.; Galon, J. ClueGO: A Cytoscape Plug-in to Decipher Functionally Grouped Gene Ontology and Pathway Annotation Networks. *Bioinforma. Appl. NOTE* **2009**, *25* (8), 1091–1093. https://doi.org/10.1093/bioinformatics/btp101.

(215) Telieps, T.; Ewald, F.; Gereke, M.; Annemann, M.; Rauter, Y.; Schuster, M.; Ueffing, N.; von Smolinski, D.; Gruber, A. D.; Bruder, D.; Schmitz, I. Cellular-FLIP, Raji Isoform (c-FLIPR) Modulates Cell Death Induction upon T-Cell Activation and Infection. *Eur. J. Immunol.* **2013**, *43* (6), 1499–1510. https://doi.org/10.1002/eji.201242819.

(216) Thäle, C.; Kiderlen, A. F. Sources of Interferon-Gamma (IFN-γ) in Early Immune Response to Listeria Monocytogenes. *Immunobiology* **2005**, *210* (9), 673–683. https://doi.org/10.1016/j.imbio.2005.07.003.

(217) Boehm U Groot M, Howard JC, K. T.; Boehm U, Klamp T, Groot M, H. J. Cellular Responses to Interferon-Gamma. *Annu Rev Immunol* **1997**, *15*, 749-95. Review. PubMed PMID: 9143706.

(218) Kak G Tiwari BK, R. M. Interferon-Gamma (IFN-γ): Exploring Its Implications in Infectious Diseases. *Biomol Concepts* **2018**, *May 30* (9(1)), 64-79. doi: 10.1515/bmc-2018-0007.

(219) Ai, W.; Li, H.; Song, N.; Li, L.; Chen, H. Optimal Method to Stimulate Cytokine Production and Its Use in Immunotoxicity Assessment. *Int. J. Environ. Res. Public Health* **2013**, *10* (9), 3834–3842. https://doi.org/10.3390/ijerph10093834.

(220) Böning, M. A. L.; Trittel, S.; Riese, P.; van Ham, M.; Heyner, M.; Voss, M.; Parzmair, G. P.; Klawonn, F.; Jeron, A.; Guzman, C. A.; Jänsch, L.; Schraven, B.; Reinhold, A.; Bruder, D. ADAP Promotes Degranulation and Migration of NK Cells Primed During in Vivo Listeria Monocytogenes Infection in Mice. *Front. Immunol.* **2020**, *10*. https://doi.org/10.3389/fimmu.2019.03144.

(221) Brady, J.; Carotta, S.; Thong, R. P. L.; Chan, C. J.; Hayakawa, Y.; Smyth, M. J.; Nutt, S. L. The Interactions of Multiple Cytokines Control NK Cell Maturation. *J. Immunol.* **2010**, *185* (11), 6679–6688. https://doi.org/10.4049/jimmunol.0903354.

(222) Takeda, K.; Tsutsui, H.; Yoshimoto, T.; Adachi, O.; Yoshida, N.; Kishimoto, T.; Okamura, H.; Nakanishi, K.; Akira, S. Defective NK Cell Activity and Th1 Response in IL-18-Deficient Mice. *Immunity* **1998**, *8* (3), 383–390. https://doi.org/10.1016/S1074-7613(00)80543-9.

(223) Nandagopal, N.; Ali, A. K.; Komal, A. K.; Lee, S. H. The Critical Role of IL-15-PI3K-MTOR Pathway in Natural Killer Cell Effector Functions. *Front. Immunol.* **2014**, *5* (APR). https://doi.org/10.3389/fimmu.2014.00187.

(224) Chaix, J.; Tessmer, M. S.; Hoebe, K.; Fuséri, N.; Ryffel, B.; Dalod, M.; Alexopoulou, L.; Beutler, B.; Brossay, L.; Vivier, E.; Walzer, T. Cutting Edge: Priming of NK Cells by IL-18. *J. Immunol.* **2008**, *181* (3), 1627–1631. https://doi.org/10.4049/jimmunol.181.3.1627.

References

(225) Makowska, A.; Franzen, S.; Braunschweig, T.; Denecke, B.; Shen, L.; Baloche, V.; Busson, P.; Kontny, U. Interferon Beta Increases NK Cell Cytotoxicity against Tumor Cells in Patients with Nasopharyngeal Carcinoma via Tumor Necrosis Factor Apoptosis-Inducing Ligand. *Cancer Immunol. Immunother.* **2019**, *68* (8), 1317–1329. https://doi.org/10.1007/s00262-019-02368-y.

(226) Arase, H.; Arase, N.; Saito, T. Interferon γ Production by Natural Killer (NK) Cells and NK1.1+ T Cells upon NKR-P1 Cross-Linking. *J. Exp. Med.* **1996**, *183* (5), 2391–2396. https://doi.org/10.1084/jem.183.5.2391.

(227) Jacobs, N.; Langers; Renoux; Thiry; Delvenne. Natural Killer Cells: Role in Local Tumor Growth and Metastasis. *Biol. Targets Ther.* **2012**, *6*, 73. https://doi.org/10.2147/btt.s23976.

(228) Combs, J.; Kim, S. J.; Tan, S.; Ligon, L. A.; Holzbaur, E. L. F.; Kuhn, J.; Poenie, M. Recruitment of Dynein to the Jurkat Immunological Synapse. *Proc. Natl. Acad. Sci. U. S. A.* **2006**, *103* (40), 14883–14888. https://doi.org/10.1073/pnas.0600914103.

(229) D'Orazio, S. E. F. Innate and Adaptive Immune Responses during Listeria Monocytogenes Infection. *Microbiol. Spectr.* **2019**, *7* (3). https://doi.org/10.1128/microbiolspec.gpp3-0065-2019.

(230) Mizuki, M.; Nakane, A.; Sekikawa, K.; Tagawa, Y. ich; Iwakura, Y. Comparison of Host Resistance to Primary and Secondary Listeria Monocytogenes Infections in Mice by Intranasal and Intravenous Routes. *Infect. Immun.* **2002**, *70* (9), 4805–4811. https://doi.org/10.1128/IAI.70.9.4805-4811.2002.

(231) Dussurget, O.; Bierne, H.; Cossart, P. The Bacterial Pathogen Listeria Monocytogenes and the Interferon Family: Type I, Type II and Type III Interferons. *Frontiers in Cellular and Infection Microbiology*. Frontiers Media S.A. 2014. https://doi.org/10.3389/fcimb.2014.00050.

(232) Dai, W. J.; Köhler, G.; Brombacher, F. Both Innate and Acquired Immunity to Listeria Monocytogenes Infection Are Increased in IL-10-Deficient Mice. *J. Immunol.* **1997**, *158* (5).

(233) Barber DF Long EO, F. M. LFA-1 Contributes an Early Signal for NK Cell Cytotoxicity. *J Immunol* **2004**, *Sep 15* (173(6)), 3653-9. PubMed PMID: 15356110.

(234) Allavena, P.; Bianchi, G.; Paganin, C.; Giardina, G.; Mantovani, A. Regulation of Adhesion and Transendothelial Migration of Natural Killer Cells. *Nat. Immun.* 15 (2–3), 107–116.

(235) Verma, N. K.; Kelleher, D. Not Just an Adhesion Molecule: LFA-1 Contact Tunes the T Lymphocyte Program. *J. Immunol.* **2017**, *199* (4), 1213–1221. https://doi.org/10.4049/jimmunol.1700495.

(236) Wang, H.; Rudd, C. E. SKAP-55, SKAP-55-Related and ADAP Adaptors Modulate Integrin-Mediated Immune-Cell Adhesion. *Trends in Cell Biology*. October 2008, pp 486–493. https://doi.org/10.1016/j.tcb.2008.07.005.

(237) Caillard, A.; Sadoune, M.; Cescau, A.; Meddour, M.; Gandon, M.; Polidano, E.; Delcayre, C.; Da Silva, K.; Manivet, P.; Gomez, A. M.; Cohen-Solal, A.; Vodovar, N.; Li, Z.; Mebazaa, A.; Samuel, J. L. QSOX1, a Novel Actor of Cardiac Protection upon Acute Stress in Mice. *J. Mol. Cell. Cardiol.* **2018**, *119*, 75–86. https://doi.org/10.1016/j.yjmcc.2018.04.014.

(238) Tripal, P.; Bauer, M.; Naschberger, E.; Mörtinger, T.; Hohenadl, C.; Cornali, E.; Thurau, M.; Stürzl, M. Unique Features of Different Members of the Human Guanylate-Binding Protein Family. *J. Interf. Cytokine Res.* **2007**, *27* (1), 44–52. https://doi.org/10.1089/jir.2007.0086.

(239) Sunderkötter, C.; Nikolic, T.; Dillon, M. J.; van Rooijen, N.; Stehling, M.; Drevets, D. A.; Leenen, P. J. M. Subpopulations of Mouse Blood Monocytes Differ in Maturation Stage and Inflammatory Response. *J. Immunol.* **2004**, *172* (7), 4410–4417. https://doi.org/10.4049/jimmunol.172.7.4410.

(240) Yona, S.; Kim, K. W.; Wolf, Y.; Mildner, A.; Varol, D.; Breker, M.; Strauss-Ayali, D.; Viukov, S.; Guilliams, M.; Misharin, A.; Hume, D. A.; Perlman, H.; Malissen, B.; Zelzer, E.; Jung, S. Fate Mapping Reveals Origins and Dynamics of Monocytes and Tissue Macrophages under Homeostasis. *Immunity* **2013**, *38* (1), 79–91. https://doi.org/10.1016/j.immuni.2012.12.001.

(241) Veiras, L. C.; Cao, D. Y.; Saito, S.; Peng, Z.; Bernstein, E. A.; Shen, J. Z. Y.; Koronyo-Hamaoui, M.; Okwan-Duodu, D.; Giani, J. F.; Khan, Z.; Bernstein, K. E. Overexpression of ACE in Myeloid Cells Increases Immune Effectiveness and Leads to a New Way of Considering Inflammation in Acute and Chronic Diseases. *Current Hypertension Reports*. Springer January 1, 2020. https://doi.org/10.1007/s11906-019-1008-x.

(242) Naso, M. F.; Liang, B.; Huang, C. C.; Song, X. Y.; Shahied-Arruda, L.; Belkowski, S. M.; D'Andrea, M. R.; Polkovitch, D. A.; Lawrence, D. R.; Griswold, D. E.; Sweet, R. W.; Amegadzie, B. Y. Dermokine: An Extensively Differentially Spliced Gene Expressed in Epithelial Cells. *J. Invest. Dermatol.* **2007**, *127* (7), 1622–1631. https://doi.org/10.1038/sj.jid.5700779.

(243) Shao, X.; Liao, J.; Li, C.; Lu, X.; Cheng, J.; Fan, X. CellTalkDB: A Manually Curated Database of Ligand–Receptor Interactions in Humans and Mice. *Brief. Bioinform.* **2020**. https://doi.org/10.1093/bib/bbaa269.

References

(244) Wood, S. M.; Meeths, M.; Chiang, S. C. C.; Bechensteen, A. G.; Boelens, J. J.; Heilmann, C.; Horiuchi, H.; Rosthøj, S.; Rutynowska, O.; Winiarski, J.; Stow, J. L.; Nordenskjöld, M.; Henter, J. I.; Ljunggren, H. G.; Bryceson, Y. T. Different NK Cell-Activating Receptors Preferentially Recruit Rab27a or Munc13-4 to Perforin-Containing Granules for Cytotoxicity. *Blood* **2009**, *114* (19), 4117–4127. https://doi.org/10.1182/blood-2009-06-225359.

(245) Zhang, M.; Bracaglia, C.; Prencipe, G.; Bemrich-Stolz, C. J.; Beukelman, T.; Dimmitt, R. A.; Chatham, W. W.; Zhang, K.; Li, H.; Walter, M. R.; De Benedetti, F.; Grom, A. A.; Cron, R. Q. A Heterozygous RAB27A Mutation Associated with Delayed Cytolytic Granule Polarization and Hemophagocytic Lymphohistiocytosis . *J. Immunol.* **2016**, *196* (6), 2492–2503. https://doi.org/10.4049/jimmunol.1501284.

(246) Fehniger, T. A.; Cai, S. F.; Cao, X.; Bredemeyer, A. J.; Presti, R. M.; French, A. R. R.; Ley, T. J. Acquisition of Murine NK Cell Cytotoxicity Requires the Translation of a Pre-Existing Pool of Granzyme B and Perforin MRNAs. *Immunity* **2007**, *26* (6), 798–811. https://doi.org/10.1016/j.immuni.2007.04.010.

(247) Ng, L. G.; Ostuni, R.; Hidalgo, A. Heterogeneity of Neutrophils. *Nature Reviews Immunology*. Nature Publishing Group April 1, 2019, pp 255–265. https://doi.org/10.1038/s41577-019-0141-8.

(248) Newbrough, S. A.; Mocsai, A.; Clemens, R. A.; Wu, J. N.; Silverman, M. A.; Singer, A. L.; Lowell, C. A.; Koretzky, G. A. SLP-76 Regulates Fcγ Receptor and Integrin Signaling in Neutrophils. *Immunity* **2003**, *19* (5), 761–769. https://doi.org/10.1016/s1074-7613(03)00305-4.

(249) Myung, P. S.; Derimanov, G. S.; Jordan, M. S.; Punt, J. A.; Liu, Q. H.; Judd, B. A.; Meyers, E. E.; Sigmund, C. D.; Freedman, B. D.; Koretzky, G. A. Differential Requirement for SLP-76 Domains in T Cell Development and Function. *Immunity* **2001**, *15* (6), 1011–1026. https://doi.org/10.1016/S1074-7613(01)00253-9.

(250) Clemens, R. A.; Lenox, L. E.; Kambayashi, T.; Bezman, N.; Maltzman, J. S.; Nichols, K. E.; Koretzky, G. A. Loss of SLP-76 Expression within Myeloid Cells Confers Resistance to Neutrophil-Mediated Tissue Damage While Maintaining Effective Bacterial Killing. *J. Immunol.* **2007**, *178* (7), 4606–4614. https://doi.org/10.4049/jimmunol.178.7.4606.

(251) Lanier, L. L. Up on the Tightrope: Natural Killer Cell Activation and Inhibition. *Nature Immunology*. Nat Immunol May 2008, pp 495–502. https://doi.org/10.1038/ni1581.

(252) Cella, M.; Miller, H.; Song, C. Beyond NK Cells: The Expanding Universe of Innate Lymphoid Cells. *Frontiers in Immunology*. Frontiers Research Foundation 2014. https://doi.org/10.3389/fimmu.2014.00282.

(253) Seki E, Tsutsui H, Tsuji NM, Hayashi N, Adachi K, Nakano H, F.-Y.; S, Takeuchi O, Hoshino K, Akira S, Fujimoto J, N. K.; Seki E Tsuji NM, Hayashi N, Adachi K, Nakano H, Futatsugi-Yumikura, T. H.; S Hoshino K, Akira S, Fujimoto J, Nakanishi K, T. O. Critical Roles of Myeloid Differentiation Factor 88-Dependent Proinflammatory Cytokine Release in Early Phase Clearance of Listeria Monocytogenes in Mice. *J Immunol* **2002**, *Oct 1* (169(7)), 3863-8. PubMed PMID: 12244183.

(254) Bernardini, G.; Sciume, G.; Bosisio, D.; Morrone, S.; Sozzani, S.; Santoni, A. CCL3 and CXCL12 Regulate Trafficking of Mouse Bone Marrow NK Cell Subsets. *Blood* **2008**, *111* (7), 3626–3634. https://doi.org/10.1182/blood-2007-08-106203.

(255) Shtrichman, R.; Samuel, C. E. The Role of Gamma Interferon in Antimicrobial Immunity. *Current Opinion in Microbiology*. Elsevier Ltd 2001, pp 251–259. https://doi.org/10.1016/S1369-5274(00)00199-5.

(256) Harty JT, B. M. Specific Immunity to Listeria Monocytogenes in the Absence of IFN Gamma. *Immunity* **1995**, *Jul* (3(1)), 109-17. PubMed PMID: 7621071.

(257) Clark, S. E.; Schmidt, R. L.; McDermott, D. S.; Lenz, L. L. A Batf3/Nlrp3/IL-18 Axis Promotes Natural Killer Cell IL-10 Production during Listeria Monocytogenes Infection. *Cell Rep.* **2018**, *23* (9), 2582–2594. https://doi.org/10.1016/j.celrep.2018.04.106.

(258) Edwards, S. W.; Say, J. E.; Hughes, V. Gamma Interferon Enhances the Killing of Staphylococcus Aureus by Human Neutrophils. *J. Gen. Microbiol.* **1988**, *134* (1), 37–42. https://doi.org/10.1099/00221287-134-1-37.

(259) Klebanoff, S. J.; Vadas, M. A.; Harlan, J. M.; Sparks, L. H.; Gamble, J. R.; Agosti, J. M.; Waltersdorph, A. M. Stimulation of Neutrophils by Tumor Necrosis Factor. *J. Immunol.* **1986**, *136* (11).

(260) Leist, M.; Gantner, F.; Bohlinger, I.; Germann, P. G.; Tiegs, G.; Wendel, A. Murine Hepatocyte Apoptosis Induced in Vitro and in Vivo by TNF-Alpha Requires Transcriptional Arrest. *J. Immunol.* **1994**, *153* (4), 1778–1788.

References

(261) Okunnu, B. M.; Berg, R. E. Neutrophils Are More Effective than Monocytes at Phagosomal Containment and Killing of Listeria Monocytogenes. *ImmunoHorizons* **2019**, *3* (12), 573–584. https://doi.org/10.4049/immunohorizons.1900065.

(262) Li, C.; Jiao, S.; Wang, G.; Gao, Y.; Liu, C.; He, X.; Zhang, C.; Xiao, J.; Li, W.; Zhang, G.; Wei, B.; Chen, H.; Wang, H. The Immune Adaptor ADAP Regulates Reciprocal TGF-B1-Integrin Crosstalk to Protect from Influenza Virus Infection. *PLoS Pathog.* **2015**, *11* (4). https://doi.org/10.1371/journal.ppat.1004824.

(263) Assoians, R. K.; Komoriya, A.; Meyers, C. A.; Miller, D. M.; Sporn, M. B. *Transforming Growth Factor-Beta in Human Platelets. Identification of a Major Storage Site, Purification, and Characterization.*; 1983; Vol. 258. https://doi.org/10.1016/S0021-9258(18)32345-7.

(264) Eisenman, J.; Ahdieh, M.; Beers, C.; Brasel, K.; Kennedy, M. K.; Le, T.; Bonnert, T. P.; Paxton, R. J.; Park, L. S. Interleukin-15 Interactions with Interleukin-15 Receptor Complexes: Characterization and Species Specificity. *Cytokine* **2002**, *20* (3), 121–129. https://doi.org/10.1006/cyto.2002.1989.

(265) Ratthé, C.; Girard, D. Interleukin-15 Enhances Human Neutrophil Phagocytosis by a Syk-Dependent Mechanism: Importance of the IL-15Rα Chain. *J. Leukoc. Biol.* **2004**, *76* (1), 162–168. https://doi.org/10.1189/jlb.0605298.

(266) Weber, A. N. R.; Bittner, Z.; Liu, X.; Dang, T. M.; Radsak, M. P.; Brunner, C. Bruton's Tyrosine Kinase: An Emerging Key Player in Innate Immunity. *Frontiers in Immunology*. Frontiers Media S.A. November 8, 2017. https://doi.org/10.3389/fimmu.2017.01454.

(267) Shi, C.; Hohl, T. M.; Leiner, I.; Equinda, M. J.; Fan, X.; Pamer, E. G. Ly6G + Neutrophils Are Dispensable for Defense against Systemic Listeria Monocytogenes Infection. *J. Immunol.* **2011**, *187* (10), 5293–5298. https://doi.org/10.4049/jimmunol.1101721.

(268) Guler, R.; Mpotje, T.; Ozturk, M.; Nono, J. K.; Parihar, S. P.; Chia, J. E.; Abdel Aziz, N.; Hlaka, L.; Kumar, S.; Roy, S.; Penn-Nicholson, A.; Hanekom, W. A.; Zak, D. E.; Scriba, T. J.; Suzuki, H.; Brombacher, F. Batf2 Differentially Regulates Tissue Immunopathology in Type 1 and Type 2 Diseases. *Mucosal Immunol.* **2019**, *12* (2), 390–402. https://doi.org/10.1038/s41385-018-0108-2.

(269) Roy, S.; Guler, R.; Parihar, S. P.; Schmeier, S.; Kaczkowski, B.; Nishimura, H.; Shin, J. W.; Negishi, Y.; Ozturk, M.; Hurdayal, R.; Kubosaki, A.; Kimura, Y.; de Hoon, M. J. L.; Hayashizaki, Y.; Brombacher, F.; Suzuki, H. Batf2/Irf1 Induces Inflammatory Responses in Classically Activated Macrophages, Lipopolysaccharides, and Mycobacterial Infection. *J. Immunol.* **2015**, *194* (12), 6035–6044. https://doi.org/10.4049/jimmunol.1402521.

(270) Nakajima, A.; Nakatani, A.; Hasegawa, S.; Irie, J.; Ozawa, K.; Tsujimoto, G.; Suganami, T.; Itoh, H.; Kimura, I. The Short Chain Fatty Acid Receptor GPR43 Regulates Inflammatory Signals in Adipose Tissue M2-Type Macrophages. *PLoS One* **2017**, *12* (7). https://doi.org/10.1371/journal.pone.0179696.

(271) Stroncek, D. F. Neutrophil-Specific Antigen HNA-2a, NB1 Glycoprotein, and CD177. *Current Opinion in Hematology*. Curr Opin Hematol November 2007, pp 688–693. https://doi.org/10.1097/MOH.0b013e3282efed9e.

(272) Xie, Q.; Klesney-Tait, J.; Keck, K.; Parlet, C.; Borcherding, N.; Kolb, R.; Li, W.; Tygrett, L.; Waldschmidt, T.; Olivier, A.; Chen, S.; Liu, G. H.; Li, X.; Zhang, W. Characterization of a Novel Mouse Model with Genetic Deletion of CD177. *Protein Cell* **2015**, *6* (2), 117–126. https://doi.org/10.1007/s13238-014-0109-1.

(273) Jerke, U.; Rolle, S.; Dittmar, G.; Bayat, B.; Santoso, S.; Sporbert, A.; Luft, F.; Kettritz, R. Complement Receptor Mac-1 Is an Adaptor for NB1 (CD177)-Mediated PR3-ANCA Neutrophil Activation. *J. Biol. Chem.* **2011**, *286* (9), 7070–7081. https://doi.org/10.1074/jbc.M110.171256.

(274) Göhring, K.; Wolff, J.; Doppl, W.; Schmidt, K. L.; Fenchel, K.; Pralle, H.; Sibelius, U.; Bux, J. Neutrophil CD177 (NB1 Gp, HNA-2a) Expression Is Increased in Severe Bacterial Infections and Polycythaemia Vera. *Br. J. Haematol.* **2004**, *126* (2), 252–254. https://doi.org/10.1111/j.1365-2141.2004.05027.x.

(275) Kuckleburg, C. J.; Newman, P. J. Neutrophil Proteinase 3 Acts on Protease-Activated Receptor-2 to Enhance Vascular Endothelial Cell Barrier Function. *Arterioscler. Thromb. Vasc. Biol.* **2013**, *33* (2), 275–284. https://doi.org/10.1161/ATVBAHA.112.300474.

(276) Shojaei, F.; Wu, X.; Zhong, C.; Yu, L.; Liang, X. H.; Yao, J.; Blanchard, D.; Bais, C.; Peale, F. V.; Van Bruggen, N.; Ho, C.; Ross, J.; Tan, M.; Carano, R. A. D.; Meng, Y. G.; Ferrara, N. Bv8 Regulates Myeloid-Cell-Dependent Tumour Angiogenesis. *Nature* **2007**, *450* (7171), 825–831. https://doi.org/10.1038/nature06348.

References

(277) Negri, L.; Ferrara, N. The Prokineticins: Neuromodulators and Mediators of Inflammation and Myeloid Cell-Dependent Angiogenesis. *Physiol. Rev.* **2018**, *98* (2), 1055–1082. https://doi.org/10.1152/physrev.00012.2017.

(278) Zhong, C.; Qu, X.; Tan, M.; Meng, Y. G.; Ferrara, N. Characterization and Regulation of Bv8 in Human Blood Cells. *Clin. Cancer Res.* **2009**, *15* (8), 2675–2684. https://doi.org/10.1158/1078-0432.CCR-08-1954.

(279) Manfredi, A. A.; Ramirez, G. A.; Rovere-Querini, P.; Maugeri, N. The Neutrophil's Choice: Phagocytose vs Make Neutrophil Extracellular Traps. *Frontiers in Immunology*. Frontiers Media S.A. February 20, 2018. https://doi.org/10.3389/fimmu.2018.00288.

(280) Maugeri, N.; Rovere-Querini, P.; Evangelista, V.; Covino, C.; Capobianco, A.; Bertilaccio, M. T. S.; Piccoli, A.; Totani, L.; Cianflone, D.; Maseri, A.; Manfredi, A. A. Neutrophils Phagocytose Activated Platelets in Vivo: A Phosphatidylserine, P-Selectin, and B2 Integrin-Dependent Cell Clearance Program. *Blood* **2009**, *113* (21), 5254–5265. https://doi.org/10.1182/blood-2008-09-180794.

(281) Manfredi, A. A.; Covino, C.; Rovere-Querini, P.; Maugeri, N. Instructive Influences of Phagocytic Clearance of Dying Cells on Neutrophil Extracellular Trap Generation. *Clin. Exp. Immunol.* **2015**, *179* (1), 24–29. https://doi.org/10.1111/cei.12320.

(282) Vorobjeva, N. V. Neutrophil Extracellular Traps: New Aspects. *Moscow University Biological Sciences Bulletin*. Pleiades journals October 1, 2020, pp 173–188. https://doi.org/10.3103/S0096392520040112.

(283) El-Benna, J.; Dang, P. M. C.; Gougerot-Pocidalo, M. A. Priming of the Neutrophil NADPH Oxidase Activation: Role of P47phox Phosphorylation and NOX2 Mobilization to the Plasma Membrane. *Seminars in Immunopathology*. Semin Immunopathol July 2008, pp 279–289. https://doi.org/10.1007/s00281-008-0118-3.

7   Appendix

7.1   Supplementary Figures

A

B
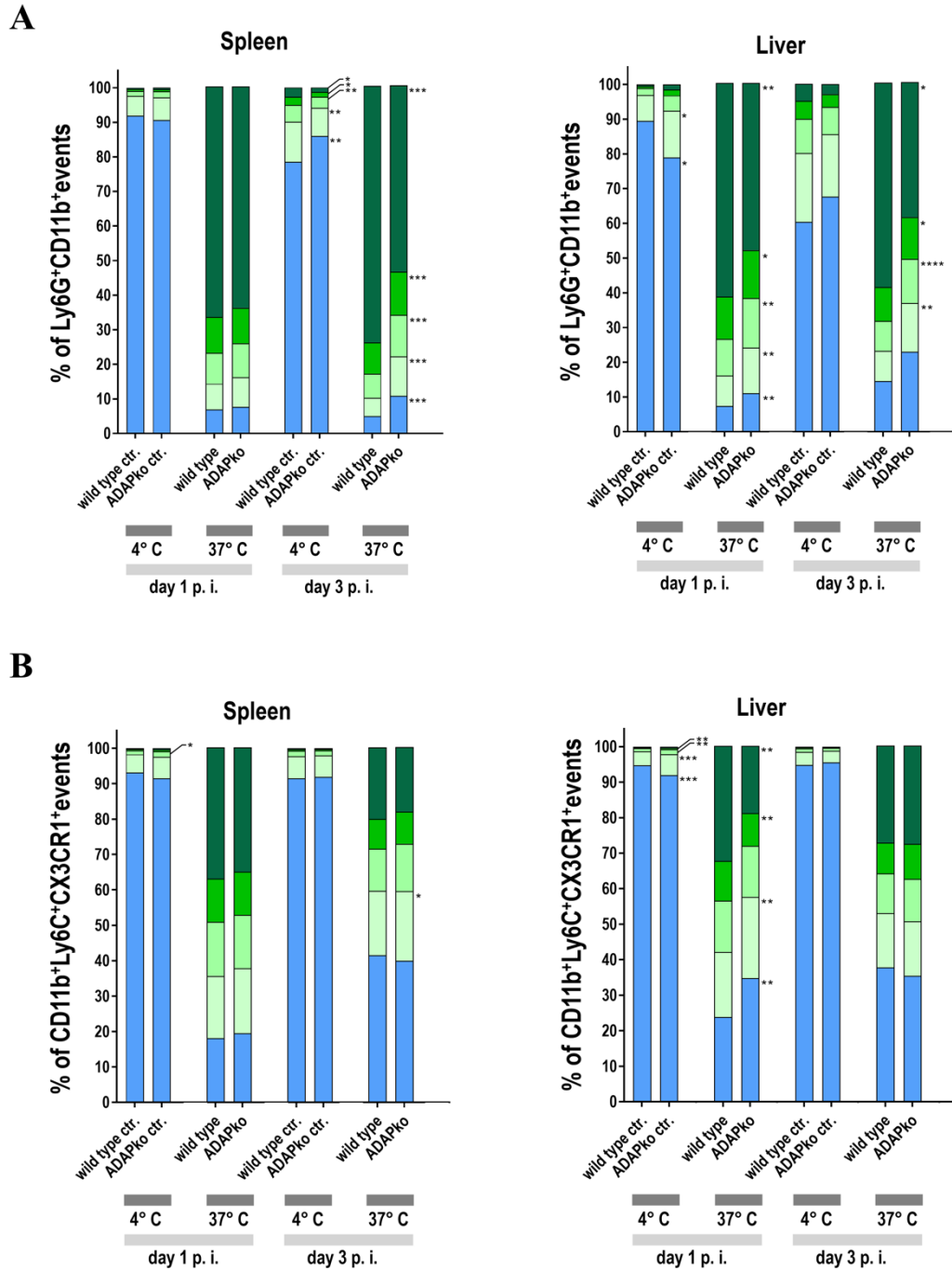
Supplement Figure 1 | *In vivo Listeria monocytogenes*-primed neutrophils and inflammatory monocytes from ADAP-deficient mice are functionally impaired in their phagocytotic capacity. Male Wild type (■) and ADAPko (□) mice (age: 10-17 weeks) were infected i. v. with 2.5 × 10⁴ CFU *Lm* and sacrificed at the indicated times post infection. Leukocytes were isolated from spleen and liver, stained for neutrophils (Ly6G⁺CD11b⁺) and

inflammatory monocytes (CX3CR1^{low}Ly6C^{high}) in reference to CD45$^+$Lin$^-$ cells and phagocytosis was assessed by a 2 h incubation of these cells with carboxylate-modified FITC-fluorescent latex microspheres at 37 °C or 4 °C serving as negative controls (ctr.) with a cell to bead ratio of 1:5. Bar charts for **(A)** neutrophils and **(B)** inflammatory monocytes show the fractioned cells according to the amount of incorporated beads (■ > 3 beads, ■ 3 beads, ■ 2 beads, ■ 1 bead, ■ 0 beads). Data are depicted as mean ± SEM for n = 6-8 individually analyzed mice per group out of two independent experiments. Statistical analyses were performed using two-tailed, unpaired t-test with Welch's correction (*p < 0.05, **p < 0.01, ***p < 0.001, ****p < 0.0001). Note: In cooperation with Prof. Ildiko Rita Dunay (Center for Behavioral Brain Sciences Magdeburg, Institute of Inflammation and Neurodegeneration Magdeburg) and M. Sc. H. P. Düsedau (Institute of Inflammation and Neurodegeneration Magdeburg). Manuscript submitted in *Frontiers in Immunology* (status: 25.06.2021).

7.2   Supplementary Tables

Table 25 | List of regulated genes from spleen- and liver-derived neutrophils 3 days post *Listeria monocytogenes* infection identified by microarray analyses from ADAPko *versus* wild type mice. Differentially regulated genes from FACS-sorted spleen and liver were identified as follows: Per genotype and organ, neutrophils from 6 mice were isolated and cells from 2 mice each were pooled, resulting in n = 3 independent replicate sample pools per organ and genotype (n for wild type liver = 2). Total RNA was isolated and analyzed by Clariom S microarray (23 samples in total). Differentially expressed transcripts in spleen/liver-derived neutrophils were determined comparing ADAPko *versus* wild type condition (fold change > ± 3-fold, FDR < 0.05). For each gene the averaged log$_2$ normalized signal intensity, fold change (ADAPko *versus* wild type), FDR and the k-means cluster (KMC) assignment are shown. Genes are sorted according to their k-means cluster number and within the clusters descendingly sorted by the average absolute fold changes. Genes above the applied fold change threshold (FC > ± 3) are in bold and color-coded (green: down-regulated, red: up-regulated). FDR values < 0.05 are bold. Table is relates to **Figure 36**.

(continued on the next page)

Annotation		Spleen				Liver				KMC Cluster ID
Array ID	Gene Symbol	ADAPko [mean log₂ SI]	wild type [mean log₂ SI]	FC (ADAPko vs. wild type)	FDR	ADAPko [mean log₂ SI]	wild type [mean log₂ SI]	FC (ADAPko vs. wild type)	FDR	
TC0500002651.mm.2	Igfbp7	7,19	7,05	1,1	1,0E+00	8,42	13,04	-24,5	1,9E-02	1
TC0X00000126.mm.2	Tspan7	4,84	5,14	-1,2	9,8E-01	6,52	10,74	-18,7	1,1E-02	1
TC0200005464.mm.2	Egfl7; Mir126a	5,24	5,83	-1,5	9,5E-01	6,85	11,03	-18,1	4,2E-03	1
TC1700001154.mm.2	Ehd3	3,39	3,41	-1,0	9,9E-01	3,64	7,75	-17,3	1,4E-02	1
TC0300001521.mm.2	Adgrl4	4,91	5,39	-1,4	9,5E-01	5,22	9,28	-16,7	1,6E-02	1
TC0800001617.mm.2	Clec4g	5,33	5,48	-1,1	9,6E-01	7,04	11,02	-15,8	8,3E-03	1
TC1600001395.mm.2	Masp1	3,93	3,61	1,3	9,8E-01	4,14	8,08	-15,4	1,7E-03	1
TC1100002783.mm.2	Sparc	4,43	4,85	-1,3	9,8E-01	7,42	11,32	-14,9	2,4E-02	1
TC0Y00000223.mm.2	Erdr1	8,92	10,36	-2,7	1,3E-01	11,63	15,31	-12,8	3,0E-04	1
TC0600002233.mm.2	Tmem176b	5,19	8,56	-10,4	1,7E-02	7,22	9,54	-5,0	2,2E-01	1
TC0300002023.mm.2	Tm4sf1	4,55	4,67	-1,1	9,9E-01	6,39	10,18	-13,8	1,2E-03	1
TC0300002998.mm.2	Bank1	8,65	11,25	-6,1	4,0E-03	9,08	12,14	-8,4	2,6E-03	1
TC0600003536.mm.2	Clec1b	9,51	11,48	-3,9	6,8E-03	9,43	12,70	-9,7	2,8E-03	1
TC1200002534.mm.2	Serpina1c	3,75	3,77	-1,0	1,0E+00	5,48	9,00	-11,5	4,8E-03	1
TC1400000940.mm.2	Pbk	5,83	9,15	-10,0	3,6E-02	7,65	8,80	-2,2	5,7E-01	1
TC0300001639.mm.2	Fabp4	5,13	5,65	-1,4	9,2E-01	8,87	12,27	-10,5	1,6E-02	1
TC1600000249.mm.2	Cldn5	3,95	4,00	-1,0	1,0E+00	4,46	7,88	-10,7	8,7E-03	1
TC1100002737.mm.2	Il4	4,63	6,42	-3,4	1,5E-02	4,67	7,72	-8,3	7,0E-04	1
TC0700002477.mm.2	Fosb	9,97	13,26	-9,8	1,0E-04	15,39	16,31	-1,9	1,8E-01	1
TC0100000524.mm.2	Adam23	3,86	3,92	-1,0	1,0E+00	3,80	7,13	-10,1	2,5E-02	1
TC0X00001715.mm.2	Gm21887	7,31	8,81	-2,8	3,9E-01	9,33	12,35	-8,1	1,9E-02	1
TC0500002508.mm.2	Apbb2	4,44	4,35	1,1	9,8E-01	4,69	7,99	-9,8	1,5E-03	1
TC1000001336.mm.2	Ptprb	2,92	3,15	-1,2	9,8E-01	3,36	6,64	-9,7	9,5E-03	1
TC0600003537.mm.2	Clec9a	4,49	6,53	-4,1	9,9E-02	5,55	8,17	-6,1	2,5E-02	1
TC0500002623.mm.2	Kdr	5,48	5,38	1,1	9,5E-01	6,67	9,82	-8,9	4,1E-02	1
TC0400002929.mm.2	Nfib	3,53	3,77	-1,2	1,0E+00	4,66	7,73	-8,4	2,1E-02	1
TC0600000664.mm.2	Aqp1	5,27	5,21	1,0	1,0E+00	5,83	8,91	-8,5	1,5E-02	1
TC0800002235.mm.2	Neil3	6,38	7,89	-2,9	1,8E-02	5,77	8,48	-6,5	3,4E-02	1
TC0800000798.mm.2	Colgalt1	6,70	7,96	-2,4	2,3E-01	7,52	10,30	-6,9	1,2E-02	1
TC1500000700.mm.2	Grap2	4,66	5,12	-1,4	9,4E-01	5,41	8,36	-7,7	4,1E-02	1
TC1700001451.mm.2	Igf2r	6,65	6,96	-1,2	8,9E-01	6,78	9,75	-7,8	1,0E-04	1
TC0700002497.mm.2	Apoe	6,97	8,59	-3,1	6,9E-02	8,23	10,73	-5,7	7,3E-03	1
TC1800000111.mm.2	Impact	8,87	9,14	-1,2	9,1E-01	10,09	12,99	-7,5	2,2E-03	1
TC0900002857.mm.2	1190002N15Rik	5,90	7,73	-3,6	7,0E-02	6,10	8,43	-5,1	2,6E-02	1
TC1200000647.mm.2	Prkch	7,62	8,82	-2,3	2,1E-01	8,70	11,30	-6,1	1,2E-02	1
TC0200002792.mm.2	Slco4a1	5,42	6,48	-2,1	9,5E-03	5,88	8,50	-6,2	7,9E-05	1
TC0600000821.mm.2	Fabp1	3,87	3,74	1,1	1,0E+00	5,20	7,98	-6,9	4,1E-02	1
TC0900000194.mm.2	Ilf3	5,94	6,54	-1,5	5,7E-01	6,47	9,12	-6,3	3,0E-04	1
TC1200000664.mm.2	Rhoj	4,38	4,32	1,0	1,0E+00	5,28	8,03	-6,8	1,8E-02	1
TC0500001992.mm.2	Cd36	4,29	5,20	-1,9	9,1E-01	5,22	7,72	-5,7	3,9E-02	1
TC0900002347.mm.2	Peak1	8,53	10,41	-3,7	3,0E-04	9,23	11,16	-3,8	1,2E-03	1
TC1800000301.mm.2	Egr1	11,47	14,06	-6,0	1,4E-02	16,16	16,65	-1,4	6,8E-01	1
TC0100003804.mm.2	Atf3	9,67	12,09	-5,4	7,0E-04	12,98	14,02	-2,1	5,3E-02	1
TC1500002309.mm.2	Cbx5	5,75	6,38	-1,6	9,6E-01	5,29	7,84	-5,8	2,6E-02	1
TC0700004132.mm.2	Rras2	5,54	5,79	-1,2	9,5E-01	5,86	8,45	-6,0	3,4E-02	1
TC1100000662.mm.2	Galnt10	8,16	10,16	-4,0	3,1E-03	8,75	10,40	-3,2	8,1E-02	1
TC0200001448.mm.2	Trp53i11	6,46	6,50	-1,0	1,0E+00	7,19	9,80	-6,1	3,9E-02	1
TC1500001410.mm.2	Klf10	6,66	8,16	-2,8	3,4E-02	8,46	10,47	-4,0	7,9E-03	1
TC0200004671.mm.2	Pcna	10,52	12,02	-2,8	9,4E-03	11,28	13,23	-3,9	6,5E-03	1
TC1700001634.mm.2	Slc9a3r2	3,90	4,88	-2,0	4,5E-01	3,96	6,20	-4,7	3,8E-02	1
TC1700002187.mm.2	Gnmt	5,43	6,56	-2,2	5,1E-01	6,23	8,40	-4,5	3,7E-02	1
TC1300002197.mm.2	Zfp367	6,39	7,33	-1,9	8,2E-01	7,60	9,84	-4,8	2,6E-02	1
TC1100000785.mm.2	Grap	5,03	5,20	-1,1	9,9E-01	5,34	7,79	-5,5	1,6E-02	1
TC0800002184.mm.2	Wwc2	7,08	7,97	-1,8	3,4E-01	7,14	9,37	-4,7	1,2E-03	1
TC0900000927.mm.2	Myo1e	7,13	7,24	-1,1	9,8E-01	6,57	8,99	-5,4	8,0E-04	1
TC1200001947.mm.2	Zbtb25	5,32	6,74	-2,7	9,5E-02	7,21	9,12	-3,8	2,0E-02	1
TC1700002787.mm.2	Ddx39b; Mir8094	9,43	10,70	-2,4	6,0E-03	10,01	12,00	-4,0	3,0E-04	1
TC0100002776.mm.2	Arl4c	4,55	6,45	-3,7	2,0E-04	5,69	7,04	-2,5	1,4E-02	1
TC1500001657.mm.2	Ndrg1	9,44	11,67	-4,7	4,0E-04	11,86	11,20	1,6	3,9E-01	1
TC1400000376.mm.2	Mmrn2	4,90	4,97	-1,1	9,9E-01	4,46	6,84	-5,2	2,9E-02	1
TC0400003343.mm.2	Nasp	4,95	5,31	-1,3	8,9E-01	4,37	6,66	-4,9	1,8E-02	1
TC0900000117.mm.2	Taf1d; Gm25500	9,03	10,40	-2,6	3,5E-02	9,76	11,60	-3,6	6,8E-03	1
TC0200003165.mm.2	Fcna	4,76	4,67	1,1	1,0E+00	4,99	7,34	-5,1	4,3E-02	1
TC0300002742.mm.2	Sars	7,07	7,83	-1,7	1,8E-01	7,54	9,67	-4,4	7,0E-04	1
TC0300001378.mm.2	Slc39a8	6,36	6,23	1,1	1,0E+00	6,12	8,44	-5,0	2,1E-03	1
TC0600000007.mm.2	Gng11	3,84	3,88	-1,0	9,8E-01	4,15	6,48	-5,0	1,2E-02	1
TC1400001432.mm.2	Dnase1l3	6,50	6,70	-1,2	9,6E-01	7,52	9,80	-4,9	2,3E-02	1
TC1500000557.mm.2	Gpihbp1	5,44	5,17	1,2	9,8E-01	5,93	8,19	-4,8	1,9E-02	1
TC0200001700.mm.2	BC052040	6,06	6,21	-1,1	9,2E-01	5,25	7,50	-4,8	2,3E-02	1
TC1200000833.mm.2	Fos	11,95	14,23	-4,8	2,3E-03	14,21	14,21	-1,0	1,0E+00	1
TC1000002043.mm.2	Amd2; Amd1	6,44	7,68	-2,4	8,9E-03	6,39	8,18	-3,4	2,3E-02	1
TC0X00000685.mm.2	Bgn	5,07	5,18	-1,1	9,8E-01	5,92	8,15	-4,7	3,0E-03	1
TC1000001298.mm.2	Nap1l1	10,63	11,91	-2,4	5,1E-02	10,40	12,12	-3,3	1,4E-02	1
TC1000002211.mm.2	Oit3	6,14	6,13	1,0	9,9E-01	6,49	8,73	-4,7	1,9E-02	1
TC1000001512.mm.2	Ppm1h; Mir8104	7,52	9,17	-3,1	9,5E-03	7,90	9,24	-2,5	1,1E-01	1
TC1800000689.mm.2	Pmaip1	7,23	9,03	-3,5	1,7E-03	8,88	10,02	-2,2	4,5E-02	1
TC0400001116.mm.2	Ssbp3	9,27	10,38	-2,2	2,5E-01	9,77	11,50	-3,3	4,1E-02	1
TC0200004383.mm.2	Meis2	3,68	3,41	1,2	1,0E+00	4,17	6,25	-4,2	8,8E-03	1
TC0200004843.mm.2	Acss1	7,06	6,96	1,1	1,0E+00	6,45	8,56	-4,3	3,6E-02	1
TC0800003236.mm.2	Usp10	7,06	7,30	-1,2	1,0E+00	7,03	9,11	-4,2	2,3E-02	1
TC1700000036.mm.2	Zdhhc14	5,28	6,24	-1,9	1,4E-01	5,18	6,95	-3,4	4,6E-02	1
TC0200003080.mm.2	Arhgap21	6,28	7,24	-2,0	6,0E-01	6,24	8,00	-3,4	2,5E-02	1
TC0600002056.mm.2	Wdr91	7,88	8,71	-1,8	6,8E-01	8,91	10,74	-3,6	4,9E-02	1
TC1200001902.mm.2	Rtn1	4,25	4,50	-1,2	9,7E-01	4,21	6,26	-4,1	2,0E-02	1
TC1000001198.mm.2	Atp2b1	10,29	11,94	-3,1	9,2E-03	11,71	12,80	-2,1	1,6E-01	1
TC0900002308.mm.2	Cul5	7,02	8,62	-3,0	2,4E-02	7,80	8,95	-2,2	3,5E-01	1
TC0200001913.mm.2	Dusp2	3,56	4,46	-1,9	2,2E-01	5,54	7,29	-3,4	8,5E-02	1
TC0400000952.mm.2	Tek	3,32	3,25	1,1	9,9E-01	3,36	5,42	-4,2	3,6E-03	1

| **142**

Appendix

		Spleen				Liver				KMC Cluster ID
Array ID	Gene Symbol	ADAPko [mean log₂ SI]	wild type [mean log₂ SI]	FC (ADAPko vs. wild type)	FDR	ADAPko [mean log₂ SI]	wild type [mean log₂ SI]	FC (ADAPko vs. wild type)	FDR	
TC0800002565.mm.2	Il27ra	4,08	4,03	1,0	1,0E+00	4,31	6,34	-4,1	2,2E-02	1
TC0400003542.mm.2	Ago1	7,67	8,30	-1,5	6,4E-01	7,31	9,14	-3,6	2,3E-02	1
TC1500002282.mm.2	Krt8	4,64	4,53	1,1	1,0E+00	5,04	7,04	-4,0	2,6E-02	1
TC0100003010.mm.2	Tmem163	6,48	6,37	1,1	9,9E-01	6,37	8,36	-4,0	1,7E-02	1
TC0100001431.mm.2	2810025M15Rik	6,73	6,16	1,5	8,7E-01	6,81	8,63	-3,5	1,5E-02	1
TC0900003055.mm.2	Dag1	7,18	7,21	-1,0	9,7E-01	6,39	8,38	-4,0	4,5E-03	1
TC0100001338.mm.2	Ptgs2	10,32	12,15	-3,6	5,2E-03	13,93	14,40	-1,4	7,3E-01	1
TC1800000503.mm.2	Dmxl1	9,37	10,09	-1,7	5,0E-01	8,99	10,67	-3,2	3,9E-02	1
TC0500001049.mm.2	Zfp326	5,57	6,32	-1,7	3,1E-01	5,63	7,29	-3,2	2,1E-02	1
TC0400002977.mm.2	Haus6	6,81	6,97	-1,1	9,7E-01	5,32	7,19	-3,7	3,5E-02	1
TC0300001409.mm.2	Adh1	5,04	4,89	1,1	9,3E-01	5,00	6,87	-3,7	2,0E-04	1
TC0600000454.mm.2	Gstk1	7,30	7,10	1,2	9,3E-01	7,09	8,92	-3,6	2,6E-02	1
TC0600000648.mm.2	Chn2	8,35	7,67	1,6	9,8E-01	7,55	9,17	-3,1	2,1E-02	1
TC0600002200.mm.2	Ezh2	6,83	7,32	-1,4	9,0E-01	7,55	9,22	-3,2	4,1E-02	1
TC1300002617.mm.2	Ipo11	5,38	5,62	-1,2	9,0E-01	5,09	6,84	-3,4	1,6E-02	1
TC1500001067.mm.2	Nr4a1	8,94	10,53	-3,0	1,4E-03	15,23	15,75	-1,4	3,8E-01	1
TC0100001568.mm.2	Sh2d1b1	6,72	7,15	-1,4	3,3E-01	6,32	7,94	-3,1	3,8E-02	1
TC0400003603.mm.2	Fam167b	6,79	6,32	1,4	9,1E-01	7,47	9,06	-3,0	4,1E-02	1
TC0900001414.mm.2	Impdh2	7,78	7,99	-1,2	9,7E-01	7,85	9,54	-3,2	4,7E-02	1
TC1600000138.mm.2	Snx29	6,79	6,69	1,1	8,7E-01	6,34	8,04	-3,3	9,7E-03	1
TC0300000453.mm.2	Tsc22d2	9,15	9,51	-1,3	3,1E-01	8,88	10,49	-3,0	8,7E-03	1
TC0600000324.mm.2	Akr1b8	5,46	5,48	-1,0	9,9E-01	6,54	8,26	-3,3	4,6E-02	1
TC1600001667.mm.2	Phldb2	6,13	6,06	1,1	1,0E+00	6,09	7,80	-3,3	1,6E-02	1
TC0100003882.mm.2	Chpf	3,29	3,16	1,1	1,0E+00	3,33	5,02	-3,2	3,4E-02	1
TC0200000620.mm.2	Hspa5	13,59	13,82	-1,2	9,2E-01	12,93	14,56	-3,1	1,6E-02	1
TC0100003129.mm.2	Nav1	5,58	5,74	-1,1	9,6E-01	5,22	6,87	-3,1	4,8E-02	1
TC0700002648.mm.2	LOC 101055953	6,59	6,85	-1,2	7,6E-01	6,19	7,79	-3,0	3,0E-02	1
TC0600000461.mm.2	Tas2r143	7,81	12,16	-20,5	6,0E-03	6,90	9,13	-4,7	2,5E-01	2
TC0300002594.mm.2	Cd101	10,41	14,57	-17,9	1,7E-05	8,58	11,05	-5,5	1,4E-03	2
TC1100002001.mm.2	Slc26a11	8,50	11,17	-6,3	3,1E-02	6,35	10,12	-13,6	1,4E-02	2
TC0600003235.mm.2	Clec1a	5,60	9,09	-11,3	1,1E-02	6,27	9,37	-8,5	2,3E-02	2
TC0600000462.mm.2	Tas2r135	6,51	10,05	-11,6	2,9E-02	4,97	7,53	-5,9	1,2E-01	2
TC0900001182.mm.2	Slc9a9	7,18	10,33	-8,9	1,0E-05	6,96	9,77	-7,0	3,0E-04	2
TC0200003401.mm.2	Strbp	7,50	10,22	-6,6	2,0E-04	7,84	11,00	-8,9	2,0E-04	2
TC0700001876.mm.2	Itgax	7,79	10,86	-8,4	4,0E-04	7,03	9,71	-6,4	8,3E-03	2
TC0700001669.mm.2	Pde3b	6,51	8,83	-5,0	2,5E-03	5,91	9,17	-9,6	9,0E-04	2
TC0300001064.mm.2	Ptpn22	8,74	11,60	-7,3	1,4E-03	8,99	11,79	-7,0	6,1E-03	2
TC0900002254.mm.2	Ncam1	5,48	9,08	-12,1	2,6E-05	5,66	4,56	2,1	3,0E-01	2
TC1900001105.mm.2	Tmem216	6,65	10,27	-12,3	1,0E-05	5,88	5,97	-1,1	9,9E-01	2
TC0800001802.mm.2	Defb40	7,39	10,65	-9,6	5,8E-03	6,71	8,61	-3,7	1,7E-01	2
TSUnmapped00000006.mm.	Rcor3	6,97	9,22	-4,8	2,6E-02	5,27	8,15	-7,4	6,1E-02	2
TC1800000184.mm.2	Mapre2	8,56	10,87	-5,0	5,7E-03	8,85	11,68	-7,1	1,7E-03	2
TC0600000463.mm.2	Tas2r126	6,64	9,79	-8,9	2,0E-04	6,67	8,24	-3,0	5,5E-02	2
TC1800000665.mm.2	Nedd4l	9,38	11,12	-3,3	1,4E-03	7,76	10,76	-8,0	9,3E-05	2
TC1100003268.mm.2	Gm10392	4,66	7,57	-7,5	2,0E-04	4,15	5,93	-3,4	3,7E-02	2
TC1100000798.mm.2	Pigl	6,77	9,47	-6,5	3,1E-03	5,98	8,02	-4,1	1,6E-02	2
TC1700000629.mm.2	Btnl2	6,22	8,94	-6,6	2,6E-03	5,77	7,71	-3,8	8,1E-02	2
TC1100000007.mm.2	Patz1; Gm11944	6,33	7,80	-2,8	7,4E-02	5,20	8,12	-7,6	9,5E-03	2
TC0200001770.mm.2	Chac1	5,79	8,77	-7,9	5,0E-04	5,75	6,99	-2,4	1,7E-01	2
TC1200002230.mm.2	Rps6ka5	9,13	11,06	-3,8	3,6E-03	8,31	10,94	-6,2	5,5E-03	2
TC1500002221.mm.2	Cers5	8,63	10,82	-4,5	3,2E-03	8,17	10,62	-5,5	4,2E-03	2
TC1200000427.mm.2	Arhgap5	4,92	7,10	-4,6	1,0E-04	3,37	5,81	-5,4	6,0E-04	2
TC1100000891.mm.2	Ctc1	7,21	9,68	-5,5	9,0E-04	5,89	8,01	-4,4	1,1E-02	2
TC0900001673.mm.2	Ccr3	7,25	9,92	-6,4	1,5E-03	5,75	7,45	-3,3	1,0E-01	2
TC1300000191.mm.2	Hist1h2bk	6,62	8,21	-3,0	2,2E-01	5,96	8,65	-6,5	3,4E-02	2
TSUnmapped00000010.mm.	Rcor3	7,15	9,14	-4,0	1,6E-02	5,90	8,33	-5,4	7,9E-03	2
TC0100001351.mm.2	Ivns1abp	10,70	11,79	-2,1	2,2E-01	9,07	11,93	-7,2	3,8E-03	2
TC1100003093.mm.2	Alox15	6,13	9,13	-8,0	1,9E-05	5,64	5,74	-1,1	9,3E-01	2
TC0200003224.mm.2	Fcnb	7,64	10,28	-6,3	2,6E-05	7,29	5,85	2,7	1,9E-02	2
TC0400003451.mm.2	Zmpste24	7,90	10,74	-7,2	2,6E-06	6,93	7,76	-1,8	1,0E-01	2
TC1500001300.mm.2	Fam105a	6,74	9,00	-4,8	2,1E-02	6,30	8,32	-4,1	1,5E-01	2
TC1100001767.mm.2	Ace	6,30	9,03	-6,6	5,5E-03	5,38	6,51	-2,2	3,3E-01	2
TC0700000756.mm.2	Siglecf	8,01	10,27	-4,8	1,2E-02	6,39	8,39	-4,0	2,4E-02	2
TC0700003015.mm.2	Fut2	4,08	6,77	-6,5	1,3E-02	6,54	7,69	-2,2	3,8E-01	2
TC1500001783.mm.2	Slc39a4	7,34	9,92	-6,0	2,0E-04	6,80	8,21	-2,7	1,4E-02	2
TC1100001127.mm.2	Abhd15	6,49	9,19	-6,5	2,1E-03	6,55	7,63	-2,1	2,3E-01	2
TC0400001000.mm.2	Gm12689	6,71	9,33	-6,2	3,3E-03	6,37	7,69	-2,5	1,5E-01	2
TC1300000175.mm.2	Hist1h2bm	8,91	10,33	-2,7	8,1E-02	8,31	10,86	-5,9	4,7E-03	2
TC0900002044.mm.2	Slc37a2	7,20	9,86	-6,4	1,5E-02	6,96	7,95	-2,0	2,5E-01	2
TC0300002324.mm.2	Syt11	4,72	7,32	-6,0	4,7E-02	5,06	6,25	-2,3	3,5E-01	2
TC1000002488.mm.2	Polr2e	9,25	10,67	-2,7	7,9E-02	8,25	10,74	-5,6	7,4E-03	2
TC1100000730.mm.2	Mprip	7,86	9,15	-2,4	5,7E-03	6,52	9,06	-5,8	3,0E-04	2
TC1500002258.mm.2	Krt80	9,96	12,43	-5,5	1,5E-02	8,04	9,48	-2,7	7,1E-02	2
TC1700000688.mm.2	H2-Q10	11,46	13,94	-5,6	6,2E-03	10,32	11,67	-2,6	6,7E-02	2
TC0600003232.mm.2	Clec12b	5,35	7,95	-6,1	1,8E-02	5,27	6,28	-2,0	4,7E-01	2
TC0800001420.mm.2	Osgin1	8,52	10,79	-4,8	1,2E-02	9,23	10,91	-3,2	1,4E-01	2
TC0800001803.mm.2	Defb38	5,29	7,95	-6,3	4,9E-03	5,17	5,91	-1,7	5,6E-01	2
TC0900002451.mm.2	Kif23	11,67	13,67	-4,0	1,9E-02	9,80	11,78	-3,9	2,3E-02	2
TC1300000967.mm.2	Mblac2	4,98	7,48	-5,7	1,0E-06	4,80	5,96	-2,3	7,9E-03	2
TC1000000708.mm.2	Bcr	9,10	10,82	-3,3	5,2E-02	8,11	10,29	-4,5	3,8E-03	2
TC1000000409.mm.2	Rtn4ip1	9,67	11,87	-4,6	7,0E-04	8,98	10,64	-3,2	3,6E-03	2
TC1500000380.mm.2	Med30	11,41	13,43	-4,1	2,3E-03	10,81	12,68	-3,6	4,2E-03	2
TC0700002080.mm.2	Mrpl23	10,10	12,19	-4,2	1,3E-02	8,96	10,74	-3,4	9,5E-03	2
TC1500000037.mm.2	Fyb	13,39	15,63	-4,7	1,8E-05	13,80	15,32	-2,9	1,6E-03	2
TC1900000915.mm.2	Ankrd13d	9,32	11,38	-4,2	1,9E-03	7,84	9,55	-3,3	3,2E-02	2
TC0300003222.mm.2	Ovgp1	8,90	11,15	-4,8	3,9E-02	7,74	9,11	-2,6	2,1E-01	2
TC1200000825.mm.2	Ylpm1	8,98	9,96	-2,0	7,2E-03	7,68	10,09	-5,3	4,2E-05	2
TC0600001709.mm.2	Lrmp	7,04	9,28	-4,7	1,6E-02	7,39	8,69	-2,5	2,8E-01	2

Appendix

Annotation		Spleen				Liver				KMC Cluster ID
Array ID	Gene Symbol	ADAPko [mean $\log_2$ SI]	wild type [mean $\log_2$ SI]	FC (ADAPko vs. wild type)	FDR	ADAPko [mean $\log_2$ SI]	wild type [mean $\log_2$ SI]	FC (ADAPko vs. wild type)	FDR	
TC0200002972.mm.2	Itga8	4,37	5,87	-2,8	1,9E-03	4,18	6,31	-4,4	4,0E-04	2
TC0400004186.mm.2	Nfia	9,44	10,98	-2,9	4,0E-02	8,92	10,99	-4,2	6,0E-03	2
TC0800001029.mm.2	Papd5	12,12	13,79	-3,2	9,0E-04	11,43	13,36	-3,8	2,3E-03	2
TC0700001391.mm.2	Arrb1	10,02	12,34	-5,0	1,1E-03	10,36	11,37	-2,0	2,9E-01	2
TC0800001805.mm.2	Defb39	7,38	9,63	-4,8	2,3E-03	7,46	8,60	-2,2	2,4E-01	2
TC1500002012.mm.2	Cerk	8,22	9,48	-2,4	1,4E-02	7,24	9,43	-4,6	4,0E-04	2
TC1900000763.mm.2	Pdcd4	11,17	12,17	-2,0	1,7E-01	10,02	12,26	-4,7	5,4E-03	2
TC0100001754.mm.2	Tlr5	8,49	10,67	-4,5	3,7E-03	6,69	7,78	-2,1	1,0E-01	2
TC0100001495.mm.2	Sele	6,62	8,96	-5,1	4,2E-03	5,65	6,28	-1,6	5,6E-01	2
TC0700001837.mm.2	Mylpf	7,03	9,00	-3,9	7,7E-03	6,58	8,01	-2,7	4,3E-02	2
TC0200002876.mm.2	Camk1d	5,82	7,73	-3,8	2,1E-05	6,31	7,79	-2,8	4,2E-03	2
TC0100003029.mm.2	Cxcr4	13,25	15,18	-3,8	2,0E-04	14,13	15,56	-2,7	5,8E-03	2
TC0900000720.mm.2	Sema7a	7,13	9,31	-4,6	1,7E-03	6,60	7,57	-2,0	3,4E-01	2
TC1900000906.mm.2	Carns1	9,12	10,84	-3,3	1,9E-03	6,88	8,53	-3,2	1,9E-02	2
TC0200002152.mm.2	Dtd1	8,37	10,08	-3,3	3,0E-04	7,10	8,77	-3,2	3,3E-03	2
TC1900000898.mm.2	BC021614	7,75	9,42	-3,2	7,1E-03	6,86	8,57	-3,3	1,0E-02	2
TC1300001563.mm.2	Hist1h2bq; Hist1h2br	9,26	11,47	-4,6	8,5E-05	8,10	8,96	-1,8	1,4E-01	2
TC0600000591.mm.2	Mpp6	5,84	7,11	-2,4	4,2E-02	5,04	7,05	-4,0	4,3E-02	2
TC1300001461.mm.2	Gpr137b	11,65	12,96	-2,5	9,5E-03	11,11	13,07	-3,9	2,5E-03	2
TC1000000422.mm.2	Prep	8,55	10,10	-2,9	7,1E-03	8,48	10,27	-3,5	6,3E-03	2
TC0800000959.mm.2	Lyl1	8,47	10,84	-5,2	5,0E-04	9,33	9,48	-1,1	8,9E-01	2
TC1700001209.mm.2	Galm	8,72	10,99	-4,8	9,0E-04	7,58	8,08	-1,4	2,0E-01	2
TC1200000567.mm.2	Klhdc2	10,82	12,20	-2,6	8,7E-02	8,34	10,20	-3,6	2,6E-02	2
TC0800000172.mm.2	Agpat5	7,17	9,26	-4,3	1,1E-03	7,27	8,19	-1,9	3,8E-01	2
TC0200002366.mm.2	Trp53inp2	8,85	11,17	-5,0	1,1E-03	8,70	8,92	-1,2	7,5E-01	2
TC0500003169.mm.2	Tpcn1	6,86	8,64	-3,4	1,0E-03	6,74	8,20	-2,7	2,3E-02	2
TC0200000585.mm.2	Fam102a	8,72	9,79	-2,1	2,2E-01	7,41	9,43	-4,1	6,7E-03	2
TC1900000026.mm.2	Cdk2ap2	12,97	14,75	-3,5	6,7E-03	12,29	13,71	-2,7	9,1E-02	2
TC1400000459.mm.2	Ear12; Ear2; Ear3	10,07	12,34	-4,8	6,6E-03	10,53	10,91	-1,3	7,3E-01	2
TC0300000694.mm.2	Fcrl1	10,20	11,35	-2,2	1,0E-01	9,01	10,95	-3,8	6,2E-03	2
TC1800000869.mm.2	Mbp	7,39	9,65	-4,8	2,7E-03	7,24	7,55	-1,2	7,8E-01	2
TC0400001163.mm.2	Calr4	5,72	7,98	-4,8	1,2E-02	5,55	5,86	-1,2	8,7E-01	2
TC0500002893.mm.2	Abcg3	7,82	10,01	-4,6	1,1E-03	8,37	8,80	-1,4	7,8E-01	2
TC1000000332.mm.2	Rev3l	5,39	6,83	-2,7	1,1E-02	5,39	7,05	-3,2	1,7E-02	2
TC0100001317.mm.2	Uchl5	11,44	12,78	-2,5	4,0E-02	10,39	12,12	-3,3	1,4E-02	2
TC1100001474.mm.2	Gngt2	12,35	14,36	-4,0	8,6E-05	12,82	13,69	-1,8	1,1E-01	2
TC0800002422.mm.2	Nr2f6	4,21	5,85	-3,1	1,5E-02	3,67	5,09	-2,7	1,6E-01	2
TC0300003226.mm.2	Gm5150	13,67	15,58	-3,8	4,8E-03	13,12	14,13	-2,0	5,7E-02	2
TC1200002077.mm.2	Entpd5	6,53	7,19	-1,6	7,4E-02	4,83	6,90	-4,2	2,0E-04	2
TC1300000183.mm.2	Hist1h2br	10,47	12,20	-3,3	1,2E-03	8,27	9,57	-2,5	7,5E-02	2
TC1200000996.mm.2	9030617O03Rik	6,91	9,02	-4,3	3,0E-04	7,01	7,52	-1,4	6,2E-01	2
TC1100000582.mm.2	Cdkn2aipnl	12,60	13,66	-2,1	1,0E-02	11,16	13,01	-3,6	9,0E-04	2
TC0500002095.mm.2	Prkag2	7,22	8,98	-3,4	1,1E-03	7,53	8,70	-2,2	4,7E-02	2
TC1000001572.mm.2	Zbtb39	11,13	13,02	-3,7	9,8E-03	9,25	10,17	-1,9	1,3E-01	2
TC0X00000151.mm.2	Atp6ap2	11,11	12,22	-2,2	1,4E-02	10,97	12,75	-3,4	3,8E-03	2
TC0700002076.mm.2	Tnni2	6,57	8,30	-3,3	8,4E-03	7,29	8,47	-2,3	8,9E-02	2
TC0100003867.mm.2	Serpinb10	9,31	11,37	-4,2	1,2E-02	8,26	7,80	1,4	2,4E-01	2
TC0100000829.mm.2	Dgkd	6,09	7,27	-2,3	1,7E-02	5,41	7,11	-3,3	2,4E-03	2
TC1100000684.mm.2	4930438A08Rik	8,76	10,52	-3,4	1,6E-02	8,34	7,25	2,1	1,9E-01	2
TC0600002354.mm.2	Vopp1	6,86	8,54	-3,2	6,0E-03	7,37	8,56	-2,3	6,2E-02	2
TC1100002862.mm.2	Flcn	11,89	13,10	-2,3	7,5E-03	12,30	13,95	-3,1	8,1E-03	2
TC1000000312.mm.2	Hdac2	5,60	6,44	-1,8	7,4E-01	4,88	6,75	-3,6	2,2E-02	2
TC1700002771.mm.2	Nme3	6,77	8,55	-3,4	4,6E-03	6,94	7,94	-2,0	1,1E-01	2
TC0200001030.mm.2	Dcaf17	7,17	8,02	-1,8	7,6E-02	5,49	7,34	-3,6	1,9E-02	2
TC1600000432.mm.2	Bex6	6,69	8,48	-3,4	4,1E-02	6,71	7,65	-1,9	5,4E-01	2
TC1800000771.mm.2	Mex3c	8,08	8,56	-1,4	8,6E-01	7,06	9,04	-3,9	1,8E-02	2
TC0400000519.mm.2	Tgfbr1	8,20	9,81	-3,1	2,5E-02	7,80	8,97	-2,3	1,3E-01	2
TC0800000756.mm.2	Isyna1	9,00	10,74	-3,3	2,0E-04	9,23	10,19	-2,0	5,5E-02	2
TC0600002941.mm.2	Vgll4	8,89	9,91	-2,0	5,6E-03	8,09	9,77	-3,2	8,0E-04	2
TC1100002695.mm.2	Rmnd5b	10,74	11,80	-2,1	1,1E-02	10,35	12,00	-3,1	4,2E-03	2
TC1100003934.mm.2	Polg2	8,18	9,78	-3,0	2,7E-03	8,42	9,54	-2,2	2,9E-02	2
TC0600000841.mm.2	St3gal5	11,41	13,22	-3,5	2,0E-04	12,04	12,74	-1,6	1,7E-01	2
TC0700003087.mm.2	Svip	9,82	11,48	-3,2	5,0E-03	8,46	9,44	-2,0	5,0E-01	2
TC1000000147.mm.2	Map3k5	12,22	13,91	-3,2	3,7E-02	11,89	12,81	-1,9	2,7E-01	2
TC1500000578.mm.2	Gm19945	10,94	12,59	-3,1	1,9E-03	10,97	11,97	-2,0	4,8E-02	2
TC1300001762.mm.2	Serpinb1a	9,99	11,78	-3,5	4,0E-02	9,20	9,91	-1,6	5,1E-01	2
TC1300001669.mm.2	Acot13	9,58	11,36	-3,4	2,3E-03	10,46	11,17	-1,6	1,4E-01	2
TC0200003436.mm.2	Scai	7,68	9,46	-3,4	2,5E-03	7,10	7,75	-1,6	2,6E-01	2
TC1700000533.mm.2	Slc37a1	8,55	10,15	-3,0	2,1E-03	7,92	8,87	-1,9	3,0E-02	2
TC0600000538.mm.2	Zfp398	5,26	6,85	-3,0	2,5E-02	5,05	6,02	-2,0	1,7E-01	2
TC0200003320.mm.2	Ralgps1	6,47	8,31	-3,6	6,3E-03	6,37	6,82	-1,4	6,6E-01	2
TC0400001135.mm.2	Lrp8	5,17	5,79	-1,5	9,0E-01	4,08	5,81	-3,3	1,1E-02	2
TC0X00002384.mm.2	Ids	8,23	8,96	-1,7	3,6E-01	6,32	7,99	-3,2	4,8E-02	2
TC0400001451.mm.2	Oscp1	7,88	9,72	-3,6	3,9E-02	8,05	8,38	-1,3	7,9E-01	2
TC0700002226.mm.2	Clcn4	7,71	8,36	-1,6	1,9E-01	7,12	8,81	-3,2	3,5E-02	2
TC1100002673.mm.2	Rufy1	7,83	8,36	-1,5	8,8E-01	5,19	6,93	-3,3	5,0E-02	2
TC0200000007.mm.2	Phxr1	11,10	12,69	-3,0	2,7E-02	12,35	13,14	-1,7	4,7E-01	2
TC1800000625.mm.2	Csf1r	11,79	13,39	-3,0	6,0E-04	11,40	12,18	-1,7	1,2E-01	2
TC1500002285.mm.2	Csad	5,74	7,63	-3,7	9,0E-04	6,28	6,25	1,0	9,5E-01	2
TC0100002576.mm.2	Tns1	6,52	7,22	-1,6	4,6E-01	5,93	7,55	-3,1	5,5E-03	2
TC1900000205.mm.2	Ddb1	6,98	7,27	-1,2	9,1E-01	5,64	7,42	-3,4	3,8E-02	2
TC0800001089.mm.2	Ogfod1	7,95	7,97	-1,0	9,6E-01	6,40	8,25	-3,6	9,8E-03	2
TC0500001572.mm.2	Abhd11	8,12	8,62	-1,4	5,3E-01	7,12	8,79	-3,2	4,0E-02	2
TC1700002267.mm.2	Satb1	10,22	10,42	-1,2	9,8E-01	8,49	10,22	-3,3	3,8E-02	2
TC1400002058.mm.2	Haus4	6,93	7,26	-1,3	4,9E-01	5,88	7,55	-3,2	3,4E-02	2
TC1400001189.mm.2	Slain1	7,33	7,41	-1,1	7,9E-01	5,71	7,40	-3,2	2,3E-02	2
TC1600000659.mm.2	Nepro	6,47	6,70	-1,2	8,1E-01	5,05	6,69	-3,1	2,9E-02	2
TC1100001183.mm.2	Rab11fip4	8,49	10,09	-3,0	2,9E-02	7,95	8,22	-1,2	8,3E-01	2

| **144**

	Annotation	Spleen				Liver				KMC Cluster ID
Array ID	Gene Symbol	ADAPko [mean log$_2$ SI]	wild type [mean log$_2$ SI]	FC (ADAPko vs. wild type)	FDR	ADAPko [mean log$_2$ SI]	wild type [mean log$_2$ SI]	FC (ADAPko vs. wild type)	FDR	
TC1400001669.mm.2	Smim4	10,54	12,13	-3,0	2,3E-02	10,11	10,40	-1,2	6,8E-01	2
TC1700001034.mm.2	Adgre1	9,25	10,92	-3,2	2,5E-03	9,30	9,34	-1,0	9,4E-01	2
TC0700003039.mm.2	Saa3	13,01	6,86	71,0	9,0E-04	15,02	10,62	21,0	5,7E-03	3
TC0200004599.mm.2	Il1a	12,89	6,66	74,9	1,0E-04	16,11	14,76	2,6	4,7E-01	3
TC1100001171.mm.2	Nos2	9,79	4,92	29,1	2,0E-04	11,87	7,12	26,8	7,0E-04	3
TC0200003278.mm.2	Ptges	10,59	7,83	6,7	4,1E-02	12,72	8,42	19,7	3,6E-03	3
TC0300003210.mm.2	Schip1; Gm21949	9,27	5,39	14,8	1,6E-05	11,81	8,44	10,4	4,0E-04	3
TC0500001025.mm.2	Spp1	11,04	6,72	20,0	8,0E-04	10,68	11,51	-1,8	7,8E-01	3
TC0900001365.mm.2	Cish	8,67	5,19	11,2	9,0E-04	9,76	7,02	6,7	7,1E-03	3
TC0600000226.mm.2	Hilpda	11,76	7,94	14,1	1,7E-03	15,27	13,65	3,1	2,1E-01	3
TC1700000846.mm.2	Clic5	9,27	6,78	5,6	2,6E-02	11,22	7,84	10,4	1,5E-02	3
TC1700000148.mm.2	Sod2	12,76	9,49	9,6	1,6E-05	14,06	11,87	4,6	2,0E-03	3
TC0300000567.mm.2	Il12a	8,86	7,04	3,5	2,0E-04	11,50	8,21	9,8	1,1E-05	3
TC0200004913.mm.2	Bcl2l1	12,04	9,22	7,1	2,0E-04	13,17	10,74	5,4	9,1E-03	3
TC0300000161.mm.2	Tnfsf10	10,03	6,88	8,9	1,0E-04	10,44	8,72	3,3	2,0E-01	3
TC1300001135.mm.2	Serf1	9,55	7,06	5,7	1,2E-03	10,65	7,98	6,3	1,9E-03	3
TC0100003057.mm.2	Ikbke	13,44	10,63	7,0	5,0E-04	14,40	12,13	4,8	1,0E-02	3
TC0200001226.mm.2	Slc43a3	10,64	7,42	9,3	2,7E-03	11,59	10,65	1,9	8,7E-01	3
TC0500002945.mm.2	Mfsd7a	8,40	6,59	3,5	5,0E-04	9,31	6,43	7,4	4,8E-05	3
TC1600001419.mm.2	Cldn1	8,89	8,65	1,2	8,6E-01	12,35	9,27	8,5	1,6E-02	3
TC1100001256.mm.2	Ccl4	11,23	8,28	7,7	4,0E-04	14,60	13,75	1,8	4,9E-01	3
TC1400001898.mm.2	Ero1l	11,16	10,09	2,1	7,0E-02	14,27	11,37	7,4	5,5E-03	3
TC0800000115.mm.2	F10	9,78	7,25	5,8	4,0E-03	10,61	8,77	3,6	1,4E-01	3
TC1300002756.mm.2	Gm21188	10,57	9,02	2,9	6,7E-02	11,77	9,12	6,3	2,5E-03	3
TC1700000489.mm.2	Pnpla1	7,76	7,08	1,6	2,6E-01	9,54	6,64	7,5	2,1E-05	3
TC1600000179.mm.2	Abcc1	8,20	6,30	3,8	1,0E-02	9,59	7,20	5,2	3,3E-03	3
TC0200002961.mm.2	Pfkfb3	10,36	8,80	3,0	1,1E-02	11,38	8,84	5,9	6,0E-04	3
TC1900000711.mm.2	Cnnm2	9,91	7,10	7,0	5,8E-03	9,83	9,08	1,7	5,4E-01	3
TC0400004171.mm.2	Isg15	13,74	12,00	3,3	4,6E-02	14,87	12,50	5,2	3,0E-02	3
TC0500002756.mm.2	Cxcl10	11,30	9,08	4,7	5,0E-04	12,98	11,09	3,7	2,5E-02	3
TC1100000792.mm.2	Adora2b	7,90	5,90	4,0	1,3E-02	9,59	7,47	4,4	1,5E-02	3
TC1000001698.mm.2	Pcmt1; BC020402	9,92	8,73	2,3	1,1E-01	10,91	8,39	5,8	1,8E-03	3
TC0600003307.mm.2	Dusp16	13,37	10,88	5,6	2,0E-03	15,17	13,95	2,3	1,8E-01	3
TC0900000184.mm.2	Icam1	12,80	10,32	5,6	8,3E-05	14,43	13,22	2,3	4,2E-02	3
TC1600000353.mm.2	Lpp	11,92	9,70	4,7	6,4E-05	12,72	11,03	3,2	3,0E-03	3
TC1000000531.mm.2	P4ha1	8,63	7,15	2,8	4,6E-03	9,80	7,65	4,4	7,1E-03	3
TC0900002676.mm.2	Mapk6	10,38	7,81	5,9	2,0E-04	10,67	11,03	-1,3	6,8E-01	3
TC0600000227.mm.2	Fam71f2	6,26	4,89	2,6	7,5E-02	9,72	7,54	4,5	4,1E-02	3
TC0700003793.mm.2	Dgat2	12,18	11,15	2,1	8,1E-02	13,09	10,84	4,8	1,5E-03	3
TC1600001092.mm.2	Mx2	9,16	7,21	3,9	1,0E-03	9,34	7,92	2,7	4,0E-02	3
TC1200001663.mm.2	Ifrd1	6,26	4,91	2,6	3,3E-01	8,45	10,42	-3,9	3,1E-02	3
TC0X00001322.mm.2	Wbp5	12,13	10,02	4,3	2,0E-04	13,20	12,10	2,1	1,4E-01	3
TC0200002300.mm.2	Cox4i2	6,24	5,83	1,3	6,0E-01	8,79	6,46	5,0	2,0E-04	3
TC1900000067.mm.2	Fosl1	6,92	7,05	-1,1	9,9E-01	12,94	10,55	5,3	1,7E-03	3
TC0400001010.mm.2	Pgm2	10,44	9,45	2,0	2,2E-01	11,31	9,22	4,3	6,2E-03	3
TC1700000496.mm.2	Cdkn1a	13,84	11,55	4,9	4,2E-06	15,99	15,61	1,3	2,1E-01	3
TC1600001559.mm.2	Fam162a	10,95	9,55	2,7	1,8E-01	12,91	11,11	3,5	3,9E-02	3
TC0100002725.mm.2	Sp110	14,55	12,68	3,6	9,0E-04	15,87	14,57	2,5	5,3E-02	3
TC1000002320.mm.2	Arid5b	14,03	12,18	3,6	2,0E-04	15,23	14,02	2,3	2,5E-02	3
TC0400001034.mm.2	Ak4	5,78	5,32	1,4	6,0E-01	7,12	4,95	4,5	1,0E-03	3
TC1100002653.mm.2	Olfr1396	6,31	6,05	1,2	9,7E-01	8,63	6,43	4,6	2,0E-03	3
TC0200001729.mm.2	Thbs1	13,98	11,86	4,3	8,3E-05	15,79	15,22	1,5	1,8E-01	3
TC0800002431.mm.2	Bst2	14,89	12,87	4,1	2,0E-04	15,17	14,40	1,7	2,1E-01	3
TC0200002589.mm.2	Snai1	7,16	6,17	2,0	3,7E-02	10,38	8,46	3,8	9,0E-04	3
TC0100002656.mm.2	Dock10	11,01	8,90	4,3	3,3E-03	11,46	11,03	1,4	6,5E-01	3
TC1700002536.mm.2	Nlrc4	5,65	4,86	1,7	1,6E-01	7,18	5,23	3,9	4,9E-02	3
TC0900002883.mm.2	Rasa2	10,47	10,13	1,3	8,9E-01	12,37	10,29	4,2	4,7E-03	3
TC1400002454.mm.2	Lacc1	8,69	7,04	3,1	3,9E-02	10,26	9,03	2,3	7,5E-02	3
TC0600003229.mm.2	Cd69	12,83	10,74	4,3	2,4E-05	15,39	15,13	1,2	6,7E-01	3
TC1000002438.mm.2	Pfkl	8,87	7,67	2,3	4,1E-02	9,90	8,29	3,1	5,8E-02	3
TC0100002461.mm.2	Klf7	13,22	12,17	2,1	2,5E-01	13,90	12,21	3,2	1,7E-02	3
TC1000003130.mm.2	Rbms2	9,12	7,45	3,2	7,0E-04	9,87	8,80	2,1	2,4E-01	3
TC0500003417.mm.2	Sh2b2	11,84	9,97	3,7	4,0E-03	13,13	12,47	1,6	3,6E-01	3
TC0600001736.mm.2	Stk38l	5,78	7,37	-3,0	1,2E-02	8,51	7,43	2,1	1,4E-01	3
TC0500001043.mm.2	Lrrc8c	10,05	8,25	3,5	3,2E-02	10,97	10,32	1,6	7,7E-01	3
TC0700003823.mm.2	Plekhb1	7,71	7,89	-1,1	9,9E-01	10,06	8,11	3,9	2,0E-04	3
TC0800000184.mm.2	Defb5	7,08	7,39	-1,2	9,9E-01	8,44	6,57	3,6	3,5E-02	3
TC1300001209.mm.2	Pde4d; Mir1904	7,81	6,17	3,1	3,0E-04	9,83	9,05	1,7	1,1E-01	3
TC1700002673.mm.2	Gm10309	7,20	6,42	1,7	5,9E-01	7,96	6,34	3,1	1,1E-02	3
TC1100003401.mm.2	Ccl3	15,71	13,86	3,6	2,4E-03	17,43	17,22	1,2	8,6E-01	3
TC1400002165.mm.2	Cdadc1	9,21	9,19	1,0	9,9E-01	10,71	8,81	3,7	1,0E-03	3
TC1200000280.mm.2	Gdap10	12,66	12,25	1,3	4,2E-01	13,29	11,53	3,4	4,6E-02	3
TC0X00003437.mm.2	Il2rg	13,25	11,47	3,4	1,0E-04	13,92	13,54	1,3	5,5E-01	3
TC1700001791.mm.2	Ccdc167	10,27	9,77	1,4	3,4E-01	11,22	9,63	3,0	8,0E-04	3
TC0400003756.mm.2	Clic4	9,74	8,04	3,2	1,5E-02	12,90	12,72	1,1	8,8E-01	3
TC1700000077.mm.2	Tagap	15,52	13,90	3,1	3,0E-04	15,40	15,42	-1,0	9,1E-01	3
TC0100003309.mm.2	Qsox1	13,78	10,30	11,1	4,3E-06	12,65	7,88	27,2	1,2E-07	4
TC0700002776.mm.2	Ffar2	14,61	11,68	7,6	2,4E-07	12,98	8,42	23,7	1,6E-09	4
TC0700002611.mm.2	Cd177	15,89	14,26	3,1	9,5E-03	14,24	9,72	23,0	5,8E-07	4
TC0300002684.mm.2	Chil3	15,66	15,11	1,5	9,1E-01	15,21	11,03	18,1	7,0E-04	4
TC0300002683.mm.2	Chil5	11,89	9,35	5,8	1,1E-03	10,91	7,55	10,3	8,3E-05	4
TC0300002685.mm.2	Chil4	12,01	11,22	1,7	6,1E-01	11,51	7,77	13,4	4,0E-04	4
TC1400001112.mm.2	Olfm4	12,30	9,77	5,8	2,6E-02	10,44	7,28	9,0	8,8E-03	4
TC1600002142.mm.2	Itgb2l	11,31	11,67	-1,3	9,7E-01	11,01	7,37	12,5	1,1E-03	4
TC0900000746.mm.2	Adpgk	12,32	12,07	1,2	9,9E-01	11,39	7,77	12,3	1,4E-05	4
TC0900001481.mm.2	Ltf	14,95	16,04	-2,1	1,5E-01	13,99	10,51	11,1	4,2E-05	4
TC1700000487.mm.2	Mapk13	12,66	10,30	5,1	3,0E-04	11,63	8,65	7,9	3,0E-04	4
TC0100002866.mm.2	Pam	12,23	9,77	5,5	1,0E-01	10,49	7,69	7,0	3,5E-02	4

| **145**

Appendix

	Annotation	Spleen				Liver				KMC Cluster ID
Array ID	Gene Symbol	ADAPko [mean log$_2$ SI]	wild type [mean log$_2$ SI]	FC (ADAPko vs. wild type)	FDR	ADAPko [mean log$_2$ SI]	wild type [mean log$_2$ SI]	FC (ADAPko vs. wild type)	FDR	
TC1300001868.mm.2	Adtrp	10,03	8,79	2,4	9,0E-02	9,32	6,00	10,0	9,2E-06	4
TC1400002578.mm.2	Dach1	9,73	9,19	1,5	7,6E-01	10,43	7,03	10,6	2,0E-03	4
TC1000007737.mm.2	Stxbp5	11,42	9,10	5,0	4,0E-03	11,09	8,28	7,0	2,1E-03	4
TC0200000222.mm.2	Il15ra	12,24	10,19	4,1	5,0E-04	11,62	8,81	7,0	1,0E-04	4
TC1900000504.mm.2	Ifit1	13,74	12,38	2,6	4,5E-02	13,21	10,30	7,6	2,2E-03	4
TC0800000659.mm.2	Ddx60	13,07	11,52	2,9	1,2E-01	12,25	9,48	6,8	5,9E-03	4
TC1400002098.mm.2	Tgm1	13,62	11,88	3,4	1,1E-03	12,60	9,96	6,2	2,0E-03	4
TC1500000660.mm.2	Triobp	14,21	13,09	2,2	3,3E-02	14,04	11,16	7,3	3,0E-04	4
TC1400001157.mm.2	Klf5	12,89	11,66	2,3	9,0E-02	11,65	8,82	7,1	1,0E-04	4
TC1100000681.mm.2	Gm12250	15,80	14,44	2,6	1,1E-02	14,96	12,22	6,7	3,0E-04	4
TC1100001140.mm.2	Flot2	12,85	10,76	4,3	8,9E-03	11,03	8,74	4,9	3,9E-02	4
TC1400002065.mm.2	Cebpe	10,29	12,10	-3,5	6,0E-02	9,64	7,14	5,7	9,5E-03	4
TC0400002220.mm.2	Tmem67	10,98	8,75	4,7	1,0E-04	9,21	7,10	4,3	9,0E-04	4
TC1700001596.mm.2	Mmp25	13,37	12,22	2,2	6,1E-02	12,49	9,73	6,8	5,0E-04	4
TC1500001062.mm.2	Acvr1b	9,31	7,16	4,5	1,7E-02	8,91	6,77	4,4	6,7E-02	4
TC0700000693.mm.2	1600014C10Rik	14,52	12,79	3,3	2,6E-02	13,32	10,92	5,3	7,1E-03	4
TC0700004516.mm.2	Ifitm6	16,52	15,06	2,8	2,4E-02	16,52	13,99	5,8	1,2E-03	4
TC0800001432.mm.2	Crispld2	11,95	9,72	4,7	8,6E-03	10,27	8,35	3,8	3,5E-02	4
TC0100000638.mm.2	Bcs1l	10,46	7,90	5,9	6,5E-03	7,88	6,70	2,3	2,5E-01	4
TC0500000928.mm.2	Anxa3	10,40	9,57	1,8	5,2E-01	9,94	7,27	6,4	3,0E-04	4
TC1300000919.mm.2	Glrx	13,59	12,40	2,3	1,4E-02	13,32	10,79	5,8	3,0E-04	4
TC1000000825.mm.2	Gm26602; LOC100862144	14,40	13,14	2,4	8,2E-02	14,17	11,67	5,7	1,2E-03	4
TC0700000396.mm.2	Ceacam10	13,47	12,45	2,0	9,9E-02	12,97	10,41	5,9	4,0E-04	4
TC1600000500.mm.2	Parp9	9,14	7,61	2,9	5,9E-02	8,93	6,61	5,0	3,2E-03	4
TC1700002315.mm.2	Lrg1	14,85	13,72	2,2	3,7E-01	14,80	12,30	5,6	2,4E-02	4
TC1900000501.mm.2	Ifit3	12,85	10,90	3,9	1,7E-02	11,67	9,70	3,9	3,4E-02	4
TC0500003436.mm.2	Muc3a; A630081J09Rik	6,82	7,37	-1,5	4,0E-01	7,69	5,03	6,3	1,1E-03	4
TC1500002183.mm.2	Rnd1	13,51	11,34	4,5	4,2E-02	11,17	9,46	3,3	1,6E-01	4
TC1900001414.mm.2	Ankrd22	13,64	13,06	1,5	4,9E-01	12,19	9,56	6,2	2,0E-04	4
TC0700004660.mm.2	Mvp	10,57	8,69	3,7	3,4E-03	9,83	7,86	3,9	1,0E-02	4
TC0200004545.mm.2	Sppl2a	14,09	12,57	2,9	3,7E-02	13,23	10,98	4,7	9,2E-03	4
TC0600001369.mm.2	Usp18	15,52	13,89	3,1	1,7E-03	15,11	12,99	4,4	9,0E-04	4
TC0300001841.mm.2	Dcun1d1	12,11	9,89	4,7	1,0E-04	10,52	9,07	2,7	1,4E-02	4
TC0500003730.mm.2	Gbp9	14,25	12,27	3,9	1,1E-03	13,20	11,43	3,4	3,3E-03	4
TC0600002958.mm.2	Tmem40	14,16	13,32	1,8	1,5E-01	14,17	11,71	5,5	4,2E-03	4
TC0600000416.mm.2	Mgam	14,84	13,86	2,0	4,9E-01	14,12	11,72	5,3	2,5E-02	4
TC1300002445.mm.2	Scamp1	9,86	7,99	3,7	8,0E-04	8,73	6,90	3,6	6,8E-03	4
TC0600002342.mm.2	Nt5c3	12,22	10,53	3,2	5,0E-03	11,67	9,72	3,9	3,8E-03	4
TC1300002767.mm.2	Zfp935	11,61	10,10	2,8	3,0E-04	10,43	8,34	4,2	2,0E-04	4
TC0300001447.mm.2	Gbp2	16,51	15,20	2,5	3,7E-02	16,00	13,83	4,5	4,3E-02	4
TC0600000852.mm.2	Capg	15,02	13,90	2,2	3,2E-03	14,69	12,45	4,7	2,2E-05	4
TC0600001481.mm.2	Parp11	8,93	6,57	5,1	6,5E-03	6,96	6,26	1,6	1,5E-01	4
TC0300002659.mm.2	Mov10	15,50	14,61	1,9	8,8E-02	14,74	12,45	4,9	1,0E-02	4
TC0800003077.mm.2	Galns	11,47	9,84	3,1	5,5E-02	10,14	8,28	3,6	2,9E-02	4
TC1700000009.mm.2	Tiam2	9,99	8,83	2,2	1,5E-01	8,21	6,04	4,5	2,9E-02	4
TC0700000847.mm.2	Gys1	10,98	11,17	-1,1	9,9E-01	11,53	9,06	5,6	1,9E-02	4
TC0900002321.mm.2	Cib2	8,23	7,48	1,7	6,1E-01	7,58	5,27	5,0	1,5E-02	4
TC0100000215.mm.2	Rab23	7,10	5,91	2,3	7,7E-02	6,26	4,13	4,4	7,9E-03	4
TC1900001422.mm.2	Ifit1bl1	15,02	13,30	3,3	4,7E-02	13,39	11,66	3,3	7,8E-02	4
TC0700001739.mm.2	Mettl9	16,32	15,37	1,9	4,4E-03	15,31	13,13	4,5	8,2E-06	4
TC1100002641.mm.2	Irgm1	14,48	13,09	2,6	8,1E-02	14,17	12,23	3,8	2,9E-02	4
TC1900001670.mm.2	Gm10197	11,14	10,69	1,4	9,2E-01	11,04	8,72	5,0	2,3E-03	4
TC1500001727.mm.2	Ly6i	13,05	11,75	2,5	2,2E-02	13,16	11,22	3,8	2,4E-03	4
TC1100003369.mm.2	Rffl	13,35	12,26	2,1	5,3E-01	12,83	10,79	4,1	4,8E-02	4
TC1800001151.mm.2	4933408B17Rik	8,45	7,12	2,5	5,5E-02	7,07	5,21	3,6	4,0E-02	4
TC1400000306.mm.2	Tkt; Mir3076	10,74	9,49	2,4	1,2E-01	9,86	7,95	3,8	3,1E-02	4
TC0500002320.mm.2	Prom1	7,84	9,01	-2,3	7,5E-02	7,90	5,95	3,9	9,5E-03	4
TC0200002405.mm.2	Tldc2	9,85	9,31	1,5	4,3E-01	9,75	7,54	4,6	1,3E-02	4
TC0100002333.mm.2	Asnsd1	12,00	10,75	2,4	2,1E-02	11,85	9,96	3,7	4,7E-03	4
TC1100004265.mm.2	Igtp	16,00	14,46	2,9	1,4E-02	14,70	13,10	3,0	2,5E-02	4
TC1300001526.mm.2	Gpr141	14,03	12,68	2,6	4,4E-02	13,13	11,37	3,4	2,4E-02	4
TC0300000367.mm.2	Mgst2	16,63	15,63	2,0	3,1E-01	16,10	14,13	3,9	9,5E-03	4
TC0500003193.mm.2	Aldh2	11,69	11,33	1,3	7,2E-01	11,04	8,83	4,6	1,9E-03	4
TC0100001222.mm.2	Chil1	15,57	14,46	2,2	1,0E-01	15,24	13,33	3,7	7,2E-03	4
TC0300000959.mm.2	Gja5	7,45	6,03	2,7	9,0E-04	6,45	4,77	3,2	5,0E-04	4
TC0200000933.mm.2	Gca	13,27	13,19	1,1	9,9E-01	12,82	10,58	4,7	1,5E-02	4
TC0100002210.mm.2	Mitd1	13,58	11,90	3,2	8,0E-04	12,50	11,14	2,6	9,6E-03	4
TC0500002504.mm.2	Rbm47	9,71	8,83	1,8	3,4E-02	8,89	6,94	3,9	4,0E-04	4
TC0100001570.mm.2	Olfml2b	9,20	10,53	-2,5	2,8E-02	7,93	6,28	3,1	1,6E-02	4
TC1000002374.mm.2	Gucd1	10,11	9,10	2,0	1,1E-01	8,39	6,55	3,6	2,2E-02	4
TC0200005181.mm.2	Znfx1	12,20	11,15	2,1	1,4E-01	12,09	10,30	3,5	1,4E-02	4
TC1500000553.mm.2	Ly6g	17,12	16,22	1,9	4,2E-01	17,02	15,16	3,6	2,1E-02	4
TC0500001844.mm.2	Alox5ap	15,87	14,85	2,0	8,9E-03	14,98	13,19	3,5	1,0E-04	4
TC0600002114.mm.2	Parp12	16,41	15,30	2,2	1,5E-03	16,03	14,28	3,3	3,0E-04	4
TC0100003887.mm.2	Nos1ap	12,73	12,76	-1,0	9,9E-01	12,30	10,14	4,5	7,1E-03	4
TC0700002951.mm.2	Siglece	14,73	14,07	1,6	7,2E-01	13,71	11,76	3,9	1,9E-02	4
TC0300000258.mm.2	Atp11b	11,85	11,20	1,6	1,8E-01	11,66	9,74	3,8	1,3E-02	4
TC1400000524.mm.2	Peli2	10,31	8,69	3,1	1,7E-02	9,18	8,00	2,3	5,3E-02	4
TC1300000273.mm.2	Cmah	14,85	13,94	1,9	1,6E-01	14,21	12,43	3,4	4,3E-02	4
TC0900003112.mm.2	Klhl18	12,20	11,07	2,2	5,5E-02	10,01	8,38	3,1	7,0E-03	4
TC1500002347.mm.2	Parp10	16,17	15,02	2,2	5,7E-02	15,86	14,24	3,1	1,6E-02	4
TC0500002528.mm.2	Atp8a1	11,93	10,99	1,9	7,9E-02	11,95	10,21	3,4	1,2E-02	4
TC0200003245.mm.2	Ntng2; 6530402F18Rik	11,44	11,92	-1,4	7,0E-01	11,91	9,95	3,9	3,5E-02	4
TC0100002588.mm.2	Rnf25	12,64	11,91	1,7	2,3E-01	11,85	10,00	3,6	1,0E-03	4
TC0400004012.mm.2	Agtrap	10,80	9,95	1,8	2,2E-02	10,51	8,73	3,4	1,0E-04	4
TC0500003297.mm.2	Stx2	12,61	11,01	3,0	2,2E-02	10,04	8,92	2,2	2,4E-01	4
TC0700002976.mm.2	Ptov1	12,06	11,80	1,2	9,3E-01	12,16	10,16	4,0	2,2E-02	4
TC1300001573.mm.2	Prss16	9,79	7,87	3,8	2,2E-02	7,91	7,47	1,4	6,4E-01	4

Appendix

Annotation		Spleen				Liver				KMC Cluster ID
Array ID	Gene Symbol	ADAPko [mean $\log_2$ SI]	wild type [mean $\log_2$ SI]	FC (ADAPko vs. wild type)	FDR	ADAPko [mean $\log_2$ SI]	wild type [mean $\log_2$ SI]	FC (ADAPko vs. wild type)	FDR	
TC0200001859.mm.2	Sqrdl	11,34	10,60	1,7	9,3E-03	10,94	9,15	3,5	2,0E-03	4
TC0700001174.mm.2	Whamm	11,37	10,67	1,6	6,4E-02	10,85	9,04	3,5	5,0E-04	4
TC0400000084.mm.2	Trp53inp1	9,96	9,18	1,7	5,6E-01	7,75	5,99	3,4	4,0E-02	4
TC1900000634.mm.2	Entpd7	10,43	9,70	1,7	3,7E-01	9,81	8,11	3,3	7,9E-03	4
TC0500003176.mm.2	Oas3	14,72	13,85	1,8	2,7E-02	13,80	12,19	3,1	2,8E-02	4
TC1400000793.mm.2	Ltb4r1	13,78	13,50	1,2	8,0E-01	13,07	11,20	3,7	6,8E-03	4
TC0500003411.mm.2	Ssc4d	8,91	8,52	1,3	1,0E+00	8,33	6,51	3,5	3,9E-02	4
TC0500003175.mm.2	Oas2	15,01	14,55	1,4	2,8E-01	13,48	11,74	3,4	1,0E-02	4
TC1900000320.mm.2	Nmrk1	10,44	10,58	-1,1	1,0E+00	11,33	9,49	3,6	2,5E-02	4
TC0400001726.mm.2	Mul1	10,45	9,85	1,5	7,2E-01	10,01	8,37	3,1	6,3E-03	4
TC0700003057.mm.2	Mrgpra2a	14,14	13,59	1,5	5,1E-01	14,48	12,82	3,2	3,8E-02	4
TC1300000624.mm.2	Hrh2	14,24	13,78	1,4	6,8E-01	12,31	10,62	3,2	4,7E-02	4
TC0600001639.mm.2	Mgst1	16,34	15,73	1,5	1,8E-01	16,08	14,49	3,0	1,2E-03	4
TC0700002632.mm.2	Lipe	12,63	12,38	1,2	9,9E-01	11,49	9,75	3,3	1,4E-02	4
TC1100001143.mm.2	Fam222b	10,65	10,20	1,4	8,3E-01	10,49	8,86	3,1	1,2E-02	4
TC0300000967.mm.2	Fmo5	9,80	10,24	-1,4	7,3E-01	10,17	8,56	3,1	6,3E-03	4
TC1000000717.mm.2	Ggt1	16,19	10,17	65,1	2,2E-05	15,24	9,04	73,4	1,0E-04	5
TC1800001595.mm.2	Lipg	14,30	7,63	101,3	2,8E-07	12,82	7,63	36,4	1,3E-05	5
TC1900000102.mm.2	Batf2	11,82	5,98	57,0	1,5E-06	12,11	6,69	42,8	1,2E-05	5
TC1800001396.mm.2	Gm4841	12,61	7,18	43,4	2,8E-07	11,45	6,34	34,7	1,8E-06	5
TC0600000182.mm.2	Cped1	13,16	7,61	46,8	1,6E-05	13,03	9,53	11,3	2,0E-03	5
TC0600002843.mm.2	Prok2	12,85	7,73	34,7	4,0E-06	12,41	8,02	21,1	5,2E-05	5
TC0500000710.mm.2	Kit	14,76	9,34	42,9	1,5E-02	13,62	10,76	7,2	2,4E-01	5
TC0700001015.mm.2	Fam169b	10,19	5,60	24,2	1,0E-04	10,00	6,83	9,0	6,7E-03	5
TC1100000120.mm.2	Abca13	10,41	7,31	8,6	1,9E-03	10,97	6,39	24,0	3,8E-05	5
TC0500000468.mm.2	Cd38	11,16	6,47	26,0	1,1E-03	11,20	8,50	6,5	4,9E-02	5
TC1800000610.mm.2	Iigp1	14,03	9,66	20,7	5,1E-06	13,02	9,76	9,6	2,0E-04	5
TC1800000606.mm.2	Gm4951	14,33	10,61	13,1	1,7E-05	13,52	9,44	16,9	6,2E-05	5
TC0200001765.mm.2	Spint1	13,82	9,60	18,7	4,6E-03	12,88	9,55	10,0	4,1E-02	5
TC1200002524.mm.2	Serpina3f	15,04	10,96	16,9	1,9E-05	14,93	12,09	7,1	7,0E-03	5
TC1600001198.mm.2	Socs1	11,34	7,05	19,7	3,2E-05	7,73	5,79	3,8	8,1E-02	5
TC0700004288.mm.2	Nupr1	13,57	10,19	10,4	8,6E-05	14,33	10,97	10,3	1,0E-04	5
TC1300000586.mm.2	Fbxw17	9,78	6,35	10,8	9,1E-05	8,51	5,83	6,4	7,5E-03	5
TC1700002816.mm.2	Cfb	14,30	13,08	2,3	5,6E-01	14,22	10,35	14,6	5,4E-03	5
TC0100002495.mm.2	Acadl	11,93	8,65	9,7	7,5E-06	11,06	8,23	7,1	2,0E-04	5
TC0500002480.mm.2	Tlr1	13,30	9,86	10,8	4,9E-05	12,17	9,69	5,6	6,3E-03	5
TC0500001663.mm.2	Fam20c	9,30	6,26	8,2	2,0E-05	9,38	6,45	7,6	3,0E-04	5
TC1900000500.mm.2	Ifit2	12,11	9,03	8,4	1,1E-03	11,15	8,27	7,4	5,7E-03	5
TC0800000111.mm.2	Atp11a	14,13	10,98	8,9	2,6E-03	13,31	10,58	6,7	1,4E-02	5
TC0500000488.mm.2	Lap3	10,59	7,44	8,9	6,5E-03	10,46	7,75	6,5	4,0E-02	5
TC1500001054.mm.2	Slc4a8	12,67	9,55	8,7	3,4E-02	12,07	9,42	6,3	2,4E-01	5
TC0200001222.mm.2	Ube2l6	13,88	11,17	6,6	7,0E-04	14,10	11,09	8,0	1,4E-03	5
TC0400003680.mm.2	Smpdl3b	10,74	8,77	3,9	2,0E-04	11,69	8,31	10,4	8,4E-06	5
TC0100001765.mm.2	Dusp10	12,63	9,06	11,9	1,4E-02	12,49	11,39	2,2	5,3E-01	5
TC0300001444.mm.2	Gbp2b; Gbp5	14,12	11,26	7,3	1,6E-03	13,61	10,86	6,7	7,1E-03	5
TC1000000571.mm.2	Ppa1	11,12	7,89	9,4	7,7E-03	10,88	8,80	4,2	1,4E-01	5
TC1800000609.mm.2	F830016B08Rik	11,09	8,27	7,1	4,4E-07	10,35	7,85	5,7	9,0E-06	5
TC0300003133.mm.2	Ifi44	11,99	9,74	4,8	4,5E-02	11,38	8,40	7,9	1,0E-04	5
TC0500002895.mm.2	Gbp10; Gbp6	15,18	12,35	7,1	8,6E-05	14,43	11,99	5,4	6,7E-03	5
TC1400002193.mm.2	Spryd7	10,44	7,47	7,8	2,0E-04	9,78	7,60	4,5	1,4E-02	5
TC1400002328.mm.2	Rhobtb2	11,01	7,62	10,5	3,0E-04	9,08	8,33	1,7	7,1E-01	5
TC1100004159.mm.2	Lgals3bp	11,99	9,01	7,9	1,1E-03	11,14	9,27	3,7	7,3E-02	5
TC0300001703.mm.2	Gyg	12,50	10,21	4,9	1,8E-05	11,73	9,04	6,5	1,4E-05	5
TC0500003729.mm.2	Gbp8	15,70	12,90	7,0	4,0E-04	15,36	13,24	4,4	1,6E-02	5
TC1100003779.mm.2	Dhx58	12,96	10,80	4,5	1,0E-04	13,01	10,31	6,5	3,0E-05	5
TC1600001775.mm.2	Gpr15	9,71	6,65	8,3	7,0E-04	7,41	6,34	2,1	1,3E-01	5
TC0900001170.mm.2	Plscr1	12,44	10,39	4,1	3,0E-04	12,57	9,94	6,2	3,0E-04	5
TC0400000698.mm.2	Slc31a1	14,92	12,47	5,5	9,1E-05	13,63	11,35	4,9	2,2E-03	5
TC0500001522.mm.2	Tpst1	12,94	10,11	7,1	5,6E-05	12,57	10,90	3,2	1,6E-02	5
TC0500002896.mm.2	Gbp11	13,51	10,95	5,9	2,0E-04	12,85	10,85	4,0	1,0E-04	5
TC0300001244.mm.2	Gclm	13,01	10,91	4,3	1,4E-02	13,09	10,63	5,5	2,5E-03	5
TC0900000412.mm.2	Vwa5a	9,48	6,49	8,0	4,0E-04	6,92	6,04	1,8	1,9E-01	5
TC1200002359.mm.2	Wars	13,93	11,16	6,8	3,0E-05	13,23	11,65	3,0	1,4E-02	5
TC1600000664.mm.2	Cd200r4	10,34	8,34	4,0	3,3E-03	10,67	8,14	5,8	7,1E-03	5
TC0X00002637.mm.2	Pdk3	12,36	10,15	4,6	1,2E-05	11,48	9,14	5,0	1,0E-04	5
TC1700002815.mm.2	C4a	9,31	6,51	7,0	5,1E-03	7,65	6,27	2,6	3,7E-01	5
TC1400002161.mm.2	Phf11a	10,64	7,89	6,7	1,8E-03	10,34	8,85	2,8	3,5E-02	5
TC1200000769.mm.2	Sipa1l1	10,40	7,86	5,8	1,0E-02	10,79	8,90	3,7	5,0E-02	5
TC0300001271.mm.2	Camk2d	14,10	11,58	5,7	1,5E-05	14,11	12,33	3,5	1,8E-03	5
TC0300000767.mm.2	Kcnn3	6,78	4,15	6,2	2,0E-05	5,70	4,16	2,9	1,4E-03	5
TC1600000765.mm.2	Cldnd1	12,25	9,38	7,3	2,3E-03	11,61	10,79	1,8	2,6E-01	5
TC0100001592.mm.2	F11r	10,51	7,86	6,3	1,0E-02	9,24	7,84	2,6	3,0E-01	5
TC0500001240.mm.2	Oasl1	12,98	11,14	3,6	1,6E-02	12,23	9,82	5,3	3,7E-02	5
TC0800002947.mm.2	Mlkl	12,65	10,29	5,1	8,0E-04	12,40	10,56	3,6	7,0E-03	5
TC0900000033.mm.2	Casp12	7,84	4,97	7,3	2,0E-04	5,29	4,83	1,4	7,2E-01	5
TC1400002162.mm.2	Phf11b	13,21	10,60	6,1	3,0E-04	13,08	11,73	2,6	2,9E-02	5
TC1900000141.mm.2	Pla2g16	14,32	11,91	5,3	6,0E-03	14,24	12,56	3,2	1,0E-01	5
TC1900000797.mm.2	Casp7	9,92	7,87	4,2	2,7E-03	9,30	7,23	4,2	1,2E-02	5
TC1900011137.mm.2	Ms4a6d	12,54	11,42	2,2	6,3E-01	12,35	9,73	6,1	4,7E-02	5
TC0800001255.mm.2	Cdh1	8,52	5,86	6,3	6,6E-03	6,44	7,30	-1,8	5,2E-01	5
TC0700003850.mm.2	Il18bp	14,99	12,97	4,0	7,0E-04	14,44	12,47	3,9	3,7E-03	5
TC1700006600.mm.2	Daxx	10,41	8,41	4,0	6,4E-03	10,20	8,25	3,9	1,8E-02	5
TC0800002842.mm.2	Psmb10	12,95	10,61	5,1	2,0E-04	13,01	11,54	2,8	9,5E-03	5
TC1700002558.mm.2	Eif2ak2	11,37	10,02	2,6	3,6E-03	11,56	9,19	5,2	4,0E-04	5
TC0300002113.mm.2	Lxn	9,09	7,14	3,9	1,0E-04	9,25	7,33	3,8	6,0E-04	5
TC0600003369.mm.2	Slco1a6	5,85	4,50	2,6	1,6E-01	6,71	4,36	5,1	9,5E-03	5
TC0400002665.mm.2	Abca1	11,08	8,72	5,2	9,4E-03	10,84	9,56	2,4	9,1E-02	5
TC0400002605.mm.2	Tbc1d2	10,70	8,66	4,1	1,1E-02	10,58	8,80	3,5	4,1E-02	5

Annotation		Spleen				Liver				KMC Cluster ID
Array ID	Gene Symbol	ADAPko [mean log$_2$ SI]	wild type [mean log$_2$ SI]	FC (ADAPko vs. wild type)	FDR	ADAPko [mean log$_2$ SI]	wild type [mean log$_2$ SI]	FC (ADAPko vs. wild type)	FDR	
TC1900000604.mm.2	Ubtd1	13,32	11,75	3,0	2,7E-03	13,33	11,14	4,6	4,0E-04	5
TC0500003731.mm.2	Gbp4	16,31	14,39	3,8	1,8E-03	16,06	14,18	3,7	1,2E-02	5
TC0400002104.mm.2	Tnfrsf18	12,33	10,38	3,9	2,6E-02	11,55	9,71	3,6	1,4E-01	5
TC0700004287.mm.2	Il27	10,74	8,62	4,3	1,0E-03	9,74	8,13	3,1	2,2E-02	5
TC1200000239.mm.2	Tssc1	11,30	9,23	4,2	3,0E-04	11,37	9,72	3,2	8,2E-03	5
TC1900001541.mm.2	Got1	10,71	8,29	5,3	1,3E-02	10,80	9,89	1,9	4,6E-01	5
TC0800000674.mm.2	Tmem192	11,38	9,49	3,7	7,5E-03	11,23	9,43	3,5	1,8E-02	5
TC1500001061.mm.2	Acvrl1	9,27	8,14	2,2	1,9E-02	9,38	7,06	5,0	8,3E-05	5
TC1500000615.mm.2	1110038F14Rik	9,42	7,34	4,2	5,8E-03	9,08	7,55	2,9	4,9E-02	5
TC0600001689.mm.2	Cmas	10,54	8,16	5,2	1,1E-03	9,92	9,01	1,9	2,6E-01	5
TC1300000157.mm.2	Aoah	13,77	12,41	2,6	8,4E-05	14,03	11,86	4,5	3,8E-06	5
TC0300001292.mm.2	Tifa	10,55	8,62	3,8	2,0E-02	10,99	9,30	3,2	1,8E-01	5
TC1100000078.mm.2	Dbnl	12,75	11,01	3,3	7,1E-03	11,85	9,97	3,7	2,4E-02	5
TC1900001123.mm.2	AW112010	14,88	12,85	4,1	3,4E-02	15,08	13,57	2,9	1,7E-01	5
TC1000001761.mm.2	Stx11	12,00	10,94	2,1	1,1E-01	12,37	10,11	4,8	2,0E-02	5
TC1400000574.mm.2	Pnp	15,88	14,20	3,2	1,1E-03	15,09	13,22	3,7	5,1E-03	5
TC0500003060.mm.2	Kctd10	8,04	6,28	3,4	1,2E-02	7,16	5,39	3,4	1,9E-02	5
TC0900000051.mm.2	Mmp27	7,98	5,73	4,8	3,0E-04	6,00	5,13	1,8	8,1E-02	5
TC1200000279.mm.2	Nampt	13,22	11,82	2,6	1,9E-02	13,15	11,19	3,9	2,1E-02	5
TC1500001728.mm.2	Ly6a	14,83	12,92	3,8	1,3E-02	14,85	13,36	2,8	4,4E-02	5
TC1100000989.mm.2	Xaf1	11,83	10,13	3,3	1,9E-02	11,99	10,30	3,2	2,0E-02	5
TC0600003139.mm.2	Tapbpl	13,56	11,71	3,6	6,1E-06	12,74	11,24	2,8	3,0E-04	5
TC1400002122.mm.2	Cenpj	10,30	8,42	3,7	1,0E-04	9,44	7,99	2,7	1,5E-02	5
TC0200003362.mm.2	Stom	11,70	9,91	3,4	3,6E-02	11,15	9,60	2,9	5,9E-02	5
TC1100000119.mm.2	Upp1	16,79	15,50	2,4	1,9E-02	16,83	14,86	3,9	2,1E-02	5
TC1400001047.mm.2	Esd	14,30	12,67	3,1	1,0E-04	14,52	12,81	3,3	3,0E-03	5
TC1200000700.mm.2	Gphn	8,40	6,75	3,1	2,0E-03	8,34	6,68	3,2	3,8E-03	5
TC1600000356.mm.2	Morf4l1-ps1	8,77	7,20	3,0	1,7E-01	8,51	6,78	3,3	3,9E-02	5
TC0700001519.mm.2	Trim6	7,37	6,41	1,9	4,2E-01	7,73	5,62	4,3	1,6E-02	5
TC0700004258.mm.2	Nsmce1	11,61	9,56	4,2	4,9E-03	10,87	9,84	2,1	1,9E-01	5
TC1900000517.mm.2	Pcgf5	11,37	10,28	2,1	2,6E-02	11,73	9,73	4,0	1,3E-03	5
TC0400003890.mm.2	Ddi2; Rsc1a1	14,20	12,11	4,3	1,0E-04	12,64	11,78	1,8	1,1E-01	5
TC0800002518.mm.2	Smad1	10,15	8,25	3,7	3,2E-02	9,77	8,54	2,3	1,3E-01	5
TC1100001657.mm.2	Ifi35	13,98	12,55	2,7	3,0E-04	14,23	12,48	3,4	2,0E-04	5
TC1100003379.mm.2	Slfn9	10,01	8,03	3,9	4,5E-03	8,38	7,32	2,1	1,5E-01	5
TC0500000627.mm.2	Rhoh	11,69	10,02	3,2	1,9E-02	11,88	10,39	2,8	1,5E-01	5
TC0300001446.mm.2	Gbp3	15,39	13,49	3,7	5,8E-03	14,50	13,33	2,3	1,1E-01	5
TC1300002774.mm.2	Zfp456	8,74	6,75	4,0	5,3E-03	7,38	6,42	2,0	1,8E-01	5
TC0200002796.mm.2	Ogfr	11,79	10,02	3,4	1,4E-03	11,58	10,26	2,5	3,0E-02	5
TC0100003591.mm.2	Pydc4	13,08	11,33	3,4	2,4E-02	13,11	11,74	2,6	4,3E-02	5
TC0100003320.mm.2	Tor3a	11,62	10,15	2,8	3,0E-03	11,63	9,99	3,1	2,8E-02	5
TC1500001749.mm.2	Naprt	7,94	6,21	3,3	3,0E-04	7,08	5,76	2,5	2,5E-02	5
TC0500000432.mm.2	Stx18	12,30	10,62	3,2	8,6E-05	11,32	9,94	2,6	1,5E-02	5
TC1700002814.mm.2	C4b	12,59	10,53	4,2	7,0E-04	11,26	10,57	1,6	3,0E-01	5
TC0300001136.mm.2	Psma5	15,71	14,05	3,2	1,7E-02	15,71	14,33	2,6	5,8E-02	5
TC1600001556.mm.2	Parp14	11,84	10,44	2,6	1,4E-02	11,78	10,14	3,1	7,2E-03	5
TC0X00000728.mm.2	Gm5936	9,91	8,12	3,5	1,6E-02	9,71	8,54	2,2	1,7E-01	5
TC1500000960.mm.2	Pced1b	8,25	6,64	3,1	4,2E-02	8,52	7,16	2,6	1,5E-01	5
TC1600001641.mm.2	Atp6v1a	10,20	8,11	4,3	1,0E-02	8,58	8,16	1,3	5,6E-01	5
TC0X00001124.mm.2	Apool	7,83	6,12	3,3	7,0E-04	7,15	5,94	2,3	5,4E-02	5
TC0400001509.mm.2	Ak2	13,20	12,07	2,2	1,3E-01	13,48	11,73	3,4	1,9E-02	5
TC1000000604.mm.2	Dnajc12	7,88	6,17	3,3	9,2E-03	7,83	6,66	2,3	1,6E-01	5
TC0600003503.mm.2	Herc6	16,27	15,01	2,4	5,8E-03	16,17	14,53	3,1	1,7E-02	5
TC1200002522.mm.2	Churc1	11,05	9,39	3,2	2,0E-02	10,71	9,50	2,3	1,1E-01	5
TC1000001988.mm.2	Zufsp	13,63	12,36	2,4	7,0E-04	13,57	11,96	3,1	1,1E-03	5
TC0900001012.mm.2	Gnb5	6,83	4,90	3,8	5,0E-04	5,92	5,29	1,6	2,3E-01	5
TC1300000904.mm.2	Erap1	10,62	8,64	4,0	2,0E-05	9,31	8,82	1,4	4,6E-01	5
TC0200005015.mm.2	Rbl1	10,15	8,13	4,1	8,6E-03	8,15	7,81	1,3	9,5E-01	5
TC1600001337.mm.2	Klhl6	13,41	11,66	3,4	4,1E-02	12,61	11,71	1,9	1,9E-01	5
TC1300000009.mm.2	Asb13	9,17	7,25	3,8	1,3E-02	8,46	7,94	1,4	5,7E-01	5
TC0500002552.mm.2	Gnpda2	8,31	6,25	4,2	7,7E-03	6,15	6,09	1,0	5,5E-01	5
TC1300002246.mm.2	Zfp429	10,00	7,97	4,1	3,7E-03	8,63	8,76	-1,1	7,7E-01	5
TC1100001661.mm.2	Tmem106a	13,99	12,39	3,0	9,5E-03	13,63	12,55	2,1	1,7E-01	5
TC1700000842.mm.2	Enpp5	8,71	6,99	3,3	8,4E-03	8,43	7,57	1,8	5,2E-01	5
TC0600000577.mm.2	Gpnmb	9,24	7,43	3,5	1,0E-04	8,41	9,05	-1,6	2,3E-01	5
TC0400002744.mm.2	Ptgr1	8,18	7,34	1,8	4,0E-02	8,57	6,88	3,2	7,2E-03	5
TC0600000565.mm.2	Gimap9	9,46	7,71	3,4	4,0E-03	8,70	8,07	1,6	5,3E-01	5
TC1400002870.mm.2	Setdb2; Phf11c; Phf11d	11,57	9,93	3,1	3,0E-04	11,34	10,50	1,8	1,1E-01	5
TC1900000221.mm.2	Ms4a6c	11,33	10,73	1,5	9,5E-01	11,73	9,97	3,4	2,0E-02	5
TC0200003599.mm.2	Cd302	9,16	8,62	1,5	6,2E-01	10,32	8,55	3,4	3,7E-02	5
TC0400002601.mm.2	Trim14	7,74	5,84	3,7	5,7E-03	5,77	5,61	1,1	5,6E-01	5
TC0500002843.mm.2	Hpse	7,63	7,12	1,4	9,4E-01	7,57	5,80	3,4	3,4E-02	5
TC1200002525.mm.2	Serpina3g	9,05	7,41	3,1	7,2E-03	8,99	8,32	1,6	4,0E-01	5
TC0900002054.mm.2	Tbrg1	12,01	10,42	3,0	2,7E-02	11,36	10,60	1,7	3,3E-01	5
TC0200004245.mm.2	Tcp11l1	5,77	3,98	3,5	4,2E-02	4,73	4,44	1,2	7,7E-01	5
TC0100003627.mm.2	Akt3	13,08	11,44	3,1	8,0E-04	12,60	12,63	-1,0	9,7E-01	5

Table 26 | List of regulated genes from spleen- and liver-derived inflammatory monocytes 3 days post *Listeria monocytogenes* **infection identified by microarray analyses from ADAPko** *versus* **wild type mice.** Differentially regulated genes from FACS-sorted spleen and liver were identified as follows: Per genotype and organ, inflammatory monocytes from 6 mice were isolated and cells from 2 mice each were pooled, resulting in n = 3 independent replicate sample pools per organ and genotype. Total RNA was isolated and analyzed by Clariom S microarray (23 samples in total). Differentially expressed transcripts in spleen/liver-derived inflammatory monocytes were determined comparing ADAPko *versus* wild type condition (fold change $> \pm 3$-fold, FDR < 0.05). For each gene the averaged $\log_2$ normalized signal intensity, fold change (ADAPko *versus* wild type), FDR and the k-means cluster (KMC) assignment are shown. Genes are sorted according to their k-means cluster number and within the clusters descendingly sorted by the average absolute fold changes. Genes above the applied fold change threshold (FC $> \pm 3$) are in bold and color-coded (green: down-regulated, red: up-regulated). FDR values < 0.05 are bold. Table is relates to **Figure 37**.

(continued on the next page)

Appendix

Annotation		Spleen				Liver				KMC Cluster ID
Array ID	Gene Symbol	ADAPko [mean log$_2$ SI]	wild type [mean log$_2$ SI]	FC (ADAPko vs. wild type)	FDR	ADAPko [mean log$_2$ SI]	wild type [mean log$_2$ SI]	FC (ADAPko vs. wild type)	FDR	
TC0400001770.mm.2	Padi2	7,54	12,41	-29,2	5,8E-03	6,32	9,92	-12,1	9,1E-03	1
TC1100001767.mm.2	Ace	8,64	12,86	-18,6	7,0E-04	6,09	9,16	-8,4	2,3E-03	1
TC0100003129.mm.2	Nav1	5,84	9,25	-10,6	7,0E-04	5,93	9,91	-15,8	1,0E-04	1
TC0800000621.mm.2	Hpgd	5,36	9,83	-22,2	1,4E-02	4,98	6,97	-4,0	1,1E-01	1
TC0200005164.mm.2	Sulf2	7,69	11,37	-12,8	2,5E-02	6,32	9,80	-11,2	1,8E-02	1
TC1100004000.mm.2	Abca9	5,67	9,37	-12,9	2,0E-03	5,83	7,37	-2,9	1,5E-01	1
TC1200001686.mm.2	Stxbp6	6,38	9,23	-7,2	2,8E-03	6,25	9,33	-8,4	6,0E-04	1
TC1700000990.mm.2	Adgre4	9,51	12,90	-10,5	3,2E-03	7,90	10,17	-4,8	1,7E-02	1
TC0400001107.mm.2	Dhcr24	5,90	8,74	-7,1	4,3E-03	5,29	8,25	-7,8	2,1E-03	1
TC0200004207.mm.2	Ldlrad3	7,13	9,57	-5,4	5,7E-02	7,16	10,36	-9,2	5,3E-03	1
TC0100000642.mm.2	Cyp27a1	10,12	12,63	-5,7	5,2E-02	9,16	12,30	-8,8	4,5E-03	1
TC1200000682.mm.2	Plekhg3	9,84	12,00	-4,5	3,8E-02	9,69	12,70	-8,1	2,0E-04	1
TC1500000037.mm.2	Fyb	12,51	15,06	-5,9	7,5E-06	12,57	15,01	-5,4	5,8E-05	1
TC0600001443.mm.2	Lpar5	6,16	9,47	-9,9	1,6E-03	5,41	5,88	-1,4	3,8E-01	1
TC0700002617.mm.2	Atp1a3	11,08	13,75	-6,4	2,0E-02	11,08	13,36	-4,9	6,6E-03	1
TC1100001677.mm.2	Cd300lg	6,76	8,67	-3,8	8,7E-02	5,63	8,52	-7,4	4,1E-02	1
TC0900003248.mm.2	Cx3cr1	5,28	8,24	-7,8	2,0E-03	5,19	6,89	-3,3	2,6E-02	1
TC1600000432.mm.2	Bex6	8,83	11,56	-6,6	2,2E-02	9,15	11,15	-4,0	9,5E-02	1
TC0600002965.mm.2	Plxnd1	9,90	12,25	-5,1	4,0E-02	9,00	11,46	-5,5	2,0E-02	1
TC1100004057.mm.2	Gm11710; Gm11711; Cd300lh	7,94	10,57	-6,2	5,8E-03	8,71	10,76	-4,1	1,5E-02	1
TC1200000647.mm.2	Prkch	9,71	11,61	-3,8	2,9E-02	9,34	11,97	-6,2	6,8E-03	1
TC1100004058.mm.2	Cd300lh; Gm11711	9,17	11,61	-5,4	4,8E-03	9,92	12,00	-4,2	8,8E-03	1
TC1200001902.mm.2	Rtn1	4,78	7,29	-5,7	6,4E-03	4,51	6,49	-4,0	8,8E-03	1
TC0900000581.mm.2	Nxpe4	9,92	12,25	-5,0	1,6E-03	8,28	10,23	-3,9	8,5E-03	1
TC1000003119.mm.2	Lrp1	13,18	14,58	-2,6	1,5E-01	11,78	14,37	-6,0	3,6E-03	1
TC1100003462.mm.2	Ypel2	4,92	7,04	-4,4	7,6E-03	4,94	6,97	-4,1	1,2E-03	1
TC0700002168.mm.2	Tmem150b	5,69	7,31	-3,1	8,2E-03	4,96	7,25	-4,9	1,2E-03	1
TC1100003870.mm.2	Map3k14	9,80	11,29	-2,8	1,9E-03	9,24	11,58	-5,1	8,8E-05	1
TC0200001798.mm.2	Stard9	9,37	11,18	-3,5	9,2E-03	9,03	11,16	-4,4	3,6E-03	1
TC0600001521.mm.2	Clec2i	8,99	11,20	-4,6	1,1E-02	9,04	10,71	-3,2	6,1E-02	1
TC0900000492.mm.2	Pvrl1	5,87	8,14	-4,8	9,2E-03	5,84	7,18	-2,5	7,6E-02	1
TC0500003024.mm.2	Adrbk2	8,41	10,09	-3,2	8,7E-03	7,73	9,77	-4,1	4,5E-03	1
TC0500003219.mm.2	Camkk2	9,36	11,58	-4,6	2,7E-03	9,63	10,85	-2,3	9,1E-03	1
TC0600005570.mm.2	Tmem176a	7,75	10,28	-5,8	3,5E-02	7,94	8,15	-1,2	9,7E-01	1
TC0300000060.mm.2	Fabp5	8,87	10,91	-4,1	1,3E-02	9,21	10,65	-2,7	9,8E-02	1
TC1500001791.mm.2	Arhgap39	10,04	11,35	-2,5	2,6E-01	9,41	11,48	-4,2	2,5E-02	1
TC0600003433.mm.2	Itpr2	7,98	8,88	-1,9	6,6E-01	7,30	9,56	-4,8	1,1E-03	1
TC0100001262.mm.2	Kif21b	8,61	10,10	-2,8	7,6E-02	7,96	9,87	-3,8	3,9E-02	1
TC0200004843.mm.2	Acss1	6,15	8,06	-3,8	2,7E-02	6,49	7,97	-2,8	1,6E-01	1
TC0700004313.mm.2	Spn	7,31	9,64	-5,0	3,2E-02	7,44	8,02	-1,5	5,4E-01	1
TC0100001018.mm.2	Phlpp1	7,78	9,46	-3,2	2,7E-02	8,13	9,85	-3,3	1,1E-02	1
TC1600001150.mm.2	Rogdi	7,48	9,52	-4,1	3,4E-02	6,52	7,76	-2,4	8,2E-02	1
TC0100002350.mm.2	Ankrd44	10,26	11,73	-2,8	6,4E-03	10,00	11,87	-3,7	1,0E-04	1
TC1000003078.mm.2	Slc16a7	5,91	6,96	-2,1	1,7E-01	4,76	6,85	-4,3	4,9E-02	1
TC0400003253.mm.2	Zfyve9	8,68	10,48	-3,5	1,1E-02	7,67	9,08	-2,7	2,0E-02	1
TC1300002002.mm.2	Sema4d	8,29	10,35	-4,2	2,9E-02	7,11	8,08	-2,0	1,1E-01	1
TC0200002580.mm.2	1500012F01Rik; Snord12	12,43	14,46	-4,1	4,6E-02	13,13	14,15	-2,0	4,2E-01	1
TC1300000735.mm.2	Dapk1	8,21	9,25	-2,1	1,7E-01	7,58	9,58	-4,0	7,0E-03	1
TC0900003115.mm.2	Nbeal2; Mir8107	9,58	10,90	-2,5	7,5E-01	8,76	10,58	-3,5	3,6E-02	1
TC0700001086.mm.2	Akap13	7,05	8,18	-2,2	4,6E-01	6,61	8,55	-3,8	4,0E-02	1
TC1700002298.mm.2	Pot1b	12,33	14,01	-3,2	1,9E-03	11,96	13,44	-2,8	3,0E-03	1
TC0800002184.mm.2	Wwc2	8,56	10,10	-2,9	2,0E-02	8,46	10,07	-3,1	3,7E-02	1
TC1900001622.mm.2	Calhm2	8,49	10,48	-4,0	1,4E-02	7,55	8,52	-2,0	1,9E-01	1
TC1300001461.mm.2	Gpr137b	10,18	12,01	-3,6	1,7E-03	10,75	11,99	-2,4	4,7E-02	1
TC1000000147.mm.2	Map3k5	10,33	11,09	-1,7	8,1E-01	9,26	11,33	-4,2	6,9E-03	1
TC1100000343.mm.2	Stk10	11,93	13,38	-2,7	3,6E-03	11,95	13,61	-3,2	1,5E-03	1
TC0100000886.mm.2	Ramp1	8,59	10,48	-3,7	2,1E-02	8,30	9,41	-2,2	9,0E-02	1
TC0700001391.mm.2	Arrb1	9,93	11,65	-3,3	1,8E-02	9,91	11,24	-2,5	4,5E-02	1
TC0800001608.mm.2	Insr	10,65	11,61	-2,0	1,2E-01	10,11	12,06	-3,9	3,5E-03	1
TC1100004051.mm.2	Cd300lb	8,34	10,09	-3,4	1,3E-02	7,45	8,74	-2,4	7,5E-02	1
TC0900001568.mm.2	Ctdspl	6,52	7,61	-2,1	3,4E-02	5,73	7,58	-3,6	8,3E-03	1
TC0300000968.mm.2	Prkab2	8,03	10,06	-4,1	3,5E-02	8,16	8,87	-1,6	2,9E-01	1
TC1100004229.mm.2	Cbr2	5,45	7,27	-3,5	2,1E-02	5,87	6,99	-2,2	4,4E-01	1
TC1100004002.mm.2	Abca6	4,95	6,82	-3,7	7,3E-05	5,11	6,09	-2,0	5,8E-02	1
TC1900000610.mm.2	Marveld1	5,91	8,06	-4,4	8,4E-03	6,52	6,74	-1,2	7,5E-01	1
TC0900001182.mm.2	Slc9a9	7,23	9,19	-3,9	1,6E-02	7,30	8,08	-1,7	7,4E-02	1
TC1900000819.mm.2	Atml1	10,19	10,94	-1,7	7,1E-01	9,15	11,10	-3,9	5,7E-03	1
TC1900000748.mm.2	Add3	11,85	13,08	-2,4	2,7E-02	10,71	12,38	-3,2	3,4E-03	1
TC0600000648.mm.2	Chn2	5,77	6,74	-2,0	1,3E-01	5,67	7,51	-3,6	4,7E-03	1
TC0200000393.mm.2	Pnpla7	10,41	11,43	-2,0	2,3E-01	9,37	11,18	-3,5	2,0E-02	1
TC0400002799.mm.2	Akna	13,13	14,20	-2,1	6,8E-01	12,09	13,87	-3,4	1,7E-02	1
TC0500003284.mm.2	Slc15a4	13,32	14,91	-3,0	1,7E-02	12,85	14,16	-2,5	3,3E-02	1
TC1100004157.mm.2	Timp2	8,28	10,21	-3,8	1,6E-03	7,99	8,70	-1,6	8,2E-02	1
TC0700001816.mm.2	Ypel3	11,41	13,24	-3,6	8,2E-03	11,78	12,68	-1,9	1,7E-01	1
TC1700000584.mm.2	Adamts10	7,49	8,27	-1,7	3,9E-01	6,16	8,05	-3,7	2,8E-02	1
TC1000000142.mm.2	Ifngr1	9,92	11,78	-3,6	4,7E-03	10,27	11,11	-1,8	4,8E-02	1
TC0700001888.mm.2	Inpp5f	6,08	8,09	-4,0	5,9E-03	5,88	6,37	-1,4	4,5E-01	1
TC1900001131.mm.2	Ms4a7	9,60	11,55	-3,9	3,9E-02	9,58	10,17	-1,5	8,4E-01	1
TC0200001782.mm.2	Mga	9,47	9,60	-1,1	9,9E-01	7,85	9,95	-4,3	3,0E-03	1
TC1100003505.mm.2	Akap1	6,14	7,20	-2,1	2,3E-01	4,97	6,65	-3,2	3,0E-02	1
TC1900000763.mm.2	Pdcd4	10,29	12,15	-3,7	1,6E-02	9,87	10,57	-1,6	4,3E-01	1
TC1100001115.mm.2	Ssh2	7,34	8,93	-3,0	4,0E-02	7,11	8,27	-2,2	2,8E-01	1
TC0100002236.mm.2	Tbc1d8	9,15	11,00	-3,6	1,6E-03	9,58	10,17	-1,5	2,0E-01	1
TC1100003663.mm.2	Arl5c	8,51	8,83	-1,3	8,9E-01	7,69	9,63	-3,8	6,0E-03	1
TC1300002463.mm.2	Iqgap2	11,26	12,29	-2,0	1,9E-01	10,59	12,19	-3,0	4,7E-03	1
TC1100002914.mm.2	Mapk7	10,98	11,89	-1,9	5,9E-01	10,17	11,82	-3,1	1,8E-02	1
TC0700000424.mm.2	Tgfb1	13,09	14,74	-3,1	1,3E-02	13,33	14,20	-1,8	2,8E-01	1
TC1300001641.mm.2	Hfe	8,70	10,49	-3,5	2,0E-02	8,80	9,26	-1,4	7,6E-01	1

Appendix

	Annotation	Spleen				Liver				KMC Cluster ID
Array ID	Gene Symbol	ADAPko [mean log₂ SI]	wild type [mean log₂ SI]	FC (ADAPko vs. wild type)	FDR	ADAPko [mean log₂ SI]	wild type [mean log₂ SI]	FC (ADAPko vs. wild type)	FDR	KMC Cluster ID
TC0600001622.mm.2	Atf7ip	11,78	12,57	-1,7	5,7E-01	11,12	12,72	-3,0	1,5E-02	1
TC0500003632.mm.2	Slc46a3	8,25	10,04	-3,5	1,5E-02	7,38	7,74	-1,3	4,2E-01	1
TC0200005136.mm.2	Pltp	4,03	5,71	-3,2	1,6E-03	3,92	4,47	-1,5	2,2E-01	1
TC1600002157.mm.2	Prdm15	6,82	6,43	1,3	9,4E-01	5,56	7,26	-3,2	9,8E-03	1
TC1800000282.mm.2	Apc	7,81	8,39	-1,5	7,5E-01	7,04	8,64	-3,0	2,7E-02	1
TC0100001663.mm.2	Sdccag8	7,92	8,35	-1,3	7,6E-01	7,35	9,01	-3,1	1,6E-02	1
TC0700003829.mm.2	P2ry6	7,82	9,51	-3,2	1,3E-03	8,17	8,49	-1,3	8,1E-01	1
TC0500003198.mm.2	Sh2b3	6,50	6,92	-1,3	5,8E-01	5,87	7,49	-3,1	4,5E-02	1
TC0X00003209.mm.2	Kctd12b	3,55	5,16	-3,1	3,8E-03	3,38	3,52	-1,1	5,5E-01	1
TC0400001677.mm.2	Id3	4,76	6,18	-2,7	6,6E-01	9,52	13,65	-17,5	2,4E-02	2
TC1700002337.mm.2	Rfx2	6,26	7,66	-2,6	2,7E-01	5,92	9,70	-13,8	9,1E-03	2
TC1700001027.mm.2	Tnfsf9	5,50	5,50	1,0	9,9E-01	7,84	11,67	-14,2	1,6E-03	2
TC0100003029.mm.2	Cxcr4	9,53	12,12	-6,1	6,0E-04	12,18	14,25	-4,2	4,0E-04	2
TC0200004196.mm.2	Gm10800	6,97	8,14	-2,3	3,6E-01	6,49	9,48	-8,0	9,9E-03	2
TC0X00001715.mm.2	Gm21887	10,79	12,36	-3,0	2,9E-01	11,92	14,58	-6,3	1,9E-02	2
TC0200004808.mm.2	Thbd	7,19	8,43	-2,4	1,5E-01	9,09	11,56	-5,6	1,1E-03	2
TC0200004676.mm.2	Gpcpd1	8,28	9,96	-3,2	1,6E-02	10,61	12,79	-4,5	1,5E-02	2
TC0Y00000223.mm.2	Erdr1	13,13	14,44	-2,5	2,0E-01	14,35	16,72	-5,2	3,3E-02	2
TC1700000655.mm.2	Gm20481	8,98	7,82	2,2	4,5E-01	9,17	11,59	-5,4	9,6E-03	2
TC0500001698.mm.2	Amz1	6,38	8,41	-4,1	3,9E-02	7,28	8,97	-3,2	2,5E-02	2
TC1700001827.mm.2	Sik1	10,21	12,54	-5,0	1,0E-04	13,74	14,90	-2,2	1,2E-02	2
TC1900001390.mm.2	Sgms1	9,10	10,36	-2,4	1,1E-01	11,53	13,68	-4,4	7,0E-04	2
TC1700001936.mm.2	Hspa1a	10,63	9,79	1,8	6,7E-01	10,54	12,79	-4,8	3,2E-02	2
TC1500001155.mm.2	Ptger4	7,25	8,41	-2,2	5,1E-01	8,63	10,68	-4,2	2,2E-02	2
TC0900000824.mm.2	Dennd4a	11,03	12,43	-2,6	1,3E-02	12,75	14,65	-3,7	1,7E-03	2
TC0800001694.mm.2	Irs2	9,88	11,00	-2,2	2,7E-01	11,22	13,24	-4,0	3,2E-02	2
TC1100000910.mm.2	Gm17305	7,26	8,55	-2,5	4,5E-01	7,89	9,79	-3,7	2,0E-02	2
TC1500001630.mm.2	Asap1	10,54	11,92	-2,6	7,6E-02	10,60	12,41	-3,5	8,2E-03	2
TC1700002324.mm.2	Ptprs	8,81	9,62	-1,8	4,3E-01	8,81	10,92	-4,3	2,9E-02	2
TC0400000529.mm.2	Nr4a3	3,93	3,93	-1,0	9,9E-01	8,22	10,54	-5,0	1,5E-02	2
TC1400001499.mm.2	Nr1d2	4,65	6,02	-2,6	1,8E-01	4,94	6,70	-3,4	3,7E-02	2
TC0700000562.mm.2	Nfkbid	9,55	9,59	-1,0	9,4E-01	11,06	13,34	-4,9	6,5E-05	2
TC1600001380.mm.2	Dgkg	8,70	10,03	-2,5	9,5E-02	9,21	10,93	-3,3	2,0E-02	2
TC0100001176.mm.2	Slc41a1	10,58	11,18	-1,5	8,4E-01	9,92	11,98	-4,2	3,9E-02	2
TC1100004144.mm.2	Tmc6	6,86	8,05	-2,3	2,0E-02	7,78	9,54	-3,4	1,2E-03	2
TC1500001410.mm.2	Klf10	7,08	8,88	-3,5	1,7E-02	9,30	10,41	-2,2	4,4E-02	2
TC0500000896.mm.2	Ccng2	9,98	10,66	-1,6	7,9E-01	9,97	11,97	-4,0	8,8E-03	2
TC1300000958.mm.2	Arrdc3	7,47	9,61	-4,4	5,1E-03	11,34	11,14	1,2	7,9E-01	2
TC1100003125.mm.2	Nlrp1b	9,46	9,78	-1,3	8,8E-01	8,62	10,67	-4,2	1,1E-02	2
TC1700001935.mm.2	Hspa1b; Hspa1a	8,47	7,48	2,0	3,6E-01	8,63	10,41	-3,4	2,5E-02	2
TC0700003839.mm.2	Art2a-ps	5,26	6,08	-1,8	1,2E-01	5,89	7,69	-3,5	3,1E-03	2
TC1400000244.mm.2	4931406H21Rik	6,77	7,65	-1,8	4,2E-01	7,02	8,79	-3,4	6,5E-03	2
TC0600003601.mm.2	Foxp1	12,00	13,02	-2,0	6,2E-02	12,11	13,77	-3,2	3,6E-03	2
TC0600002056.mm.2	Wdr91	10,75	11,81	-2,1	3,9E-01	11,51	13,12	-3,1	3,4E-02	2
TC0600003236.mm.2	Clec7a	12,56	14,41	-3,6	6,0E-04	13,89	14,50	-1,5	2,7E-01	2
TC1600001770.mm.2	St3gal6	7,07	8,11	-2,1	3,4E-01	7,98	9,58	-3,0	3,2E-02	2
TC0400001715.mm.2	Eif4g3	7,01	7,60	-1,5	2,7E-01	6,97	8,73	-3,4	8,1E-03	2
TC1500000835.mm.2	Tbc1d22a	7,35	7,92	-1,5	7,7E-01	7,97	9,73	-3,4	1,8E-02	2
TC0200003592.mm.2	Baz2b	10,37	10,72	-1,3	8,2E-01	10,48	12,27	-3,5	7,8E-03	2
TC1000000529.mm.2	Sowahc	11,84	12,38	-1,5	8,0E-01	13,52	15,20	-3,2	1,6E-02	2
TC1300000498.mm.2	Cd83	5,57	6,07	-1,4	9,0E-01	7,26	8,95	-3,2	4,6E-02	2
TC0200001396.mm.2	Phf21a	10,11	10,68	-1,5	7,1E-01	10,18	11,81	-3,1	5,7E-03	2
TC0700000024.mm.2	Leng8	8,85	9,49	-1,6	6,1E-01	8,55	10,15	-3,0	2,2E-02	2
TC0900002281.mm.2	Sik2	7,15	7,27	-1,1	9,5E-01	6,57	8,33	-3,4	3,4E-03	2
TC0500003418.mm.2	Cux1	10,36	10,40	-1,0	1,0E+00	9,99	11,75	-3,4	6,5E-03	2
TC1100002455.mm.2	Gm17332	3,39	3,45	-1,0	9,2E-01	3,42	5,12	-3,3	3,7E-02	2
TC0700002424.mm.2	Ccdc9	7,52	7,60	-1,1	9,8E-01	7,55	9,24	-3,2	9,1E-03	2
TC0100000292.mm.2	Il1r2	14,64	9,60	33,1	4,6E-08	15,31	13,46	3,6	5,5E-03	3
TC0700000575.mm.2	Dmkn	9,97	6,66	10,0	6,0E-04	10,39	8,44	3,9	3,4E-03	3
TC0200004599.mm.2	Il1a	9,41	6,50	7,5	3,2E-02	12,28	11,95	1,3	8,1E-01	3
TC0900003313.mm.2	Ccr1	12,52	10,34	4,5	8,5E-03	13,37	11,90	2,8	1,2E-01	3
TC0700004487.mm.2	Adam8	10,65	8,15	5,6	1,6E-02	10,94	10,73	1,2	3,1E-01	3
TC0200005030.mm.2	Tgm2	10,81	8,49	5,0	7,6E-03	12,79	12,13	1,6	6,2E-01	3
TC1700000932.mm.2	Trem1	13,44	11,34	4,3	9,2E-03	15,39	15,88	-1,4	9,8E-01	3
TC0900000497.mm.2	Usp2	9,16	7,34	3,5	2,4E-02	9,58	8,48	2,2	3,9E-01	3
TC1400001182.mm.2	Irg1	13,73	11,66	4,2	1,0E-02	13,93	14,29	-1,3	7,2E-01	3
TC0700002173.mm.2	Ube2s	8,37	6,64	3,3	1,6E-02	8,49	7,52	2,0	1,6E-01	3
TC1300002204.mm.2	Ctsl	12,10	10,36	3,3	7,6E-03	12,57	11,88	1,6	1,3E-01	3
TC1900000111.mm.2	Ehd1	11,63	9,75	3,7	1,7E-03	11,96	12,02	-1,0	9,0E-01	3
TC1000001621.mm.2	Mmp19	9,63	7,92	3,3	4,2E-02	9,57	9,53	1,0	7,0E-01	3
TC0600003084.mm.2	Clec4e	15,04	13,39	3,1	3,9E-02	15,60	15,83	-1,2	8,9E-01	3
TC0700003793.mm.2	Dgat2	10,41	8,80	3,0	4,4E-02	10,54	10,76	-1,2	8,8E-01	3
TC1100001267.mm.2	Wfdc21	15,97	11,75	18,6	3,3E-03	16,05	11,60	21,7	8,0E-04	4
TC0300002376.mm.2	S100a9	15,18	12,07	8,7	1,5E-03	15,56	10,72	28,7	4,2E-05	4
TC0700003039.mm.2	Saa3	15,51	11,61	14,9	1,9E-02	16,34	12,39	15,5	8,4E-03	4
TC1000000823.mm.2	Elane	12,68	9,08	12,1	6,4E-03	12,41	8,41	16,0	3,0E-03	4
TC1700002315.mm.2	Lrg1	11,13	7,27	14,5	1,6E-03	10,94	8,10	7,2	1,0E-03	4
TC1000000822.mm.2	Prtn3	14,10	10,87	9,4	7,0E-04	14,24	10,65	12,1	4,0E-04	4
TC0300000811.mm.2	S100a8	16,16	13,00	8,9	9,6E-03	16,88	13,37	11,5	1,2E-02	4
TC1100001171.mm.2	Nos2	9,70	6,05	12,5	5,8E-03	9,88	7,39	5,6	8,7E-03	4
TC0400003792.mm.2	C1qb	10,99	9,15	3,6	4,2E-01	12,00	8,15	14,4	2,9E-02	4
TC1500001054.mm.2	Slc4a8	12,44	9,91	5,8	7,4E-02	12,63	9,20	10,8	1,0E-02	4
TC0200003303.mm.2	Lcn2	16,63	13,33	9,9	4,6E-03	16,64	13,98	6,3	1,1E-02	4
TC1500001940.mm.2	Cenpm	9,09	6,91	4,6	1,9E-02	9,90	6,69	9,3	3,1E-02	4
TC0600003250.mm.2	Klra17	10,34	7,66	6,4	8,0E-04	10,35	7,65	6,5	5,0E-04	4
TC0200001854.mm.2	AA467197; Mir147	12,79	10,11	6,4	2,0E-02	12,90	10,28	6,2	3,0E-03	4
TC0400003793.mm.2	C1qc	9,62	7,61	4,0	6,0E-02	10,09	7,06	8,2	1,2E-02	4
TC1400002065.mm.2	Cebpe	9,27	6,62	6,3	6,7E-03	9,89	7,45	5,5	3,0E-02	4

(continued on the next page) | **151**

Appendix

Annotation		Spleen				Liver				KMC Cluster ID
Array ID	Gene Symbol	ADAPko [mean log$_2$ SI]	wild type [mean log$_2$ SI]	FC (ADAPko vs. wild type)	FDR	ADAPko [mean log$_2$ SI]	wild type [mean log$_2$ SI]	FC (ADAPko vs. wild type)	FDR	
TC0800001833.mm.2	Gm15056	8,27	8,43	-1,1	1,0E+00	9,18	5,83	10,2	3,4E-03	4
TC0200004511.mm.2	Gatm	9,15	7,75	2,6	2,7E-01	9,78	6,81	7,8	2,2E-03	4
TC0500001732.mm.2	Kdelr2	11,37	9,50	3,7	3,3E-01	12,23	9,66	5,9	4,7E-02	4
TC0X00003434.mm.2	Ubl4a	11,33	9,56	3,4	1,2E-01	11,82	9,23	6,0	3,6E-02	4
TC1900001340.mm.2	Insl6	9,53	8,29	2,4	3,0E-01	9,64	6,89	6,7	8,0E-03	4
TC0600003079.mm.2	C3ar1	9,99	7,50	5,6	1,9E-02	9,78	8,18	3,0	5,7E-03	4
TC0700000847.mm.2	Gys1	9,94	8,44	2,8	3,1E-01	9,71	7,21	5,6	2,3E-02	4
TC1100003161.mm.2	Aspa	7,37	5,41	3,9	1,7E-01	8,37	6,29	4,2	3,0E-02	4
TC0100001574.mm.2	Fcgr4	14,57	13,84	1,7	2,4E-01	15,02	12,46	5,9	2,0E-03	4
TC1100001222.mm.2	Ccl12	7,56	5,86	3,3	1,1E-01	7,79	5,76	4,1	1,9E-02	4
TC0900001170.mm.2	Plscr1	10,14	8,48	3,2	4,8E-03	10,69	8,69	4,0	9,8E-03	4
TC0900001883.mm.2	Spc24	8,98	7,48	2,8	9,8E-02	9,60	7,62	3,9	2,5E-02	4
TC1600001559.mm.2	Fam162a	9,88	9,44	1,4	8,6E-01	11,70	9,30	5,3	2,1E-03	4
TC1100000015.mm.2	Selm	11,29	10,21	2,1	2,7E-01	12,53	10,36	4,5	3,9E-02	4
TC0600001839.mm.2	Asns	7,98	6,86	2,2	1,9E-01	8,78	6,66	4,4	1,1E-03	4
TC0700003850.mm.2	Il18bp	12,52	11,05	2,8	2,1E-02	12,24	10,44	3,5	2,0E-03	4
TC1900001418.mm.2	Ch25h	5,42	3,87	2,9	2,1E-02	5,26	3,55	3,3	5,6E-03	4
TC0700000990.mm.2	Vimp	12,08	10,69	2,6	8,5E-02	12,15	10,35	3,5	1,5E-02	4
TC1700002204.mm.2	Guca1a	8,24	8,30	-1,0	9,8E-01	9,70	7,42	4,9	1,9E-03	4
TC1600000508.mm.2	Gm5483	6,83	5,90	1,9	2,4E-01	7,16	5,17	4,0	3,0E-03	4
TC1000000469.mm.2	Nus1	12,61	11,35	2,4	9,1E-02	12,93	11,15	3,4	4,2E-02	4
TC0700004258.mm.2	Nsmce1	11,35	10,81	1,5	7,1E-01	12,05	9,96	4,3	8,3E-03	4
TC0400000523.mm.2	Sec61b	12,47	11,44	2,0	1,3E-01	12,88	11,00	3,7	9,8E-03	4
TC0700002128.mm.2	Tarm1	14,66	12,99	3,2	1,3E-02	14,55	13,23	2,5	9,1E-03	4
TC0600000928.mm.2	Bola3	9,10	8,85	1,2	9,5E-01	10,41	8,31	4,3	5,4E-03	4
TC0900002054.mm.2	Tbrg1	8,93	8,37	1,5	4,1E-01	9,40	7,45	3,9	4,7E-02	4
TC0900002764.mm.2	Hmgn3	9,70	9,23	1,4	8,8E-01	10,29	8,39	3,7	3,1E-02	4
TC1500001542.mm.2	Mrpl13	9,53	8,70	1,8	7,6E-01	9,99	8,33	3,2	3,2E-02	4
TC1900001124.mm.2	Ms4a8a	10,52	9,65	1,8	2,3E-01	11,06	9,45	3,1	6,5E-03	4
TC0900001008.mm.2	Arpp19	12,69	12,04	1,6	6,2E-01	13,23	11,53	3,3	1,0E-02	4
TC1500002059.mm.2	Rabl2	7,79	7,51	1,2	9,0E-01	8,42	6,57	3,6	3,0E-03	4
TC0500002756.mm.2	Cxcl10	12,82	11,13	3,2	2,0E-02	12,16	11,54	1,5	2,2E-01	4
TC0300001621.mm.2	Mrps28	9,19	8,55	1,6	3,9E-01	10,34	8,65	3,2	4,2E-02	4
TC0500002649.mm.2	Spink2	8,92	8,38	1,5	8,3E-01	10,04	8,33	3,3	4,8E-02	4
TC1100001443.mm.2	Mrpl27	12,79	12,22	1,5	7,4E-01	13,39	11,69	3,2	4,2E-02	4
TC1900000401.mm.2	Gm3873	12,78	12,51	1,2	9,9E-01	13,32	11,51	3,5	4,8E-02	4
TC1000001946.mm.2	Hint3	12,54	11,96	1,5	7,1E-01	13,31	11,63	3,2	2,2E-02	4
TC0700002143.mm.2	Lair1	12,63	11,94	1,6	4,5E-01	13,07	11,46	3,1	4,5E-03	4
TC0700003769.mm.2	Aqp11	4,40	4,77	-1,3	9,1E-01	5,72	4,01	3,3	4,4E-02	4
TC0X00003420.mm.2	Uxt	13,35	12,85	1,4	6,3E-01	13,74	12,11	3,1	4,7E-03	4
TC0300000530.mm.2	Lekr1	6,65	6,38	1,2	9,8E-01	7,11	5,40	3,3	3,9E-02	4
TC0700004508.mm.2	Bet1l	10,52	10,43	1,1	9,8E-01	11,36	9,67	3,2	1,0E-02	4
TC1400001535.mm.2	Mrps16	8,03	8,03	1,0	1,0E+00	8,89	7,29	3,0	1,9E-02	4
TC1900001140.mm.2	Ms4a3	11,75	6,59	35,8	7,0E-04	11,99	5,79	73,6	2,0E-04	5
TC0200001935.mm.2	Mertk	10,89	7,56	10,1	1,3E-02	9,62	6,25	10,3	3,7E-02	5
TC1700001522.mm.2	Fpr1	12,36	9,91	5,5	1,7E-02	11,38	8,34	8,2	2,3E-03	5
TC0900001461.mm.2	Ngp	12,51	11,76	1,7	7,8E-01	8,99	5,46	11,6	8,0E-04	5
TC1900000102.mm.2	Batf2	11,52	8,96	5,9	6,7E-03	10,54	7,79	6,8	4,1E-03	5
TC0500000468.mm.2	Cd38	13,24	10,39	7,2	3,3E-02	12,76	10,62	4,4	6,0E-02	5
TC0300001255.mm.2	Sec24d	10,29	7,64	6,3	8,5E-03	9,47	7,16	5,0	2,5E-02	5
TC0200001765.mm.2	Spint1	16,15	14,29	3,6	1,9E-01	15,64	12,79	7,2	1,5E-02	5
TC1500000852.mm.2	Creld2	13,62	11,45	4,5	3,9E-02	13,64	10,99	6,3	4,6E-02	5
TC1800001396.mm.2	Gm4841	13,52	11,54	4,0	8,9E-03	12,70	10,00	6,5	6,0E-04	5
TC1700001596.mm.2	Mmp25	9,99	6,99	8,0	2,0E-04	9,45	8,20	2,4	1,3E-01	5
TC0900001391.mm.2	Gmppb	11,25	9,01	4,7	2,0E-04	10,60	8,18	5,4	8,0E-04	5
TC1400000501.mm.2	Cdkn3	8,16	6,22	3,8	6,7E-02	7,95	5,31	6,2	2,6E-02	5
TC1700001757.mm.2	Fkbp5	10,22	7,57	6,3	3,9E-02	8,66	6,80	3,6	2,5E-01	5
TC0500001614.mm.2	Cldn15	11,50	9,50	4,0	9,4E-02	11,27	8,70	5,9	1,5E-02	5
TC0500001240.mm.2	Oasl1	12,46	9,56	7,4	1,6E-02	10,71	9,71	2,0	2,8E-01	5
TC0300001448.mm.2	Ccbl2	9,91	7,87	4,1	1,9E-03	9,68	7,32	5,1	1,8E-03	5
TC1000000571.mm.2	Ppa1	14,38	12,30	4,2	1,7E-01	13,68	11,42	4,8	4,6E-02	5
TC1600001198.mm.2	Socs1	9,78	7,03	6,7	4,7E-03	7,34	6,19	2,2	1,5E-01	5
TC0100001170.mm.2	Fam72a	8,66	6,94	3,3	3,6E-01	8,23	5,76	5,6	3,3E-02	5
TC0200002232.mm.2	Gins1	8,70	7,63	2,1	6,0E-01	8,79	6,06	6,6	1,7E-02	5
TC0200005494.mm.2	Phpt1	12,38	11,09	2,5	6,8E-01	12,92	10,37	5,9	4,9E-02	5
TC1100000119.mm.2	Upp1	14,91	12,90	4,0	1,2E-02	14,49	12,44	4,1	3,4E-03	5
TC0300002053.mm.2	P2ry13	9,84	8,68	2,2	4,5E-01	8,75	6,20	5,9	6,0E-03	5
TC0300000161.mm.2	Tnfsf10	10,13	8,37	3,4	9,5E-02	8,82	6,64	4,5	1,0E-02	5
TC0100001570.mm.2	Olfml2b	7,22	4,89	5,1	4,9E-03	6,93	5,42	2,9	3,7E-02	5
TC1600000699.mm.2	Retnlg	10,61	8,70	3,8	1,6E-01	10,03	8,08	3,9	3,4E-03	5
TC1700000835.mm.2	Pla2g7	14,73	13,53	2,3	3,4E-01	14,37	11,97	5,3	4,8E-03	5
TC1300000919.mm.2	Glrx	12,52	10,31	4,6	1,6E-03	11,95	10,50	2,7	5,0E-03	5
TC0100002495.mm.2	Acadl	12,12	9,91	4,6	2,8E-03	11,57	10,13	2,7	4,4E-03	5
TC1500000553.mm.2	Ly6g	8,41	6,89	2,9	7,6E-02	8,18	6,03	4,4	3,1E-03	5
TC1200002524.mm.2	Serpina3f	14,86	12,96	3,7	8,7E-02	13,85	12,16	3,2	2,3E-02	5
TC0200000933.mm.2	Gca	12,11	11,14	2,0	2,7E-01	11,27	8,99	4,9	5,4E-03	5
TC1700000214.mm.2	Fpr2; Fpr3	11,27	10,05	2,3	1,7E-01	11,36	9,24	4,4	4,7E-03	5
TC1200002525.mm.2	Serpina3g	11,12	9,66	2,8	3,0E-02	10,23	8,26	3,9	3,1E-03	5
TC0200004913.mm.2	Bcl2l1	7,88	6,41	2,8	3,1E-01	7,97	6,02	3,9	1,5E-02	5
TC1100004265.mm.2	Igtp	14,69	12,94	3,4	2,9E-02	13,99	12,33	3,2	3,6E-03	5
TC0800000111.mm.2	Atp11a	13,63	11,29	5,1	2,8E-02	12,21	11,75	1,4	1,9E-01	5
TC1500000615.mm.2	1110038F14Rik	11,12	9,92	2,3	1,9E-01	10,78	8,79	4,0	3,8E-02	5
TC1000000175.mm.2	H60b; Raet1a; Raet1b; Raet1c; Raet1d; Raet1e	7,61	5,55	4,2	1,1E-02	6,82	5,83	2,0	2,0E-02	5
TC1100003115.mm.2	Scimp	12,41	11,07	2,5	2,7E-01	11,48	9,66	3,5	7,0E-03	5
TC1700000487.mm.2	Mapk13	7,42	5,90	2,9	8,7E-03	7,54	5,92	3,1	6,8E-03	5
TC1000002572.mm.2	Nfyb	8,53	8,12	1,3	4,3E-01	8,81	6,61	4,6	1,7E-02	5
TC1600000322.mm.2	Dnajb11	11,66	9,79	3,6	4,5E-02	10,86	9,73	2,2	9,8E-02	5
TC0X00001071.mm.2	Pgk1	9,19	7,90	2,5	8,4E-02	9,16	7,42	3,3	1,1E-02	5

Appendix

Annotation		Spleen				Liver				KMC Cluster ID
Array ID	Gene Symbol	ADAPko [mean log$_2$ SI]	wild type [mean log$_2$ SI]	FC (ADAPko vs. wild type)	FDR	ADAPko [mean log$_2$ SI]	wild type [mean log$_2$ SI]	FC (ADAPko vs. wild type)	FDR	
TC0800000770.mm.2	Il12rb1	8,78	6,73	4,2	3,5E-03	6,46	5,80	1,6	7,7E-02	5
TC0500000689.mm.2	Dcun1d4	5,40	3,99	2,7	2,2E-02	4,96	3,34	3,1	7,0E-03	5
TC0200002407.mm.2	Rpn2	8,67	6,99	3,2	2,7E-02	8,46	7,17	2,4	1,9E-01	5
TC0200002150.mm.2	Sec23b	11,95	10,35	3,0	2,9E-02	11,59	10,29	2,5	5,2E-02	5
TC0X00002238.mm.2	Mospd1	11,81	10,81	2,0	3,4E-01	11,30	9,52	3,4	7,1E-03	5
TC0900000050.mm.2	Mmp8	15,00	13,32	3,2	1,0E-02	14,73	13,59	2,2	6,8E-03	5
TC0200003224.mm.2	Fcnb	8,53	6,89	3,1	1,9E-02	8,09	6,91	2,3	2,4E-02	5
TC0800001132.mm.2	Usb1	11,44	9,61	3,6	6,0E-03	10,09	9,25	1,8	3,7E-01	5
TC0300000037.mm.2	Zc2hc1a	8,23	7,32	1,9	2,0E-01	7,84	6,05	3,5	1,5E-02	5
TC0300002030.mm.2	Commd2	10,41	10,10	1,3	8,4E-01	10,40	8,37	4,1	4,8E-02	5
TC0400004014.mm.2	Fbxo6	10,61	9,77	1,8	4,6E-01	10,54	8,74	3,5	5,0E-02	5
TC0X00002847.mm.2	2610002M06Rik	9,79	8,98	1,8	6,1E-02	10,16	8,37	3,5	8,0E-04	5
TC1100003340.mm.2	Tefm	9,84	9,18	1,6	8,4E-01	9,09	7,24	3,6	8,9E-03	5
TC0200000620.mm.2	Hspa5	16,06	14,33	3,3	8,2E-03	15,39	14,52	1,8	1,4E-01	5
TC0700000693.mm.2	1600014C10Rik	13,04	12,06	2,0	3,9E-01	12,81	11,15	3,2	3,9E-02	5
TC0X00002189.mm.2	Rap2c	11,24	10,30	1,9	2,5E-01	10,34	8,69	3,2	1,3E-02	5
TC1400002161.mm.2	Phf11a	11,57	10,90	1,6	6,1E-01	11,43	9,69	3,3	2,5E-02	5
TC1600000664.mm.2	Cd200r4	11,61	10,85	1,7	4,3E-01	10,81	9,15	3,2	4,7E-02	5
TC1100000681.mm.2	Gm12250	15,09	14,28	1,8	3,4E-01	14,23	12,60	3,1	1,1E-02	5
TC1700002110.mm.2	Cenpq	8,41	7,95	1,4	8,1E-01	7,72	5,96	3,4	4,0E-02	5
TC0100000300.mm.2	Il18rap	7,76	5,95	3,5	3,3E-02	7,01	6,71	1,2	3,4E-01	5
TC0900000786.mm.2	Anp32a	11,81	11,15	1,6	3,9E-01	11,09	9,44	3,1	4,2E-02	5
TC1100002091.mm.2	Inpp5j	8,91	7,24	3,2	4,8E-03	7,24	6,73	1,4	1,1E-01	5
TC1300002339.mm.2	Rfesd	10,57	10,22	1,3	9,9E-01	10,66	8,97	3,2	8,4E-03	5
TC0500002755.mm.2	Cxcl9	15,07	15,00	1,1	8,9E-01	14,68	12,96	3,3	1,3E-03	5
TC0200001011.mm.2	Phospho2	8,32	8,34	-1,0	9,6E-01	8,15	6,56	3,0	2,5E-02	5

7.3 Ehrenerklärung

Ich versichere hiermit, dass ich die vorliegende Arbeit ohne unzulässige Hilfe Dritter und ohne Benutzung anderer als der angegebenen Hilfsmittel angefertigt habe; verwendete fremde und eigene Quellen sind als solche kenntlich gemacht.

Ich habe insbesondere nicht wissentlich:

- Ergebnisse erfunden oder widersprüchlich Ergebnisse verschwiegen,
- statistische Verfahren absichtlich missbraucht, um Daten in ungerechtfertigter Weise zu interpretieren,
- fremde Ergebnisse oder Veröffentlichungen plagiiert,
- fremde Forschungsergebnisse verzerrt wiedergegeben.

Mir ist bekannt, dass Verstöße gegen das Urheberrecht Unterlassungs- und Schadensersatzansprüche des Urhebers sowie eine strafrechtliche Ahndung durch die Strafverfolgungsbehörden begründen kann.

Ich erkläre mich damit einverstanden, dass die Arbeit ggf. mit Mitteln der elektronischen Datenverarbeitung auf Plagiate überprüft werden kann.

Die Arbeit wurde bisher weder im Inland noch im Ausland in gleicher oder ähnlicher Form als Dissertation eingereicht und ist als Ganzes auch noch nicht veröffentlicht.

Magdeburg, 28.06.2021

_____

Martha Böning